DEVELOPMENT OF A HIGH POWER SINGLE-MODE LASER FOR NON-LINEAR OPTICS APPLICATIONS

by

C.G. Sawyers

Ph.D. July 1981

UNIVERSITY OF SOUTHAMPTON

DEVELOPMENT OF A HIGH POWER SINGLE-MODE LASER FOR NON-LINEAR OPTICS APPLICATIONS

by

C.G. Sawyers

A thesis submitted for the degree of

Doctor of Philosophy

Department of Electronics

Faculty of Engineering and Applied Science

July 1981

UNIVERSITY OF SOUTHAMPTON

ABSTRACT

FACULTY OF ENGINEERING AND APPLIED SCIENCE

ELECTRONICS

Doctor of Philosophy

DEVELOPMENT OF A HIGH POWER SINGLE-MODE LASER FOR NON-LINEAR OPTICS APPLICATIONS

by Craig George Sawyers

In the first part of this thesis an investigation is made into the feasibility of using a stable resonator which incorporates an intra-cavity telescope as a means of extracting high power pulsed radiation in a TEM_{00} mode from a Nd:YAG laser. An analysis of this telescopic resonator is presented and experimental results are described. TEM_{00} mode operation has been verified with an output energy of 350mJ when the resonator was operated with a fixed Q, and 100mJ when Q-switched.

For many applications it is found that operation of the laser on a single-longitudinal cavity mode is desirable. In the second part of this thesis the conditions necessary to obtain single-frequency operation of a pulsed laser are discussed. The application of one technique, referred to in this thesis as pre-lase triggered Q-switching, has been investigated experimentally as applied to the telescopic resonator. Single-mode operation has been obtained for $\sim$60% of laser shots, and guidelines are given as to how this fraction may be increased.

The thesis is concluded by describing the application of the output from the telescopic resonator to two non-linear optical processes: frequency doubling and Raman scattering. In each case it is shown that with the laser operating single-frequency, good agreement is obtained between detailed theoretical prediction and experimental observation.

CONTENTS

CHAPTER ONE

INTRODUCTION

Since the invention of the laser over two decades ago, a large amount of work in resonator design has been directed towards achieving high power laser operation of pulsed lasers with a diffraction limited output beam, and good shot-to-shot repeatability. In practice, this implies the need to work with a large mode volume. The work has been motivated by the requirements of both industrial and scientific applications. Industrial lasers used in a number of materials processing applications (cutting, welding and drilling) need to have high output power and excellent long and short term stability (see, e.g. Steffen et al., 1972). In the field of scientific applications the interpretation and prediction of the behaviour in various laser interactions, e.g. non-linear optical processes, can be significantly simplified if the laser provides a well defined spatial and temporal excitation. For example, most attempts at a theoretical description of non-linear optical processes assume incident laser beams to be Gaussian (Ward and New, 1969; Bjorklund, 1975; Cotter et al., 1975).

Our own requirement for a high power, diffraction limited Nd:YAG laser arose from a preliminary investigation of stimulated Raman scattering in liquid nitrogen. Published literature on this process had suggested that the optical and material properties of liquid nitrogen were conducive to high efficiency Raman conversion (Grasyuk et al., 1977; Sinnott et al., 1977; Efimovskii et al., 1977; Grasiuk and Zubarev, 1978; Grasiuk, 1980; Grun et al., 1969). Our first experiments, performed with an unstable resonator Nd:YAG laser (Hanna and Laycock, 1979; Laycock, 1978) and a custom designed and built liquid nitrogen cell (Sawyers, 1979), indicated that a major obstacle to the spatial quality of the Raman shifted (Stokes) beam was thermal blooming of the medium at laser repetition rates greater than 1Hz (Wild and Maier, 1980; Smith, 1977; Baklushina et al., 1977, Kormer et al., 1979). However, even when the repetition rate was reduced to the extent that thermal blooming was negligible, spatial distortion of the Stokes and transmitted pump was still observed. Since the output beam from a diffraction coupled unstable resonator is in the form of an annulus, it was not possible to make any accurate prediction of the expected Stokes beam profile. Shortly after these results had been obtained, a new Nd:YAG laser was purchased

from J.K. Lasers Ltd., under the tradename "Hyper Yag". This involved a new stable resonator design, incorporating an intracavity telescope (Sarkies, 1979). This laser featured an output beam which had a much smoother intensity profile than that of the unstable resonator, and in that respect was far superior for our applications. Subsequent results obtained using this laser to pump liquid nitrogen suggested that it would be desirable to operate the laser on a single-longitudinal mode. At first, an attempt was made to achieve this by applying to the Hyper Yag laser a technique in which the laser incorporates frequency selection and the Q-switch is opened in two stages (Hanna et al., 1971; Hanna et al., 1972 (two papers)), known variously as two-step Q-switching, slow Q-switching, or, as we shall refer to it in this thesis, pre-lase Q-switching. Disappointing results were obtained when this was applied to the Hyper Yag, in that the reliability of single-mode operation was poor, and the transverse intensity profile of the beam showed shot-to-shot instability. This led us to conclude that the Hyper Yag was operating on several transverse modes, and that reliable and repeatable single-longitudinal mode operation would only be secured when the laser operated on a single transverse mode. We therefore embarked on a programme of research aimed towards the operation of the Hyper Yag (from now on referred to as a telescopic resonator) with a single transverse TEM_{00} mode and a single-longitudinal mode.

Our first priority was to find out if the telescopic resonator was capable of supporting a large volume TEM_{00} mode with good reliability. In the following investigations it was essential to have a detailed knowledge of the expected spot-sizes at various locations within the cavity. Our early attempts at analysing the cavity in terms of ray-matrices (Kogelnik, 1965; Kogelnik and Li, 1966) were frustrated by the unwieldy form of the results, and we consequently relied on numerical ray-matrix calculations using a digital computer (Clarke, 1980). Using these predictions as a guide, an appropriate aperture size and telescope magnification could be chosen to select a large volume TEM_{00} mode. Interactive use of the computer program and experimental work led to a resonator design suitable for fixed-Q operation which produced an output energy of 350mJ in a diffraction limited beam. Eventually, an analytical approach was developed (Hanna et al., 1981 (two papers); M.A. Yuratich, Private Communication), providing simple, approximate design formulae which agree with exact calculations to the extent that the computer program has been dispensed with. In Chapters Two and Three of this thesis

we present the analysis of the telescopic resonator and the experimental work performed to verify the single transverse mode behaviour of the laser, both when operated fixed-Q and Q-switched.

In Chapter Four we consider the question of linewidth narrowing in pulsed lasers, and in particular the requirements for single-longitudinal mode operation. One finds that the reliability and repeatability of single-mode operation has an ultimate limitation, arising from changes in resonator length from shot to shot, and in the analysis of Chapter Four we derive an expression for the expected reliability of single-mode operation. The chapter ends with a description of the experimental results obtained for single-longitudinal mode operation of the telescopic Nd:YAG laser.

We conclude the thesis in Chapter Five by describing the application of the output from the telescopic resonator to two non-linear optical processes: frequency doubling and Raman scattering. Good agreement is obtained between theoretical prediction and experimental measurement for both these processes.

CHAPTER TWO

TELESCOPIC RESONATORS FOR LARGE VOLUME TEM_{00} MODE OPERATION

Sections 2.1, 2.2 and 2.3 of this chapter, and also Appendix 1, appear as submitted for publication to the Journal of Optical and Quantum Electronics. Minor modifications, such as renumbering of equations and figures, have been made to make its presentation compatible with the rest of this thesis.

The final sections of this chapter are concerned with expanding on several points raised in sections 2.1 to 2.3, but which could not be elaborated on in the paper. We also discuss some important practical points arising as a result of the experimental work performed on the resonator, although detailed discussion of the experimental work is reserved for presentation as Chapter Three.

Abstract to the Paper

A stable resonator incorporating a suitably adjusted telescope gives reliable operation of a Nd:YAG laser with a large volume TEM_{00} mode. The telescope adjustment is chosen to minimise the effects of focal length variations in the laser rod and at the same time ensures the optimum mode-selection properties of a confocal resonator. Simple approximations applied to the ray transfer matrices allow a detailed analysis of the resonator to be performed. This analysis yields simple design equations relating the mode spot-sizes, resonator length, telescope magnification and defocussing, and diffraction losses. Experimental results show excellent agreement with the results of this analysis.

2.1 Introduction

By introducing a suitably adjusted telescope into a Q-switched Nd:YAG laser resonator we have been able to obtain reliable operation with a large volume TEM_{00} mode (Hanna et al., 1981). The basic principle behind the resonator design is that of choosing a telescope adjustment which compensates the thermal lensing in the laser rod (thus permitting a large spot-size) and at the same time ensuring that the spot-size is insensitive to fluctuations in focal length of the

thermal lens. In order to illustrate the principles of the design, the discussion in the above paper was given in terms of a simplified resonator in which the telescope and laser rod were assumed short compared to the overall resonator length and located close to one mirror. In fact, for accurate calculations in practical resonators these assumptions are too restrictive and in this paper we derive the necessary design equations taking into account the finite length of resonator occupied by the laser rod and telescope. However, before introducing the resonator analysis we first briefly review some of the previous approaches to operation of Nd:YAG lasers with high power and low beam divergence.

It has long been appreciated that by compensating the thermal lens induced in solid state laser rods, one can increase the TEM_{00} mode spot-size and thus extract more energy in a diffraction-limited beam (Stickley, 1966). However, it is found that in general this compensation needs to be very precise if the mode size is to be comparable to typical laser rod diameters. Fluctuations in the focal length of this thermal lens (due to pump fluctuations) then lead to large spot-size fluctuations and thus unreliable performance of the laser. Steffen, Lörtscher and Herziger (1972) pointed out this important effect of focal length fluctuations but also showed that stable resonators could be designed which are insensitive to these fluctuations. They referred to these resonators as 'dynamic stable resonators'. In one of their designs the resonator used two plane mirrors with the laser rod close to one mirror and the mirrors spaced by half the focal length of the rod's thermal lens. While this design did permit reproducible operation of a Nd:YAG laser with large volume TEM_{00} mode, it suffered from an inconveniently long resonator. Another design made use of a short radius convex mirror at one end of the resonator. This produces a large spot-size at the other, concave, resonator mirror (the laser rod is located here) and allows a conveniently short resonator to be used. At about the same time Chesler and Maydan (1972) also reported using a convex-concave resonator with a c.w. Nd:YAG laser. In a later paper Lörtscher et al. (1975) gave further details of the performance of their convex-concave resonator and their results amply confirm that it is possible to obtain reliable operation with a large volume TEM_{00} mode (up to 850mJ fixed-Q output was obtained from a pulsed Nd:YAG laser). However, the

disadvantage of the convex-concave resonator is that the spot-size is very small at the convex mirror and this effectively precludes its use in high power Q-switched lasers. Thus Q-switched Nd:YAG lasers continued to be operated with conventional stable resonators which either result in a very multimode output when the full aperture of the laser rod is used or result in a small output energy when apertured down to give TEM_{00} operation.

An important advance was made with the application of unstable resonator techniques to the Q-switched Nd:YAG laser (Herbst et al., 1977) since this allowed the extraction of a large energy in a low divergence beam. The advantages of this were immediately apparent in such applications as harmonic generation. However, the diffraction-coupled output beam from an unstable resonator also has disadvantages associated with its non-uniform intensity profile. (Hanna and Laycock, 1979). These shortcomings have stimulated a search for other means (e.g. Brassart et al., 1977) of producing high output energy in a low divergence beam, but with a smooth intensity profile. Sarkies (1979) reported using a telescope in a Nd:YAG resonator. An attractive feature of the telescope is that it allows easily controllable adjustment to compensate thermal lensing under varied pumping conditions. Although the output of his laser was not TEM_{00}, Sarkies found that a good working compromise could be achieved with high output power and low beam divergence. We undertook our investigation of the telescopic resonator with a view to gaining a fuller understanding of its behaviour and in particular of seeing whether a large volume TEM_{00} mode could be obtained. In the course of our investigation we discovered that Steffen et al. (1972) had suggested a telescopic resonator configuration as one means of realising a dynamic stable resonator. In their publications they make no mention of having used a telescopic resonator and yet it offers two advantages over their convex-concave resonator. These are (i) the easily controllable adjustment mentioned above, and (ii) the fact that it avoids the very small spot on the resonator mirror, and can therefore allow operation at the power levels typical of a Q-switched Nd:YAG laser. There is a third attractive feature, which applies to all dynamic stable resonators, namely that the diffraction losses produced by such resonators are the same as those of an equivalent symmetric *confocal* resonator. This result, which we derive in Appendix 1, has not been referred to in earlier discussions of dynamic stable resonators. However, it has an important

bearing on the problem of TEM_{00} mode selection since it is the confocal geometry that provides the greatest degree of mode selectivity (Li, 1965). This feature, and the two advantages referred to above, have enabled us to obtain Q-switched TEM_{00} outputs of greater than 100mJ from a Nd:YAG laser with excellent reliability and without any damage problems.

2.2 Theory of the Telescopic Resonator

2.2.1 Preliminary remarks

First we write down the standard result (Kogelnik and Li, 1966) for the Gaussian beam spot-sizes w_1 and w_2 at the mirrors 1 and 2 (curvatures R_1 and R_2 respectively) of an empty resonator, as shown in figure 2.1. Expressed in terms of the g parameters, $g_1 = 1 - L/R_1$ and $g_2 = 1 - L/R_2$, we have

$$\frac{\pi w_1^2}{\lambda} = L\left[\frac{g_2}{g_1(1 - g_1g_2)}\right]^{\frac{1}{2}} \qquad 2.1$$

and

$$\frac{\pi w_2^2}{\lambda} = L\left[\frac{g_1}{g_2(1 - g_1g_2)}\right]^{\frac{1}{2}} \qquad 2.2$$

We shall be concerned, in the discussion that follows, with resonators containing a laser medium which exhibits a thermally-induced lensing behaviour, having a focal length f_R. At first we shall assume the laser medium to be adjacent to mirror 2, with the lens f_R incorporated in the curvature R_2. It can be seen from equation 2.2 that the spot-size, w_2, in the laser medium can be made arbitrarily large by appropriate choice of R_1, R_2 and L. For example, with $g_1 = 1$ (i.e. R_1 plane), then as $g_2 \to 1$ so $w_2 \to \infty$. In practice, however, such a choice of parameters leads to a situation in which the spot-size w_2 is extremely sensitive to the value of g_2 and fluctuations in the value of f_R will cause variations of w_2 which are too great to permit reliable selection of the TEM_{00} mode. In fact, it can be shown from equation 2.2 that the fractional change, dw_2/w_2, of spot-size due to a fractional change, dg_2/g_2, is given by

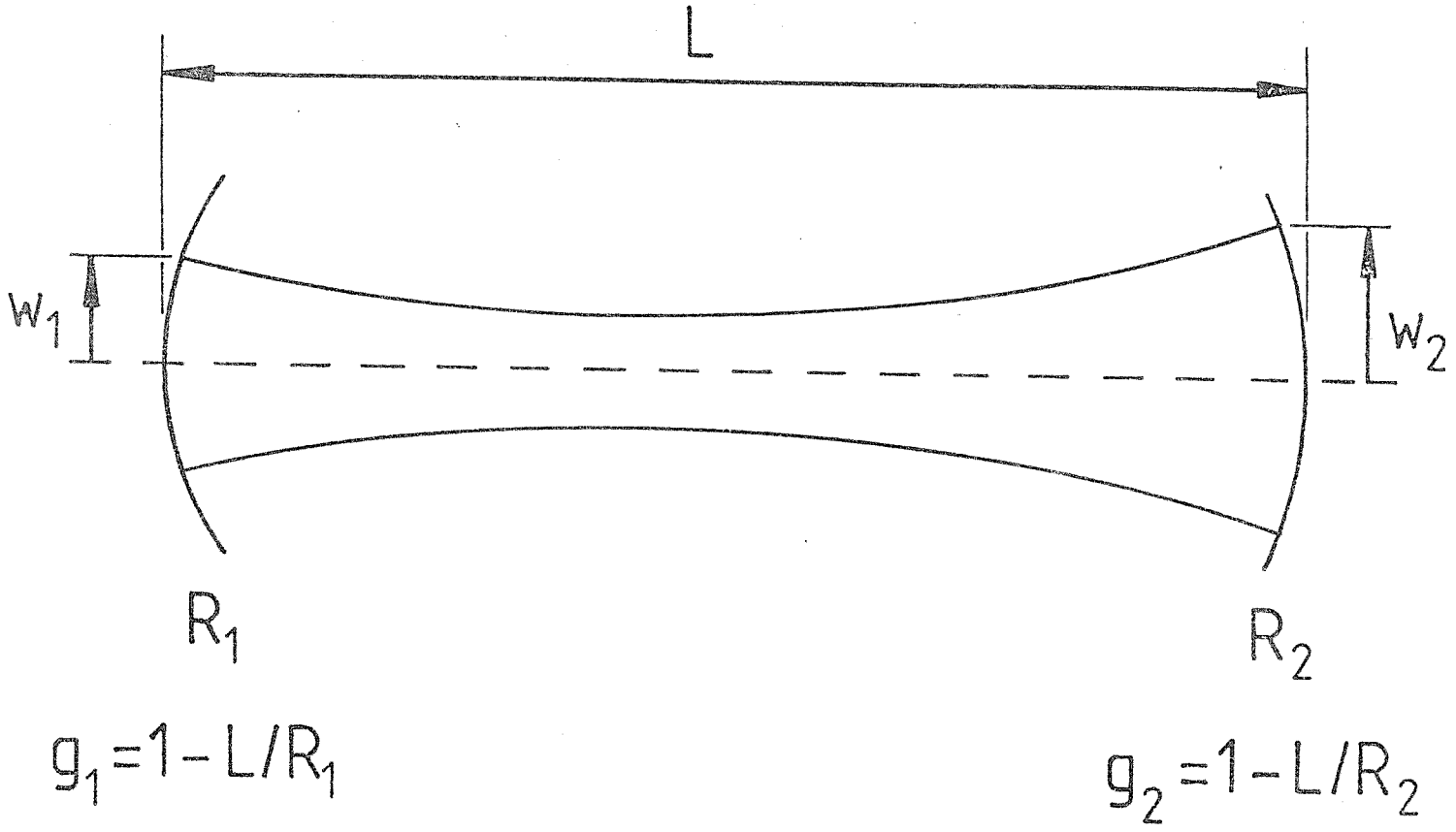

Figure 2.1: Empty resonator

$$\frac{dw_2}{w_2} = \frac{1}{4}\frac{(2g_1g_2 - 1)}{(1 - g_1g_2)}\frac{dg_2}{g_2} \qquad 2.3$$

Thus as $g_1g_2 \to 1$ the spot-size w_2 becomes sensitively dependent on g_2 and hence f_R. However, if one chooses $g_1g_2 = \frac{1}{2}$ then 2.3 shows that spot-size w_2 (but not w_1) becomes insensitive to variations of g_2. This property was first exploited by Steffen et al. (1972) in a resonator having two plane mirrors, with the laser rod close to mirror 2 (thus $g_1 = 1$, $g_2 = 1 - L/f_R$), and the mirror separation, L, given by $L = f_R/2$, hence ensuring $g_1g_2 = \frac{1}{2}$. Substitution of $g_1 = 1$, $g_2 = \frac{1}{2}$ in equations 2.1 and 2.2 gives

$$w_1^2 = \frac{\lambda L}{\pi} \qquad 2.4$$

and

$$w_2^2 = 2\frac{\lambda L}{\pi} = \frac{\lambda f_R}{\pi} \qquad 2.5$$

In this way, if f_R is large, then a large value of w_2 can be obtained (one can always introduce a lens to compensate the thermal lens thus making f_R effectively large). The disadvantage of this approach, however, is that the resonator is inconveniently long. It is worth noting here that this is actually a half-confocal resonator and an aperture placed at one mirror would therefore offer the ideal mode-selectivity characteristic of a confocal resonator (see Appendix I).

Another resonator design, which retains the condition $g_1g_2 = \frac{1}{2}$, but allows a short length L, involves choosing mirror 1 to be a very short radius convex mirror, i.e. R_1 -ve and $|R_1| \ll L$, hence making $g_1 \gg 1$. Thus g_2 is also positive but $g_2 \ll 1$, i.e. R_2 corresponds to a concave reflector ($R_2 > 0$) whose radius of curvature is slightly greater than L. An examination of equations 2.1 and 2.2 shows that $w_1^2 = (g_2/g_1) \cdot w_2^2$ and since $g_1g_2 = \frac{1}{2}$, this gives

$$w_1^2 = \frac{1}{2g_1^2} w_2^2 \,, \qquad 2.6$$

and

$$w_2^2 = \frac{2\lambda L}{\pi} g_1 \qquad 2.7$$

Comparing equations 2.5 and 2.7 it can be seen that a large spot w_2 can be produced in the laser medium (still assumed at mirror 2) with a short L provided g_1 is large. However, equation 2.6 shows that this implies a very small w_1. Thus although this resonator was successfully demonstrated (Steffen et al., 1972; Lörtscher et al., 1975) for a fixed-Q Nd:YAG laser it would be unsuitable for a Q-switched laser.

The telescopic resonator which we now describe provides a compromise between the two resonator designs given above. To compare its performance with these two resonators we anticipate the results of our analysis and quote here the expressions for w_1 and w_2, in the situation where (i) mirror 1 is plane, (ii) the telescope, of magnification M, is assumed short and is placed close to the rod, which itself is at mirror 2, and (iii) the telescope is adjusted to ensure insensitivity of spot-size w_2 to variations of f_R. Our analysis shows that w_1 and w_2 are given by

$$w_1^2 = \frac{L\lambda}{\pi} \qquad 2.8$$

and

$$w_2^2 = 2\frac{L\lambda}{\pi}M^2 \qquad 2.9$$

Thus, compared with the long resonator described by equations 2.4 and 2.5, for the same spot-size w_2, the length of the telescopic resonator can be reduced by M^2, although this makes w_1 smaller by a factor M than the corresponding value in the long resonator. On the other hand, when the telescopic resonator is compared with a convex-concave resonator of the same length and same spot-size w_2, then g_1 in equation 2.7 takes the value M^2 and it follows from equation 2.6 that the spot-size w_1 in the telescopic resonator is M times larger than the spot-size w_1 on the convex mirror.

2.2.2 Derivation of an equivalent resonator for the telescopic resonator

In making these preliminary remarks about the telescopic resonator we chose a simplified resonator as an illustration. In practice, the simplifications made, such as assuming a short telescope

and short laser rod, are too sweeping for accurate calculation. We now consider a telescopic resonator, shown in figure 2.2, for which the simplifying assumptions have been dropped. Both mirrors are assumed curved and the resonator contains a telescope of magnification $M = -f_2/f_1$ and a lens, focal length f_R, representing the laser rod. The length L now refers to the length of that part of the resonator occupied by the contracted beam. The telescope lenses are spaced by $d + \delta$ where $d = f_1 + f_2$ and δ is referred to as the telescope defocussing.† The centre of the laser rod is spaced an optical distance ℓ_2 from the telescope lens f_2, and the mirror R_2 is spaced a further optical distance ℓ_1 from the rod centre.

We shall find it convenient to treat a mirror of curvature R as a plane mirror with an adjacent lens of focal length R in front of it. This approach has the merit of allowing the resonator properties to be calculated in terms of the single-pass ray-transfer matrix elements, where a single pass takes one from the left-hand plane mirror (plane 1) to the right-hand plane mirror (plane 2).

The analysis is aimed at finding simplified expressions for the spot-sizes w_1, w_2 and in particular at finding the value of δ which makes w_2 insensitive to variations of f_R. Our procedure is first to consider the case where mirror 2 is in fact adjacent to the rod, and the rod is short, so $\ell_1 = 0$, and where the rod is in the focal plane of the telescope objective (lens f_2) so $\ell_2 = f_2$. This gives compact and exact results which exhibit the main features of the telescopic resonator. It is then possible to relax the above restrictions, and introduce arbitrary spaces ℓ_2, ℓ_1; the formulae are more complex, and we discuss their approximations.

It is readily shown that the ray matrix of the telescope f_1, $d + \delta$, f_2 is

$$\begin{bmatrix} M - \dfrac{\delta}{f_1} & d + \delta \\ \dfrac{\delta}{f_1 f_2} & \dfrac{1}{M} - \dfrac{\delta}{f_2} \end{bmatrix} \qquad 2.10$$

† Strictly, if the resonator length is to remain fixed as the telescope defocussing is varied, L should be replaced by $L - \delta$. We shall ignore this small correction, however, as it can be shown that it has a negligible effect.

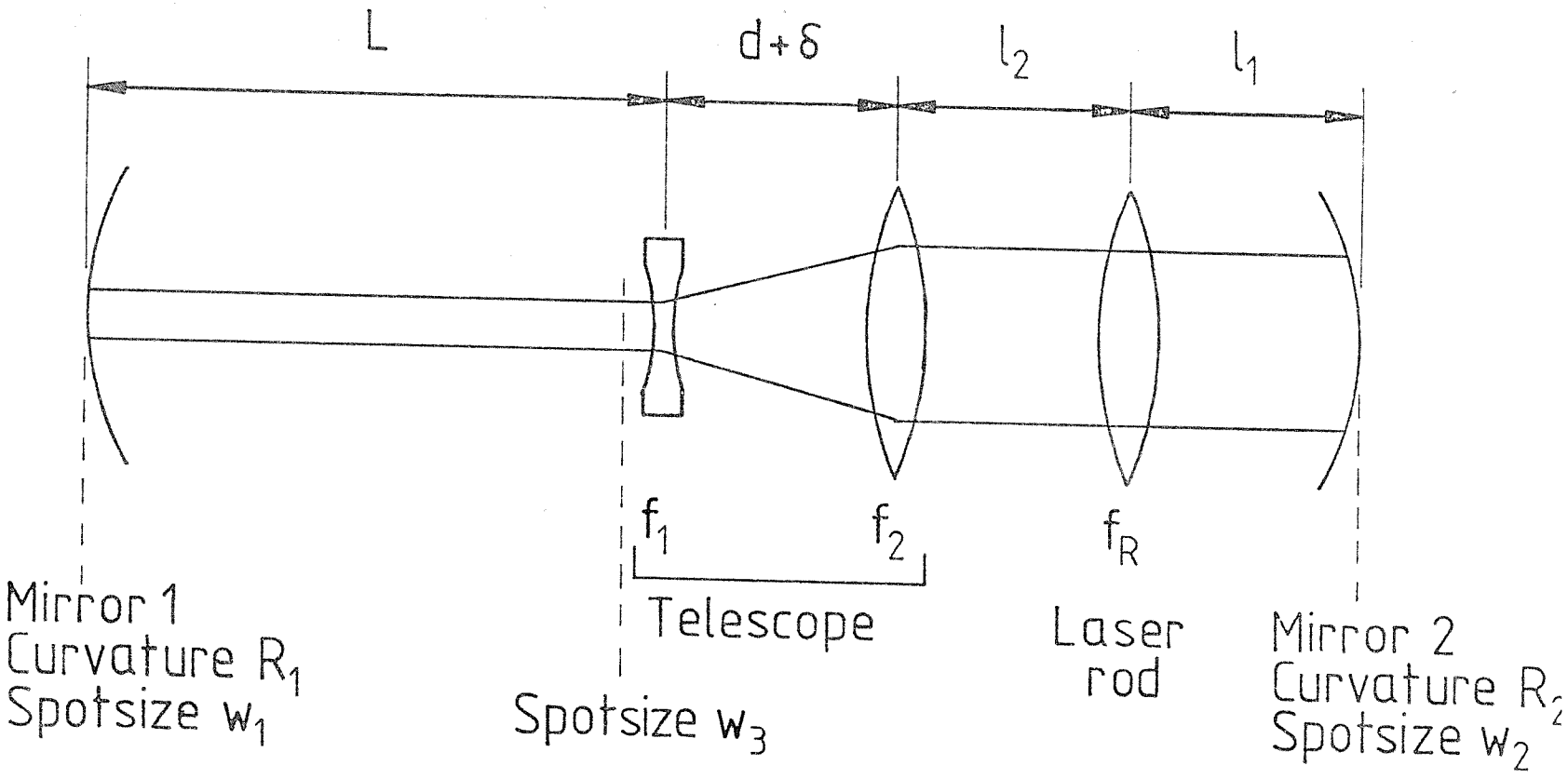

Figure 2.2: The telescopic resonator

This matrix may be factorised *exactly* into a space $-f_1$, a 'thin telescope', a thin lens f_T and a space $-f_2$:

$$\begin{bmatrix} 1 & -f_2 \\ 0 & 1 \end{bmatrix} \cdot \begin{bmatrix} 1 & 0 \\ \frac{-1}{f_T} & 1 \end{bmatrix} \cdot \begin{bmatrix} M & 0 \\ 0 & \frac{1}{M} \end{bmatrix} \cdot \begin{bmatrix} 1 & -f_1 \\ 0 & 1 \end{bmatrix} \qquad 2.11$$

where the ray matrix of the thin telescope is

$$\begin{bmatrix} M & 0 \\ 0 & \frac{1}{M} \end{bmatrix} \qquad 2.12$$

and the thin lens' focal length is

$$\frac{1}{f_T} = \frac{\delta}{f_2^2} \qquad 2.13$$

The effect of the thin telescope is to expand the beam waist by a factor M and to reduce the beam curvature by a factor M, so that there is a beam discontinuity in its plane. Note that the telescope defocussing is described by a single element, the lens f_T. Equation 2.11 provides a key to the telescopic resonator. It shows that the resonator is exactly equivalent to one containing the following sequence of elements; a lens R_1, a space L', where

$$L' = L - f_1 \qquad 2.14$$

the thin telescope, a lens pair f_T, f_R separated by a space $\ell_2 - f_2$, a space ℓ_1 and a lens R_2. By choosing $\ell_2 = f_2$, the lenses f_T and f_R are made adjacent and form a compound lens. Since $1/f_T$ is proportional to δ, the compound lens has an adjustable focal length, which can be used to precisely compensate its rod lens component f_R. By making the further restriction that $\ell_1 = 0$, we have a compound lens of focal length R_2', where

$$\frac{1}{R_2'} = \frac{1}{f_T} + \frac{1}{f_R} + \frac{1}{R_2} \qquad 2.15$$

The restricted resonator with $\ell_2 = f_2$ and $\ell_1 = 0$ is depicted in figure 2.3. Its *exact* single-pass ray matrix is

$$\begin{bmatrix} A & B \\ C & D \end{bmatrix} = \begin{bmatrix} G_1 & ML' \\ -\dfrac{(1 - G_1G_2)}{ML'} & G_2 \end{bmatrix} \qquad 2.16$$

where the G parameters are given by

$$G_1 = M\left[1 - \frac{L'}{R_1}\right] \qquad 2.17(a)$$

$$G_2 = \frac{1}{M}\left[1 - \frac{M^2L'}{R_2'}\right] \qquad 2.17(b)$$

With the help of these equations one can express spot-sizes in either of the commonly used ways, viz. in terms of A, B, C, D, or in terms of G_1, G_2. The latter are particularly convenient for a discussion of resonator stability. The G parameters defined here are a generalisation of the usual parameters g_1, g_2 for an empty resonator, and if we let M = 1, i.e. the telescope is removed, then $G_1 \to g_1 = 1 - L/R_1$ and $G_2 \to g_2 = 1 - L/R_2$.

As shown by Baues (1969) the spot-sizes are given by

$$\frac{\pi w_1^2}{\lambda} = \sqrt{-\frac{BD}{AC}} \qquad 2.18(a)$$

$$\frac{\pi w_2^2}{\lambda} = \sqrt{-\frac{AB}{CD}} \qquad 2.18(b)$$

It is convenient to normalise the spot-sizes to $\lambda L'$, bearing in mind that typically L' is approximately equal to the length L of resonator occupied by the contracted beam.

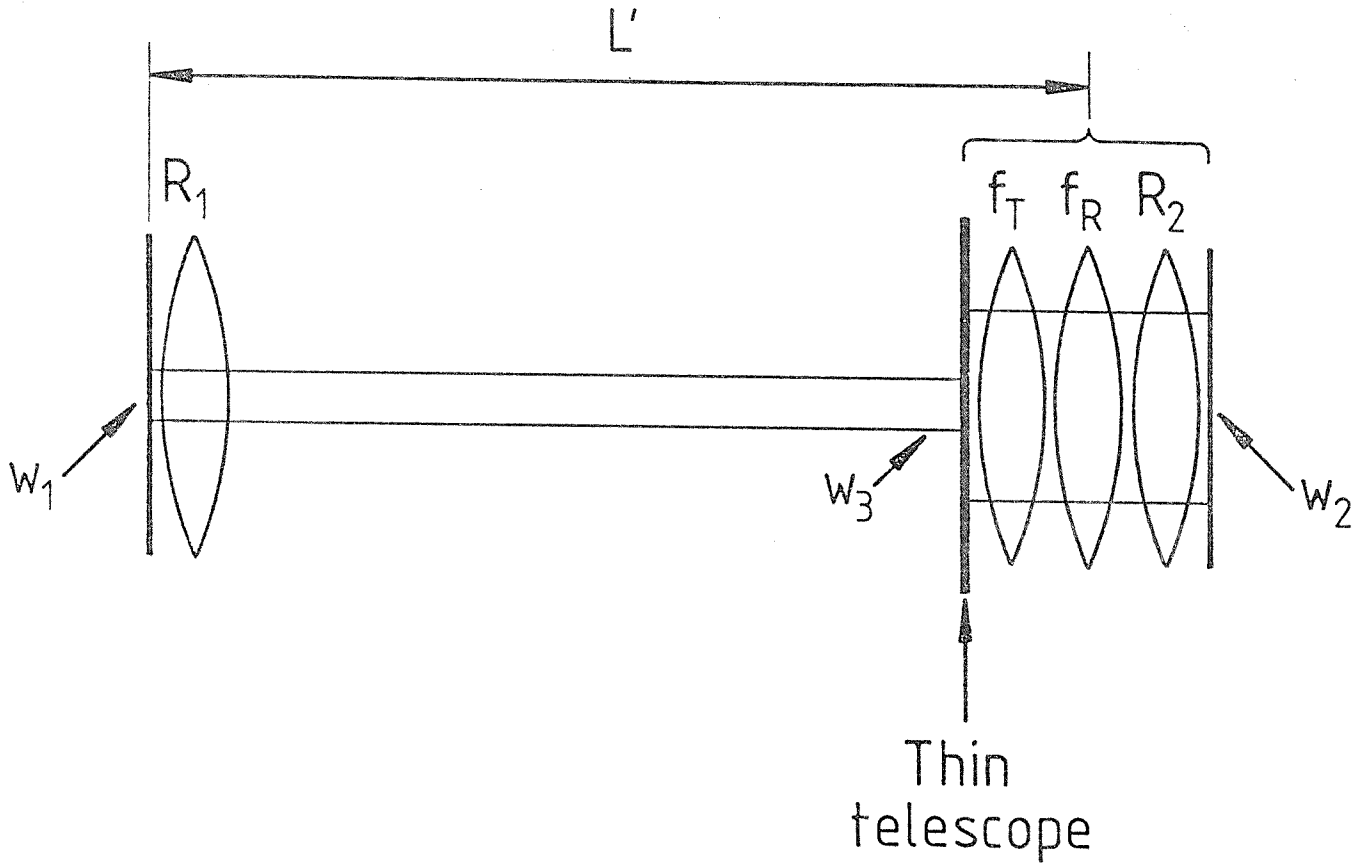

Figure 2.3: Equivalent telescopic resonator with both thin telescope and laser rod located at mirror 2

Thus the normalised spot-sizes W are,

$$W_1 = \left[\frac{\pi w_1^2}{\lambda L'}\right]^{\frac{1}{2}} = \left[\frac{M^2 G_2}{G_1(1 - G_1G_2)}\right]^{\frac{1}{4}} \qquad 2.19(a)$$

$$W_2 = \left[\frac{\pi w_2^2}{\lambda L'}\right]^{\frac{1}{2}} = \left[\frac{M^2 G_1}{G_2(1 - G_1G_2)}\right]^{\frac{1}{4}} \qquad 2.19(b)$$

and at the entrance to the telescope, i.e. at the lens f_1, the spot-size is

$$W_3 = \left[\frac{\pi w_3^2}{\lambda L'}\right]^{\frac{1}{2}} = \frac{W_2}{M} \qquad 2.19(c)$$

Figure 2.4 shows the behaviour of the spot-sizes W_1, W_2, W_3 as a function of G_2 with G_1 and M fixed. From equations 2.15 and 2.17, these curves also represent the dependence of spot-sizes on telescope defocussing δ. A number of important results are indicated in this figure. First we note that the spot-size W_2 is insensitive to variations of G_2 when $G_2 = 1/2G_1$, i.e. when $G_1G_2 = \frac{1}{2}$, and this is therefore the desired operating point. In fact a comparison of equations 2.19(b) with 2.2 is enough to show that the earlier condition $g_1g_2 = \frac{1}{2}$ now becomes $G_1G_2 = \frac{1}{2}$. The spot-sizes W_2, W_3, W_1 for $G_1G_2 = \frac{1}{2}$ are indicated in figure 2.4 as $\sqrt{2MG_1}$, $\sqrt{2G_1/M}$ and $\sqrt{M/G_1}$ respectively. Thus the ratio of spot-sizes, W_2/W_1, is $G_1\sqrt{2}$, an important quantity to bear in mind when considering the question of damage to components in the contracted beam. For the particular case where mirror 1 is plane, G_1 then has the value M and the normalised spot-sizes W_2, W_3, W_1 are $\sqrt{2}M$, $\sqrt{2}$ and 1 respectively, a result previously quoted in equations 2.8 and 2.9. From figure 2.4 it can be seen that the minimum of W_2 is quite flat and from equation 2.19(b) one can show that a 10% change of G_2 about the operating point $G_1G_2 = \frac{1}{2}$ (i.e. G_2 varying from $0.4/G_1$ to $0.6/G_1$) causes only a 1% increase in W_2. The spot-size W_1 does, however, vary and $(dW_1/dG_2)_{G_1G_2 = \frac{1}{2}} = (MG_1)^{1/2}$. The figure also indicates that as one approaches the boundaries of stable operation (at $G_2 = 0$ and $G_1G_2 = 1$) the spot-size W_2 diverges, whereas the spot-size W_1 goes to

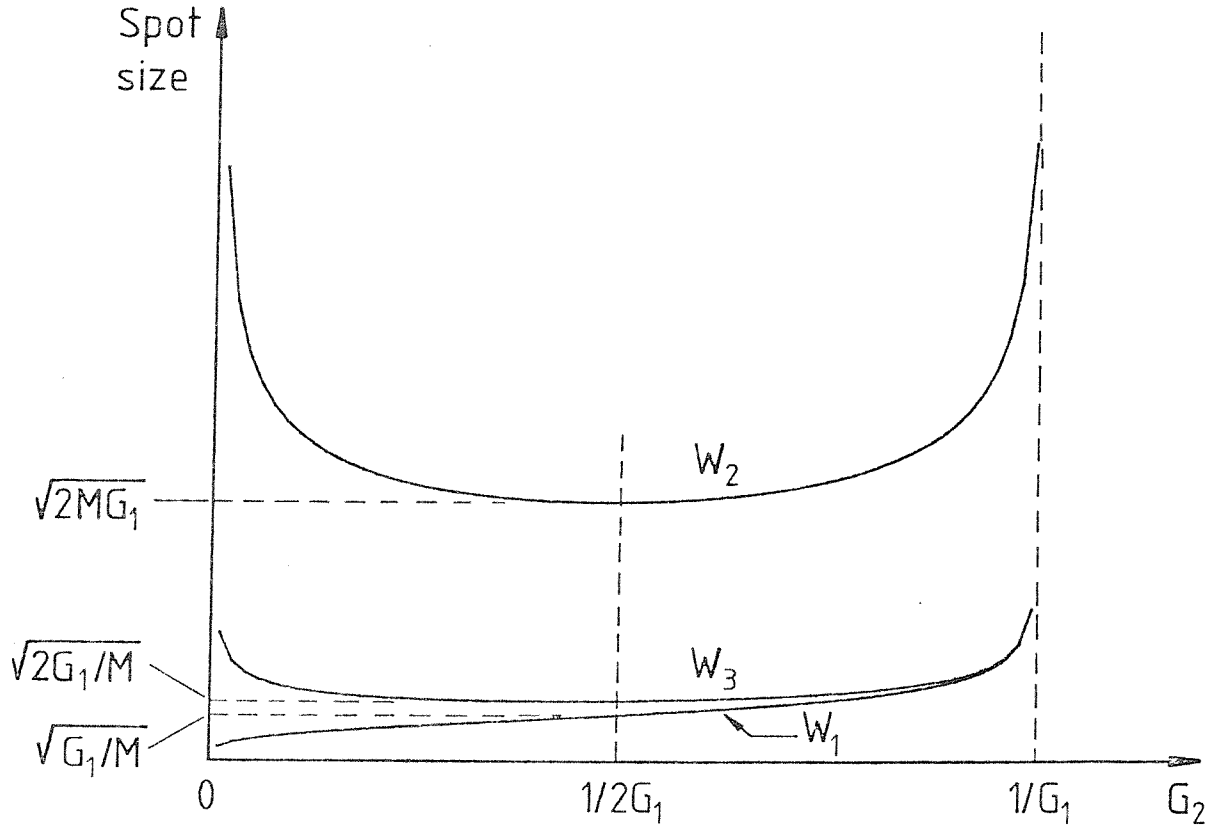

Figure 2.4: Normalised spot-sizes W_1, W_2, W_3 versus G_2 for fixed values of M and G_1

zero as $G_2 \to 0$ and diverges as $G_1G_2 \to 1$. In section 2.2.3 we discuss the choice of δ which optimises G_2 and hence the performance of the telescopic resonator.

The stability behaviour can be illustrated with reference to the G_1G_2 plane, of which the positive quadrant is shown in figure 2.5. The stable region is enclosed by the G_1, G_2 axes and the hyperbola $G_1G_2 = 1$. The locus of ideal adjustment $G_1G_2 = \frac{1}{2}$ is also a hyperbola, passing essentially through the centre of the stable region. An empty resonator with mirror 1 plane ($G_1 = 1$) and mirror 2 concave with $R_2 > L$ (hence $G_2 > 0$) is represented by a point on the line PQ. The point U represents the half confocal resonator, Q the plane-plane resonator. If a thin telescope of magnification M is inserted adjacent to mirror 2 in the resonators represented by the line PQ, they will then be represented by points on the line RS, with the point S corresponding to the plane-plane resonator and the point V corresponding to the ideal operating point. As the magnification M is increased, so the range of values of G_2 for stable operation is decreased.

Having discussed the properties of the telescopic resonator with the particular choice $\ell_2 = f_2$ and $\ell_1 = 0$, we now consider arbitrary spacings. Whereas the first case allowed us to derive exact and compact expressions, in the case of arbitrary spacings the exact expressions are very cumbersome. Exact results can, of course, be obtained on a computer, but our aim here is to show that in fact the expressions derived above remain quite adequate for practical spacings.

Any ray matrix can be put into the form of equation 2.16, and with appropriate parameters G_1', G_2', L'' say, all the discussion relating to figure 2.4 and equations 2.18 and 2.19 for the spot-sizes still applies. However, the expressions for G_1', G_2', L'' (and hence A, B, C, D) in terms of the physical resonator parameters will now differ from the G_1, G_2, L' of equations 2.14, 2.17. From 2.18 it is seen that the spot-sizes vary as $B^{\frac{1}{4}}$, and so any small error in B will be insignificant. On the other hand, the spot-sizes vary as $1/C^{\frac{1}{4}}$ and $1/D^{\frac{1}{4}}$, and so errors in C or D will have a large effect on the spot-sizes, since the limits of the stable region are defined by $C = 0$ and $D = 0$. We conclude that when making approximations, C and D need more care than B; A can be regarded as a derived parameter since $AD - BC = 1$.

Consider first the case where $\ell_2 \neq f_2$. The matrix elements are readily determined, and may be put into the form

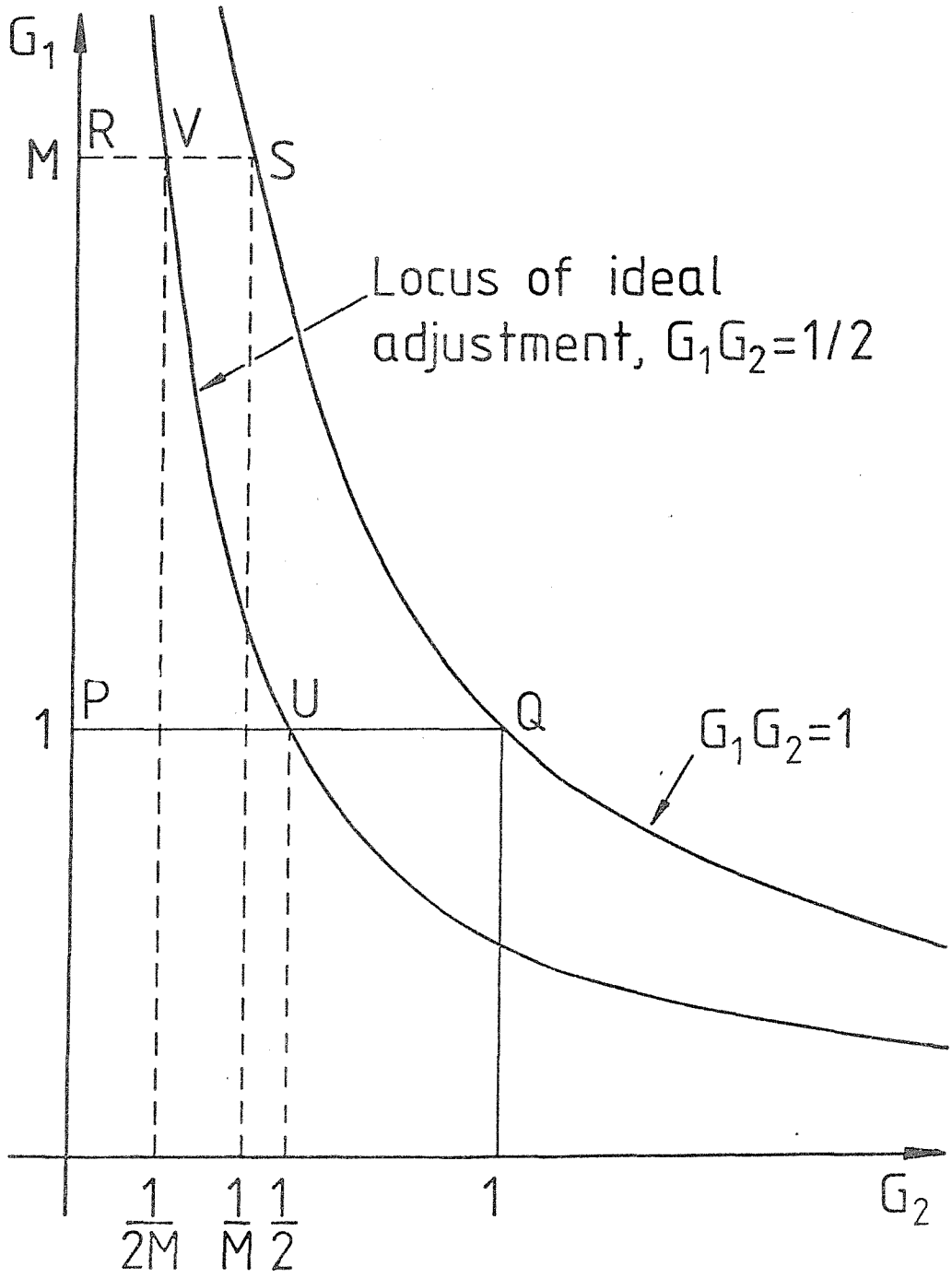

Figure 2.5: Stability diagram. The line PQ represents stable empty resonators with mirror 1 plane ($G_1 = 1$). The line RS represents stable resonators with thin telescope adjacent to mirror 2, and mirror 1 plane ($G_1 = M$)

$$A = M\left(1 - \frac{\Delta}{f_T}\right)\left[1 - \frac{L'}{R_1}\left(1 + \frac{\Delta}{M^2L'\left(1 - \frac{\Delta}{f_T}\right)}\right)\right] \qquad 2.20(a)$$

$$B = ML'\left(1 - \frac{\Delta}{f_T}\right)\left[1 + \frac{\Delta}{M^2L'\left(1 - \frac{\Delta}{f_T}\right)}\right] \qquad 2.20(b)$$

$$C = -\frac{1}{ML'}\left(1 - \frac{\Delta}{f}\right)\left[1 - M\left(1 - \frac{L'}{R_1}\right)\left(\frac{1}{M} - \frac{ML'}{R_2''}\right)\right] \qquad 2.20(c)$$

$$D = \frac{1}{M}\left(1 - \frac{\Delta}{f}\right)\left(1 - \frac{M^2L'}{R_2''}\right) \qquad 2.20(d)$$

where

$$\Delta = \ell_2 - f_2 \qquad 2.21(a)$$

$$\frac{1}{f} = \frac{1}{f_R} + \frac{1}{R_2} \qquad 2.21(b)$$

$$\frac{1}{R_2''} = \frac{1}{f_T} + \frac{1}{f - \Delta} \qquad 2.21(c)$$

In practice,

$$|\Delta| << |f|, |f_T|, M^2L' \qquad 2.22$$

or can be made so by design. Thus the term Δ/f can be dropped from equation 2.20(d), giving

$$D = G_2' \simeq \frac{1}{M}\left(1 - \frac{M^2L'}{R_2''}\right) \qquad 2.23(a)$$

Note that the limit of the stable region defined by D = 0 is still an *exact* function of R_2'', and hence of the defocussing δ. Turning to equation 2.20(c), then with G_2' defined by equation 2.23(a) and by comparison with element C in equation 2.16 it is seen that a suitable choice of G_1', and hence of A, is

$$A = G_1' \simeq M\left(1 - \frac{L'}{R_1}\right) \qquad 2.23(b)$$

As with D, this choice gives the zero of element C *exactly*. B can be approximated by dropping the terms Δ/f_T and $\Delta/M^2L'(1 - \Delta/f_T)$, giving

$$B \simeq ML', \; L'' = L' \qquad 2.23(c)$$

(It is seen that we have effectively approximated A in the same way as B.) To summarise, we have found that by making the assumptions in equation 2.22, then our earlier treatment of the telescopic resonator comes through with the one change, of R_2' to R_2''. Moreover, as $|\Delta| \ll |f|$ from equation 2.22, then we can generally ignore the change, and use the original equations 2.15 to 2.17.

Figure 2.6(a) shows the actual resonator lenses f_T, f_R, R_2 and their spacings Δ, ℓ_1. Figures 2.6(b) and (c) respectively depict the special case $\Delta = \ell_1 = 0$ treated earlier, and the case $\Delta \neq 0$, $\ell_1 = 0$ just examined. The last case we wish to examine, $\Delta = 0$, $\ell_1 \neq 0$, is shown in figure 2.6(d). By comparing with figure 2.6(c) it is apparent that the expressions 2.20 can again be used, but with the changes $1/f_T \to 1/f_T + 1/f_R$, $\Delta \to \ell_1$, and $1/f \to 1/R_2$. The inequalities corresponding to equation 2.22 are $\ell_1 \ll |R_2|, \; |1/f_T + 1/f_R|^{-1}, \; M^2L'$, and which again are satisfied in practice. Hence the only change from the first expressions 2.15 to 2.17 is that R_2' is replaced by R_2'', where

$$\frac{1}{R_2''} = \frac{1}{f_T} + \frac{1}{f_R} + \frac{1}{R_2 - \ell_1} \qquad 2.24$$

Again ℓ_1 can often be omitted, for example in the instance where mirror 2 is plane. However, whereas Δ is the difference of two comparable lengths, $\Delta = \ell_2 - f_2$, and so always tends to be small, ℓ_1 may give a

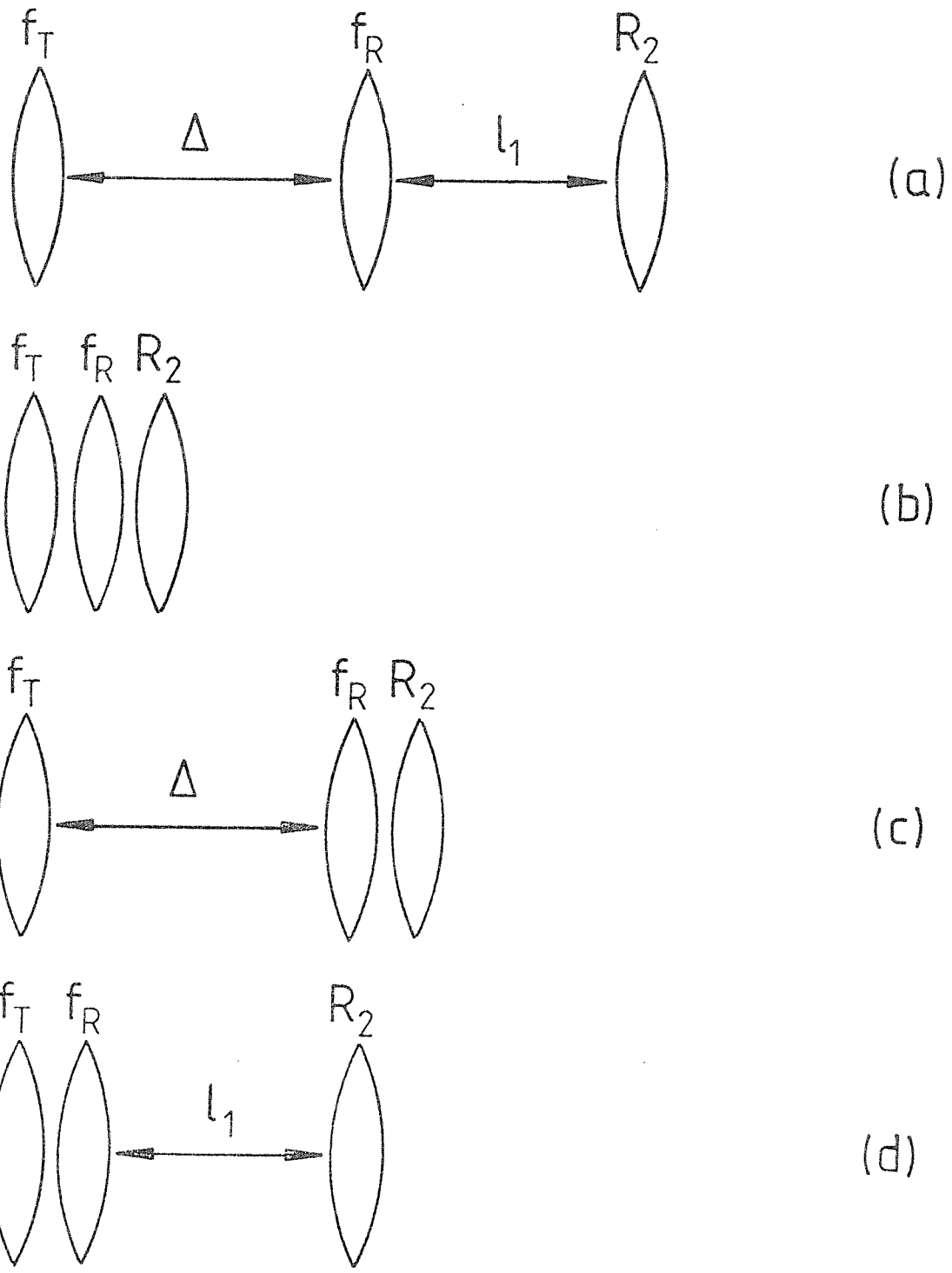

Figure 2.6: Various cases of resonator lens combinations

significant correction in equation 2.24, and hence to the predicted defocussing δ in f_T.

2.2.3 Choice of resonator parameters and telescope defocussing

In the previous section we have shown that the telescopic resonator can be characterised by the values G_1, G_2 of its equivalent resonator containing a thin telescope. We concluded that the telescopic resonator should be adjusted so that its equivalent resonator satisfies the condition $G_1G_2 = \frac{1}{2}$. This can be achieved by adjusting the telescope defocussing δ, since this determines f_T (through equation 2.13), hence R_2' (through equation 2.15) and finally G_2 (through equation 2.17(b)). Thus with G_1G_2 put equal to $\frac{1}{2}$ we find that δ_{opt} is given by

$$\delta_{opt} = f_2^2 \left[\frac{1}{M^2 L'} \left(1 - \frac{M}{2G_1} \right) - \frac{1}{f_R} - \frac{1}{R_2} \right]$$

$$= f_2^2 \left[\frac{1}{2M^2 L'} \left(\frac{1 - 2\frac{L'}{R_1}}{1 - \frac{L'}{R_1}} \right) - \frac{1}{f_R} - \frac{1}{R_2} \right] \qquad 2.25$$

Once the resonator parameters M, f_2, L, R_1, R_2 have been chosen and f_R is known, then δ_{opt} can be calculated from equation 2.25. The value of f_R depends on the operating conditions (repetition rate and pump energy) and provided its dependence is known, one can then calculate the necessary change of δ_{opt} for changed operating conditions. The effect of a change in f_R is to change R_2' and hence G_2. This simply translates the curves in figure 2.4 parallel to the G_2 axis. A change of δ has exactly the same effect since it changes f_T and hence R_2'. Thus the curves of figure 2.4 also indicate the dependence of spot-sizes on telescope defocussing. This behaviour provides an experimental means of identifying whether one is operating at the optimum point. As G_1G_2 is made to depart from its optimum value by changing the telescope defocussing it is found that the laser output energy drops and the beam quality degrades. This drop in performance shows a symmetric behaviour on either side of the optimum so that, for example, a plot of output energy versus δ will exhibit a rather flat maximum and thus can be used to locate δ_{opt} roughly. Fine adjustment of δ is usually then required

for final optimisation of performance.

We have indicated how δ_{opt} can be calculated once the resonator parameters are chosen. We now consider some of the factors that influence the choice of these parameters. Obviously one cannot give here an all-embracing strategy for the optimum selection of these parameters since they are influenced by the operating conditions of the laser. For example, if the laser is Q-switched then it is likely that damage limitations of components in the contracted beam will be a major factor in deciding the energy to be extracted. This influences the choice of spot diameter in the laser rod. Under fixed-Q conditions quite different considerations apply and the maximum spot-size in the laser rod may then be determined by inhomogeneities caused by thermally-induced birefringence (Koechner, 1976). If damage is the main limitation then one must seek a compromise between the convenience of a short resonator with its greater risk of damage and the inconvenience of a long resonator. This choice can be illustrated most clearly by considering a resonator with mirror 1 plane ($G_1 = M$, and, since $G_1G_2 = \frac{1}{2}$, then $G_2 = 1/2M$) for which equations 2.19(a) and 2.19(b) yield

$$w_1^2 = \frac{L'\lambda}{\pi} \qquad 2.26$$

$$w_2^2 = \frac{2L'\lambda M^2}{\pi} \qquad 2.27$$

Equation 2.27 shows that for a given w_2, the smaller one makes L' (by choosing a larger M), the smaller is w_1. This increases the risk of damage due to the higher energy density and also, since the resonator is shorter, due to the shorter pulse duration. The damage limitations of dielectric coatings have led us to use an uncoated plane parallel plate of fused silica as the reflector for the contracted beam and this then serves as the output mirror.

The laser used in our experiments has a 75mm x 9mm Nd:YAG rod pumped by twin flash-lamps. We have operated this laser with TEM_{00} spot diameters ($2w_2$) up to 5mm and it is likely that at repetition rates of less than 10Hz, where thermally-induced birefringence effects remain small (Koechner, 1976), even larger spot-sizes would be feasible. A typical set of resonator parameters that we have used for most of our work are as follows:- L = 0.34m, M = 4, f_1 =-0.05m (hence f_2 = 0.20m and

d = 0.15m), ℓ_2 = 0.25m, ℓ_1 = 0.51m. Hence L' = 0.39m (from equation 2.14), w_1 = 0.36mm (from equation 2.26), w_2 = 2.1 mm (from equation 2.27). The overall optical length of the resonator was 1.25m and when the output energy E was ∿100mJ the pulse duration τ was measured to be 30ns (FWHM). The peak intensity at the resonant reflector is then $2E/\pi w_1^2\tau = 2E/\lambda\tau L'$, which for our parameters gave a value of 1.6Gw/cm^2. This is to be compared with values for the damage threshold of spectrosil B, when subjected to 10ns pulses of 1.06μm radiation, viz. 5Gw/cm^2 (R. Wood, Private Communication). The spot-size w_3 at the small lens of the telescope is, according to equation 2.19(c), $\sqrt{2}$ greater than w_1. We have found that AR coatings on this lens are liable to damage and an uncoated lens of BK7 is therefore used. Apart from the use of uncoated optics in the contracted beam we have not made any serious attempt to optimise the damage threshold. Our laser has been operated with the resonator parameters listed above, producing Q-switched outputs of ∿100mJ for ∿10^6 shots so far with no sign of damage.† To optimise the damage threshold one would need to examine the various trade-offs, such as increasing the resonator length, decreasing the magnification, etc., and equations 2.19(a) and 2.19(b) provide the basis on which to carry out this optimisation analytically. The simplicity of the design equations 2.13 to 2.19 and 2.25 makes their use very straightforward.

For the exact calculation of spot-sizes one needs to know f_R. Using a He-Ne laser we have measured the mean focal length of the laser rod for various average pump input powers P and find that the focal length (in metres) is given by $f_R = 2.7/P(kw)$. We have assumed that this measured value of focal length corresponds to the actual value which prevails at the time when laser oscillation occurs. Thus we assume that transient focal length variations during pumping, such as observed by Baldwin and Riedel (1967), are small compared to the mean focal length. This assumption appears to be valid for our operating conditions since the observed changes of δ_{opt} (i.e. the necessary telescope readjustment) for given changes of pump power P were found to agree with those predicted by equation 2.25 with $f_R(m)$ put equal to 2.7/P(kw) and both $1/R_1$ and $1/R_2$ put equal to zero, i.e.

---

†In deliberate attempts to induce damage we found that a small damage speck could be produced on the spectrosil flat when the laser output energy reached 150 to 170mJ.

$$\delta_{opt} = f_2^2 \left(\frac{1}{2M^2 L'} - \frac{1}{f_R} \right) \qquad 2.28$$

This equation therefore provides a very simple prescription for change of telescope adjustment with change in average pump power. Typically we have operated the laser with a modest repetition rate ($\sim$8Hz) and $f_R \sim 7$m. It should be noted that under conditions involving a high average output power from the laser (such as where a high repetition rate is used) it is possible for the Pockels cell to contribute a noticeable negative lensing due to absorption of the laser radiation. This was noticed by observing that δ_{opt} shifted in value when the Pockels cell was added to the resonator (between the laser rod and mirror 2) while it was operating under fixed-Q conditions with 350mJ TEM_{00} output at 18Hz repetition rate. The effects of such a lens, of focal length f_p, can be included in the foregoing analysis simply by adding $1/f_p$ to the term $1/f_R$ in equations 2.15, 2.25 and 2.28. From the observed shift of δ_{opt}, the value of f_p was estimated from equation 2.28 as -20m. This is consistent with the value calculated (following J.P. Gordon et al., 1965) by assuming an absorption coefficient in the KD^+P Pockels cell corresponding to 95% deuteration (R. Wood, Private Communication). However, under our typical operating conditions (100mJ output at 8Hz) the Pockels cell lensing was not significant.

We conclude this section by showing, in figure 2.7, the calculated spot-sizes w_1, w_2, w_3 versus telescope defocussing δ for the typical set of resonator parameters quoted earlier. The calculations have been made in two ways, (i) using exact ray-transfer matrices throughout, shown as solid curves in figure 2.7, and (ii) using equations 2.14 to 2.19, shown as dotted curves. The excellent degree of accuracy obtainable from the approximate equations is apparent.

2.3 Choice of Mode-Selecting Aperture

The TEM_{00} mode is selected by means of a circular aperture which is accurately centred onto the laser axis by micrometer adjustment. One can in principle use an aperture either in the contracted or expanded beam (provided the aperture size is appropriate, see Appendix I), but we have chosen the latter for two reasons, (i) for convenience, since the larger aperture is less liable to damage, (ii) the resonator

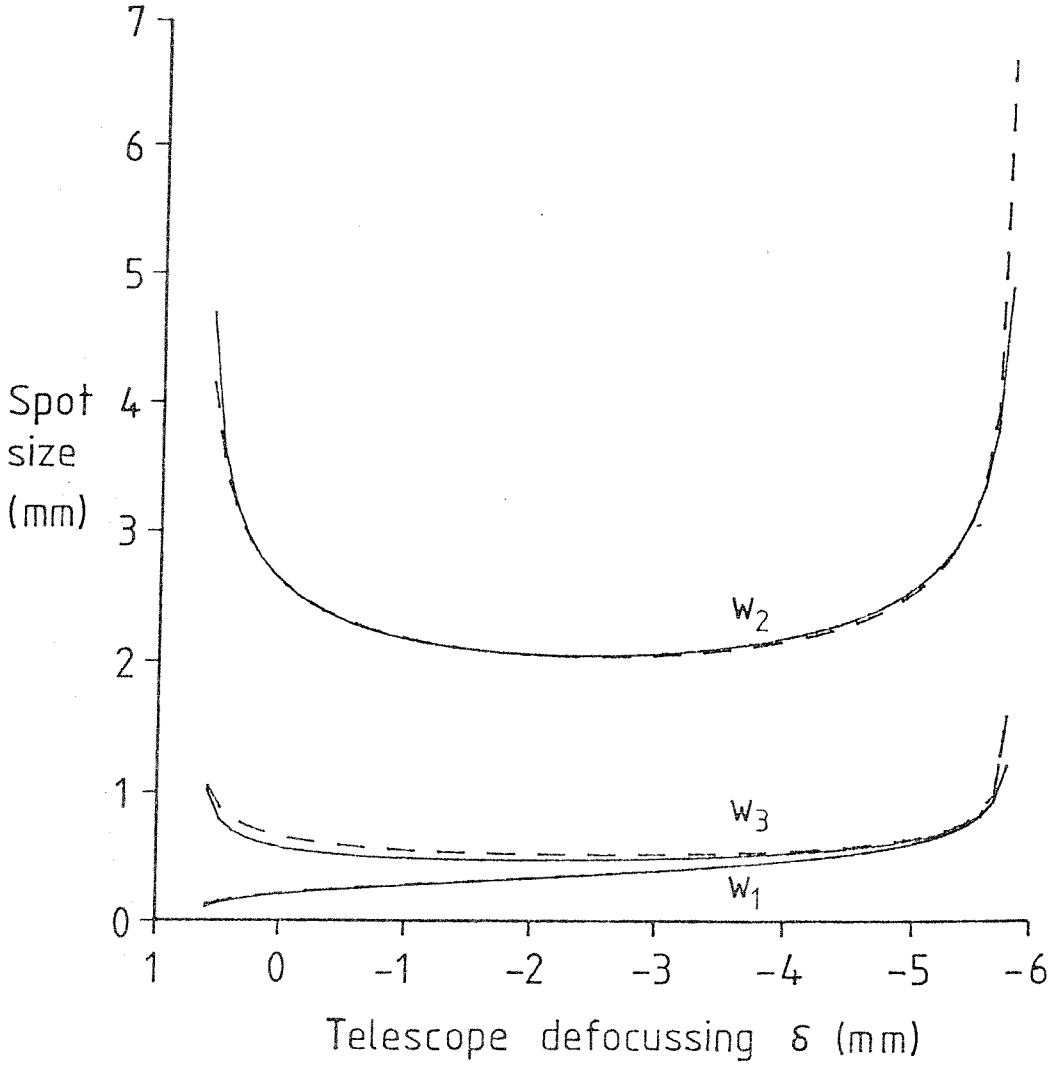

Figure 2.7: Calculated spot-sizes versus telescope defocussing for the typical resonator parameters indicated in the text. The solid curves were obtained using exact ray transfer matrices throughout and the dotted curves using the approximate equations 2.14 to 2.19.

is designed to minimise variations in spot-size of the expanded, but not of the contracted, beam.

The aperture introduces round trip diffraction losses L_{00} and L_{10} respectively for the TEM_{00} and TEM_{10} modes. The degree of mode-selection (i.e. ratio of TEM_{00} power to TEM_{10} power) resulting from q round trips is thus given by $(1 - L_{00}/1 - L_{10})^q$. The losses L_{00} and L_{10} can be found exactly using the results of Li (1965) provided the aperture (which is assumed to be the dominant cause of diffraction loss) is located at a resonator mirror. First, however, we consider a rough estimate of loss which can be made by calculating that fraction of the power in the Gaussian beam (spot-size w) intercepted by an aperture of diameter 2a. For a TEM_{00} mode this is given by (see e.g. Casperson and Lunnam, 1975)

$$L_{00} = e^{-2a^2/w^2} \qquad 2.29$$

and for a TEM_{10} mode,

$$L_{10} = \left(1 + \frac{2a^2}{w^2}\right) e^{-2a^2/w^2} \qquad 2.30$$

Like Lörtscher et al. (1975) we have used an aperture size such that a is nominally equal to 1.5w, thus giving $L_{00} = 0.011$ and $L_{10} = 0.061$, according to equations 2.29 and 2.30. If one considers a typical Q-switched Nd:YAG laser where q may be $\sim$35, the above values of loss would then imply, $(1 - L_{00}/1 - L_{10})^q \simeq 6$. One thing that is apparent from this calculation is that the degree of mode selection is sensitively dependent on the values of L_{00} and L_{10}. In Appendix I we show how an exact calculation of L_{00} and L_{10} can be made, using an equivalence relation between the actual resonator used and a symmetric resonator for which exact diffraction loss calculations have been performed (Li, 1965). The result from the Appendix is quoted here, viz. that a round trip of the telescopic resonator, starting from the aperture (diameter 2a, located at mirror 2 in the expanded beam) produces the same diffraction loss as a single-pass through a *confocal* symmetric resonator of Fresnel number $a^2/ 2\lambda M^2 L'(1 - L'/R_1)$, where $L' = L - f_1$, (equation 2.14). Li (1965) has shown that the confocal geometry provides the greatest mode selectivity, and it is a useful feature of the telescopic resonator that it is able to exploit this property. From Li's paper (his figure 8) one can see that for a TEM_{00}

loss of 0.01, the TEM_{10} loss is 0.12, thus giving a value for $(1 - L_{00}/1 - L_{10})^q$ of $\sim$60 for q = 35.

Despite this large selectivity it must be borne in mind that the mode-selection is a sensitive function of L_{00} and L_{10}, and hence of aperture size. It is therefore advisable, in selecting the aperture size, to have available a range of closely spaced aperture sizes so that one can find in practice which gives the most satisfactory performance. Using the parameters already quoted for our resonator and the aperture diameter 2a = 6.25mm, the above expression for Fresnel number yields the value 0.74. With this Fresnel number, Li's calculations give round trip losses for our resonator of L_{00} = 0.008, L_{10} = 0.10, thus giving a generous degree of mode-selection over the 35 or so round trips when Q-switched. The very small diffraction loss for the TEM_{00} mode suggests that little or no diffraction ring structure would be visible in the output beam since the mode is only very slightly truncated. This is indeed the case and figure 2.8 shows a sequence of burn patterns on photographic film. These were taken at 4m from the output resonant reflector. Figure 2.9 shows the TEM_{00} mode intensity profile as observed on a diode array, confirming the smooth, structureless profile indicated by the burn patterns. Spot-sizes measured using the diode array agree within experimental accuracy with TEM_{00} spot-sizes predicted by our analysis.

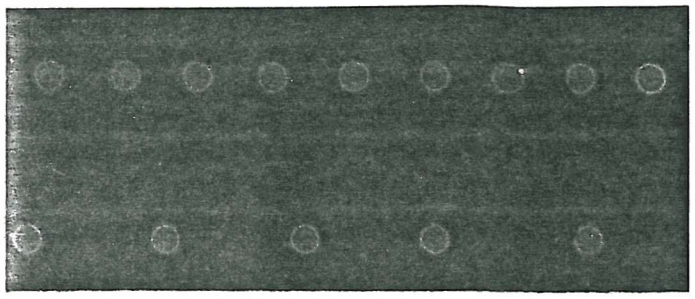

Figure 2.8: Sequence of burns on photographic paper. These were taken at 4m from the resonant reflector, at an output energy of ∿100mJ, and a repetition rate of 8Hz

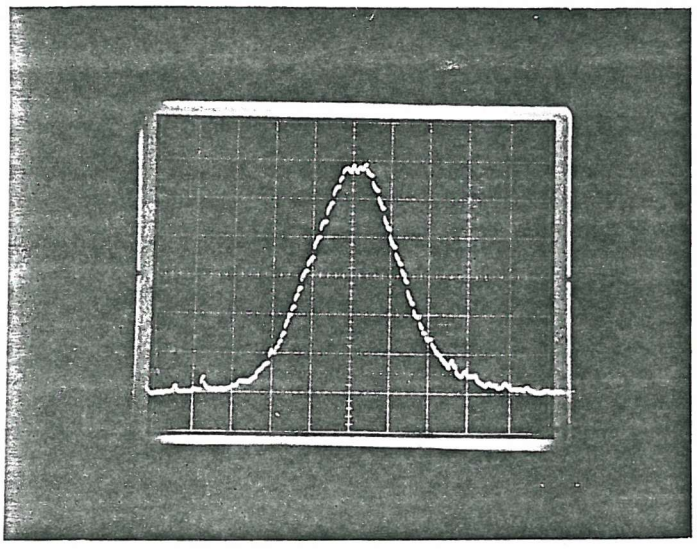

Figure 2.9: Beam profile as monitored by a diode array

2.4 Thermal Lensing of the Pockels Cell Q-Switch

It was noted in section 2.2.3 that the Pockels cell can contribute an additional negative lens to the cavity as a result of absorption of the laser radiation. This effect modifies the optimum telescope defocussing, δ_{opt}, via equation 2.25.

This lensing effect was noticed early in the experimental programme on the telescopic resonator as a result of the cavity alignment procedure being used at that time. Satisfactory results as regards beam divergence and profile had been obtained with the laser operating fixed-Q with an output energy of 350mJ without a Pockels cell in the cavity. The Pockels cell was then introduced into the resonator and the laser operated without any voltage applied to the cell. A degraded beam profile (assessed by visual inspection of burn patterns taken on blackened photographic paper) was observed. This led us to believe that the Pockels cell was acting like a lens, with the result that the telescope spacing was no longer optimised. However, use of a Mach-Zehnder interferometer indicated that the cell crystal faces were polished plane parallel to better than $\lambda/8$ at 1.06μm, so we concluded that the lensing effect was induced as a result of absorption of the laser radiation. The resonator configuration used to confirm this is illustrated in figure 2.10. The cavity is formed by a 5m radius 100% reflectivity mirror, and a plane 30% reflectivity mirror which served as the output coupler. A 7.5mm diameter aperture was used to restrict oscillation to the TEM_{00} mode when the resonator was in optimum adjustment. The pump energy was 42J and the repetition rate was 17.5Hz. The laser output energy was measured as a function of telescope lens spacing for the two cases:

(1) with the Pockels cell present, and

(2) with the Pockels cell removed from the cavity.

For each telescope setting the 5m radius mirror was adjusted to re-optimise the cavity for maximum output. For convenience, the output energy was measured using a J.K. Lasers energy monitor. This instrument is only in

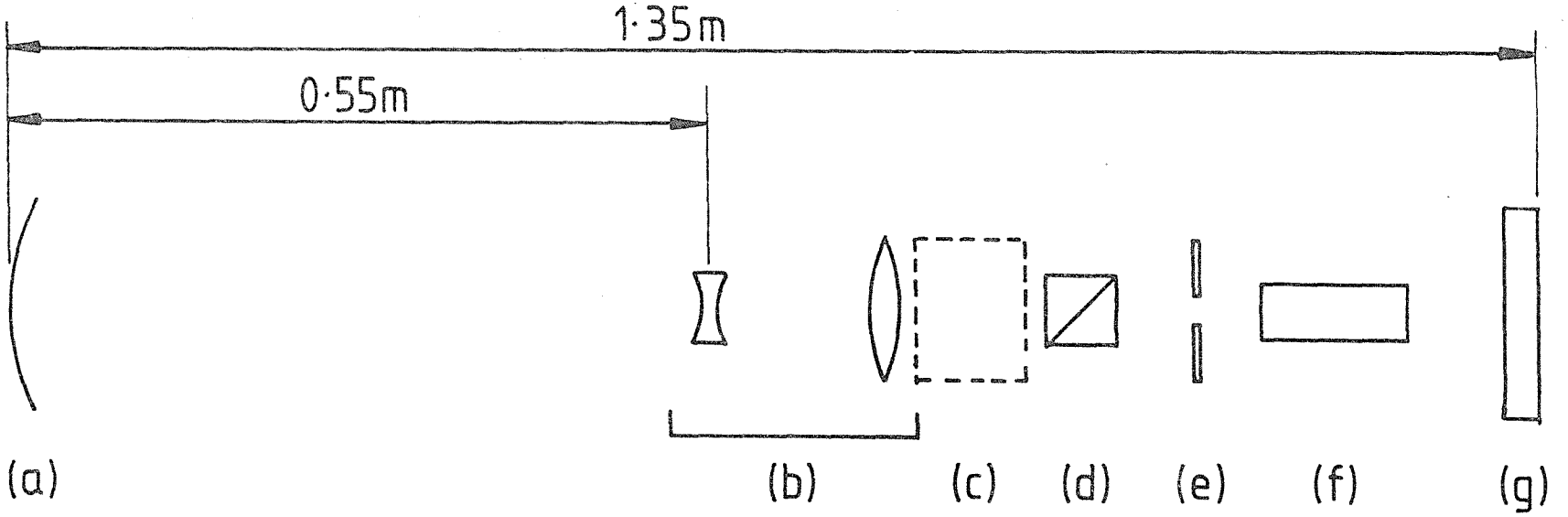

(a) Mirror. 5m radius, 100% reflectivity
(b) Telescope. Magnification = 4
(c) Position of Pockels cell.
(d) Dielectric polariser.
(e) Aperture. 7·5mm dia.
(f) Laser rod.
(g) Mirror. Plane, 30% reflectivity.

Figure 2.10: The fixed-Q telescopic resonator used to measure the shift in optimum telescope lens spacing as a result of thermal lensing in the Pockels cell. The focal lengths of the telescope lenses were +20cm and -5cm

rough calibration, and consequently the results, illustrated in figure 2.11, are normalised, in each case, to the maximum output energy. Figure 2.12 shows the corresponding burn patterns taken ∿30cm from the output coupler, and in conjunction with figure 2.11 clearly shows a shift of ∿+2mm in the optimum telescope lens spacing.

One can easily show from equation 2.25 that the change in optimum telescope lens spacing, $\Delta\delta_{opt}$, caused by the addition of a Pockels cell of focal length f_p, is given by

$$\Delta\delta_{opt} = -\frac{f_2^2}{f_p} \qquad 2.31$$

For our set-up we have $\Delta\delta_{opt}$ = 2mm, f_2 = 20cm, giving f_p = -20m.

An analysis of the thermal lensing exhibited by absorbing elements in a laser beam has been performed by Gordon et al. (1965). They derive the following expression for focal length, f, of an absorbing sample when placed in a Gaussian laser beam of average power P, and spot-size w, using the simplifying assumption that the change in refractive index of the sample is parabolic with radial distance from the beam axis.

$$f = \frac{kn\pi w^2}{\alpha P \ell \frac{dn}{dT}} \qquad 2.32$$

In equation 2.32 k is the thermal conductivity, n is the refractive index, α is the absorption coefficient and ℓ is the length of the sample. This expression is valid provided two conditions are met: (i) that only changes in refractive index contribute to the focussing effect, i.e. that changes in the physical dimensions of the sample have no effect; (ii) that the time between laser pulses is much less than a characteristic thermal relaxation time constant given by

$$t_c = \frac{w^2}{4D} \qquad 2.33$$

where $D = k/\rho C_p$ is the thermal diffusivity of the sample, ρ is the density and C_p the specific heat. Using w = 2.5mm and values for the

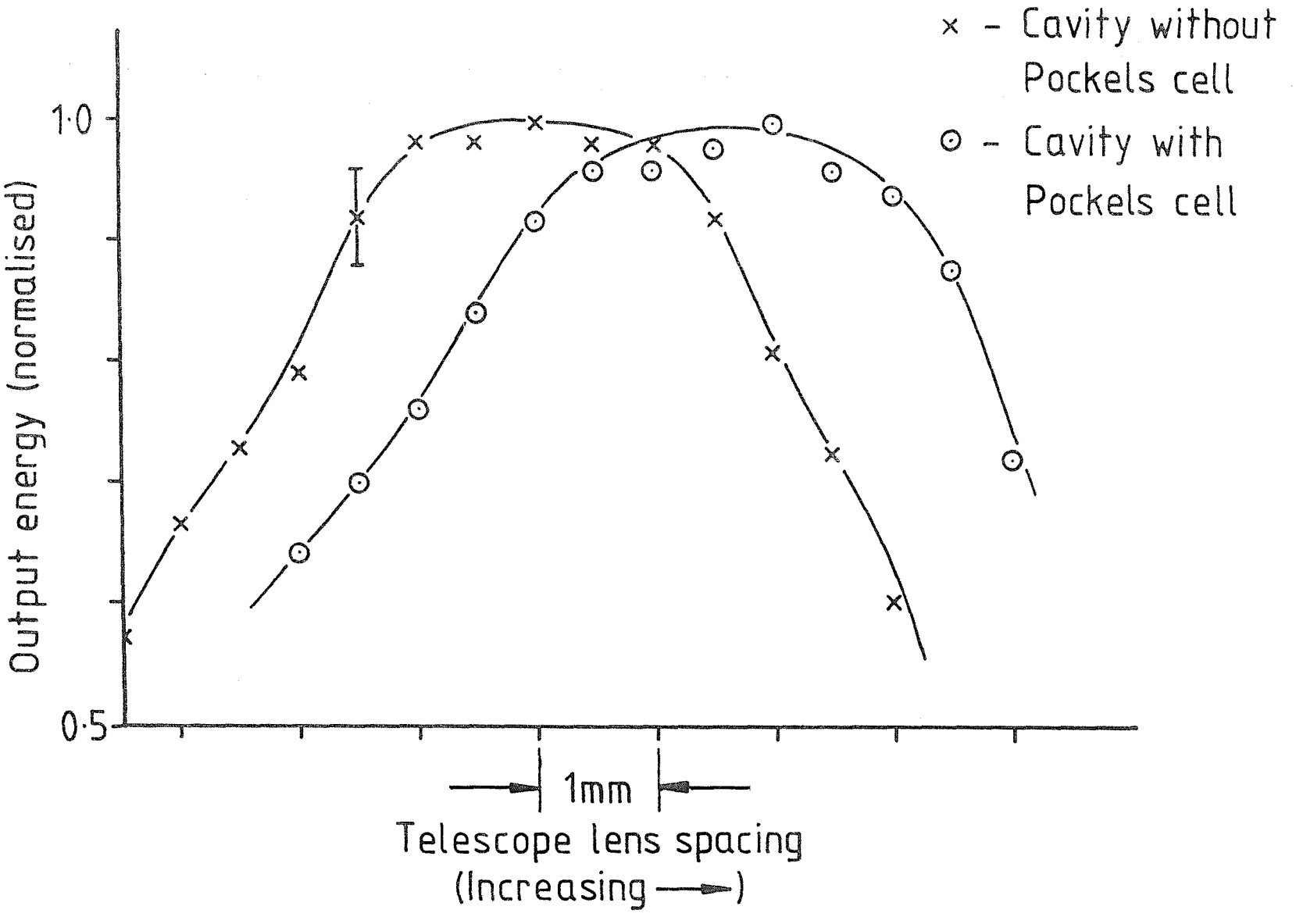

Figure 2.11: Normalised laser output energy as a function of telescope lens spacing, measured before and after addition to the cavity of the Pockels cell

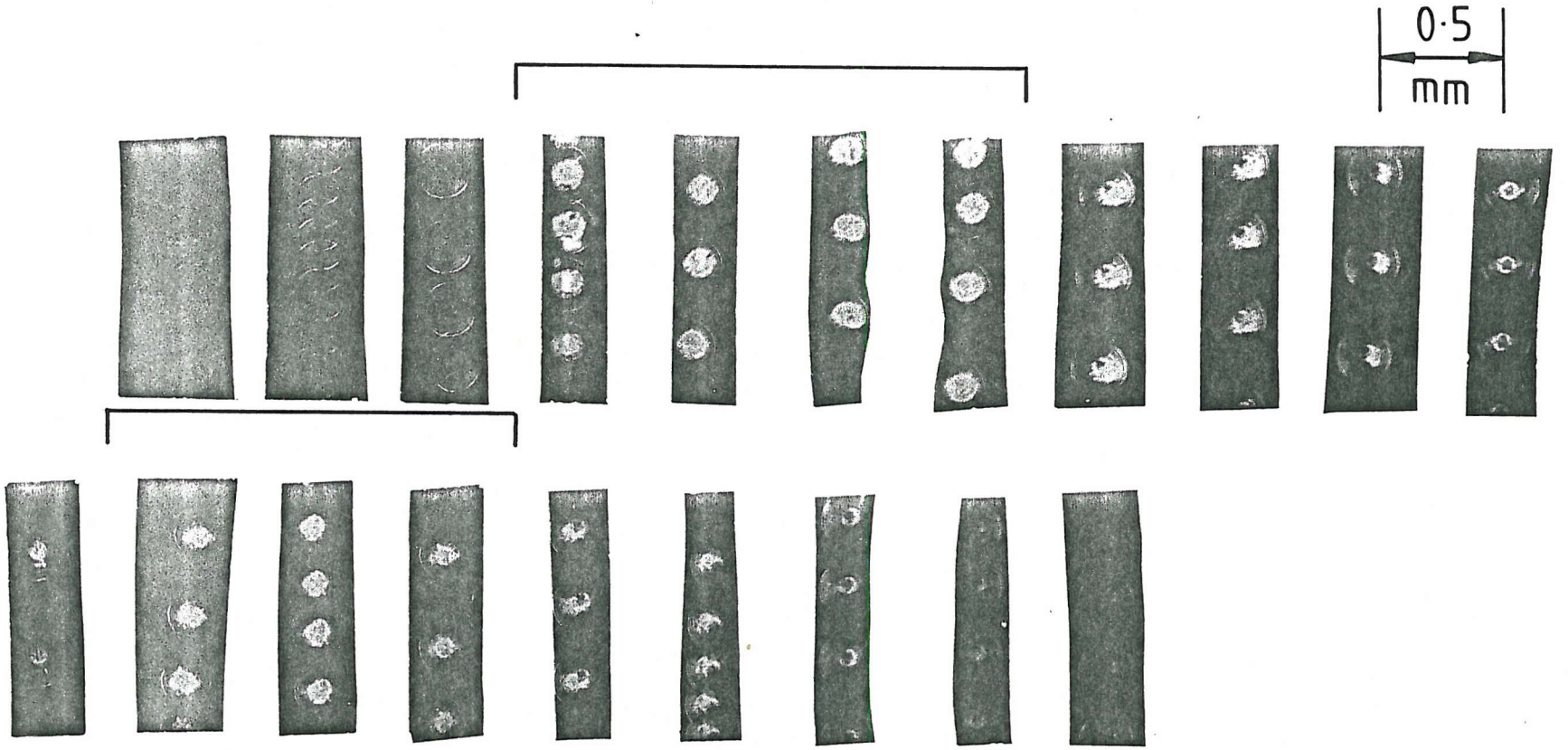

Figure 2.12: A sequence of burn patterns illustrating the shift in optimum telescope spacing upon insertion of the Pockels cell. The upper sequence was obtained without the Pockels cell in the cavity, the lower sequence with. The braces indicate the region of telescope adjustment over which acceptable profiles were obtained in each case

other constants appropriate to KD*P (these are listed in table 2.1 for convenience), we find t_c = 1.7s. Since we are working at ∿18Hz, condition (ii) is certainly met. Furthermore, the crystal is immersed in a refractive index matching fluid, therefore curvature of the crystal faces caused by thermal expansion will not contribute to the focussing effect, and so condition (i) is also met.

To use equation 2.32 to calculate the induced focal length, we need to know the value of absorption coefficient for our crystal. The absorption coefficient of KD*P depends on the degree of deuteration, varying linearly from $\alpha = 0.12\text{cm}^{-1}$ for undeuterated KDP to $\alpha \simeq 0$ for 100% deuterated KD*P (R. Wood, Private Communication). Unfortunately, the exact deuteration for our crystal is not known, but for the purpose of calculation we assume a typical figure of 95%, giving $\alpha = 6 \times 10^{-3}\text{cm}^{-1}$.

Inserting values from table 2.1 into equation 2.32 gives f = -22m, where we have used P = 5.2W (corresponding to 300mJ laser output at 17.4Hz) and ℓ = 1.5cm for our Pockels cell crystal. This agrees well with the experimental measurement of f ≃ -20m, but this must be regarded as fortuitous since we have, in calculating the power incident on the Pockels cell, assumed in effect that the Pockels cell is mounted outside the laser resonator. In practice, the relationship between output power and the power which circulates each way through the Pockels cell is not straightforward, and may be significantly different from the simple estimate of 5.2W we have used above.

As a result of this observation of Pockels cell lensing, we now take the additional precaution in the alignment procedure of plotting output energy against telescope lens spacing. After first setting the telescope lens spacing for perfect adjustment for visible light using an autocollimater, an additional calculated adjustment is made to compensate for dispersion in the lenses. Using equation 2.25, the required value of δ_{opt} is calculated and also introduced to the lens spacing. The resulting spacing is usually sufficiently accurate for laser action to occur once the resonator mirrors are aligned. A plot of output energy vs. spacing accompanied by a sequence of burn patterns then allows the optimum setting to be found. Once set in this way, no further adjustment of the telescope should be necessary, and any change in operating conditions of the laser such as repetition rate or pumping energy can be compensated for by adjusting the telescope lens spacing according to equation 2.25.

Table 2.1: Some optical and thermal properties of KD*P

QUANTITY	REFERENCE	VALUE
Thermal conductivity, k	(a)	$1.88 \times 10^{-2} Wcm^{-1}K^{-1}$
Heat capacity, C_p	(b)	$0.87 Jg^{-1}K^{-1}$
Density, ρ	(b)	$2.34 gcm^{-3}$
dn/dT	(c)	$-5.1 \times 10^{-5} K^{-1}$
Ordinary refractive index, n_o	(d)	1.47

(a) Y.S. Touloukian et al., 1970. Value measured at T = 300°K, parallel to optic axis.

(b) C.J. West and C. Hull, 1933.

(c) M. Yamazaki and T. Ogawa, 1966. Value calculated at T = 300°K.

(d) W. Koechner, 1976.

2.5 Mode Selecting Apertures: A Practical Point Concerning Their Design

The mode selecting apertures we have used in our work on laser resonators are made by drilling a hole of the required diameter in a flat disc of brass or steel, and then countersinking one side, as shown in figure 2.13. During our work we found that the laser would only function reliably with TEM_{00} mode output when the countersunk side of the aperture faced the laser rod (see figure 2.14(b)). This behaviour has been observed both with the telescopic resonator using a 6.25mm diameter aperture and also with conventional small volume TEM_{00} mode resonators incorporating 2mm diameter apertures.

We illustrate this in figure 2.15, where we show Q-switched burn patterns at the 80mJ output level. These were obtained using the telescopic resonator referred to in section 2.2.3 and discussed more fully in Chapter Three. The aperture is situated between the laser rod and the 100% reflectivity mirror, and the laser output is taken from the contracted beam end of the laser. One can clearly see a tendency for the laser to break into TEM_{01} mode oscillation with the aperture arranged as in figure 2.14(a).

In the telescopic resonator it was possible to induce this behaviour only by adjusting the aperture to be off centre from the beam axis. In the conventional resonator, however, this behaviour was always observed when the countersunk side of the aperture faced away from the laser rod, regardless of aperture centring, and oscillation was occasionally observed on modes of higher order, up to TEM_{11}.

It would appear that this behaviour is due to feedback from the plane face of the aperture and mirror M_1 (see figure 2.14(a)). In figure 2.14(b), any light incident from the left on the aperture is reflected out of the cavity by the chamfered lip on the aperture, thereby suppressing oscillation.

This is clearly a point of some practical importance in the design and setting-up of a laser oscillator since it may not be immediately obvious that poor laser performance can result from incorrect aperture design or orientation.

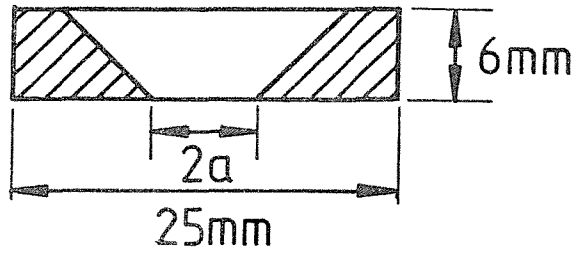

Figure 2.13: Cross-section of a mode-selecting aperture

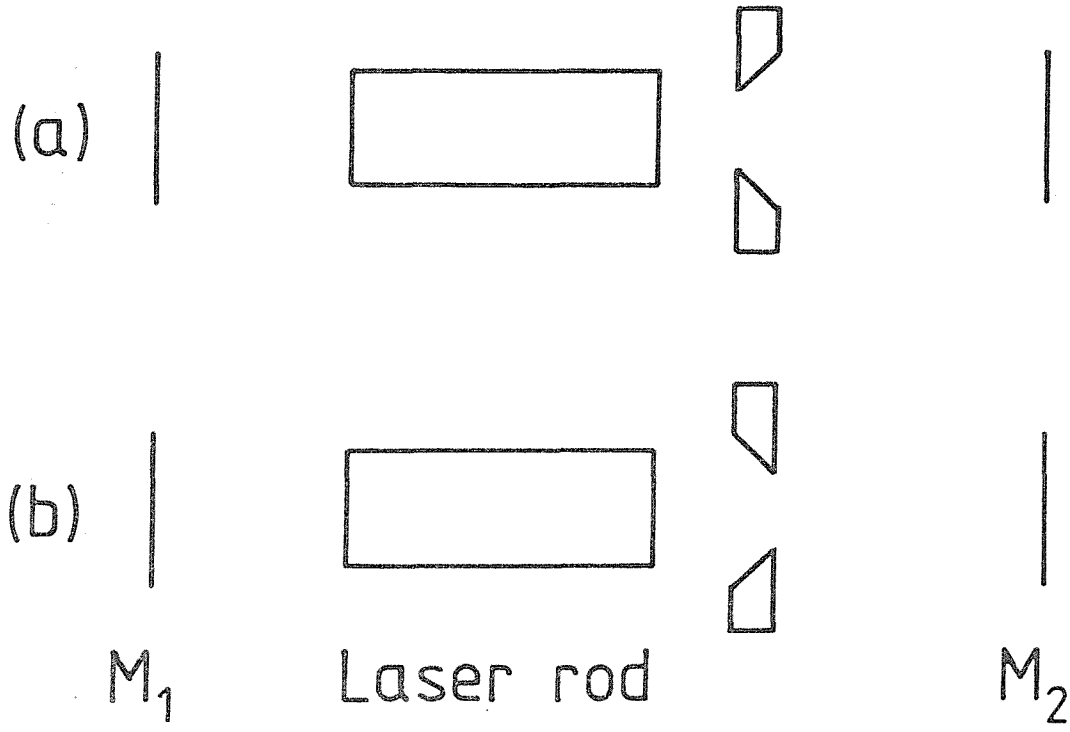

Figure 2.14: The two possible orientations of the aperture relative to the laser rod and resonator mirrors, M_1 and M_2

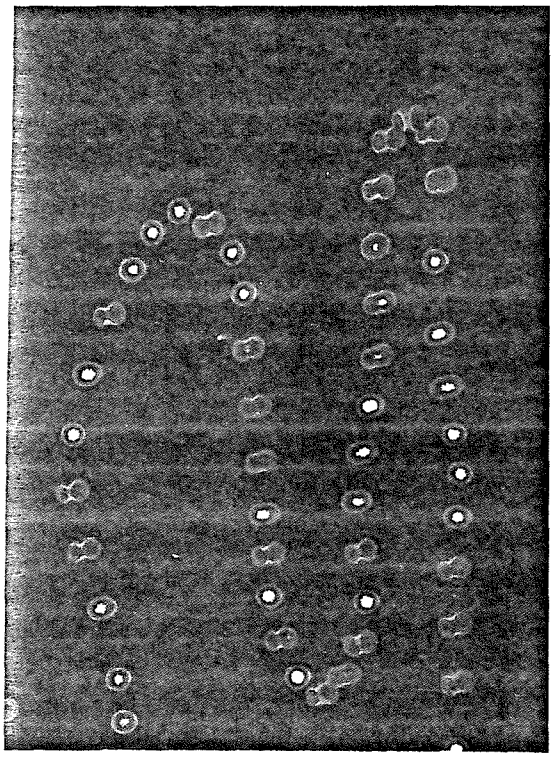

Figure 2.15: A sequence of burn patterns illustrating the effect of having the aperture oriented as shown in figure 2.14(a)

2.6 Pockels Cell Alignment

The correct alignment of the Pockels cell crystal relative to the laser beam is with the crystallographic x or y axis parallel to the polarisation vector and the z, or optic, axis parallel to the propagation direction. When aligned in this way, the crystal behaves isotropically with zero applied voltage, and therefore does not alter the polarisation of the laser beam. However, if the z axis is misaligned, the resulting optical anisotropy can lead to a cavity loss via the intracavity polariser. Since the crystal is uniaxial under zero field conditions, orientation of the x and y axes is unimportant as regards cavity loss. (A field-dependent phase shift effect caused by x, y axis misalignment is discussed in section 4.3.3.) It is useful, therefore, to derive an expression for cavity loss as a function of angular misalignment of z axis from propagation direction.

The system of coordinates is shown in figure 2.16. XZ is the plane of polarisation of the laser beam and Z is the propagation direction. The optic axis makes an angle θ with the propagation direction, and an angle χ with the plane of polarisation. By varying χ with θ fixed, one finds that the greatest power loss from the polariser in figure 2.17 occurs for values of χ obeying $\chi = (90n + 45)^{o}$; $n = 0, 1, 2, 3$. For our worst-case calculation of alignment tolerance we will take $\chi = 45^{o}$. One can write the phase shift between the ordinary and extraordinary components of the beam after passing through a length ℓ of crystal

$$\phi = \frac{2\pi\ell}{\lambda} (n_e(\theta) - n_o) \qquad 2.34$$

where $n_e(\theta)$ and n_o are the extraordinary and ordinary refractive indices. $n_e(\theta)$ is related to θ by the following expression

$$\frac{1}{n_e^2(\theta)} = \frac{\sin^2\theta}{n_e^2} + \frac{\cos^2\theta}{n_o^2} \qquad 2.35$$

which after some manipulation can be rewritten

$$n_e(\theta) = n_o \left\{ 1 + \frac{(n_o^2 - n_e^2)}{n_e^2} \sin^2\theta \right\}^{-\frac{1}{2}} \qquad 2.36$$

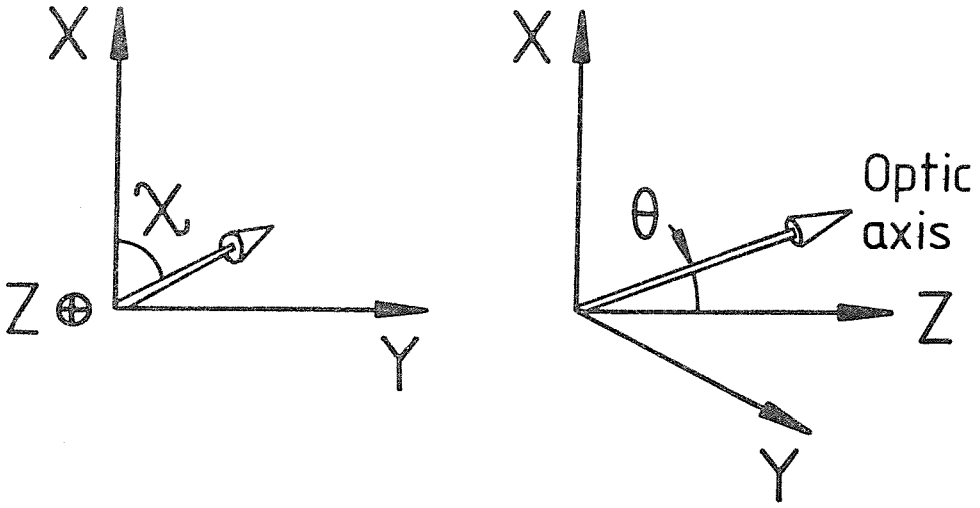

Figure 2.16: System of coordinates used in the evaluation of cavity loss as a result of Pockels cell misalignment

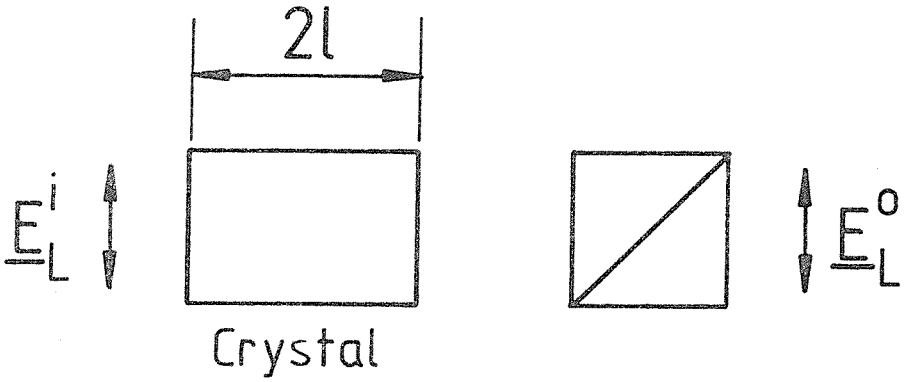

Figure 2.17: The Pockels cell crystal inside the laser cavity

In general, $n_o^2 - n_e^2$ will be much smaller than unity, and also, since we are considering small misalignments, $\sin^2\theta \simeq \theta^2 << 1$. We can therefore write

$$n_e(\theta) - n_o \simeq \theta^2 \frac{n_o}{2n_e^2}(n_e - n_o)(n_e + n_o) \qquad 2.37$$

Furthermore, since $n_o \simeq n_e$, we can simplify equation 2.37 further

$$n_e(\theta) - n_o \simeq \theta^2 (n_e - n_o) \qquad 2.38$$

The Pockels cell inside the laser cavity is shown in figure 2.17. The effective crystal length is 2ℓ since light passes twice through the cell on each round trip. One can easily show that the transmission of this optical system is given by

$$T \equiv \left[\frac{E_L^o}{E_L^i}\right]^2 = \frac{1}{2}(1 + \cos\phi) \qquad 2.39$$

From equations 2.39, 2.38 and 2.34 we can write the transmission T as a function of θ

$$T = \frac{1}{2}\left\{1 + \cos\left[\frac{4\pi\ell}{\lambda}(n_e - n_o)\theta^2\right]\right\} \qquad 2.40$$

This is illustrated in figure 2.18 using the following parameters: $\lambda = 1.064\mu m$, and for our crystal $\ell = 1.5cm$, $n_e - n_o = 0.04$. If we take as our criterion for low loss operation that the transmission must be greater than, say, 0.95, we therefore require $\theta < 8mrad$. Now θ is measured internally, so the external alignment angle is greater by a factor of n, i.e. $\theta_{ext} < 12mrad$.

The Pockels cell alignment procedure we have used in the course of our work involves centering the 'Maltese cross' pattern (see e.g. Koechner, 1976) on the resonator axis. This is done by illuminating the crystal with a He-Ne laser beam which has first been carefully aligned parallel to the resonator optical axis. The beam is diffused by passing it through a lens tissue, resulting in a bright central spot surrounded by scattered light. When the crystal is placed between crossed polarisers, a pattern of a dark cross surrounded by a series of

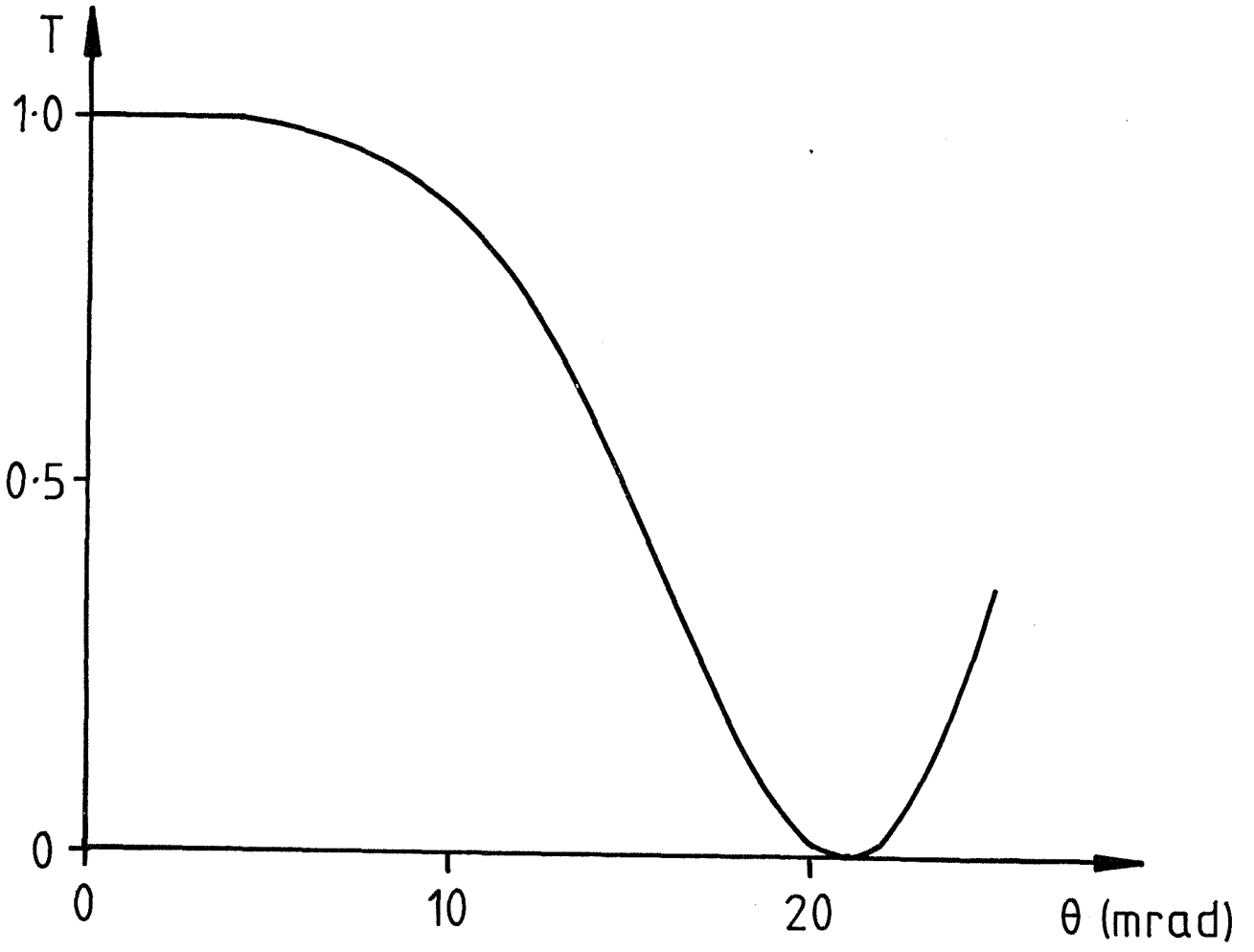

Figure 2.18: Transmission, T, of the Pockels cell/polariser combination shown in figure 2.17 as a function of crystal tilt, θ

circles appears (see e.g. Born and Wolf, 1975). The line connecting the centre of the cross to the lens tissue is parallel to the z axis.† The Pockels cell is now brought into alignment by tilting it so that the centre of the cross coincides with the bright unscattered component of the He-Ne beam. When this is performed carefully we estimate that it is possible to align the Pockels cell optic axis to the resonator axis to better than 2mrad (measured externally to the crystal). Since this is well within the required criterion $\theta_{ext} < 12$mrad, we conclude that Pockels cell losses as a result of crystal misalignment should be negligible in practice.

2.7 Conclusion

We have ended this chapter by introducing some additional discussion of three practical points mentioned only briefly in earlier sections. We show that under conditions of high average power laser operation that absorption of the radiation by the Pockels cell can induce a thermal lens of sufficiently short focal length to require a correction to the lens spacing of the telescope, and provide an approximate expression which can be used to estimate the significance of this effect. Furthermore, our practical investigations have led us to adopt a particular design and orientation of mode selecting aperture: if incorrectly designed, significant distortion of the transverse mode occurs. Finally, an estimate of the angular alignment tolerance on the Pockels cell is made, and the alignment procedure we have adopted, the "Maltese cross" method, is described.

Thus, in conclusion we have shown that a telescopic resonator can provide a reliable means of generating a large volume TEM_{00} mode in a Nd:YAG laser, permitting Q-switched operation at the 100mJ level. An analytical description of this type of resonator has been developed which reduces to a few simple design equations. We have found that these equations describe the experimentally observed behaviour with a degree of completeness and accuracy beyond what was expected. This indicates that a very thorough design calculation could be made, e.g. to maximise output energy while keeping clear of damage problems, and the results of

---

†This is only strictly true if the crystal faces are polished perpendicular to the optic axis.

such a calculation could be trusted with confidence. It is expected that a similar exercise could be extended to other optically pumped solid state lasers, notably Nd doped glass and ruby.

CHAPTER THREE

EXPERIMENTAL WORK ON THE TELESCOPIC RESONATOR

3.1 Introduction

In this chapter we consider the experimental development of the telescopic resonator.

Of central importance to our investigation of the telescopic resonator is the measurement of angular divergence and intensity profile of the output beam, since these give a quantitative and objective measure of the transverse mode structure. We therefore begin this chapter with a discussion of techniques which may be used to perform these measurements, and describe the technique which we have developed to allow their accurate and quick determination.

A previous investigation of the telescopic resonator by Herbst et al. (1977) gave poor results as regards transverse beam quality and output energy. Our own initial problems with the resonator have led us to adopt a careful alignment procedure, of which we give a detailed account in section 3.3. We conclude the chapter with the key results of the experimental programme on the resonator.

3.2 Beam Spot-Size and Divergence Measurements: Method

To provide a framework for discussion of experimental techniques, we begin this section by making some general points concerning the diffraction behaviour of Gaussian beams.

Suppose a laser oscillates only on the TEM_{00} transverse mode, with a spot-size at the beam waist, w_0. For such a beam, the angular divergence is given by

$$\theta = \frac{\lambda}{\pi w_0} \qquad 3.1$$

and the spot-size at a distance z from the waist

$$w(z) = w_0 \left\{ 1 + \left[\frac{\lambda z}{\pi w_0^2} \right]^2 \right\}^{\frac{1}{2}} \qquad 3.2$$

(see, e.g. Kogelnik and Li, 1966). Consider the situation where the

beam has propagated to the far field, which we define by the condition

$$\left[\frac{\lambda z}{\pi w_0^2}\right]^2 >> 1 \qquad 3.3$$

In this case, one can write, using equations 3.2 and 3.1

$$\frac{w(z)}{z} \simeq \frac{\lambda}{\pi w_0} = \theta \qquad 3.4$$

In principle, then, one would measure w_0 at the waist, and w(z) at a distance z satisfying equation 3.3. The calculated value of θ from equation 3.1 is then compared to w(z)/z. If they are equal, we say that the beam is 'diffraction limited'.

There are, however, three major problems which arise when we attempt a practical measurement of these quantities.

(a) To measure the spot-size, one requires to measure the intensity profile of the beam. How can this be performed reliably, quickly and accurately?

(b) The measurement of w_0 in the scheme outlined above relies on the laser forming a waist outside the cavity. For general applicability, however, one needs to devise a scheme which can handle the situation where the waist is formed inside the cavity.

(c) One may have to allow the beam to propagate inconveniently far to reach the far field. This can be seen by considering a typical laser output characterised by w_0 = 2mm, λ = 1μm, for which the condition for far field diffraction is z >> 13m.

The intensity distribution in the laser beam can be monitored in three ways. (i) The beam can be photographed. After development, the resulting image is analysed using a microdensitometer. When using this technique great care must be exercised to ensure operation on the linear portion of the film characteristic, and subsequent development and analysis of the image is time consuming. (ii) A detector mounted behind a pinhole can be moved mechanically across the beam on a calibrated, accurate translation stage. This method, however, requires a lot of laser operation time, and gives no information on the intensity

profile of a single laser pulse. (iii) The beam may be monitored using a scanning photodiode array (S.P.A.). In this technique, the intensity distribution of the incident beam is 'stored' on a linear array of silicon photodiodes, which are then sequentially sampled and displayed on an oscilloscope. In this way it is possible to monitor the profile of an individual laser pulse. Furthermore, the control electronics is set to clearly indicate when the diodes are operating outside the region of linear response. For these reasons we have chosen to use an S.P.A. for our measurements of beam profile, and therefore restrict out later discussions to the use of this instrument.

The problem of propagation to the far field may be overcome by focussing the beam, as illustrated in figure 3.1. We note that the beam waist is not, in general, formed in the focal plane of the lens, but at a distance which depends on the spot-size w and wavefront curvature R of the beam which is incident on the lens. This can be seen by considering the lens as consisting of two parts, the first of which corrects the wavefront curvature and presents plane wavefronts to the second, of focal length $f' = (1/f - 1/R)^{-1}$. One can then show that the beam waist occurs at a distance $z_f = f'/(1 + (\lambda f'/\pi w^2))$ from the lens.

As a result of the high degree of collimation of a laser beam, the diameter of the beam waist formed after passing through a lens is very small for typical, practical values of lens focal length. To illustrate this we assume that a beam, spot-size w_0, is incident on the back focal plane of a lens of focal length f. The beam is focussed to a waist w_{0f} in the front focal plane of the lens. It is easy to show that w_{0f} is given by

$$w_{0f} = \frac{f\lambda}{\pi w_0} \qquad 3.5$$

Taking typical values for w_0, λ and f (appropriate to our experimental arrangement) of 2mm, 1μm and 1m respectively, we find from equation 3.5 that $w_{0f} = 160\mu m$. Our S.P.A. has a diode spacing of 100μm, and if this was placed at the beam focus to monitor the profile, the spatial resolution would be clearly inadequate. We therefore image the waist with a second lens, arranged to give a magnification M > 1. The general experimental arrangement we have used is shown in figure 3.2, where for

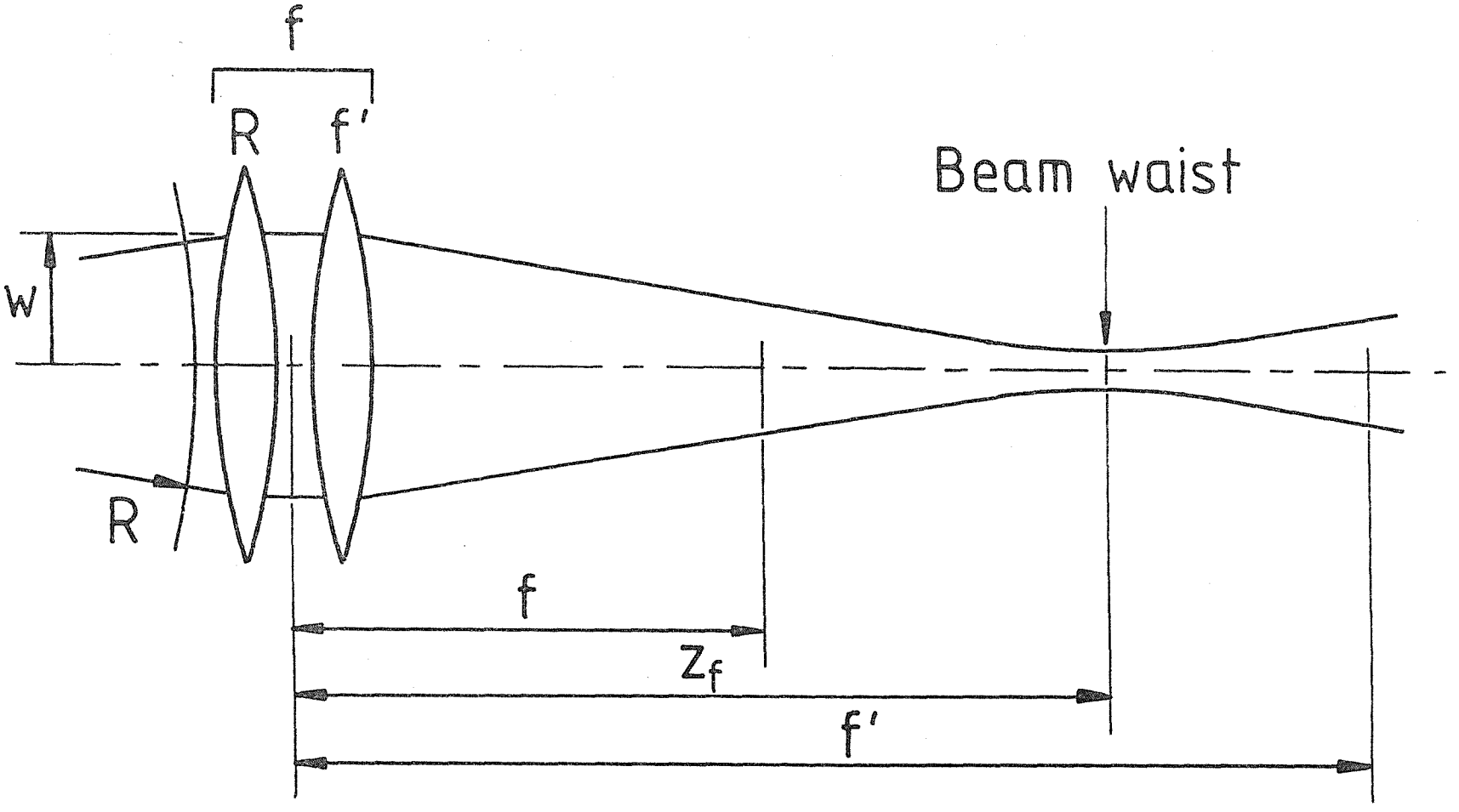

Figure 3.1: Use of a lens, focal length f, to form a beam waist at a distance z_f from the lens

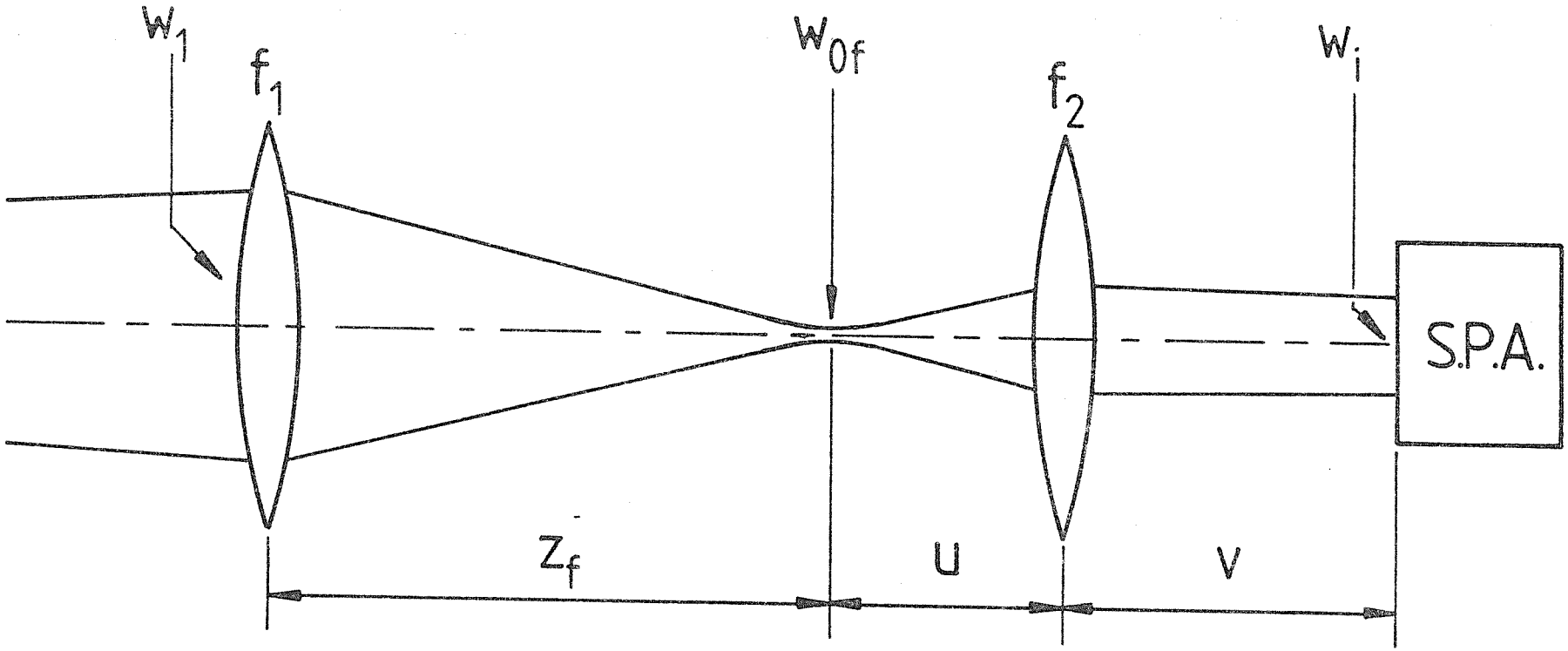

Figure 3.2: Experimental arrangement used to measure the waist spot-size, w_{0f}, and profile formed by a lens of focal length f_1

clarity various attenuators have been omitted. The laser beam is incident from the left on a lens of focal length f_1 and brought to a waist with spot-size w_{0f}, at a distance z_f from the lens. Note that in general $z_f \neq f_1$. Having located the waist formed by this first lens a second lens of focal length f_2 is used to image the waist onto the S.P.A., giving an image spot-size $w_i = Mw_{0f}$, where $M = v/u$ is the geometrical magnification. This can be measured by examining the signal from the photodiode array, and w_{0f} deduced from $w_{0f} = w_i/M$. If the incident beam were a pure TEM_{00} mode then the spot-size w_1 at lens 1 would be given by equation 3.2 with $z = z_f$ and $w_0 = w_{0f}$. This calculated value is compared with the measured value of w_1 obtained by replacing lens 1 with the S.P.A. If equal, then the beam is diffraction limited.

In practice, there is always an error δ_1 associated with the location of the waist formed by lens 1, and an error δ_2 in the placing of the S.P.A. In this case, $w_i \neq Mw_{0f}$ since the object plane of the imaging system no longer contains the waist. To calculate the magnitude of this effect, we find the beam magnification, defined by $M' = w_i/w_{0f}$, for the arrangement illustrated in figure 3.3. By using the ABCD law for Gaussian beams (Kogelnik, 1965), one can show that M' is given by

$$M' = M\left\{\left[1 + \frac{\delta_2}{Mf_2}\right]^2 + \left[\left[\frac{\delta_2}{M^2} + \delta_1\left[1 + \frac{\delta_2}{Mf_2}\right]\right]\frac{\lambda}{\pi w_{0f}^2}\right]^2\right\}^{\frac{1}{2}} \qquad 3.6$$

Clearly, when the system is in perfect alignment, i.e. when $\delta_1 = \delta_2 = 0$, then $M' = M = v/u$ as required. For the practically important case $\delta_2/Mf_2 << 1$, $\delta_2/M^2 << \delta_1$, we can write a more compact, approximate expression.

$$M' \simeq M\left\{1 + \left[\frac{\delta_1\lambda}{\pi w_{0f}^2}\right]^2\right\}^{\frac{1}{2}} \qquad 3.7$$

As an example, consider our earlier illustration, where a waist of 160μm diameter was formed by a 1m focal length lens. In our experiments we have found it convenient to use a magnification M = 7, accomplished by using a 15cm focal length lens with u = 17.1cm, v = 120cm. To locate the small beam waist we have used either an infra-red phosphor

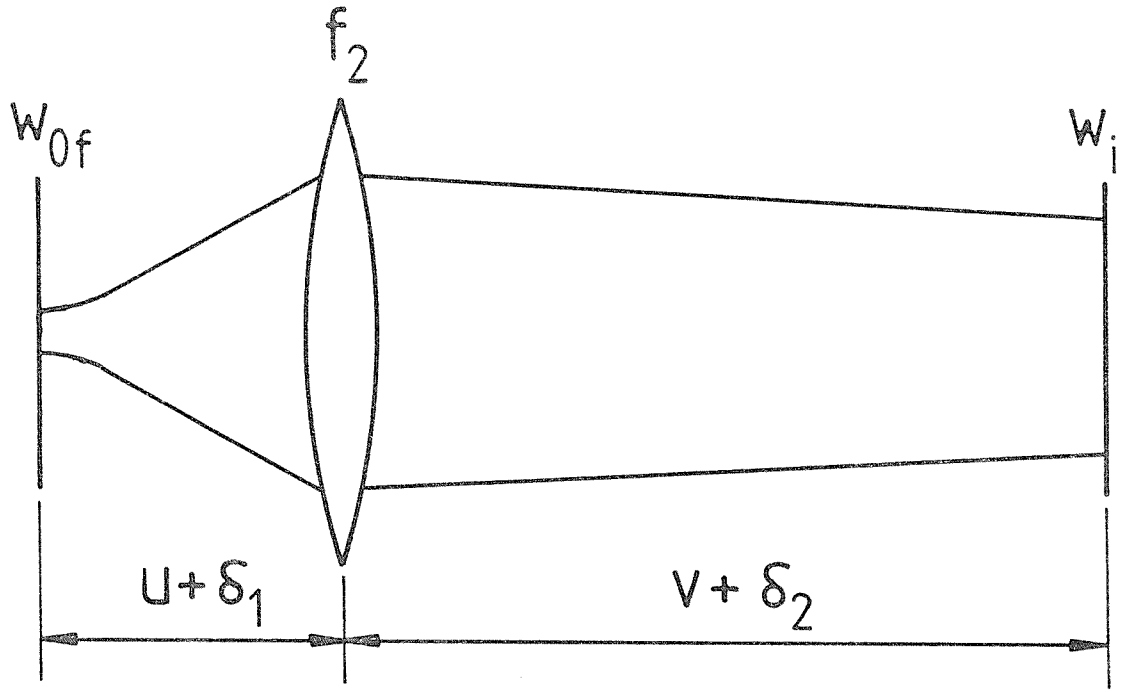

Figure 3.3: Errors δ_1 and δ_2 in the object and image distances u and v

card or exposed photographic paper, with an estimated accuracy of $\delta_1 = \pm 2$cm. Inserting M = 7, λ = 1μm, w_{0f} = 160μm into equation 3.7 gives $M' = 7.2$. This would give rise to an error in deducing w_{0f} of $0.2/7 \equiv 3\%$, thus illustrating the high degree of accuracy that one might expect in beam divergence measurements performed by this method.

3.3 Cavity Alignment Procedure

3.3.1 Telescope alignment

When setting up a telescopic resonator, one of the most important aspects of alignment is finding the correct telescope spacing. In the course of our work we have found that this can be easily and conveniently achieved in two stages.

(i) The spacing of the lenses is first adjusted so that the telescope is exactly collimated. This is achieved by viewing a plane mirror through the telescope using an autocollimator. The lens spacing is then adjusted to form a sharp image of the autocollimator cross wires. A calculated correction is now made for dispersion, using the dispersion formula for BK7 glass (the material used for our telescope lenses). This is given in the Schott glass catalogue as

$$n_\lambda^2 = A_0 + A_1\lambda^2 + A_2\lambda^{-2} + A_3\lambda^{-4} + A_4\lambda^{-6} + A_5\lambda^{-8}$$

where

$$\begin{aligned} A_0 &= 2.2718929 \\ A_1 &= -1.0108077 \times 10^{-2} \\ A_2 &= 1.0592509 \times 10^{-2} \\ A_3 &= 2.0816965 \times 10^{-4} \\ A_4 &= -7.6472538 \times 10^{-6} \\ A_5 &= 4.9240991 \times 10^{-7} \end{aligned}$$

where λ is in microns. We assume that by using the autocollimator, the telescope is correctly adjusted for $\lambda \sim 500$nm, and so the required correction is

$$d_{1.06} - d_{.5} = d_{.5}\left[\frac{n_{.5} - n_{1.06}}{n_{1.06} - 1}\right] = 3 \times 10^{-2} d_{.5}$$

To this is added the design value of δ_{opt} calculated using equation 2.25.

(ii) With the telescope adjusted in this way, and inserted in the resonator, the resonator mirrors are aligned using an autocollimator and/or He-Ne laser. With the laser operating fixed-Q, the laser output energy is now measured as a function of telescope lens spacing, and a graph similar to figure 2.11 plotted. We have also found in practice that examination of burn patterns taken at each telescope setting can aid the exact location of the optimum lens spacing. One can see this by observing the characteristic behaviour of burn patterns as a function of δ, as illustrated in figure 2.12.

3.3.2 Resonator alignment

There are many possible modes of operation for a telescopic resonator, e.g. fixed-Q, fast Q-switched, pre-lase Q-switched (see Chapter Four), and for each of these configurations the beam may be extracted from the contracted or expanded beam end of the cavity, or indeed both. It is clearly impractical to give an all embracing alignment procedure which covers all telescopic resonators, and providing a separate procedure for each resonator would involve much repetition. We therefore give the alignment procedure we have adopted for the most elaborate cavity we have used, a slow Q-switched resonator in which the output is taken from the contracted beam end of the laser. Experimental results obtained from this laser are reserved until the experimental section of Chapter Four, and we restrict our discussion here to the required steps to bring the cavity into alignment.

The final cavity configuration is illustrated in figure 3.4. In order to suppress spurious frequency selection effects, components such as the Pockels cell windows have, where possible, been wedged, and components with parallel faces, such as the laser rod, tilted (see section 4.2.5). Certain parts of the alignment procedure refer specifically to a laser system built onto a commercial J.K. Lasers optical rail, for which there is no facility for tilting or laterally translating most of the components. For a laser system built using a more adaptable mounting arrangement, these comments can be either ignored or altered as required.

(1) The laser rod and its pumping chamber are bolted to the laser rail in the required position, and a He-Ne laser aligned along its axis.

(2) The telescope lenses are added in roughly the right positions on the laser rail. Each lens is tilted or displaced so that reflections

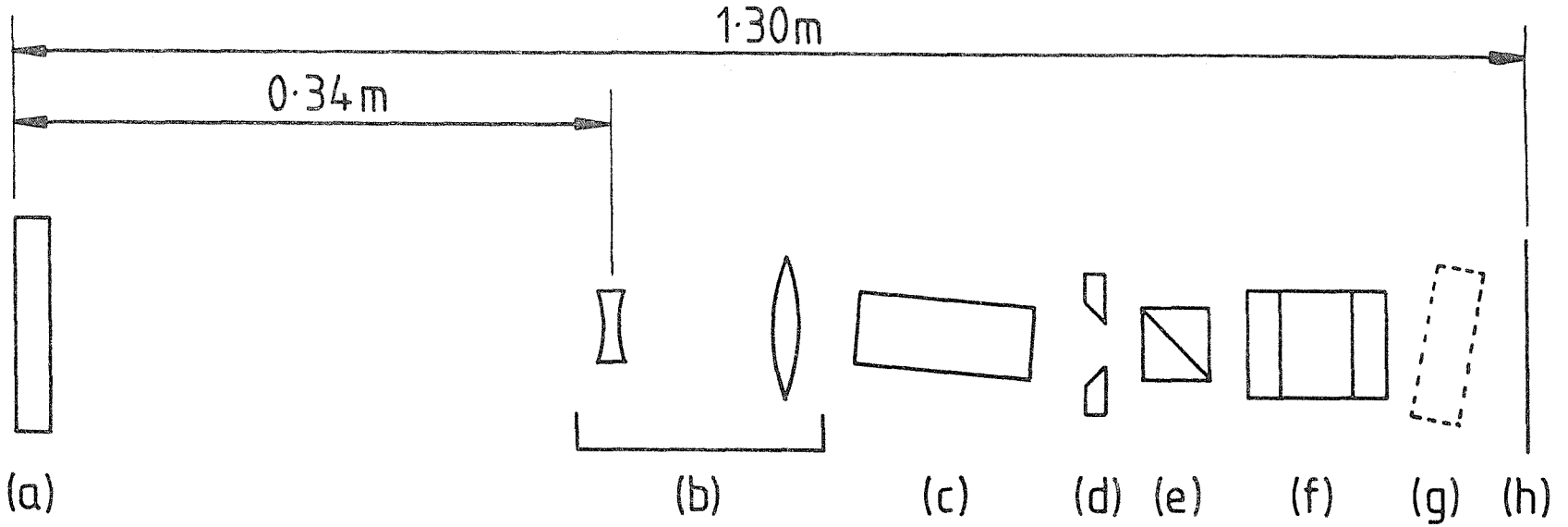

(a) Resonant reflector. 6mm thick.
(b) Telescope. Magnification = 4
(c) Laser rod.
(d) Aperture. 6·25mm dia.
(e) Dielectric polariser.
(f) Pockels cell.
(g) Position of tilted etalon.
(h) Plane mirror. 93% reflectivity.

Figure 3.4: Q-switched telescopic resonator. The focal lengths of the telescope lenses were +20cm and -5cm

from the lens' surfaces do not pass back through the laser rod. The lens spacing can now be set, as discussed at the beginning of this section.

(3) In order to suppress spurious frequency selection introduced by parallel faces in the Pockels cell, it is necessary to prepare the cell by fitting wedged windows. Although it is also preferable to have the faces of the crystal wedged, it was not possible to have our existing parallel-faced crystal modified. Consequently our work has been performed with a parallel-faced crystal in a cell fitted with windows wedged to 30'. Care should be taken when fitting the windows to ensure that the included angle between any two of the six faces is greater than $\sim$30'. This can be conveniently performed by using an autocollimator.

(4) The Pockels cell and wedged dielectric stack polariser are temporarily fitted to the rail to allow alignment of the high reflectivity resonator mirror. With this mirror fitted, reflections from the various faces in the cavity are viewed using an autocollimator held to the left of mirror (h) (see figure 3.4). The weak reflection from the end of the laser rod can be identified by moving a piece of card back and forth in front of the rod, and the mirror brought into alignment by tilting it so that the strong reflection from its coated surface coincides with the weak reflection from the rod face.

(5) The pumping chamber is now unbolted from the rail and one end packed to tilt the rod axis away from the rail axis by greater than $\sim$30'. The pumping chamber is then rebolted to the rail. We have typically used a packing of $2\frac{1}{2}$-3mm for our laser system, resulting in a rod tilt of $\sim$50'. This ensures the suppression of gain-enhanced etalon effects caused by the rod faces being parallel to the high reflectivity mirror. We have adopted this alignment procedure to allow easy realignment if the high reflectivity mirror is accidentally moved, or after it has been removed for cleaning. If this should happen, the packing can be removed from the chamber and the autocollimator used to realign the mirror to rod faces as detailed in step (4). The rod can now be repacked and the cavity mirror alignment reoptimised.

(6) Steps (4) and (5) effectively determine the optical axis of the laser system. Because of the tilt of the laser rod this will not, in general, coincide with the axis of the Pockels cell or polariser. This problem was compounded in our laser system because the laser rod axis

was displaced from the mechanical axis of the rail by ∿1.5mm, with the result that the total axis misalignment was ∿3.5mm. This means that the laser beam may be partially apertured by the polariser mount, or, more seriously, may strike the cylindrical electrodes of the Pockels cell crystal. This leads to irreversible damage, and repair can only be effected by replacement of the (expensive) crystal. The polariser and Pockels cell must therefore be translated by inserting packing pieces of the correct thickness between their mounts and the laser rail.

(7) The Pockels cell may now be aligned. Alignment of the x and y axes is performed by visually aligning the cell to its mount, where we have assumed that the crystal has been aligned correctly relative to the cell by the manufacturer (see section 4.3.3). Alignment of the optic axis of the crystal to the resonator axis is performed using the Maltese Cross method (section 2.6), after first aligning the He-Ne laser to be perpendicular to the high reflectivity mirror. The next stage in the alignment procedure is simplified if the He-Ne laser is also aligned to pass roughly down the rod axis.

(8) The resonant reflectoris now added. To ensure that a resonant reflector reflectivity maximum coincides with the gain maximum of the Nd:YAG rod we have taken the precaution of controlling the temperature of the reflector using an oven. The procedure we have used to ensure coincidence of the peaks is discussed in section 4.4.1.

With the He-Ne laser aligned as in step (7), the diverging lens of the telescope is translated so that the beam falls roughly in the centre of the resonant reflector. A piece of card with a small hole in it is now used to view the reflection from the resonant reflector. The reflector is now tilted to align the reflection along the He-Ne beam. This is first done coarsely by placing the card between the telescope and the reflector, and then finely by placing the card between the telescope and rod.

(9) The laser is now run, fixed-Q, at a level somewhat above the expected threshold, and at the required repetition rate. If steps (2) and (8) have been performed carefully, experience has shown that the laser, although unoptimised, should oscillate. The resonant reflector should now be adjusted to maximise the output energy.

(10) The dielectric polarisers we have used in our laser are intended for use at (nominally) Brewster's angle. As a result of manufacturing

tolerances, however, it is generally necessary to adjust the angle of the polariser to optimise the laser output energy. This should now be done, and possibly rechecked after steps (11) and (12) since a small misalignment of $\sim 1^{o}$ can cause a severe drop in laser output energy.

(11) Following section 3.3.1, the telescope lens spacing is now optimised. Once correctly set for these operating conditions, the telescope can be easily readjusted to reoptimise the cavity if the pump energy and/or repetition rate are changed, by using equation 2.25.

(12) The aperture is now added, taking care that the countersunk side faces the laser rod (see section 2.5) and is centred on the resonator axis. This is performed by adjusting the aperture position to maximise the output energy. Experience has shown a number of possible causes of severe shot-to-shot fluctuations in output energy, and/or poor beam profile. These are listed below. Generally, any misadjustment or malfunction which raises the laser threshold will tend to produce fluctuations in output energy, because typically operating conditions are only a factor of 1.5 above the optimum threshold.

(a) Resonator mirror misalignment or telescope lens spacing incorrect.

(b) Angle of polariser incorrect.

(c) Aperture incorrectly centred on resonator axis, or partial aperturing of the beam by the Pockels cell or polariser.

(d) Damaged optical component(s) in the cavity.

(e) Contaminated coolant, ageing flashlamps, or ageing discharge capacitors.

(13) The cavity may now be Q-switched, taking care to work a safe margin below the damage threshold of the resonant reflector and diverging telescope lens.

(14) A discussion of the alignment of the intracavity etalon and the temperature setting of the resonant reflector are reserved until we have discussed pre-lase Q-switching more fully in Chapter Four.

3.4 Tests on Practical Telescopic Resonators

During the experimental work performed on the telescopic resonator, several cavity configurations were used and tested. One aspect of performance which was common to all the resonators is that

they produced a diffraction limited output beam, with very little structure in the near field, and no detectable structure in the far field. To prevent repetition of beam profile measurements and presentation of visually identical burn patterns, we restricte our discussion to general points concerning the resonators, broadly following the chronological evolution of the design.

Initial development work on the telescopic resonator was carried out as a result of numerical calculations which indicated the feasibility of such a resonator for large volume TEM_{00} mode operation. These calculations were carried out using a computer program (P.E.L. Clarke, 1980) which analyses an optical system in terms of the ray transfer matrices of its components.

The first cavity design is shown in figure 3.5.† This laser was operated fixed-Q with an output energy of ∿350mJ for a flashlamp pump energy of 56J.

The far field beam profile was measured using the technique outlined in section 3.2, where beam attenuation has been introduced by reflection from the faces of two prisms placed between lens 1 (focal length Im) and the beam focus. This is illustrated in figure 3.6. The far field beam profile at the focus of this lens was measured using the arrangement shown in figure 3.2, with f_2 = 15cm. Distances u, v were 17.3cm and 114cm respectively, corresponding to a magnification of 6.6. Additional attenuation was found to be necessary, and this was introduced by placing neutral density filters just in front of the photodiode array. A typical far field profile using this method is shown in figure 3.7(a). The castellation of the trace which can be seen in the wings of the beam is generated by the array electronics and does not represent regular structure in the beam profile. The spot-size displayed in figure 3.7(a) is 140 ± 10μm, and if diffraction limited would correspond to a spot-size at lens 1 (and hence at the laser output) of $2.4 \begin{smallmatrix} + 0.2 \\ - 0.1 \end{smallmatrix}$mm. This is in very good agreement with theoretical prediction, using equations 2.23(b) (for G_1') and 2.19(b) (for w_2). With the laser parameters that we used, and shown in figure 3.5, these give an output spot-size of 2.39mm, where we have assumed that the telescope is in perfect adjustment. The

---

†The resonator mirrors were a 5m radius 100% reflectivity mirror and a 6mm thick resonant reflector. The 5m mirror was used because this is how the laser was originally supplied. Subsequent analysis of the telescopic resonator, however, showed that there is no advantage to be gained by using curved mirrors. The telescope consisted of a 20cm focal length plano-convex lens, and a -5cm plano-concave lens, both of which were antireflection coated.

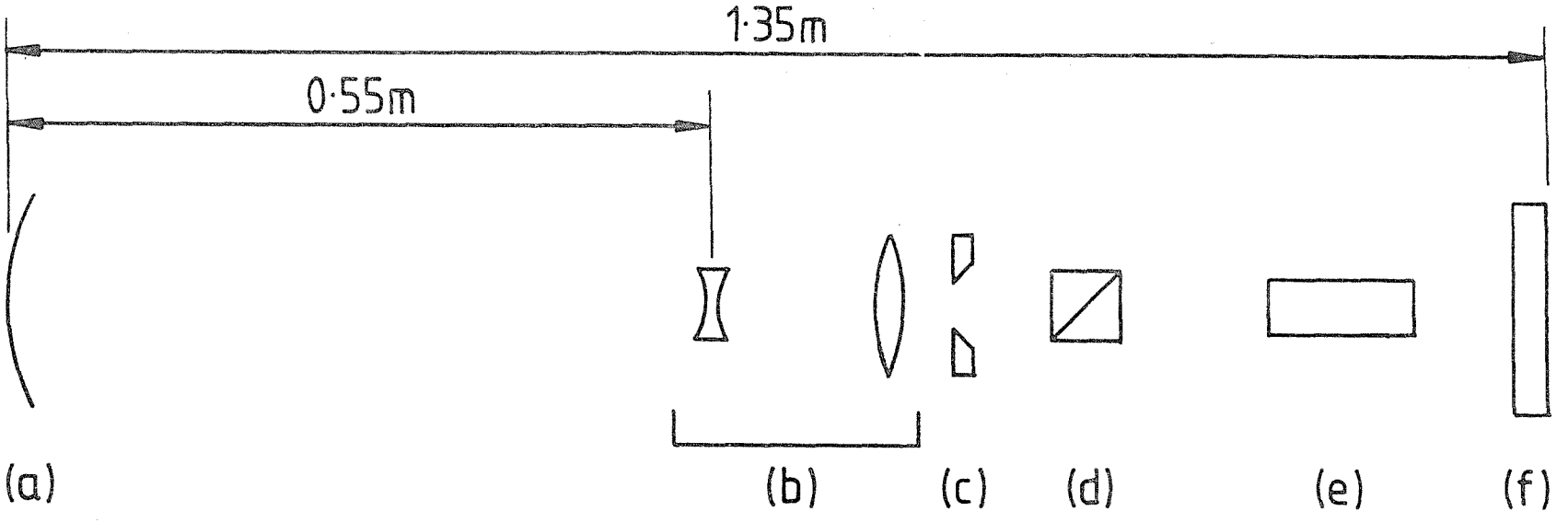

(a) Mirror. 5m radius, 100% reflectivity.
(b) Telescope. Magnification = 4
(c) Aperture. 7·5mm dia.
(d) Dielectric polariser.
(e) Laser rod.
(f) Resonant reflector. 6mm thick.

Figure 3.5: The fixed-Q telescopic resonator. The focal lengths of the telescope lenses were +20cm and -5cm

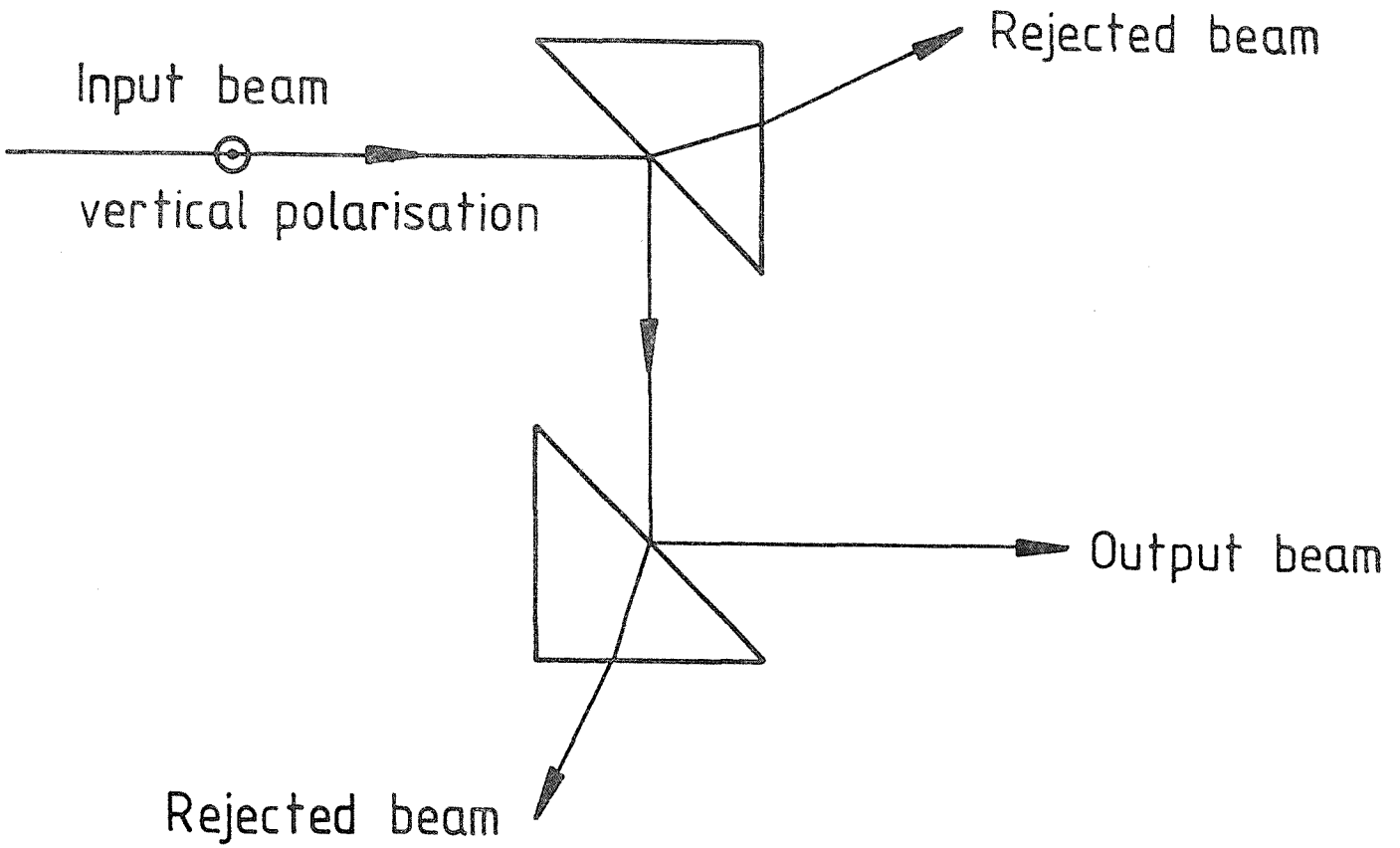

Figure 3.6: Beam attenuator used when measuring beam profiles. The output beam energy is ∿0.8% of the input beam energy

(a)

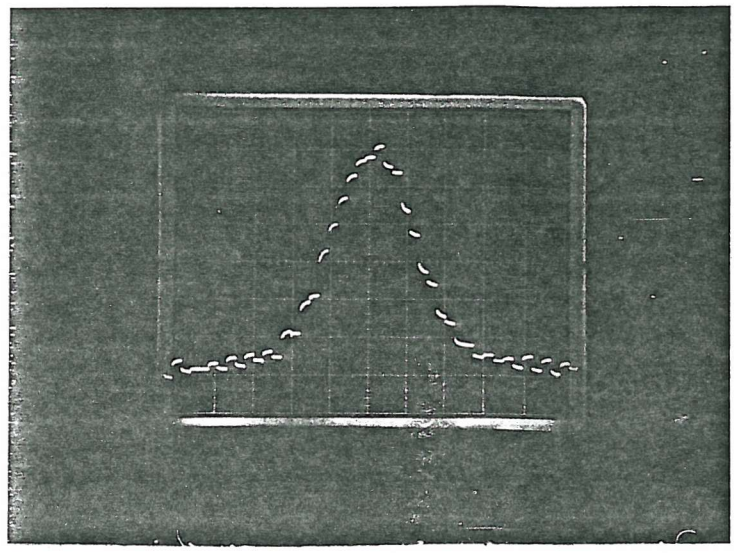

(b)

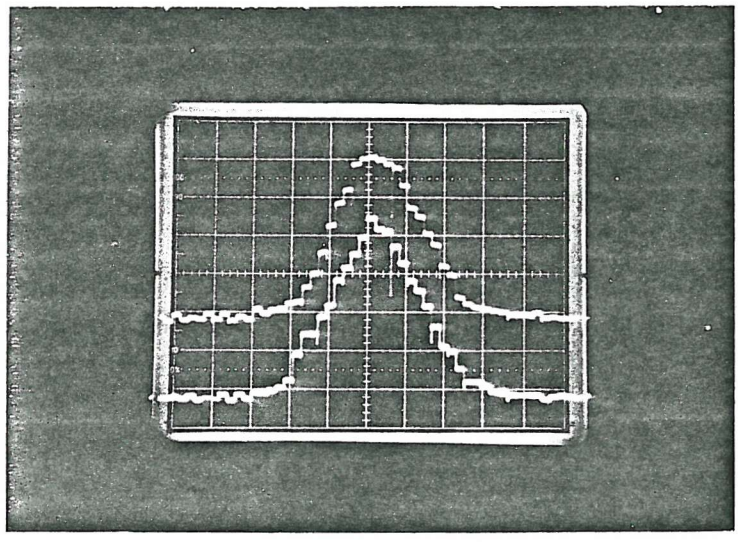

Figure 3.7: Beam profiles for the fixed-Q resonator measured on a diode array. (a) Far field, horizontal plane. (b) Near field: upper trace horizontal plane, lower trace vertical plane

measured near field profile is shown in figure 3.7(b). This was obtained by imaging the plane of the laser output coupler onto the photodiode array with a magnification of 0.44 using a 15cm focal length lens. Figure 3.7(b) gives a spot-size of 2.4 ± 0.2mm, and experimentally confirms that the beam is diffraction limited.

An attempt at Q-switching this resonator was unsuccessful since damage occurred to the coatings on the -5cm telescope lens and 5m radius mirror. This led us to investigate the possibility of extracting the beam from the high intensity end of the cavity using the resonant reflector, and at the same time using an uncoated -5cm lens in the telescope.

The cavity arrangement, which we have subsequently used with minor modifications for our work on slow Q-switching and non-linear optics, is illustrated in figure 3.8. The cavity mirrors are now both plane, since there is no useful advantage gained by using curved mirrors. The output coupler is in the contracted beam end of the cavity and the high reflectivity dielectric coated mirror in the expanded beam. Although it is in principle possible to place the Pockels cell and polariser in either the contracted or expanded end of the cavity, one is restricted in practice to using the expanded end of the cavity for reasons of damage. Furthermore, it was found that if the Pockels cell was placed between the rod and the telescope, parasitic oscillations as a result of reflection of radiation from the cell could result in premature Q-switching of the laser during pre-lase triggered Q-switching. We were therefore restricted to using the Pockels cell and polariser between the mirror and laser rod.

In addition to the increase in output power mentioned above, one further advantage of this laser as compared to that illustrated in figure 3.5 concerns the relative distances required for the beams to propagate to the far field. For the fixed-Q resonator one finds from equation 3.3 that the far field condition is $z >> 16m$, as compared to $z >> 0.6m$ for the Q-switched resonator. We illustrate this effect experimentally in figure 3.9, which shows the output from the fixed-Q laser after 9m (and therefore not yet in the far field) compared to the output from the Q-switched laser after 4½m. This shows that extraction of the beam from the contracted end of the laser produces a cleaner spot close to the laser. One must also bear in mind, however, that the high intensity of this beam close to the laser may be above the damage

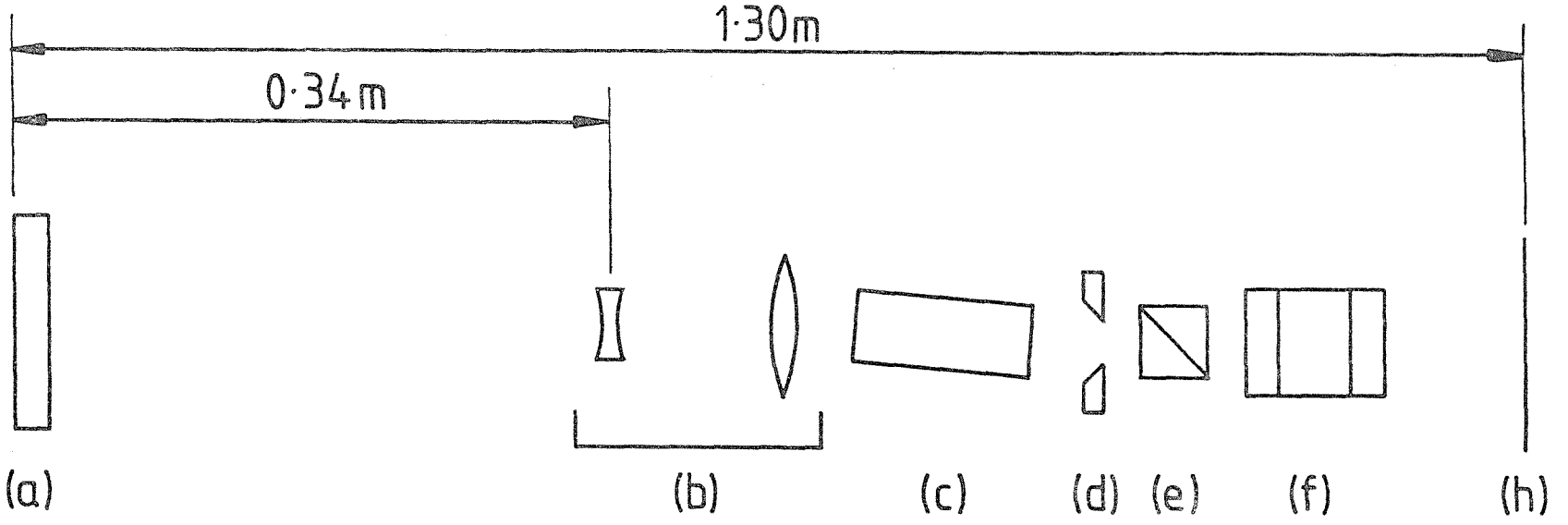

(a) Resonant reflector. 6mm thick.

(b) Telescope. Magnification = 4

(c) Laser rod.

(d) Aperture. 6·25mm dia.

(e) Dielectric polariser.

(f) Pockels cell.

(h) Plane mirror. 93% reflectivity.

Figure 3.8: Q-switched telescopic resonator. The focal lengths of the lenses were +20cm and -5cm

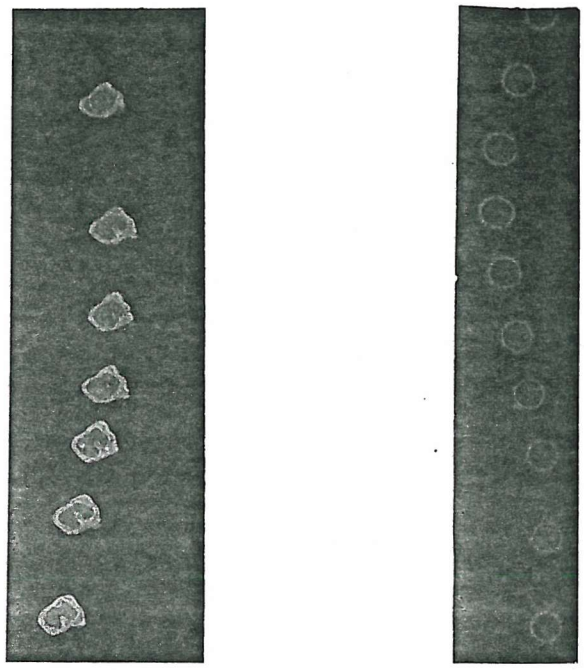

Figure 3.9: Sequences of burns taken for the fixed-Q resonator (left) at a distance of 9m, and the Q-switched resonator (right) at a distance of $4\frac{1}{2}$m

threshold for non-linear crystals, such as KDP, used to frequency double the laser radiation.

Beam profile measurements performed on this laser both when operated fixed-Q and fast Q-switched, confirmed that the output was diffraction limited to within the limits of experimental accuracy (estimated as ±10%). A typical beam profile taken at a distance of ∿2½m from the output coupler is shown in figure 3.10.

Tests were performed to find out how stable the beam quality was during prolonged laser operation, and how much energy could be extracted from the laser before damage to the resonant reflector or -5cm lens occurred. The laser was first operated continuously for 1 hour at 8Hz repetition rate with an 80mJ output without adjustment. Every 5 minutes the beam profile was checked using photographic paper at a distance of ∿4½m from the laser output, and the energy measured by allowing 80 consecutive shots to fall on a cone calorimeter. The burn patterns were all visually identical, with perfect circularity and complete lack of structure. The output energy remained constant to within an experimental accuracy of ±5%. These initial results have been amply consolidated on a much longer time scale, with the laser operating on a day-to-day basis for some four months, with only very occasional realignment.

As we mentioned above, the critical components in the laser cavity as regards optical damage are the resonant reflector and diverging telescope lens. It is important, therefore to establish at what output energy damage occurs, and therefore decide upon a practical operating energy somewhat less than the damage threshold.

This was performed by operating the laser fast Q-switched at a fixed 8Hz repetition rate, and then slowly increasing the output energy until damage to the resonant reflector was observed. The output energy was first set to 70mJ, and the laser run for ∿5 minutes. The pump energy was then increased to give an increase in output energy of ∿10mJ, and the telescope adjusted according to equation 2.25 to compensate for the change in rod lensing. A further five minutes were allowed to elapse while carefully observing the resonant reflector and lens. This process was continued until damage to the reflector occurred at a laser output of ∿170mJ, accompanied with a drop in energy of ∿20mJ and degraded burn patterns. This was repeated several times, using a different section of

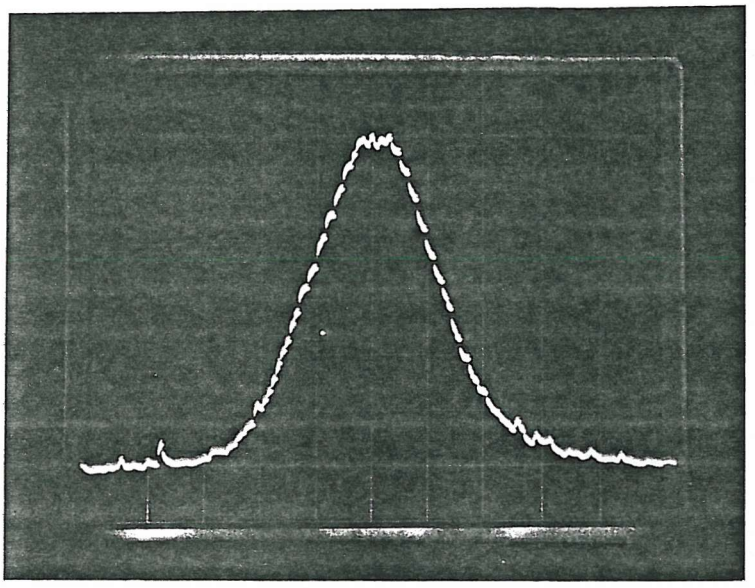

Figure 3.10: Beam profile taken ∿2½m from the output coupler of the Q-switched resonator, measured using a diode array

the resonant reflector for each test, and showed that damage always occurred in the range 150-170mJ output energy. In subsequent experiments we have allowed a safety factor of two, and operated the laser with an output of ∿80mJ, with no further damage.

It is of importance when considering ease of resonator alignment to know how the laser output varies with the tilt of the resonator mirrors. This has been measured for both mirrors with the laser operating fixed-Q, and the results are shown in figure 3.11. A rule of thumb criterion often applied to mirror alignment tolerances states that the amount by which a resonator mirror may be tilted away from perfect alignment must be much less than the divergence of the beam incident upon it. This is indeed the case for the telescopic resonator, where we have marked the relevant beam divergences on the abscissa. Note that this means that the alignment tolerance is easier for the mirror in the contracted beam by a factor of the telescope magnification as compared to the mirror in the expanded end of the cavity. In practice this means that it is easier to realign the laser (for instance when a drop in output power is noticed) by adjusting the contracted beam mirror (in our case, the output coupler).

The full width half maximum pulse duration for our typical fast Q-switched operating conditions is ∿30ns. This has been measured by using a vacuum photodiode and transient digitiser. Care was taken to filter the signal with a low pass filter which removed the high frequency, longitudinal mode beating without broadening the pulse envelope significantly. The pulse duration can be measured more accurately, however, when the laser is pre-lase Q-switched, since this technique generates a pulse with a smooth temporal profile. Such a measurement was performed, and confirms the above result of 30ns. This is in good agreement with calculation, following the analysis of Wagner and Lengyel (1963), which gives 33ns for our pumping conditions.

3.5 Conclusion

In this chapter we have discussed the approach used to align the resonator, including adjustment of the telescope, and the techniques used to measure the beam divergence and intensity profile. Various laser designs have been tried, of which two were discussed in this chapter. The first, operated fixed-Q, gave 350mJ TEM_{00} output. This design was not suitable for Q-switched operation for reasons of damage. A modified

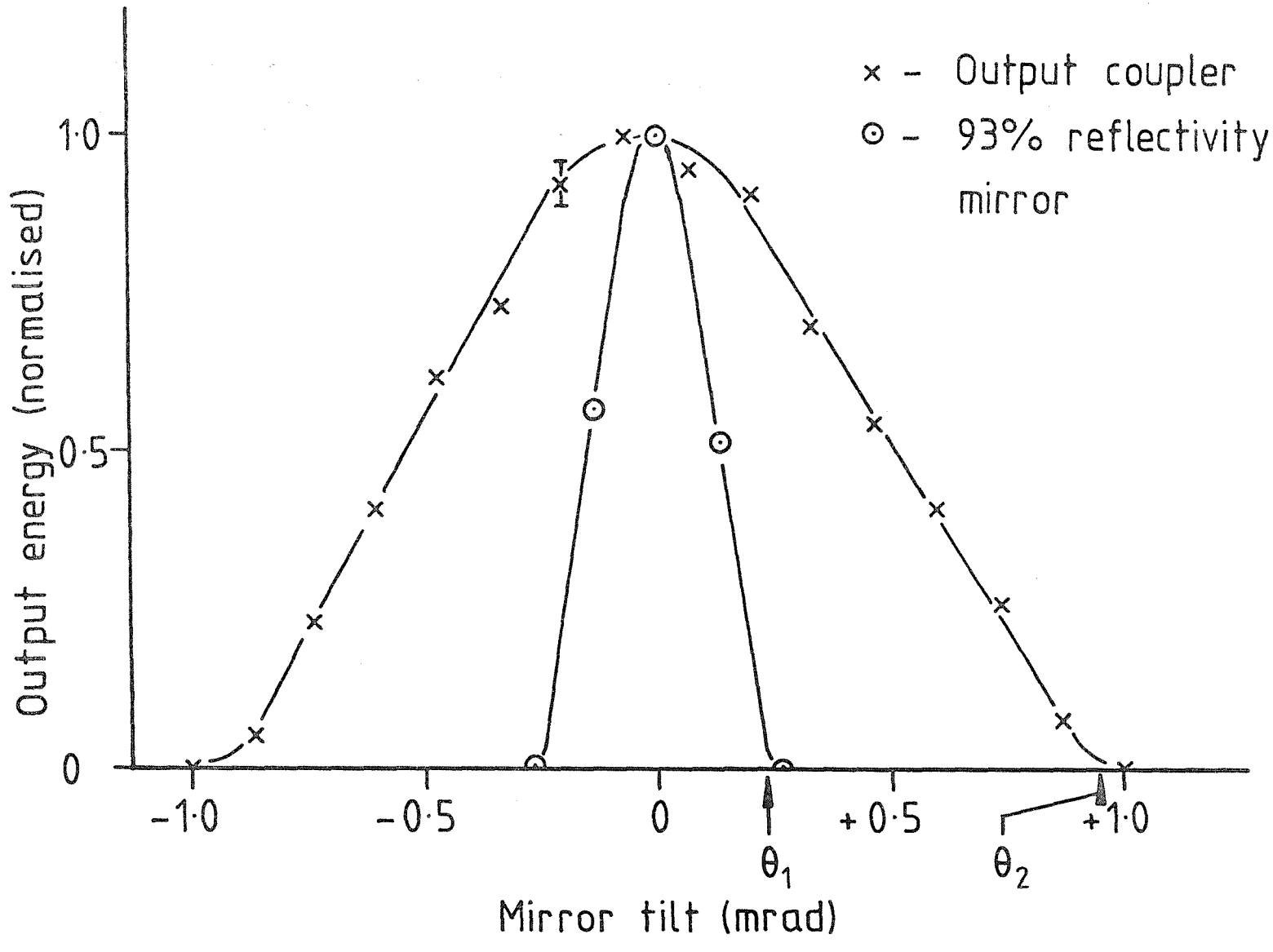

Figure 3.11: Normalised laser output energy as a function of resonator mirror tilt. θ_1 and θ_2 are the calculated beam divergences in the contracted and expanded beam

design in which the mirror in the contracted beam was an uncoated resonant reflector was successfully operated with a typical Q-switched output of 100mJ. Excellent beam quality and repeatability was observed. The observed damage threshold for the resonant reflector was significantly greater than the typical maximum operating condition that we adopted (100mJ), and it is possible that with small design changes and suitable precautions an output of 200mJ could be reliably obtained.

CHAPTER FOUR

LINE NARROWING

4.1 Introduction and Review

There are three main areas of application for a high power single-frequency laser source.

(i) In experiments on non-linear optics. The smooth temporal shape of the laser pulse allows one to make careful quantitative measurements of the process under study. For example, in Chapter Five of this thesis we present the results of experiments performed on frequency doubling of single-frequency pulsed Nd:YAG radiation. The resulting single-frequency 532nm wavelength light was used to pump stimulated electronic Raman scattering (SERS) on the 6s-5d transition of Caesium, and allowed an accurate experimental measurement of the Raman gain coefficient for atomic Caesium which was in good agreement with theoretical prediction.

(ii) Very high power oscillator/amplifier Nd:Glass laser systems used in fusion and laser compression experiments are required to produce a very short, i.e. less than 1ns, pulse. This can be achieved by using a mode-locked oscillator followed by a fast electro-optic switch arranged to select only one spike for subsequent amplification. Alternatively, one can use a single-longitudinal mode oscillator followed by a switch to 'slice' out a 1ns pulse. The oscillator must produce a smooth temporal profile, since any random mode beating would mean that a different energy would be sliced out on every shot. Too much energy produced by the oscillator can have disastrous effects later in the amplifier chain, where optical components, such as dielectric polarisers, are operated very close to their damage threshold. This means that the oscillator must operate on a single-longitudinal mode.

(iii) In studies of vibrating systems using double pulse holography, one requires that the coherence length of the laser light be greater than the dimensions of the object under study. This indicates the need for a single mode laser in these applications.

From now on, we will restrict our discussion principally to Nd:YAG lasers, although the principles of operation and formulae we derive later in this chapter are equally applicable to other solid state lasers, e.g. ruby.

In lasers using low gain media the number of longitudinal modes on which the laser will operate can be restricted by using a simple frequency-selective element in the cavity such as a Fabry-Perot etalon (Hercher, 1969), or a resonant reflector. With Nd:YAG, however, and with most other Q-switched solid state lasers, the gain at the time of Q-switching is very large, and the Q-switched pulse takes typically a few tens of cavity round trips to build up from noise to saturation. This technique is known as 'fast' Q-switching. To restrict lasing to a single longitudinal mode an etalon with very high selectivity is needed, and this is exceedingly difficult to realise in practice. The way in which single longitudinal mode operation of the laser can be achieved with conventional frequency-selective elements is to increase the number of round trips experienced by the laser radiation before saturation occurs. This essentially means that the laser must be Q-switched in two stages. Initially the laser cavity is arranged to be very lossy so that it is operating just above lasing threshold. This gives the radiation several hundred transits of the cavity before saturation, and, with a suitable intracavity etalon or resonant reflector, the frequency spread of this radiation will have narrowed to a single longitudinal mode of the laser cavity. The Q-switch is now fully opened and the single mode radiation is amplified, thus extracting essentially all of the stored energy in the laser. In practice, this type of operation can be achieved either actively or passively. In passive Q-switching using a saturable absorber Q-switch, the low-level linear loss of the saturable dye provides the conditions required for the long pulse build-up. Subsequent bleaching of the dye then Q-switches the laser. This technique has been successfully used with both ruby (e.g. Hercher, 1965), and more recently with Nd:YAG (e.g. Owyoung and Jones, 1977) using Eastman Kodak 14015 (BDN) dye. Active Q-switching can be accomplished in four ways: fast Q-switching, two step Q-switching, pre-lase triggered Q-switching and feedback controlled Q-switching. Only the final three techniques offer the possibility of the long pulse build-up times required for single-frequency laser operation. For convenience we refer to any Q-switching technique which results in long pulse build-up times, either active or passive, as 'slow' Q-switching.

(i) Two-step Q-switching (Hanna et al., 1971). In this technique The Pockels cell Q-switch is operated at three voltage levels, illustrated in figure 4.1. Initially the voltage is set at the quarter-wave voltage of the Pockels cell, $V_{\lambda/4}$. When fast Q-switched, the voltage drops from $V_{\lambda/4}$ to 0 at time t_2. When two-step Q-switched, the driving circuitry for the Pockels cell supplies the waveform shown by the solid line in figure 4.1, where time, t_1, and voltage, V_T, are variable. V_T was set so that a weak laser pulse occurred approximately 1μs after t_1, this being the time required for the pulse to build up from noise. For their resonator (∿75cm long) this corresponds to ∿220 round trips. The frequency-selective element they used was a two-plate resonant reflector, and had sufficient selectivity to narrow the bandwidth of the laser to one longitudinal mode. At time $t_2 = t_1 + 800ns$ the voltage drops to zero as in fast Q-switching, and the stored energy is extracted in a single mode. The best output energy they obtained was 6mJ in a pulse of duration 27ns (FWHM). This corresponds to a peak power of 210kW (see section 5.2.1).

The main drawback with two-step Q-switching is that one has no control over the circulating power in the laser cavity when the Q-switch is opened fully. Since times t_1 and t_2 are fixed relative to one another and synchronised to the flashlamps, any shot-to-shot fluctuations in pump energy affect the population inversion, and hence the laser gain, at the times of switching. This leads to an uncertainty in the number of round trips experienced by the radiation before Q-switching, and therefore also in the degree of mode selection obtained. Furthermore, opening the Q-switch in two steps results in fewer cavity transits than one would like, since the first step must produce a significant net gain in the laser. One way of achieving more round trips is to allow the laser gain to pass through zero net gain slowly, thereby ensuring very slow initial growth of the laser pulse. A technique using this slow growth is known as pre-lase triggered Q-switching.

(ii) Pre-lase triggered Q-switching (Hanna et al., 1972, two papers). In this technique the Pockels cell voltage is adjusted to a value, V_T, which only just allows the laser to reach threshold. In practice this means that if the laser output is monitored on a photodiode without Q-switching the laser, about 5-10 normal mode laser spikes are observed. The Q-switch is triggered open at a time t_2, when the circulating power

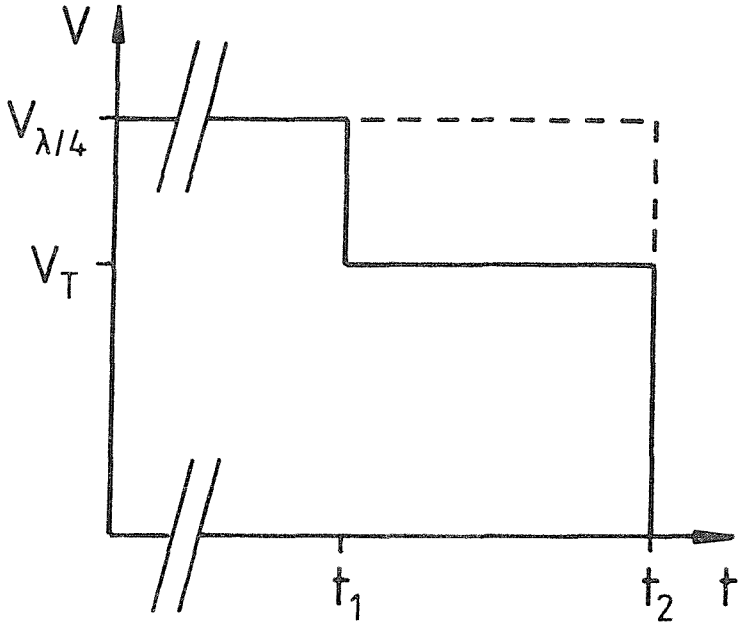

Figure 4.1: Voltage waveforms appearing at the Pockels cell Q-switch during two-step Q-switching (solid line), and 'fast', i.e. conventional, Q-switching (broken line)

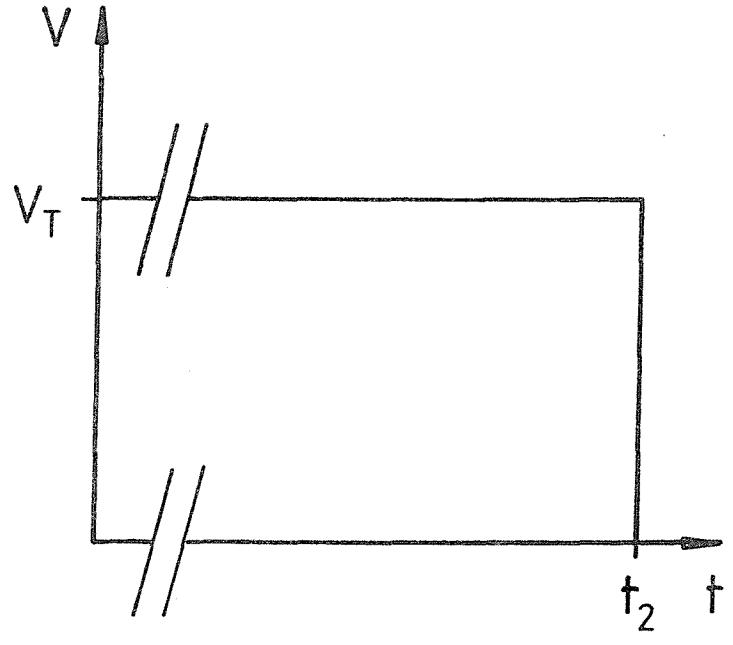

Figure 4.2: Voltage waveform appearing at the Pockels cell Q-switch during pre-lase triggered Q-switching

in the laser cavity reaches a preset trigger level. This is achieved by monitoring (with a photodiode) the laser light rejected by the intracavity polariser, as shown in figure 4.3. The signal from the photodiode triggers a Marx bank voltage multiplier to provide a high voltage, fast risetime signal (∿1kV, 5ns) to trigger the Krytron Pockels cell switch. Frequency selection was accomplished by using either a two-plate resonant reflector, or a tilted intracavity etalon.

We restrict ourselves to this rather brief description of pre-lase triggered Q-switching since the technique is discussed in some detail in the later sections of this chapter.

(iii) Feedback controlled Q-switching (Luther-Davies and Del Pizzo, 1979). In this scheme, shown schematically in figure 4.3, very long build-up times (∿100μs) are achieved in the following way. With the photodiode blocked and no trigger signal applied to the Q-switch, the D.C. bias +V is adjusted so that normal mode lasing just occurs. (As with pre-lase triggered Q-switching, this means that in practice a few normal mode spikes are observed.) The level of radiation within the cavity is monitored using a photodiode. The signal from the photodiode is amplified using an H.F. amplifier capable of a maximum output signal of 300V with a risetime <15ns. The amplified signal is returned to the P.C. in such a way that an increase in laser output tends to increase cavity losses. This use of negative feedback gives stabilisation of the laser output, and Luther-Davies has shown that such an arrangement can give low-level output pulses lasting ∿100μs. At some time in this 100μs window the trigger signal is applied to the P.C. crowbar switch to open the Pockels cell. The precise switching time during this 100μs does not appear to be critical. These figures represent ∿5 x 10^4 cavity round trips for his experimental arrangement, or approximately 100 times the number of round trips that one can obtain using pre-lase triggered Q-switching. This relaxes the requirements for frequency-selective elements dramatically: Luther-Davies reports reliable single-mode operation using only a thin, single-plate uncoated resonant reflector output coupler as a reflection etalon.

In the next sub-section of this chapter we review the existing theory of linewidth narrowing (Sooy, 1965; Hanna et al, 1972), and derive expressions for the degree of narrowing that can be expected in cases of particular experimental interest. These are (i) Fast Q-

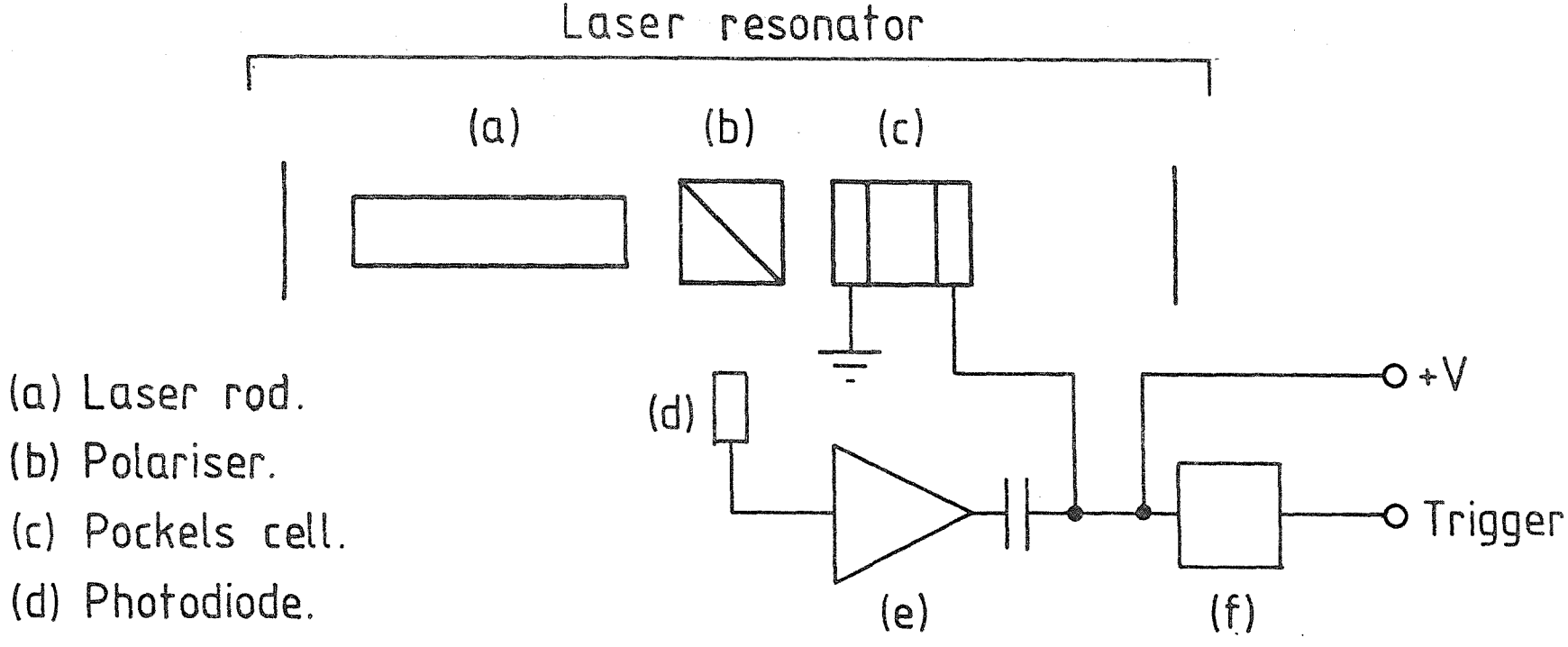

Figure 4.3: Feedback controlled Q-switching

switching, both with and without frequency selection, (ii) Slow Q-switching, also with and without frequency selection. Operation of the laser without frequency selection means that no frequency-selective optical elements are incorporated in the cavity, and the final linewidth develops as a result of gain narrowing of the laser fluorescence. In the case of additional frequency selection we restrict our discussion to the use of intracavity transmission etalons or single-plate resonant reflectors, although in principle the analyses we present can also be applied to laser cavities containing dispersive prisms, diffraction gratings or birefringent filters. It will be shown that one convenient practical way of achieving single-frequency laser operation in a high-gain solid state Q-switched laser is by using slow Q-switching with frequency selection. The other cases discussed give varying degrees of linewidth narrowing, and the analyses are included since in some applications it may be desirable to restrict the laser linewidth without necessarily using single-mode radiation.

We turn our attention now to single-frequency operation, and to some of the problems associated with obtaining reliable operation of a single-mode laser system. One can find that a design based on the equations derived in section 4.2 has more than adequate mode selection in principle, but in practice produces disappointing results. There are three principal reasons why this should be so.

(i) In the analysis of slow Q-switching presented in section 4.2, it is assumed that a transmission peak of the mode selecting etalon is centred on the gain maximum of the laser emission. (For illustration we assume here that mode selection is accomplished using an intracavity transmission etalon, but the following argument is equally valid for other frequency-selective devices.) It is further assumed that a longitudinal mode of the laser cavity is coincident with these. In practice, it is easy to ensure that the etalon is correctly tuned to the laser line centre by angle tuning and temperature control, but for most conventional laser cavities it is more difficult to control the laser mode frequency. This is because the resonator is a large structure which contains a long air path and is therefore subject to mechanical and thermal changes which make frequency stabilisation that much more difficult. This has a severe effect on the calculated degree of mode selectivity. We illustrate this by anticipating two results from later sections of this chapter.

One finds that for a laser which is slow Q-switched and incorporates mode selection, the ratio of the powers at the strongest lasing mode, P_n, and the adjacent mode, P_m, is given by

$$\frac{P_n}{P_m} \simeq e^{\varepsilon q_{eff}} \quad \text{for} \quad \varepsilon << 1,$$

where ε is a dimensionless number which is a measure of the degree of mode selection and q_{eff} is the number of round trips of growth before Q-switching. A typical value for ε is 5×10^{-2}, and from section 4.2 we find $q_{eff} \simeq 500$ implying that the ratio of mode powers is

$$\frac{P_n}{P_m} = 7.2 \times 10^{10}.$$

This would appear to be more than adequate mode selection. If we now allow the laser modes to be positioned randomly from shot-to-shot, and ask what is the ratio of single-mode to two-mode shots, we find (section 4.3.1)

$$r = \varepsilon\left[\frac{q_{eff}}{\ell nN}\right] - 1,$$

where $\frac{P_n}{P_m} > N$ is our criterion for single-mode operation. Typically we might take $N = 10^4$ to be an acceptable ratio of mode powers, and using values for δ and q from above we find $r = 1.7$, indicating that only 63% of the shots will be single-frequency by our criterion $N > 10^4$. Clearly, this means that one must interpret calculations of mode selectivity with some care.

(ii) Perturbations to the cavity length of mirror alignment during the build-up time of the single-mode pulse will reduce the effective degree of mode selection, since these will result in scanning of the mode frequencies of the laser. There are three possible causes of such perturbations. Firstly, thermal scanning of the laser rod optical thickness during the flashlamp pump pulse. Secondly, air turbulence in exposed sections of the laser cavity causing local refractive index changes in the air. Thirdly, vibration of the optical rail on which the laser is assembled. This can be caused by ambient noise in the laboratory or the mechanical shock delivered by the flashlamps as they discharge.

These effects can all be measured or estimated. The amount by which the laser rod changes optical thickness may be calculated from the physical and optical properties of the laser host and the estimated heat input to the rod. Vibrations of the rail may be measured interferometrically, but air turbulence effects are more difficult to quantify. Calculations and measurements of these effects for the laser system described in this thesis are presented in section 4.3.2.

(iii) It is possible for the Pockels cell Q-switch to introduce a change in effective cavity length on a nanosecond time scale during switching. This occurs if the x and y crystallographic axes of the Q-switch crystal are not aligned parallel and perpendicular to the polarisation of the laser. In this case, the Pockels cell introduces a voltage-dependent phase shift which can shift the cavity mode frequencies when the Pockels cell bias voltage is removed. This means that the single-mode which has developed during the pulse build-up time is no longer matched to the cavity modes after Q-switching and therefore experiences a lower loop gain. Other modes could then subsequently grow faster than this initially favoured mode and thus lead to a significantly broadened bandwidth in the final output. In section 4.3.3 we derive an expression for the voltage-dependent phase shift, and conclude that for our experimental arrangement a significant phase shift is possible only in cases of gross misalignment.

A further source of cavity-mode frequency displacement results from the presence of an intracavity etalon (Bhawalkar et al., 1977). Associated with each etalon transmission maximum is a corresponding frequency-dependent phase shift. This leads to frequency pulling of modes adjacent to the selected mode, and this effect must be taken into account when performing mode selection calculations since it can reduce the degree of mode selection. In section 4.3.4 we briefly review the theory developed by Bhawalkar, which results in an equation which can only be solved numerically, and also present an approximate solution which can be used to easily deduce whether the effect is significant for a particular experimental arrangement. Calculations performed for the cavity under study in this thesis indicate only a 5% shift in cavity modes, so the effect is only of minor significance.

4.1.1 A note on notation

In order to present equations in a compact and simple form, we use the following notations.

(i) Linewidths are all full width at half maximum, and have the symbol Γ, subscripted to identify which particular linewidth is being referred to. For instance, the laser linewidth when slow Q-switched would be Γ_{SQ}, and the laser fluorescence linewidth would be Γ_F.

(ii) The free spectral range of an etalon or interferometer has the symbol Δ, again subscripted as appropriate. We use, for instance, Δ_L to represent the intermode spacing of the laser resonator, and Δ_E for the free spectral range of an etalon.

(iii) We characterise a mode selecting etalon by the parameters Δ_E, F_E and C_E; the free spectral range, transmission finesse and contrast of the etalon respectively. It will be found that equations for mode selectivity take a particularly simple form if they are expressed in terms of Δ_E, C_E, although it is sometimes convenient to use finesse instead of contrast to illustrate certain points, and so we use both C_E and F_E throughout this chapter. Δ_E, F_E and C_E are related to the refractive index, n, thickness, t, and face reflectivities R_1, R_2, by the following well-known relations

$$\Delta_E = \frac{1}{2nt}$$

$$F_E = \frac{\pi\sqrt{R}}{(1 - R)} \qquad \text{I a,b,c,d}$$

$$C_E = \frac{(1 + R)^2}{(1 - R)^2}$$

where $R = \sqrt{R_1 R_2}$.

4.2 Review of the Theory of Laser Linewidth

In this section we derive expressions for the laser linewidth for four cases of experimental interest: (i) Fast Q-switching in the absence of mode selection, (ii) Fast Q-switching, but with additional

mode selection, (iii) Slow Q-switching in the absence of mode selection, (iv) Slow Q-switching, but with additional mode selection. We assume that mode selection is accomplished by using either an intracavity transmission etalon, or a single-plate resonant reflector.

To facilitate calculations performed in this chapter, a number of relevant parameters have been collected in table 4.1. The properties of Nd:YAG have been drawn from Koechner (1976), and the laser parameters apply to the telescopic resonator discussed in Chapter Three and also in the final sections of this chapter.

We begin by deriving expressions for the growth of a laser cavity mode of frequency ω_n. The final results, equations 4.6 and 4.12, correspond to those obtained by Sooy (1965), but are derived in a different, and more general way. The total power gain at time t for one round trip of the laser cavity is determined by

$$G_n(t) = R_{1n}R_2\exp\{2\sigma_n N(t)\ell\} \qquad 4.1$$

where σ_n is the stimulated emission cross-section for the n^{th} cavity mode, N(t) is the population inversion at time t, ℓ is the length of the laser medium, and R_{1n}, R_2 are the resonator reflectivities. R_{1n} is subscripted with an n to model a frequency-dependent reflectivity or cavity loss. Note that equation 4.1 is only valid above laser threshold.

Suppose the n^{th} laser mode reaches threshold at time t_n, and in general $t = t_n + q_nT$, where q_n is the number of cavity round trips after threshold has been reached for mode n, and T is the cavity round trip time. We can then write

$$G_n(t_n + q_nT) = R_{1n}R_2\exp\{2\sigma_n N(t_n + q_nT)\ell\} \qquad 4.2$$

The intracavity power grows from a noise power, P_{n0}, at time t_n, reaching a value after q_n round trips of

$$P_n(t_n + q_nT) = P_n(t_n + (q_n - 1)T)G_n(t_n + (q_n - 1)T) \qquad 4.3$$

which can easily be deduced by considering the first round trip after threshold is reached, when the power has grown from P_{n0} to $P_n(t_n + T) = P_{n0}G_n(t_n)$, and generalising to the q_n^{th} round trip. One

Table 4.1: Numerical data on Nd:YAG, and laser parameters relevant to numerical examples included in this chapter

(a) Physical and Optical Properties of Nd:YAG
(taken from Koechner (1976))

Specific heat, σ_h	$0.59 Wsg^{-1}K^{-1}$
Thermal expansion coefficient, k	$7.5 \times 10^{-6}C^{-1}$
dn/dT	$7.3 \times 10^{-6}K^{-1}$
Fluorescence linewidth, Γ_F	$4.0 cm^{-1}$
Stimulated emission cross-section, $\sigma(\omega_0)$	$8.8 \times 10^{-19} cm^2$
Laser transition frequency, ω_0	$9398 cm^{-1}$
Photon energy at 1.06μm	$1.86 \times 10^{-19} J$
Refractive index at 1μm, n	1.82
Density	$4.65 gcm^{-3}$

(b) Laser Parameters

Laser rod length, ℓ	7.5cm
Laser rod diameter, ϕ	9.5mm
Laser rod volume, V	$5.32 cm^3$
Resonator optical length, L	1.3m
Resonator free spectral range, $\Delta_L = 1/2L$	$3.85 \times 10^{-3} cm^{-1}$
Round trip time, T = 2L/c	8.67ns
Pumping pulse duration	200μs

can now show by induction that $P_n(t_n + q_nT)$ is given by

$$P_n(t_n + q_nT) = P_{n0}\prod_{p=1}^{q_n} G_n(t_n + (q_n - p)T) \qquad 4.4$$

Substituting for $G(t_n + (q_n - p)T)$ from equation 4.1 into equation 4.4 gives

$$P_n(t_n + q_nT) = P_{n0}(R_{1n}R_2)^{q_n}\exp\left\{2\sigma_n\ell \sum_{p=1}^{q} N(t_n + (q_n - p)T)\right\} \qquad 4.5$$

which we now apply separately to fast and slow Q-switching.

(a) Fast Q-switching. When fast Q-switched, the loop gain of our Nd:YAG laser at the time of maximum inversion is so large that only ∿30 cavity round trips are required for the giant pulse to build up from noise (see Appendix 2). This corresponds to ∿0.26μs for a cavity length (optical) of 1.3m, and is much less than the pump pulse duration (∿200μs). Thus, only a small change in the inversion occurs during this pulse build-up period, and $N(t_n + (q_n - p)T) = N(t_s) \simeq$ constant, where t_s is the time at which switching occurs. In this case, equation 4.5 simply reduces to

$$P_n(t) = P_{n0}(R_{1n}R_2)^{q_n}\exp\left\{2\sigma_n\ell N(t_s)\right\}^{q_n} \qquad 4.6$$

The term inside the exponential accounts for normal gain narrowing (in Sooy's terminology 'gain differentiation'), and the term $(R_{1n}R_2)^{q_n}$ takes into account additional mode selection incorporated into the laser cavity ('loss differentiation').

(b) Slow Q-switching. For slow Q-switching we have to include the time-dependence of the inversion since this is responsible for pushing the loop gain above unity. Using Sooy's notation we write

$$N(t) = \gamma t - \mu \qquad 4.7$$

where $\gamma = dN(t)/dt$ is the pumping rate. Use of a constant pump rate is justified since the amount of time required for pulse growth is still much less than the pump pulse duration. (An analysis of the conditions in our laser indicates that pulse growth takes place over ∿5μs, whereas

the pump pulse duration is ∿200μs.)

From equation 4.7 we find that the required form for the population inversion for insertion into equation 4.5 is

$$N(t_n + (q_n - p)T) = N(t_n) + \gamma T(q_n - p) \qquad 4.8$$

and it is easily shown that

$$\sum_{p=1}^{q_n} N(t_n + (q_n - p)T) = q_n(N(t_n) + \frac{\gamma T}{2}(q_n - 1)) \qquad 4.9$$

Further, the threshold condition for the population inversion, defined by $G_n(t_n) = 1$, yields for $N(t_n)$

$$N(t_n) = - \frac{\ell n(R_{1n}R_2)}{2\sigma_n \ell} \qquad 4.10$$

From equations 4.5, 4.9 and 4.10, we find the mode power after q_n round trips is given by

$$P_n(t_n + q_nT) = P_{n0}\exp\{\sigma_n \ell \gamma T q_n(q_n - 1)\} \qquad 4.11$$

which can be written in its more familiar form by inserting $q_n = (t - t_n)/T$ and approximating $q_n - 1 \simeq q_n$ (usually a good approximation. We shall see shortly that q_n is typically greater than 100). This gives

$$P_n(t) = P_{n0}\exp\{\sigma_n \ell \gamma (t - t_n)^2/T\} \qquad 4.12$$

For later use, and also for illustration, we will now obtain numerical estimates for γ and q_n. A measurement of the stored energy in the laser rod was made by using a simple two-mirror resonator comprising a 5m radius of curvature 100% reflectivity mirror and a single-plate resonant reflector separated by 1m. The discharge capacitors were set to 750V, corresponding to a pump energy of 56J with a repetition rate of 12Hz. These are typical values used when the laser system is run on a day-to-day basis. The multimode fixed Q output obtained in this way was ∿800mJ, and is a measure of the total stored energy in the $^4F_{3/2}$ upper laser level. However, only the R_2 sub-level contributes to the laser gain, and this contains 40% of the stored energy. We therefore

calculate an inversion density of $3.2 \times 10^{17} cm^{-3}$, using values from table 4.1. A rough estimate of γ can be obtained by assuming that the population inversion increases linearly with time over the flashlamp pump pulse duration. We therefore find $\gamma \simeq 3.2 \times 10^{17}/200 \times 10^{-6} = 1.6 \times 10^{21} cm^{-3} s^{-1}$. To calculate q_n we first consider the intracavity power level at which the photodetector triggers the Q-switch. (The photodetector was located at the high reflectivity mirror, whose transmission was 7%.) For the photodetector used, a Hewlett-Packard 5082-4220 PIN photodiode, we find the following relevant parameters: Responsivity at 1.06μm $\simeq 5 \times 10^{-2} AW^{-1}$, sensitive area $= 2 \times 10^{-3} cm^2$. The triggering level of the electronics is 1V across a load resistance of 50Ω, and we therefore calculate a total beam power of 25W to trigger the Q-switch, taking into account that the detector samples only a small fraction of the laser beam (whose area is $0.13 cm^2$ for the telescopic resonator). The intracavity beam power at the time of triggering is therefore 25/0.07 = 360W. For a single-mode pulse of 30ns duration we calculate a starting noise power $P_{n0} \simeq 2.7 \times 10^{-12} W$ (Appendix 2). Thus, the exponent in equation 4.11 is simply $\ell n(360/2.7 \times 10^{-12}) = 32$. Inserting parameter values from table 4.1 into equation 4.11, we calculate q = 620. Note that although we have calculated q for our particular experimental arrangement, the total number of cavity transits is rather insensitive to the actual values taken for $P_n(t)$ and P_{n0}. However, this value of q must be regarded as an underestimate, since the pump rate, γ, is not constant over the pump pulse duration. In practice, the variation of inversion with time would have a smooth maximum, and Q-switching would be effected just prior to the maximum. Hence γ could be less than, and consequently q greater than, the simple estimates obtained above.

To clarify the application of equations 4.6, 4.11 and 4.12 to fast and slow Q-switching, we preface the following sub-sections with some general comments on line narrowing.

Around the time of maximum laser output, the spectrum of the laser will, in general, contain a number of cavity modes, with frequency spacing Δ_L, illustrated in figure 4.4(a). The peak power in each mode is determined by an envelope function which results from gain narrowing and the presence (if any) of frequency selective intracavity components. The linewidth of the laser is defined as the FWHM of the envelope function. This condition can be written

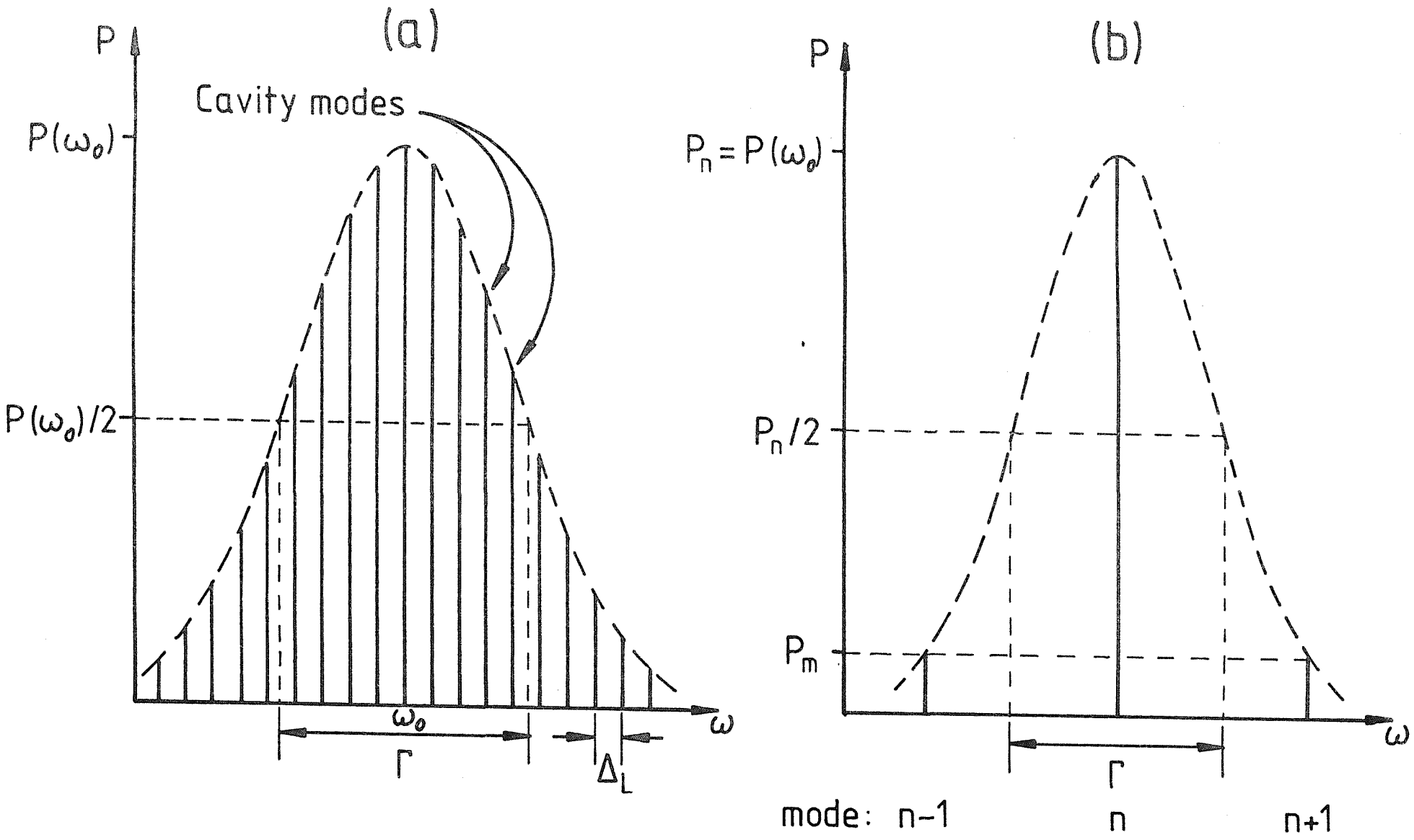

Figure 4.4: (a) Frequency spectrum of a multi-longitudinal mode laser

(b) Frequency spectrum of a single-longitudinal mode laser

$$P(\omega_0 \pm \Gamma/2) = P(\omega_0)/2 \qquad 4.13$$

and we note that $\Gamma/2$ need not correspond to an integral number of cavity mode spacings. This quite general definition of linewidth applies whatever the degree of narrowing; however, for 'single-mode' laser operation, illustrated in figure 4.4(b), which we define formally by the inequality

$$\Gamma < 2\Delta_L \qquad 4.14$$

a more relevant quantity is the ratio of cavity mode powers for adjacent modes, P_n/P_m, with $m = n \pm 1$. In the following analysis we always assume mode n is coincident with the envelope peak at frequency ω_0, unless otherwise stated.

In the case $\Gamma > 2\Delta_L$, i.e. multi-longitudinal mode operation, we find it useful to rewrite equations 4.6 and 4.12 as a continuous function of frequency, which can be obtained formally by allowing Δ_L to tend to zero. Hence, equation 4.6 becomes

$$P_\omega(t) = P_0(R_\omega R_2)^{q_\omega}\exp\{2\sigma(\omega)\ell N(t_s)\}q_\omega \qquad 4.15$$

and 4.12

$$P_\omega(t) = P_0\exp\{\sigma(\omega)\ell\gamma(t - t_\omega)^2/T\} \qquad 4.16$$

where we have dropped the frequency-dependence from the noise power (This approximation is justified since frequency differences $\omega_n - \omega_m$ are small in comparison to the laser frequency ω_0.), and also the numerical subscript from R_1 for clarity,

4.2.1 Fast Q-switching with no additional mode selection

From equation 4.15, we find the ratio of powers for frequencies ω_1 and ω_2

$$\frac{P_{\omega 1}(t_s)}{P_{\omega 2}(t_s)} = \exp\{2(\sigma(\omega_1) - \sigma(\omega_2))\ell N(t_s)\}q \qquad 4.17$$

where it has been assumed that frequencies ω_1 and ω_2 reach threshold at

the same time, so that $q_{\omega 1} = q_{\omega 2} = q$.

To calculate the laser linewidth, we consider the case where $\omega_1 = \omega_0$, $\omega_2 = \omega_0 \pm \Gamma_{FQ}/2$, and use equation 4.13 to write $P_{\omega 0}(t_s)/P_{\omega 2}(t_s) = 2$. The fluorescence has a Lorentzian lineshape given by

$$\sigma(\omega) = \sigma(\omega_0) / \left[1 + (2(\omega - \omega_0)/\Gamma_F)^2\right] \qquad 4.18$$

centred at $\omega = \omega_0$ with a linewidth Γ_F. Writing $\omega - \omega_0 = \omega_2 - \omega_0 = \pm \Gamma_{FQ}/2$, where Γ_{FQ} is the fast Q-switched laser linewidth, we find

$$\sigma(\omega_0) - \sigma(\omega_2) = \sigma(\omega_0)(\Gamma_{FQ}/\Gamma_F)^2 / \left[1 + (\Gamma_{FQ}/\Gamma_F)^2\right] \qquad 4.19$$

Inserting these results into equation 4.17 and solving for Γ_{FQ}/Γ_F gives

$$\frac{\Gamma_{FQ}}{\Gamma_F} = \left\{ \frac{\ell n 2}{2\sigma(\omega_0)\ell N(t_s)q - \ell n 2} \right\}^{\frac{1}{2}} \qquad 4.20$$

The $\ell n 2$ in the denominator of equation 4.20 can usually be ignored, since it will be found that $2\sigma(\omega_0)\ell N(t_s)q >> \ell n 2$ for typical parameter values, and so the Q-switched laser linewidth is then given by

$$\Gamma_{FQ} = \Gamma_F \left\{ \frac{\ell n 2}{2\sigma(\omega_0)\ell N(t_s)q} \right\}^{\frac{1}{2}} \qquad 4.21$$

We estimate that for a typical loop gain of 3, the number of round trips required to bring the intracavity power up to the megawatt level (a typical saturation level) is about 30 (Appendix 2), so using $N(t_s) = 3.2 \times 10^{17} cm^{-3}$ from the earlier example in this section we calculate $\Gamma_{FQ} = 0.29 cm^{-1}$, where we have made use of table 4.1 for the remaining parameters. Because of the square root dependence of linewidth on the various parameters in equation 4.21, and the insensitivity of q to the values taken for starting noise power and final laser power, we find that the Q-switched laser linewidth remains fairly constant for quite large changes in operating conditions.

4.2.2 Fast Q-switching with additional mode selection

We must now take account of the frequency dependence of the mirror reflectivity, and obtain from equation 4.15

$$\frac{P_{\omega 1}(t_s)}{P_{\omega 2}(t_s)} = \left[\frac{R_{\omega 1}}{R_{\omega 2}}\right]^q \exp\{2(\sigma(\omega_1) - \sigma(\omega_2))\ell N(t_s)\}q \qquad 4.22$$

where we have again assumed that all the modes reach threshold simultaneously. Proceeding in the same way as we did in section 4.2.1 by putting $\omega_1 = \omega_0$, $P_{\omega 0}(t_s)/P_{\omega 2}(t_s) = 2$, we obtain

$$\exp\left\{2(\sigma(\omega_0) - \sigma(\omega_2))\ell N(t_s) + \ell n\left[\frac{R_{\omega 0}}{R_{\omega 2}}\right]\right\}q = 2 \qquad 4.23$$

Writing $\frac{R_{\omega 0}}{R_{\omega 2}} = 1 + \varepsilon$, where $\varepsilon = \varepsilon_R$ or ε_T for a resonant reflector or intracavity transmission etalon respectively. We show in section 4.2.5 that $\varepsilon_R = (\pi\Gamma_{FQE}/2\Delta_E)^2/C_E$ and $\varepsilon_T = 2(F_E\Gamma_{FQE}/\Delta_E)^2$ where $\Gamma_{FQE} = 2\Delta$ is the final laser linewidth. In practice one finds that ε_R, ε_T are much less than unity, so we can write $\ell n(R_{1n}/R_{1m}) \simeq \varepsilon$. Using equation 4.18 we find $\sigma(\omega_0) - \sigma(\omega_2) \simeq \sigma(\omega_0)(\Gamma_{FQE}/\Gamma_F)^2$. Inserting these results into equation 4.23 yields

$$\varepsilon\left[2\sigma(\omega_0)\ell N(t_s)\left[\frac{\Gamma_{FQE}}{\Gamma_F}\right]^2\frac{1}{\varepsilon} + 1\right]q = \ell n2 \qquad 4.24$$

Using typical values $\Gamma_{FQE}/\Gamma_F = 10^{-2}$, $\varepsilon = 10^{-2}$ and values for other parameters from table 4.1, we find the quantity in brackets $\simeq 1 + 4 \times 10^{-2} \simeq 1$. Inserting ε_R, ε_T in equation 4.24 gives

$$\Gamma_{FQE} = \left[C_E\frac{\ell n2}{q}\right]^{\frac{1}{2}}\frac{2\Delta_E}{\pi} \quad \text{for a resonant reflector} \qquad 4.25(a)$$

$$\Gamma_{FQE} = \left[\frac{\ell n2}{q}\right]^{\frac{1}{2}}\frac{\Delta_E}{F_E} \quad \text{for a transmission etalon} \qquad 4.25(b)$$

Typically one might use an uncoated resonant reflector output coupler with $\Delta_E = 0.5\text{cm}^{-1}$, $C_E \simeq 1$. Using $q = 32$, equation 4.25(a)

gives $\Gamma_{FQE} = 0.047\text{cm}^{-1}$. For an intracavity transmission etalon with $\Delta_E = 0.5\text{cm}^{-1}$, $F_E = 5$ equation 4.25(b) gives $\Gamma_{FQE} = 0.015\text{cm}^{-1}$. These examples show that with the introduction of a mode selector of only modest selectivity, e.g. an uncoated plate output coupler or a low finesse intracavity etalon, one can obtain a significant narrowing of the laser linewidth (c.f. 0.29cm^{-1} with no mode selection). However, with a 1.3m optical length resonator these linewidths still represent several longitudinal modes lasing with comparable power.

4.2.3 Slow Q-switching with no additional mode selection

Using equation 4.16 we write the ratio of mode powers

$$\frac{P_{\omega 1}(t_s)}{P_{\omega 2}(t_s)} = \frac{\exp\{\sigma(\omega_1)\ell\gamma(t_s - t_{\omega 1})^2/T\}}{\exp\{\sigma(\omega_2)\ell\gamma(t_s - t_{\omega 2})^2/T\}} \qquad 4.26$$

where t_s is the time at which switching occurs. We now have to take account of the fact that different modes reach threshold at different times. We will see in section 4.2.4 that this can have the effect of reducing the expected amount of mode selection for slow Q-switched lasers incorporating frequency-selective elements. However, in the present context it has little effect under our typical operating conditions.

We now put $\omega_1 = \omega_0$, and using equation 4.10 find

$$N(t_{\omega 0})(\sigma(\omega_0) - \sigma(\omega_2)) - \sigma(\omega_2)\gamma(t_{\omega 2} - t_{\omega 0}) = 0 \qquad 4.27$$

Substituting for $\sigma(\omega_0) - \sigma(\omega_2)$ from equation 4.18 into equation 4.27, assuming $(\Gamma_{SQ}/\Gamma_F)^2 << 1$, and $\sigma(\omega_0) \simeq \sigma(\omega_2)$, gives the difference between the times that frequencies ω_0 and ω_2 reach threshold as

$$t_{\omega 2} - t_{\omega 0} = t_p \left[\frac{\Gamma_{SQ}}{\Gamma_F}\right]^2 \qquad 4.28$$

where $t_p = N(t_n)/\gamma$ is the pump pulse duration. Using equation 4.28 in equation 4.26, using $P_{\omega 0}(t_s)/P_{\omega 2}(t_s) = 2$ and ignoring terms in $(\Gamma_{SQ}/\Gamma_F)^4$ and $(\Gamma_{SQ}/\Gamma_F)^6$ we find, after some algebra

$$\frac{\Gamma_{SQ}}{\Gamma_F} = \left\{ \frac{\ell n 2}{2\sigma(\omega_0)\ell N(t_s) q \left[1 + qT/2t_p\right]} \right\}^{\frac{1}{2}} \qquad 4.29$$

The second term in the square brackets accounts for modes m and n reaching threshold at different times. Inserting values for q = 620, T = 8.67ns and t_p = 200μs gives $qT/2t_p = 1.3 \times 10^{-2} << 1$, and this allows us to rewrite equation 4.29 as

$$\Gamma_{SQ} = \Gamma_F \left\{ \frac{\ell n 2}{2\sigma(\omega_0)\ell N(t_n) q} \right\}^{\frac{1}{2}} \qquad 4.30$$

Note that this is exactly the same as equation 4.21 for fast Q-switching with no extra mode selection. This is as one would expect, since the mechanism is identical in the two cases, namely gain narrowing. Inserting the same parameter values into equation 4.30 as we did for equation 4.21, but replacing q with the value appropriate for slow Q-switching, q = 620 gives $\Gamma_{SQ} = 0.066\text{cm}^{-1}$. For a 1.3m long resonator, this value corresponds to ∿17 longitudinal modes, and indicates that additional mode selection is required to secure operation on only one mode.

4.2.4 Slow Q-switching with additional mode selection

One can easily verify that the laser linewidth for a slow Q-switched laser incorporating a frequency-selective etalon is given by equation 4.25. This equation may be used to deduce the amount of narrowing produced as a result of spurious etalon effects within the laser cavity caused by uncoated parallel surfaces. However, in practice one is more concerned with this technique as a way of securing single-mode laser operation, and it is therefore more relevant to consider the ratio of adjacent mode powers rather than the laser linewidth.

From equation 4.12 we find

$$\frac{P_n(t_s)}{P_m(t_s)} = \frac{\exp\{\sigma_n \ell\gamma (t_s - t_n)^2/T\}}{\exp\{\sigma_m \ell\gamma (t_s - t_m)^2/T\}} \qquad 4.31$$

This can be rewritten in the following form

$$\frac{P_n(t_s)}{P_m(t_s)} = \exp\{\sigma_m \ell\gamma\left[(t_s - t_n)^2 - (t_s - t_m)^2\right]/T\}$$
$$\times \exp\{\ell\gamma(t_s - t_n)^2(\sigma_n - \sigma_m)/T\} \qquad 4.32$$

Whence

$$\frac{P_n(t_s)}{P_m(t_s)} = \exp\{\sigma_m \ell\gamma\left[-(t_n - t_m)((t_s - t_n) + (t_s - t_m))\right]/T\}$$
$$\times \exp\{\ell\gamma(t_s - t_n)^2(\sigma_n - \sigma_m)/T\} \qquad 4.34$$

Consider the second exponential term in equation 4.3.4. This can be rewritten as

$$\exp\{\sigma_n \ell\gamma(t_s - t_n)^2/T\} \left\{1 - \frac{\sigma_m}{\sigma_n}\right\} ,$$

and we recognise the term in the first set of curly brackets as the quantity we calculated at the end of the introduction to this section, ≈32. One can easily show that $1 - \sigma_m/\sigma_n \simeq (2\Delta_L/\Gamma_F)^2 = 3.7 \times 10^{-6}$ for our example, so we can safely set the exponential term equal to unity, and $\sigma_m/\sigma_n = 1$. Therefore

$$\frac{P_n(t_s)}{P_m(t_s)} = \left\{\frac{R_{1n}}{R_{1m}}\right\}^{(q_m + q_n)/2} \qquad 4.35$$

This expression differs from that obtained by Sooy in the power to which the round trip mode discrimination, R_{1n}/R_{1m}, is raised. In Sooy's analysis the approximation $t_s >> t_m - t_n$ was used, with the result that $(q_m + q_n)/2 \equiv q$. However, this approximation is only valid for small amounts of mode selectivity. One can see this by using equations 4.7 and 4.10 to write q_{eff} in terms of q_n and ε

$$q_{eff} = \frac{q_m + q_n}{2} = q_n - \frac{\varepsilon}{4\sigma(\omega_0)\gamma\ell T} \qquad 4.36$$

where q_{eff} is the effective number of round trips and $\varepsilon \equiv \varepsilon_T = 8(F_E\Delta_L/\Delta_E)^2$ for a transmission etalon (see section 4.2.5). For typical values quoted in table 2.1, we find the effective number of round trips $q_{eff} = 620 - 140 = 480$. This represents a significant decrease in mode selectivity compared with the assumption $q_{eff} = 620$: taking $q_{eff} = 620$ gives $P_n(t_s)/P_m(t_s) = 5.0 \times 10^{13}$, and with $q_{eff} = 480$ $P_n(t_s)/P_m(t_s) = 4.0 \times 10^{10}$. Note that equations 4.35 and 4.36 are only valid if mode m actually reaches threshold before switching occurs. This is because the equation we used as our starting point, equation 4.1, is only valid above laser threshold.

4.2.5 Mode selection using Fabry-Perot etalons

We conclude section 4.2 by considering the mode selectivity introduced by using either a resonant reflector or an intracavity transmission etalon.

(i) Resonant reflector

Consider a resonant reflector whose faces have power reflectivities R_1, R_2. At normal incidence the etalon power reflectivity is given by

$$r = \frac{(\sqrt{R_1} - \sqrt{R_2})^2 + 4R\sin^2\delta/2}{(1 - R)^2 + 4R\sin^2\delta/2} \qquad 4.37$$

where $\delta/2 = 2\pi nt/\lambda$, $R = \sqrt{R_1R_2}$, n and t are the refractive index and thickness of the etalon and λ is the wavelength. We show in Appendix 3 that the optimum discrimination between adjacent cavity modes is obtained for $R_1 = R_2$, whence equation 4.37 reduces to

$$r = \frac{4R}{(1 - R)^2} \frac{\sin^2\delta/2}{1 + \frac{4R}{(1 - R)^2}\sin^2\delta/2} \qquad 4.38$$

Consider the case where a reflection maximum of the etalon is coincident with the laser fluorescence maximum, frequency ω_0. In the notation used earlier we can write

$$R_{\omega 0} = \frac{4R}{(1 + R)^2} \qquad 4.39$$

For a frequency ω displaced by $\Delta = \omega_0 \pm \omega$ from the reflection maximum one can easily show that

$$R_\omega \simeq \frac{4R}{(1+R)^2} \cdot \frac{1}{1 + \left[\pi\frac{\Delta}{\Delta_E}\right]^2 \frac{1}{C_E}} \qquad 4.40$$

where C_E is the contrast of the etalon, $C_E = \left[\frac{1+R}{1-R}\right]^2$. We therefore find the frequency discrimination, $\frac{R_{\omega 0}}{R_\omega}$, for one round trip is

$$\frac{R_{\omega 0}}{R_\omega} \simeq 1 + \varepsilon_R \qquad 4.41(a)$$

where

$$\varepsilon_R = \left[\pi\frac{\Delta}{\Delta_E}\right]^2 \frac{1}{C_E} \qquad 4.41(b)$$

is the fractional mode discrimination per round trip

Note that the maximum value of ε_R occurs for $R = 0$, $C_E = 1$, and is given by

$$\varepsilon_{RMAX} = \left[\pi\frac{\Delta}{\Delta_E}\right]^2$$

(ii) Intracavity transmission etalon

A similar analysis for a transmission etalon yields the frequency discrimination per round trip

$$\frac{R_{\omega 0}}{R_\omega} \simeq 1 + \varepsilon_T \qquad 4.42(a)$$

where

$$\varepsilon_T = 2\left[\pi\frac{\Delta}{\Delta_E}\right]^2 (C_E - 1) = 2\left[\frac{2\Delta F_E}{\Delta_E}\right]^2 \qquad 4.42(b)$$

In contrast to the resonant reflector, one can in principle obtain as large a value of mode selectivity as required by using a high reflectivity coated etalon, since $C_E \to \infty$ as $R \to 1$. In practice, other factors such as absorption in the plate material and walk-off loss limit the maximum attainable finesse. The factor of two in equation 4.42(b) as compared with equation 4.41(b) arises from the fact that light passes through the transmission etalon twice per cavity round trip,

but only once in the case of a resonant reflector.

From equation 4.35 we obtain for the ratios of mode powers the expressions

$$\frac{P_n(t_s)}{P_m(t_s)} = e^{\epsilon_R q_{eff}} \quad \text{for a reflection etalon} \qquad 4.43(a)$$

$$= e^{\epsilon_T q_{eff}} \quad \text{for a transmission etalon} \qquad 4.43(b)$$

where ϵ_R, ϵ_T are given by equations 4.41(b) and 4.42(b) respectively, and we have made use of the approximation $(1 + x)^n \simeq e^{nx}$ for $x \ll 1$.

For easy reference, we summarise the main results of section 4.2 in table 4.2. Numerical estimates quoted in the text are included by way of examples.

(iii) Additional mode selection can be introduced if the laser rod faces are aligned to the end mirror of the resonator, as shown in figure 4.5. At first sight, the degree of mode selection that this might produce would appear to be very small since typical anti-reflection coatings might have a reflectivity of $\sim$0.25%. We will now show that the presence of a gain medium modifies the effective reflectivity of mirror M and considerably increases the mode selectivity of the structure.

A resonant reflector employing unequal reflectivity coatings R_1, R_2 has its power reflectivity given by

$$r = \frac{(\sqrt{R_1} - \sqrt{R_2})^2 + 4\sqrt{R_1 R_2}\sin^2(\delta/2)}{(1 - \sqrt{R_1 R_2})^2 + 4\sqrt{R_1 R_2}\sin^2(\delta/2)} \qquad 4.44$$

From figure 4.5, one can see that for a round trip of the etalon from F_1 to M and back to F_1, the power has changed from P, say, to G^2R_2P, so the effective reflectivity of mirror M is G^2R_2. Using this in equation 4.44 gives

$$r = \frac{(\sqrt{R_1} - G\sqrt{R_2})^2 + 4G\sqrt{R_1 R_2}\sin^2(\delta/2)}{(1 - G\sqrt{R_1 R_2})^2 + 4G\sqrt{R_1 R_2}\sin^2(\delta/2)} \qquad 4.45$$

Table 4.2: Summary of laser linewidth formulae

Laser configuration		Equation	Approximations	Typical value calculated in text
Fast Q-switched. No mode selection.	$\Gamma_{FQ} = \Gamma_F \left\{ \frac{\ell n 2}{2\pi(\omega_0)\ell N(t_s)q} \right\}^{\frac{1}{2}}$	4.21	$\left[\frac{\Gamma_{FQ}}{\Gamma_F} \right]^2 << 1$	$0.29 cm^{-1}$
Fast Q-switched with additional mode selection.	$\Gamma_{FQE} = \left\{ \frac{C_E \ell n 2}{q} \right\}^{\frac{1}{2}} \frac{2\Delta_E}{\pi}$ for a resonant reflector	4.25(a)	$\left[\frac{\pi \Gamma_{FQE}}{2\Delta_E} \right]^2 \cdot \frac{1}{C_E}, \frac{\sigma(\omega_0)\ell N(t_s)}{\Gamma_F^2} \cdot \frac{4}{\pi^2} \Delta_E C_E << 1$	$0.047 cm^{-1}$ ($\Delta_E = 0.5 cm^{-1}$, $C_E = 1$)
	$\Gamma_{FQE} = \left\{ \frac{\ell n 2}{q} \right\}^{\frac{1}{2}} \frac{\Delta_E}{F_E}$ for a transmission etalon	4.25(b)	$2\left[\frac{F_E \Gamma_{QE}}{\Delta_E} \right]^2, \frac{\sigma(\omega_0)\ell N(t_s)}{\Gamma_F^2} \left[\frac{\Delta_E}{F_E} \right]^2 << 1$	$0.015 cm^{-1}$ ($\Delta_E = 0.5 cm^{-1}$, $F_E = 5$)
Slow Q-switching. No mode selection.	$\Gamma_{SQ} = \Gamma_F \left\{ \frac{\ell n 2}{2\sigma(\omega_0)\ell N(t_n)q} \right\}^{\frac{1}{2}}$	4.30	$\left[\frac{\Gamma_{SQ}}{\Gamma_F} \right]^2, \frac{qT}{2t_p} << 1$	$0.066 cm^{-1}$

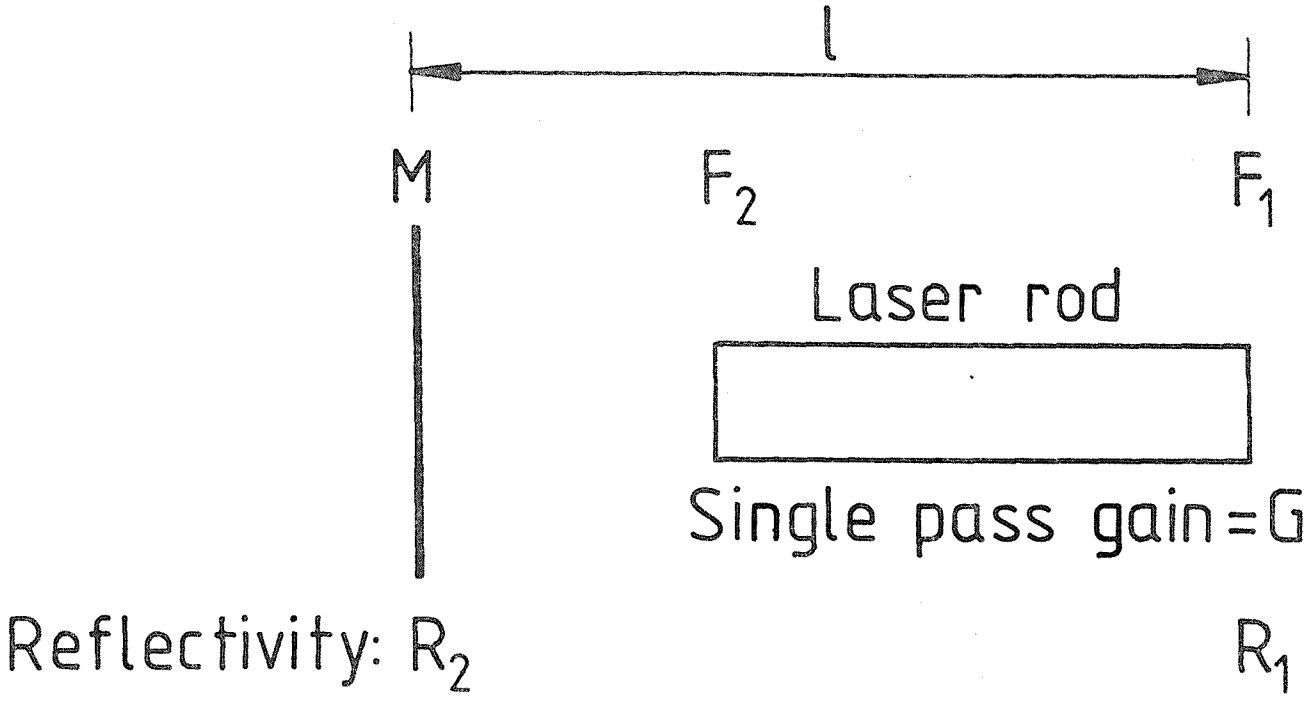

Figure 4.5: Section of a laser resonator in which face F_1 of the laser rod is parallel to the plane resonator mirror M

Equation 4.45 can now be used to derive an expression for mode selectivity. However, it is instructive to consider first how the reflectivity of the etalon changes as a function of G. Differentiation of equation 4.45 with respect to $\delta/2$ yields

$$\frac{dr}{d(\delta/2)} = \frac{4G\sqrt{R_1R_2}(1 - G^2R_2)(1 - R_1)\sin\delta}{((1 - G\sqrt{R_1R_2})^2 + 4G\sqrt{R_1R_2}\sin^2\delta/2)^2} \qquad 4.46$$

and so r has extrema at $\delta = 0, \pi, 2\pi, \ldots$. The second differential of r has the following values

$$\frac{d^2r}{d(\delta/2)^2} = \frac{8G\sqrt{R_1R_2}(1 - G^2R_2)(1 - R_1)}{(1 - G\sqrt{R_1R_2})^4} \qquad \delta = 0, 2\pi, 4\pi, \ldots \qquad 4.47(a)$$

$$\frac{d^2r}{d(\delta/2)^2} = \frac{-8G\sqrt{R_1R_2}(1 - G^2R_2)(1 - R_1)}{(1 + G\sqrt{R_1R_2})^4} \qquad 4.47(b)$$

$$\delta = \pi, 3\pi, 5\pi, \ldots$$

Equation 4.47(a) takes the same sign as $1 - G^2R_2$, whereas equation 4.47(b) takes the opposite sign. Therefore whether we have a maximum or minimum depends on the sign of $1 - G^2R_2$, i.e. whether G^2R_2 is less than or greater than unity. For a passive etalon, i.e. one which contains no gain medium, we are always concerned with $G^2R_2 < 1$ and so always have minima at $\delta = 0, 2\pi, 4\pi, \ldots$ and maxima at $\delta = \pi, 3\pi, 5\pi, \ldots$. If, however, we have a gain medium within the etalon such that $G^2R_2 > 1$, the etalon reflectivity has maxima at $\delta = 0, 2\pi, 4\pi, \ldots$ and minima at $\delta = \pi, 3\pi, 5\pi, \ldots$. We illustrate this effect by considering the value of the reflectivity for values of even or odd multiples of π. From equation 4.41

$$r_e = \frac{(\sqrt{R_1} - G\sqrt{R_2})^2}{(1 - G\sqrt{R_1R_2})^2} \quad , \quad \text{for } \delta = 0, 2\pi, 4\pi, \ldots \qquad 4.48(a)$$

$$r_o = \frac{(\sqrt{R_1} + G\sqrt{R_2})^2}{(1 + G\sqrt{R_1R_2})^2} \quad , \quad \text{for } \delta = \pi, 3\pi, 5\pi, \ldots \qquad 4.48(b)$$

r_e and r_o are plotted as a function of G^2R_2 for $R_1 = 0.5$ in figure 4.6, and the crossing of r_o and r_e can clearly be seen at $G^2R_2 = 1$. The value of R_1 chosen for this example is much larger than one would have in practice for an antireflection coating (say $R_1 \simeq 2.5 \times 10^{-3}$), but the behaviour of r_e and r_o for G^2R_2 close to unity is more clearly illustrated for large R_1.

To find the degree of mode selectivity introduced by this device we proceed in the usual way, assuming that $\Delta_L\pi << \Delta_E$ and obtain

$$\frac{R_{1n}}{R_{1m}} = 1 + \varepsilon_{RG} \qquad 4.49(a)$$

where

$$\varepsilon_{RG} = \left[\frac{\Delta_L}{\Delta_E}\right]^2 \cdot 4\pi^2 G\sqrt{R_1R_2}\left[\frac{1}{(1 - G\sqrt{R_1R_2})^2} - \frac{1}{(\sqrt{R_1} - G\sqrt{R_2})^2}\right] \qquad 4.49(b)$$

is the fractional mode discrimination per round trip for a resonant reflector containing a gain medium.

Using values of $R_2 = 1$, $R_1 = 2.5 \times 10^{-3}$ and $G = 7$ appropriate to the telescopic resonator, we find that $1/(1 - G\sqrt{R_1R_2})^2 >> 1/(\sqrt{R_1} - G\sqrt{R_2})^2$ and so rewrite equation 4.45(b)

$$\varepsilon_{RG} \simeq \left[\frac{\Delta_L}{\Delta_E}\right]^2 \frac{4\pi^2 G\sqrt{R_1R_2}}{(1 - G\sqrt{R_1R_2})^2} \qquad 4.50$$

we now recognise $\pi^2 G\sqrt{R_1R_2}/(1 - G\sqrt{R_1R_2})^2 = F_{EG}^2$ where F_{EG} is the finesse of the etalon containing a gain medium. Therefore equation 4.46 can be written

$$\varepsilon_{RG} \simeq 4\left[F_{EG}\frac{\Delta_L}{\Delta_E}\right]^2 \qquad 4.51$$

This suggests that the mode selection introduced by this type of resonant reflector is analogous to that introduced by a passive

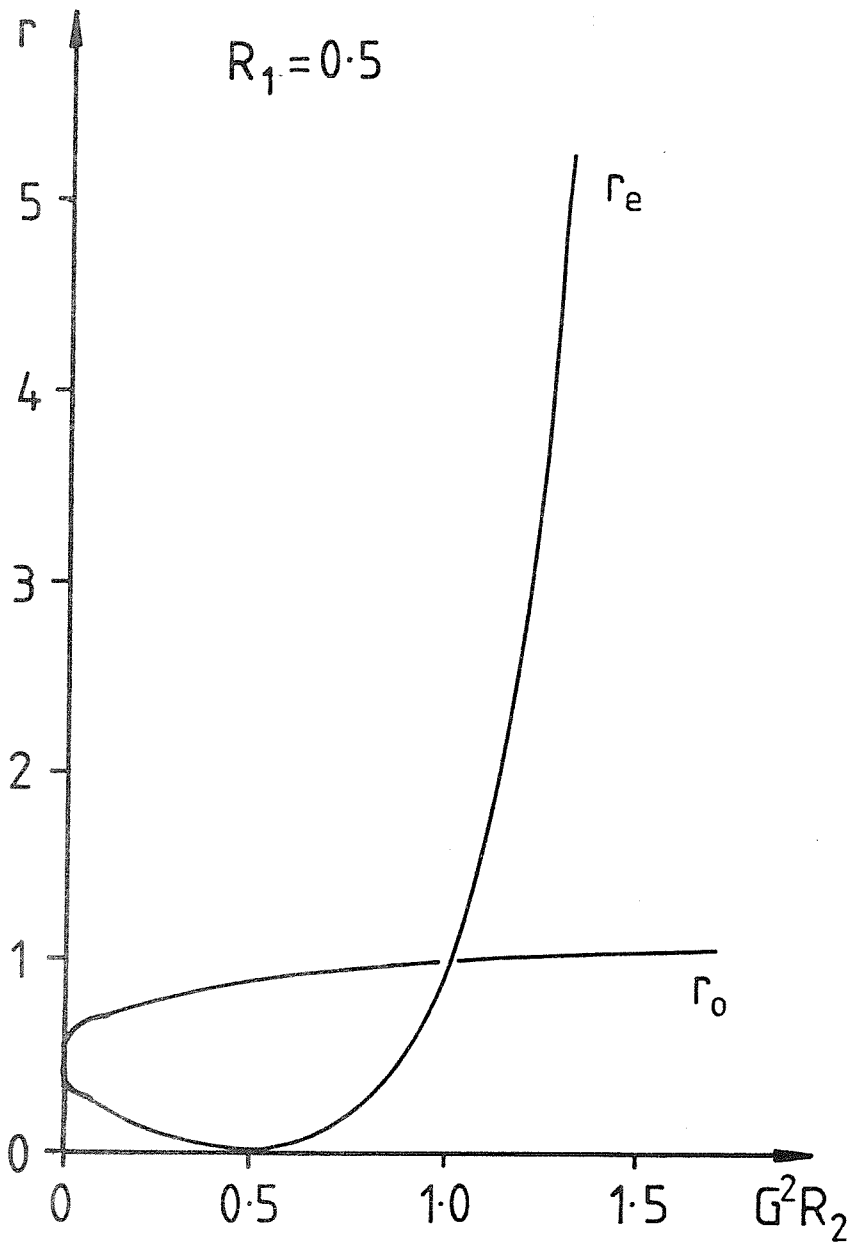

Figure 4.6: Reflectivities r_o and r_e versus G^2R_2 for an etalon containing a gain medium

intracavity transmission etalon, rather than a resonant reflector.

For values of R_1, R_2, G listed above we calculate $F_E = 2.9$, and in the telescopic resonator we have approximately $\Delta_E = 2.5 \times 10^{-2}$, $\Delta_L = 3.8 \times 10^{-3}$. Using equation 4.51 we find $\varepsilon_{RG} = 0.78$. Therefore, using equation 4.35 we calculate

$P_n(t_s)/P_m(t_s) = 3.3 \times 10^7$ for $q = 30$, which means that single longitudinal mode operation is possible using this device, even for a fast Q-switched laser. Clearly this structure is in principle capable of very large mode selectivity. However, in the above discussion we have failed to consider the fact that thermal lensing of the laser rod will reduce the effective finesse of the device, which will in practice degrade the mode selectivity somewhat.

Experimental work has been performed on this structure by Bua and co-workers (1972). They obtained single-mode operation of a ruby laser by carefully aligning the laser rod faces parallel to the 100% reflector of the resonator (R_2 in figure 4.5). We briefly examined this effect in the telescopic resonator, and showed that it could indeed produce single-mode operation, but only with poor reliability. This is thought to have been caused by shot-to-shot variation of the alignment of the laser rod and mirror arising as a result of the 'O' ring rod mounting used on our pumping chamber. Because of this we did not pursue the technique any further, choosing to concentrate our attention on intracavity mode selection using a transmission etalon.

4.3 Practical Limitations and Their Effect on the Reliability and Pulse Repeatability of Slow Q-Switched Lasers

As we stated in the introduction to this chapter, a number of factors contrive to degrade the performance of a single-mode laser system. Most of these are mechanical or thermal in origin, and can be eliminated by using a super-Invar mounting structure for the resonator enclosed in a temperature-stabilised box (Owyoung and Jones, 1978). This is an expensive solution, and for a commercial system one would like to use a simpler, and cheaper, mounting structure. It is therefore useful to get some idea of the magnitude of these effects to evaluate possible improved resonator construction.

4.3.1 The effect of random fluctuations in cavity length on mode selection

In sections 4.2.2 and 4.2.4 we assumed that mode n was coincident with the laser gain maximum and a loss minimum of the mode selector. We confine ourselves here to single-mode operation of the laser system, and investigate the effect on mode selectivity of a random location of cavity modes relative to the modes of the frequency-selective element. From equations 4.35 and 4.36 we recall that the ratio of mode powers is given by $P_n(t_s)/P_m(t_s) = \{R_{1n}/R_{1m}\}^{q_{eff}}$. Consider two adjacent cavity modes m and n positioned relative to a reflectivity maximum (loss minimum) of the mode selector at frequency ω_0, as shown in figure 4.7, where $\Delta_{Lm} + \Delta_{Ln} = \Delta_L$ the cavity mode spacing. We write $R_{1n} = 1 - \varepsilon_n$, $R_{1m} = 1 - \varepsilon_m$, where $\varepsilon_{m,n}$ are defined for a resonant reflector and transmission etalon by equations 4.41(b) 4.42(b). Then we have

$$\frac{P_n(t_s)}{P_m(t_s)} \simeq \{(1 - \varepsilon_n)(1 + \varepsilon_m)\}^{q_{eff}} \simeq \{1 - \varepsilon_n + \varepsilon_m\}^{q_{eff}} \qquad 4.52$$

where use has been made of the approximation $\varepsilon_{m,n} << 1$. It is useful to remove Δ^2 from equations 4.41(b), 4.42(b) and write $\varepsilon = \varepsilon'\Delta^2$ where $\varepsilon'_R = (\pi/\Delta_E)^2/C_E$, $\varepsilon'_T = 8(F_E/\Delta_E)^2$. Writing $\Delta_{Lm} = \Delta_L - \Delta_{Ln}$ we obtain from equation 4.52

$$\frac{P_n(t_s)}{P_m(t_s)} = \{1 + \varepsilon'(\Delta_L^2 - 2\Delta_L\Delta_{Ln})\}^{q_{eff}} \qquad 4.53$$

As a criterion for single-mode operation we take $P_n(t_s)/P_m(t_s) \geq N$, where we may, for instance, choose $N = 10^5$ as a practical value. This enables us to write

$$q_{eff}\varepsilon'(\Delta_L^2 - 2\Delta_L\Delta_{Ln}) \geq \ell nN \qquad 4.54$$

from equation 4.53, where we have used $(1 + x)^n \simeq e^{nx}$ for $x << 1$. This gives

$$\Delta_{Ln} \leq \frac{\Delta_L}{2} - \frac{\ell nN}{2\Delta_L q_{eff}\varepsilon'} = \Delta'_{Ln} \qquad 4.55$$

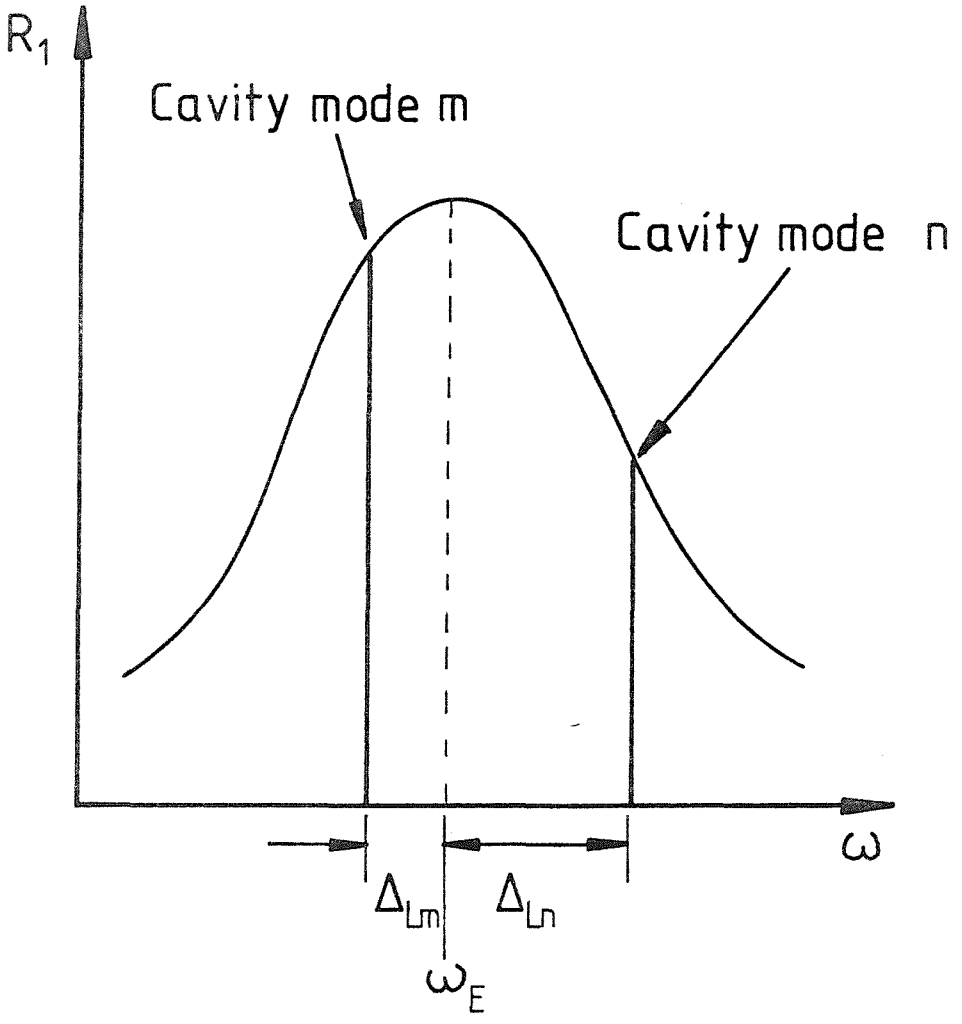

Figure 4.7: General location of two cavity modes m and n relative to a reflectivity maximum of the mode selector

is the requirement for single-mode operation. Suppose now that Δ_{Ln} changes in a random way from shot-to-shot. Single mode operation will be secured for $0 < \Delta_{Ln} \leq \Delta'_{Ln}$, and two-mode operation for $\Delta'_{Ln} < \Delta_{Ln} \leq \Delta_L/2$. Therefore the ratio of single-mode to two-mode shots will be

$$r = \frac{\Delta'_{Ln}}{\Delta'_{Ln} - \Delta_L/2} = \varepsilon \left[\frac{q_{eff}}{\ell nN} \right] - 1 \qquad 4.56$$

where we have replaced $\varepsilon' \Delta_L^2$ by ε in this final result.

We can now see a fundamental limitation on the reliability of single-mode operation caused by our lack of control over cavity mode position. The relative mode powers calculated from equations 4.39 go as $e^{\varepsilon q_{eff}}$, whereas in equation 4.56 r goes as εq_{eff}; a doubling of either ε or q_{eff} can cause a dramatic increase in $e^{\varepsilon q_{eff}}$, but at most a factor of two difference is made to r. A numerical example may serve to clarify this point further. If two modes are mixed with a ratio of mode powers N:1, one can show that $k \approx 4/\sqrt{N}$ where k is the ratio of peak-to-peak sinusoidal modulation of power at the difference frequency between the modes to the mean power (see Appendix 4). One might choose as one's criterion for single-mode operation that less than 1% modulation is observed when displaying the laser pulse on an oscilloscope. This corresponds to $N = 16/k^2 = 1.6 \times 10^5$. Suppose further that the laser system has $\varepsilon = 0.05$ and $q_{eff} = 500$. This gives a maximum ratio of mode powers $e^{\varepsilon q_{eff}} = 7.2 \times 10^{10}$. However, using $N = 1.6 \times 10^5$ we find r = 1.2. This means that only 55% of the shots will be single-frequency despite the fact that there appears to be a generous amount of mode selection. Equation 4.56 is shown in graphical form in figure 4.8.

4.3.2 Transient and random cavity length changes

There are three readily identifiable causes of cavity length changes: (i) Changes in the optical length of the laser rod caused by pump-induced thermal effects; (ii) Air turbulence in exposed portions of the laser cavity; (iii) Vibrations of the laser support rail. In the following subsections we assess the magnitude of these effects, including experimental measurements of support rail vibration for our mounting system (J.K. Lasers Ltd. rail).

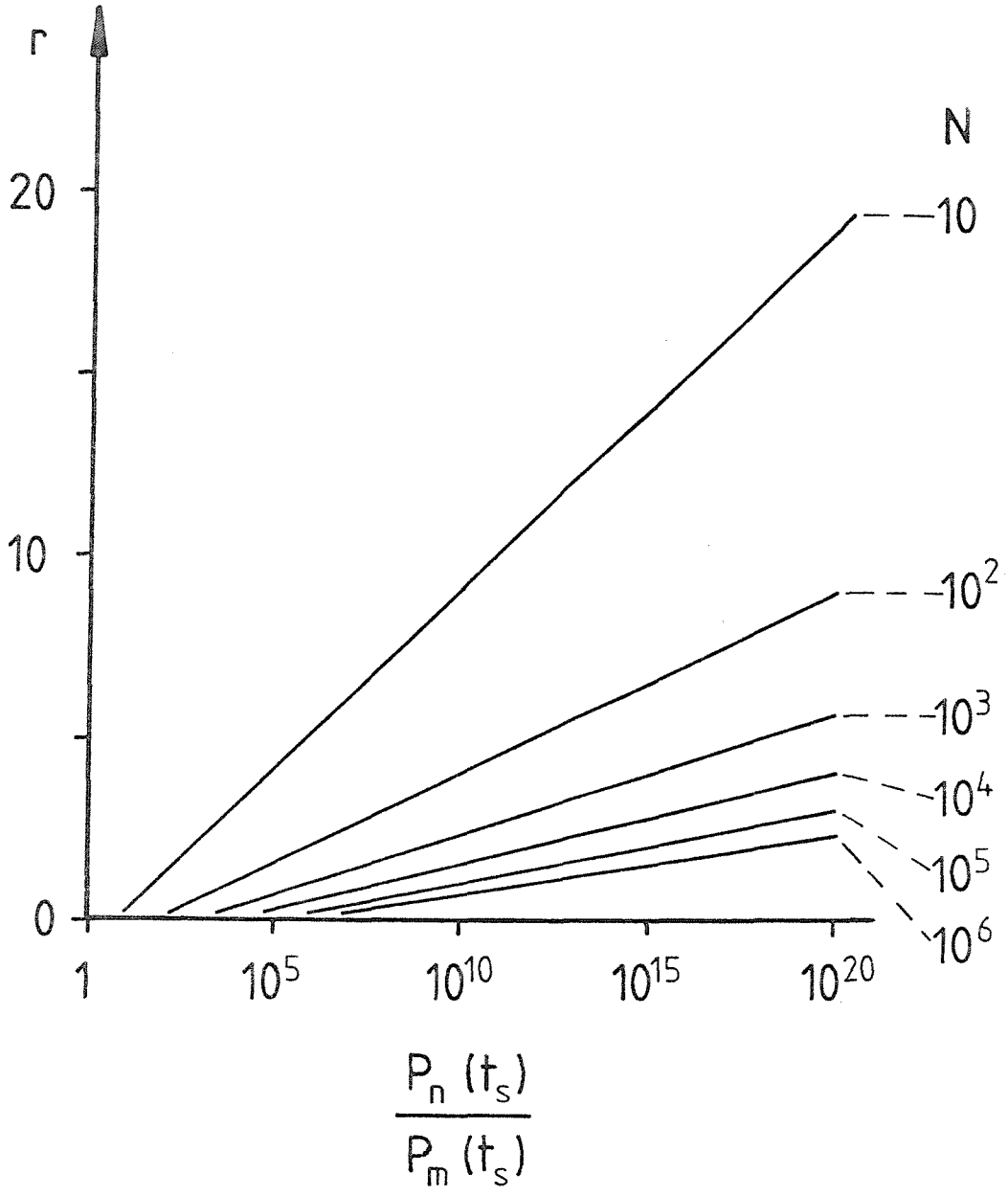

Figure 4.8: The ratio of single-mode to two-mode laser shots, r, as a function of the maximum possible ratio of mode powers, $P_n(t_s)/P_m(t_s)$, with the acceptable minimum ratio of mode powers, N, as a parameter

(i) Thermal effects in the laser rod

One can readily show that the change in optical length of the laser , $\Delta\ell'$, is related to the temperature rise ΔT by

$$\Delta\ell' = \Delta T \ell \left\{ \frac{dn}{dT} + (n-1)k \right\} \qquad 4.57$$

where n is the refractive index of the laser rod, k is the thermal expansion coefficient and ℓ is the physical rod length. Numerical values for k, n, dn/dT and ℓ are known (table 4.1), but we need an estimate of ΔT to be able to use equation 4.57.

During slow Q-switching we are concerned not only with random changes in cavity length on a shot-to-shot basis, but also in transient changes during the pulse build-up time of $\sim 5\mu s$. It is rather difficult to calculate an accurate value of ΔT for this period, but we make a worst-case estimate by assuming that 1J of heat energy is released in the rod during this $5\mu s$. Temperature rise is related to release of energy by $\Delta T = E/m\sigma_h$, where m is the mass of the object and σ_h is the specific heat. From table 4.1 we can calculate $\Delta T = 7 \times 10^{-2}{}^{o}K$ for a heat input of 1J, for our 3" x $\frac{3}{8}$" diameter laser rod. This gives $\Delta\ell' = 70nm$, or $\sim\lambda/15$, and can therefore probably be neglected for our experimental arrangement.

(ii) Air turbulence in the laser cavity

Air movement is usually accompanied by temperature fluctuations. These give rise to refractive index fluctuations, and consequently to cavity length fluctuations if portions of the resonator are exposed. It is very difficult to quantify precisely the magnitude of this effect, but a worst-case estimate is again possible by assuming an overall temperature rise of $\sim 0.1^{o}C$ in the $5\mu s$ pulse build-up time. One can easily show that the change in optical cavity length $\Delta\ell'$ is given by

$$\Delta\ell' = -\Delta T \ell \alpha (n - 1) \qquad 4.58$$

where ΔT is the temperature rise, n is the refractive index of the air and α is related to the refractive index by $dn/dT = -\alpha(n - 1)$. For air at $15^{o}C$ for a wavelength of $1\mu m$ we find $\alpha = 3.66 \times 10^{-3}$, $n - 1 = 2.7 \times 10^{-4}$,

and so $\Delta\ell' = -1.3\Delta T\mu m$ for a 1.3m long cavity. Using $\Delta T \sim 0.1^{o}C$ from above, we find that $\Delta\ell' \simeq \lambda/8$ at 1.06μm.

We anticipate that in practice $\Delta T << 0.1^{o}C$ in 5μs, and so it is probably safe to neglect this effect in the build-up of an individual laser pulse. However, on a shot-to-shot basis it only requires an overall temperature fluctuation of $\pm 0.2^{o}C$ to shift the cavity modes by half an intermode spacing, i.e. the amount required to move from maximum suppression of adjacent modes to two modes of equal generated power (see section 4.3.1). We therefore recommend that for maximum repeatability and reliability the laser cavity be enclosed in a draught-free and preferably temperature-controlled box.

(iii) Vibration of the laser rail

The rail on which the laser described in this thesis was mounted is illustrated in figure 4.9, and is a standard 1.5m double rail made by J.K. Lasers Ltd. The material used is 12.5mm thick aluminium plate, the various sections being held together with Allen head screws. The entire assembly is supported on four aluminium pillars, and the height of the emerging laser beam is finely adjusted using the four adjusting screws shown. A beam height of 19cm was used since this matched the Newport Research Corporation optical mounts that were used for holding extra-cavity optical components. The various optical elements comprising the laser are mounted on one side of the rail only, and are secured using three screws per component through the holes illustrated in figure 4.9. Although this has the effect of strengthening the rail it was felt that the structure was still inherently flimsy and an interferometer was built onto the rail to quantify the amplitude of rail vibration.

The experimental arrangement is illustrated in figure 4.10. The interferometer comprised two uncoated, wedged, $\lambda/20$ etalon blanks mounted onto the laser rail using standard J.K. Lasers mounts. The plate separation was about 10cm, and one mirror was located 2.5cm in from the adjusting screw. The parallelism of the two plates was carefully adjusted using an autocollimator. A He-Ne laser beam was passed through the plates, and adjusted to be roughly perpendicular to them by observing the back reflection. The back reflected beam was intercepted using an uncoated, wedged flat, and the angle of the He-Ne beam finely adjusted by observing the interference fringes on the

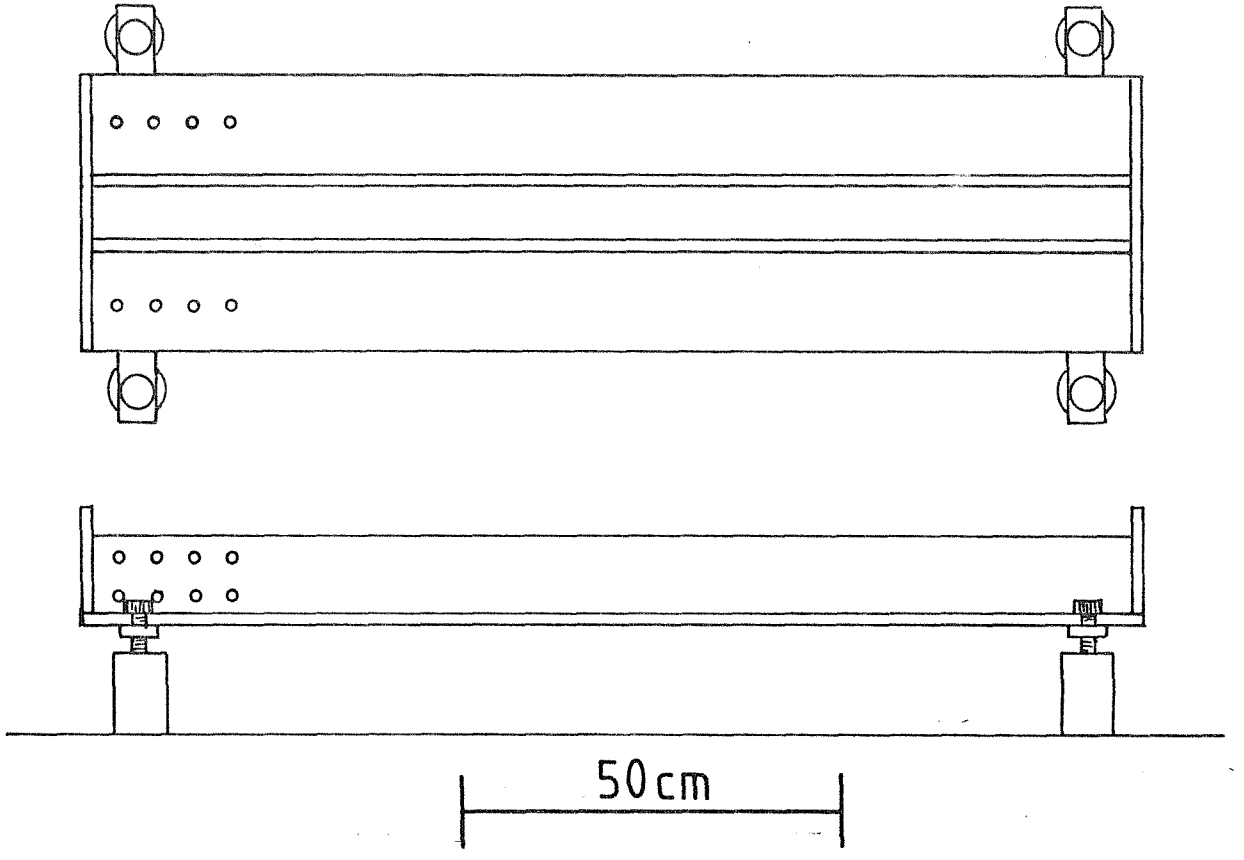

Figure 4.9: The J.K. Lasers optical rail

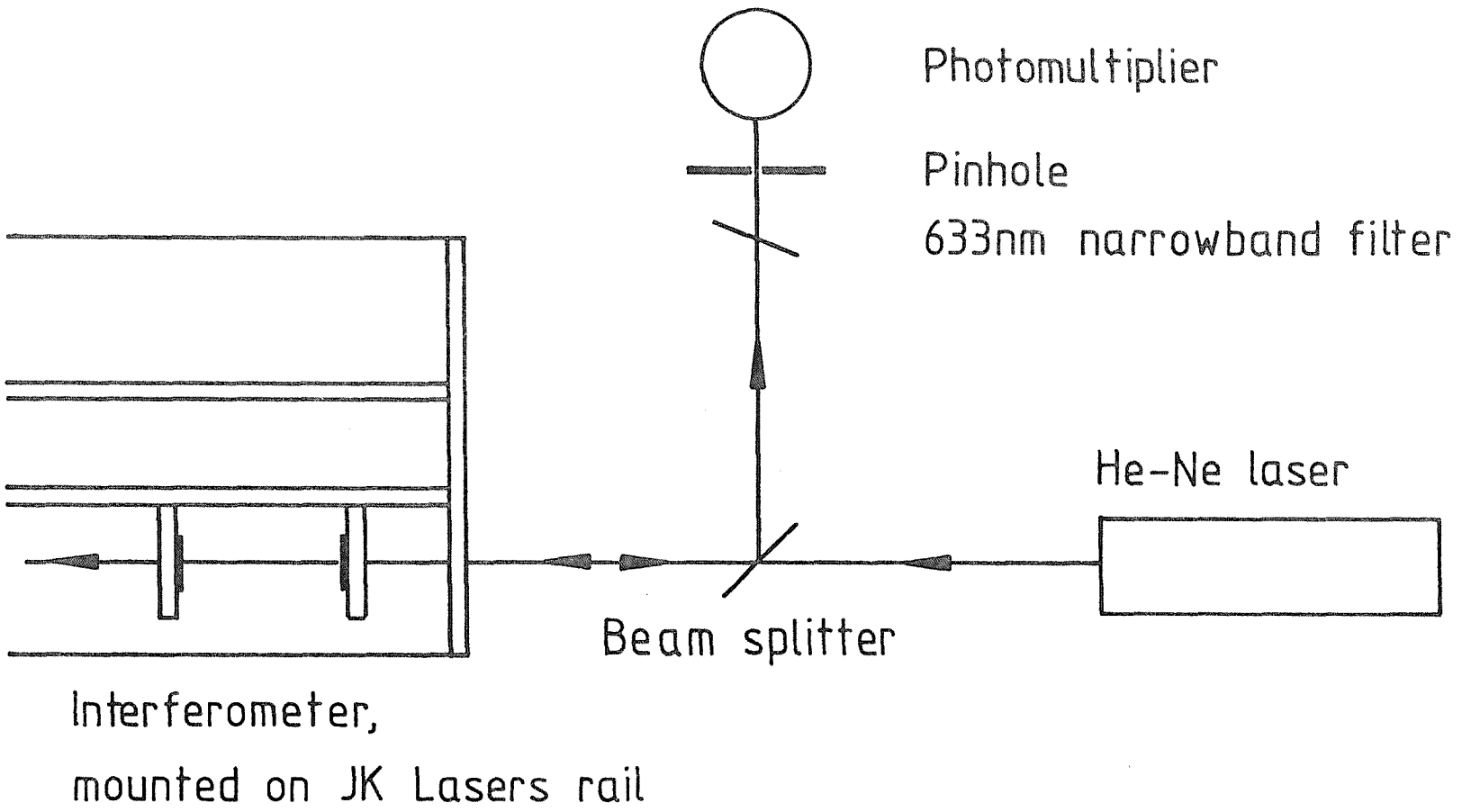

Figure 4.10: Experimental arrangement used to measure the amplitude of rail vibration

backward beam. To attenuate stray room light a 633nm narrowband filter and aperture were used, and the amount of reflected light measured using a photomultiplier. For convenient observation, the signal was displayed using a transient digitiser and television monitor.

Using this arrangement, it was immediately obvious that the rail was very susceptible to both mechanical vibration coupled through the bench, and also to airborne vibrations. Sharp sounds, such as handclaps, were readily picked up by the rail.

Before it is possible to quantify any results, it is necessary to know how an amplitude of mirror vibration measured using the interferometer relates to the amplitude of vibration for mirrors placed at opposite ends of the rail, since this is what one has in practice in the laser resonator. Preliminary measurements indicated that the rail vibrated with a resonance frequency of about 1.7kHz. Taking the speed of sound in aluminium to be $5100ms^{-1}$ we can identify this as the fundamental flexing vibration of the rail, shown in figure 4.11.

The amplitude of rail vibration at a point x is given by

$$A(x,t) = A_0 \sin\left[\frac{\pi x}{L}\right] \sin\left[\frac{\pi v t}{L}\right] \qquad 4.59$$

To calculate the mirror vibration we need to know the gradient of $A(x,t)$

$$\frac{dA(x,t)}{dx} = A_0 \frac{\pi}{L} \cos\left[\frac{\pi x}{L}\right] \sin\left[\frac{\pi v t}{L}\right] \qquad 4.60$$

and so the difference in gradient at points x_1, x_2 is

$$\Delta = \left.\frac{dA(x,t)}{dx}\right|_{x_2} - \left.\frac{dA(x,t)}{dx}\right|_{x_1} = A_0 \frac{\pi}{L}\left[\cos\left[\frac{\pi x_2}{L}\right] - \cos\left[\frac{\pi x_1}{L}\right]\right] \sin\left[\frac{\pi v t}{L}\right] \qquad 4.61$$

Equation 4.61 simply describes the oscillation of the angle between the two mirrors placed at x_1, x_2. Let the beam height above the laser rail be L. The amplitude of vibration of the two mirrors is then simply $\delta x = h\Delta$, and so the peak-to-peak value is given by

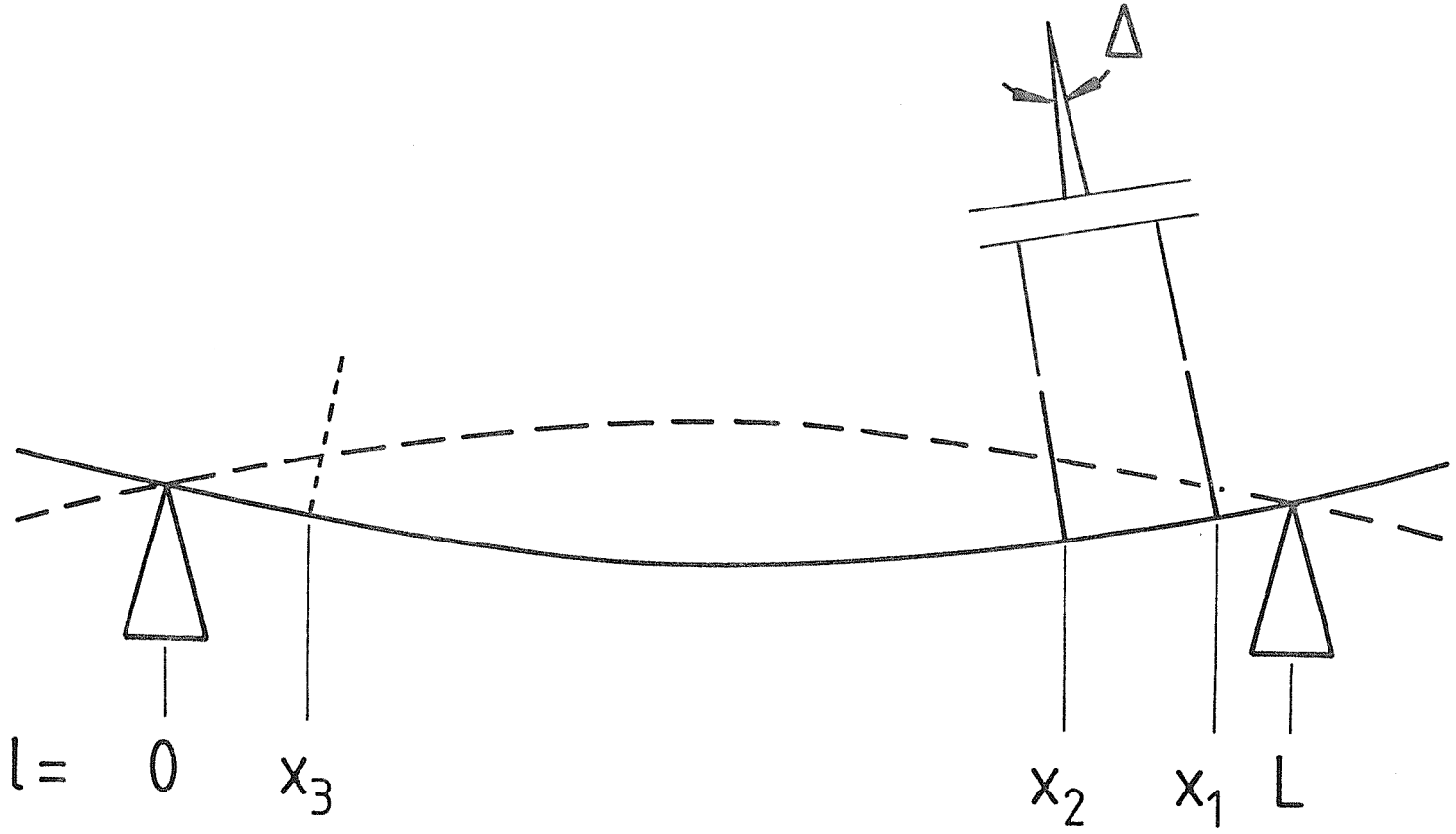

Figure 4.11: The model of the flexing behaviour of the J.K. Lasers optical rail

$$\delta x_{p-p} = h\Delta_{p-p} = 2\pi \frac{h}{L} A_0 \left[\cos\left[\frac{\pi x_2}{L}\right] - \cos\left[\frac{\pi x_1}{L}\right]\right] \qquad 4.62$$

Finally, for mirrors placed at x_1, x_3 we can write

$$\delta x'_{p-p} = 2\pi \frac{h}{L} A_0 \left[\cos\left[\frac{\pi x_3}{L}\right] - \cos\left[\frac{\pi x_1}{L}\right]\right] \qquad 4.63$$

and so δx_{p-p} and $\delta x'_{pp}$ are related by

$$\frac{\delta x'_{pp}}{\delta x_{pp}} = \frac{\cos\left[\frac{\pi x_3}{L}\right] - \cos\left[\frac{\pi x_1}{L}\right]}{\cos\left[\frac{\pi x_2}{L}\right] - \cos\left[\frac{\pi x_1}{L}\right]} \qquad 4.64$$

For the experimental arrangement used, $x_1 = 132.5$, $x_2 = 127.5$ and $x_3 = 2.5$cm. The spacing between the rail supports L = 135cm giving, from equation 4.64, $\delta x'_{pp}/\delta x_{pp} = 150$.

The peak-to-peak amplitude of mirror vibration was determined in the following way. Large relative mirror displacements induced by applying finger pressure to the two mirror mounts caused the interferometer to scan through several orders of interference. This allowed the maximum and minimum value of the reflected power to be marked on the transient digitiser monitor, representing a relative mirror movement of $\lambda/4$. Once the monitoring system had been calibrated in this way, displacements of the mirrors less than $\lambda/4$ could be easily measured.

To measure δx_{pp} under conditions relevant to normal operation of the laser, the flashlamps were run at 56J total input (750V capacitor charging voltage) at a repetition rate of 12Hz. The mirror vibration was again at a frequency of 1.7kHz, and had a peak-to-peak amplitude of $\lambda/32$ for He-Ne wavelength, or 20nm. Therefore for mirrors positioned at x_3, x_1, we find $\delta x'_{pp} = 150 \times 20 = 3000$nm, or about $3\lambda_{YAG}$. To find out the worst-case change of cavity length during the pulse build-up time of 5μs, we take the maximum rate of change of the vibration, $2\pi\delta x'_{pp}/\tau$ where $\tau = 2L/v$ is the period of vibration. Using numbers from above, this gives a worst-case rate of change of cavity length of $\lambda/30$

per microsecond, indicating that one might expect a change of $\lambda/6$ during the 5μs build-up time. This represents a severe shift of cavity modes, and one might expect a laser system built on this type of rail to give rather poorer performance as regards degree of mode selection than simple theory would predict. As will be found later in this chapter, this appeared qualitatively to be the case, although no data acquisition equipment was available to quantitatively confirm this. However, some initial results have been obtained using an upgraded Nd:YAG laser with a telescopic resonator whose construction incorporates some of the recommendations made in this thesis. Its behaviour when slow Q-switched is considerably more stable and predictable, typically producing more than 500 consecutive shots at the 100mJ level with no discernible mode beating. This laser has its optical components fixed directly and securely to the surface of a Newport Research Corporation optical table, which possesses excellent long and short term mechanical stability. We therefore conclude that mechanical stability is of prime importance in construction of single-frequency laser oscillators.

4.3.3 Transient phase shift induced by the Pockels cell

Consider the section of laser cavity illustrated in figure 4.12(a). The polariser passes horizontally polarised radiation, and this is incident on a Pockels cell. The correct angular orientation is such that the field-induced crystallographic axes x', y' of the Pockels cell crystal make an angle of 45° with the input polarisation. When aligned in this way the Pockels cell does not introduce any additional, field-dependent, phase shift to the horizontally polarised component. At angles other than 45°, however, a field-induced phase shift can give rise to a net change of cavity length after opening of the Pockels cell. We now assess the magnitude of this effect.

The Pockels cell orientation is shown in figure 4.12(b), and we assume that the z axis of the crystal is parallel to the propagation vector of the laser beam and perpendicular to mirror M. Resolving $\underline{E_L}$ onto the x' and y' axes gives for the field components at the input to the cell

$$\underline{E^i_{x'}} = |E_L|\,\hat{\underline{i}}\cos\theta \qquad 4.65(a)$$

$$\underline{E^i_{y'}} = |E_L|\,\hat{\underline{j}}\sin\theta \qquad 4.65(b)$$

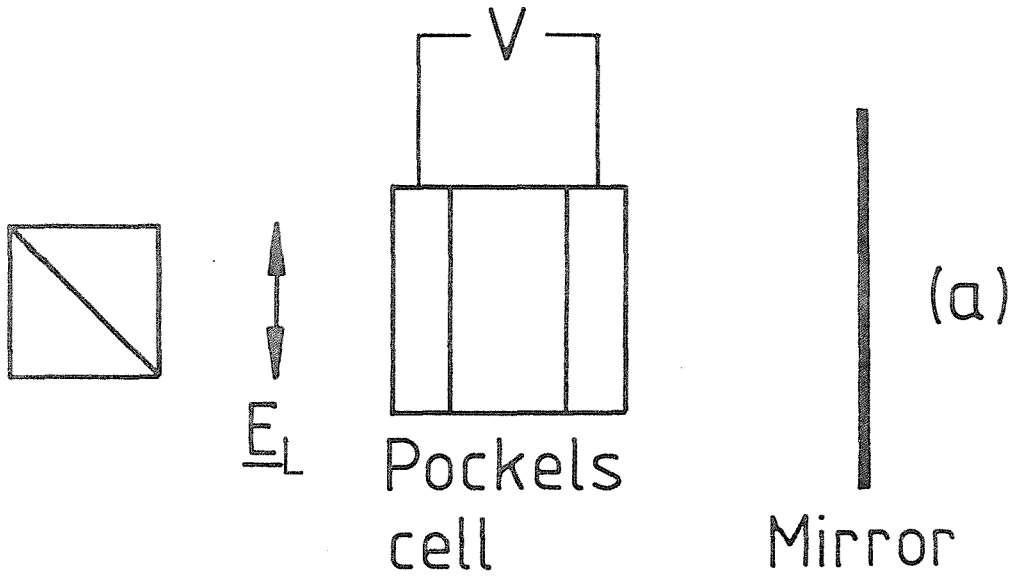

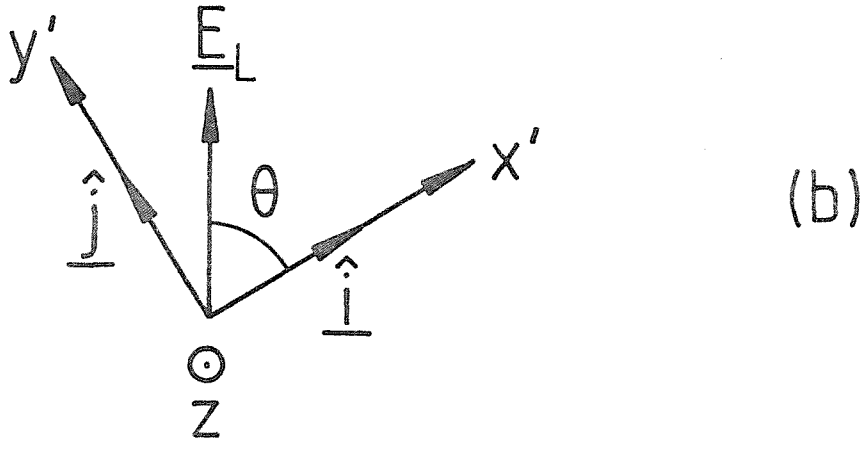

Figure 4.12: (a) Section of laser resonator containing the Pockels cell

(b) Voltage induced axes of the Pockels cell, x', y', and their orientation relative to the laser polarisation

where $\hat{i}$ and $\hat{j}$ are unit vectors in the x′ and y′ directions respectively The voltage-induced phase shifts for components in the x′ and y′ directions are $+\delta/2$ and $-\delta/2$ respectively, where $\delta = \frac{2\pi}{\lambda} n_o^3 r_{63} V$ and n_o is the ordinary index of refraction, r_{63} is the electro-optic coefficient and V is the applied voltage.

Reflection from the mirror followed by a second pass through the crystal induces a second phase shift of $\delta/2$, making a total phase shift of δ. Therefore, the fields in the x′, y′ directions after the return trip are

$$\underline{E}^o_{x'} = |E_L| \hat{i} e^{i\delta} \cos\theta \qquad 4.66(a)$$

$$\underline{E}^o_{y'} = |E_L| \hat{j} e^{-i\delta} \sin\theta \qquad 4.66(b)$$

and the total output field is just $\underline{E}_o = \underline{E}^o_x + \underline{E}^o_y$. To find the field E^o_L transmitted by the polariser we use

$$E^o_L = \frac{\underline{E}^o \cdot \underline{E}_L}{|E_L|} = |E_L| \left\{ e^{i\delta} \cos^2\theta + e^{-i\delta} \sin^2\theta \right\} \qquad 4.67$$

Note in passing that $\theta = 45^o$ gives $E^o_L = |E_L| \cos\delta$, showing that for this correct orientation there is no additional phase shift introduced by the Pockels cell voltage. Equation 4.67 can be rewritten as

$$E^o_L = |E_L| \left\{ \cos^2\delta + (2\cos^2\theta - 1)^2 \sin^2\delta \right\}^{\frac{1}{2}} e^{i\delta'}$$

where

$$\delta' = \cos^{-1} \left[\frac{1}{(1 + (2\cos^2\theta - 1)^2 \tan^2\delta)} \right]^{\frac{1}{2}} \qquad 4.68$$

is the voltage-dependent phase shift. The change in optical path length associated with this phase shift is

$$\Delta L = \frac{\lambda}{2\pi} \delta' \qquad 4.69$$

and $\Delta L = \lambda/4$ will shift cavity modes by half an intermode spacing. In figure 4.13 we plot n, where $\Delta L = \lambda/n$ is the change in cavity length, against $\Delta\theta = \theta - 45^o$, where $\Delta\theta$ is the angular misalignment of the Pockels cell axes. $V/V_{\lambda/4}$ is chosen as a parameter.

With the laser system described in this thesis, alignment of the Pockels cell is performed visually, with the assumption that the x

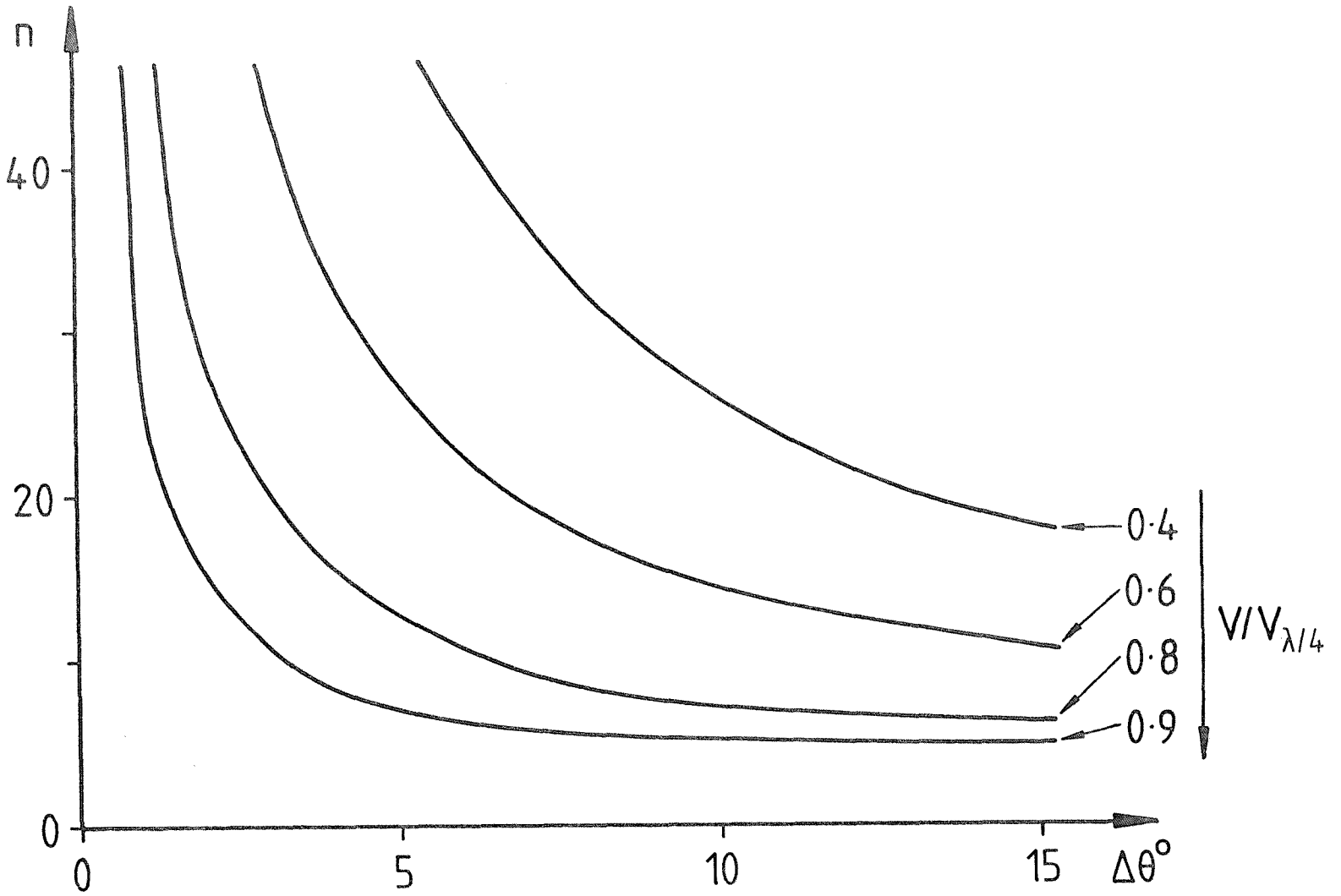

Figure 4.13: Transient change of cavity length as a function of angular misalignment of the Pockels cell, $\Delta\theta$. The ordinate is in terms of n, where λ/n is the change in cavity length. $V/V_{\lambda/4}$ is a parameter

and y crystallographic axes are aligned by the manufacturer relative to the Pockels cell mount. We estimate a worst-case misalignment of $\Delta\theta = \pm 5^{o}$, and assume a Pockels cell voltage when slow Q-switching less than 2.6kV. For our cell, the quarter-wave voltage at 1.06μm is 3.4kV, giving $V/V_{\lambda/4} = 0.77$. From figure 4.13 we find that the transient cavity length change during switching is less than $\lambda/10$, and this probably is not significant. However, one must be careful when working with voltages near $V_{\lambda/4}$, in which case cavity length changes can approach $\lambda/4$.

4.3.4 Cavity mode pulling caused by dispersion in an intracavity etalon

Bhawalkar and co-workers (1977) have considered how the frequency-dependent phase shift associated with each Fabry-Perot transmission maximum affects the mode spacing of a laser resonator in which it is placed. They showed that this can have a significant effect in the case of a dye laser having a cavity length of 10cm when using an intracavity etalon characterised by $\Delta_E = 1.2\text{cm}^{-1}$, $F_E = 8$, where they found that adjacent cavity modes were shifted by 0.25 of a cavity mode spacing. We briefly consider this effect, and assess its importance for our experimental arrangement.

A Fabry-Perot etalon introduces a phase shift ϕ to transmitted light given by

$$\tan\phi = \frac{\sin\delta}{1/R - \cos\delta} \qquad 4.70$$

where the etalon is assumed to have equal face reflectivities R, and δ is the phase shift associated with a double traversal of the etalon. Consider the case illustrated in figure 4.14, where an etalon transmission peak is centred on a laser cavity mode. One can show that the phase shift for a frequency detuning Δ from the etalon transmission maximum (frequency ω_E)

$$\tan\phi = \frac{\sin(2\pi\Delta/\Delta_E)}{1/R - \cos(2\pi\Delta/\Delta_E)} \qquad 4.71$$

The resonance condition for the p^{th} axial mode of a laser operating on the TEM_{00} transverse mode can be written

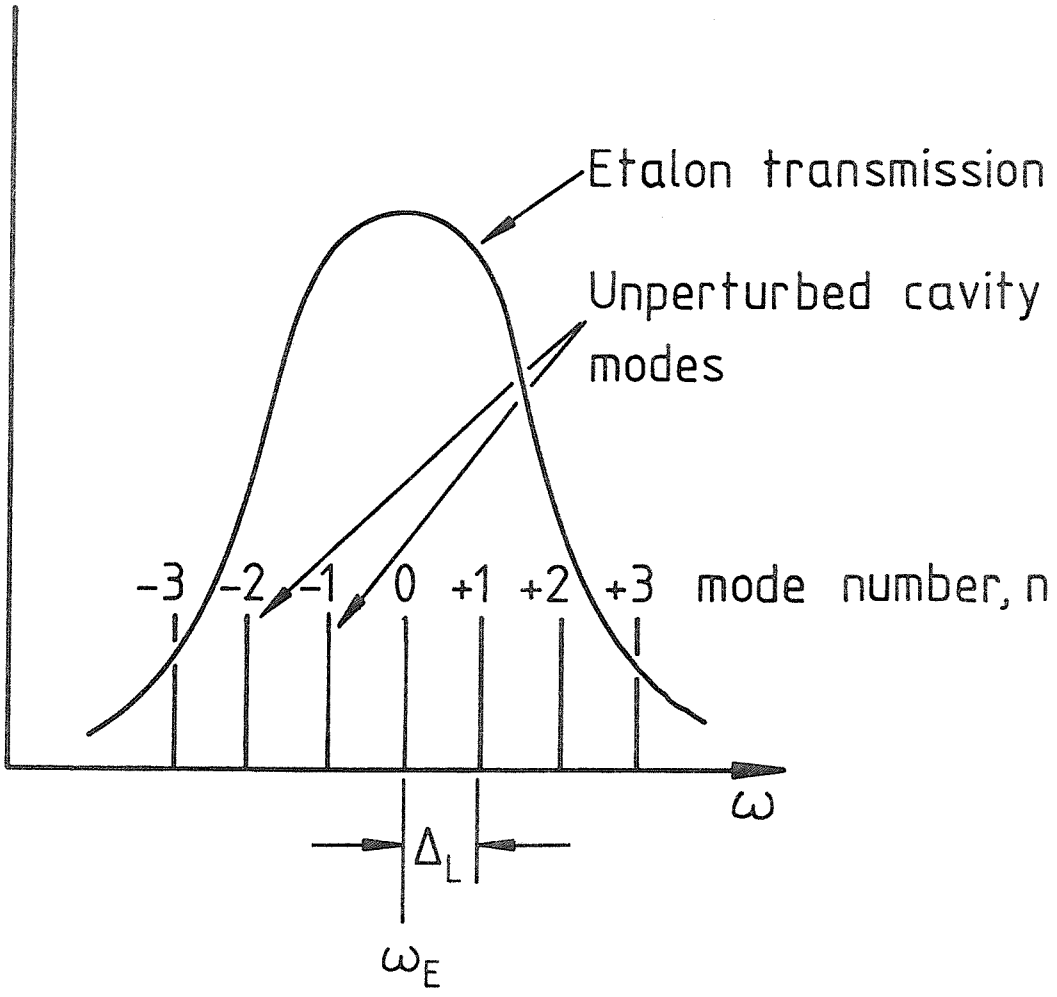

Figure 4.14: Notation used in the derivation of equation 4.73

$$\frac{\pi\omega}{\Delta_L} + \phi_o + \phi = p\pi \qquad 4.72$$

where $\omega = \omega_E + \Delta$ is the frequency of the p^{th} laser mode and ϕ_o is a phase shift associated with laser resonator mirrors and diffraction effects (assumed to be constant over the wavelength range of interest). Δ_L is the unperturbed cavity mode spacing, given by $\Delta_L = 1/2L$, where L is the cavity length. From equations 4.71 and 4.72 we can write a transcendental equation in Δ

$$\Delta = \Delta_L \left\{ n - \frac{1}{\pi} \tan^{-1} \left[\frac{\sin(2\pi\Delta/\Delta_E)}{1/R - \cos(2\pi\Delta/\Delta_E)} \right] \right\} \qquad 4.73$$

where the mode number n is now counted from n = 0 at $\omega = \omega_E$. Equation 4.73 can be solved numerically for Δ for given parameters. We can, however, obtain an approximate solution by using the approximation $2\pi\Delta R/\Delta_E(1 - R) \ll 1$, and obtain the fractional shift of the n^{th} mode frequency

$$\alpha_n = 1 - \frac{\Delta}{n\Delta_L} \simeq \frac{2\,\frac{\Delta_L}{\Delta_E}\,\frac{R}{1-R}}{1 + 2\,\frac{\Delta_L}{\Delta_E}\,\frac{R}{1-R}} \qquad 4.74$$

Equation 4.74 predicts a constant fractional shift regardless of mode number n. Numerical solution of equation 4.73 indicates that α_n gets smaller for increasing n, and that equation 4.74 is valid only for small n. We illustrate this by using two examples.

(i) Cavity used by Bhawalkar et al.

For their cavity we find $\Delta_L = 0.05\text{cm}^{-1}$, $\Delta_E = 1.2\text{cm}^{-1}$, R = 0.8. Equation 4.74 gives $\alpha_n = 0.25$. Numerical solution of equation 4.73 gives the following values for n = 1, 2 and 3.

n	$1 - \Delta/n\Delta_L$
1	0.22
2	0.14
3	0.10

(ii) Telescopic resonator

For this cavity we have $\Delta_L = 3.8 \times 10^{-3} cm^{-1}$, $\Delta_E = 0.35 cm^{-1}$, $R = 0.72$, and so from equation 4.74, $\alpha_n = 5.3 \times 10^{-2}$. Exact solution yields

n	$1 - \Delta/n\Delta_L$
1	5.3×10^{-2}
2	5.1×10^{-2}
3	4.8×10^{-2}

We find some indirect evidence of this effect by measuring the intermode beat frequency using a vacuum photodiode and transient digitiser. Without the etalon, a beat period of 7.9ns is measured under fast Q-switching conditions. This corresponds to an optical cavity length of 119cm, in good agreement with the measured value of 120cm. With the etalon ($\Delta_E = 0.35 cm^{-1}$, $R = 0.72$) inserted and angle tuned so that strong lasing on two modes was observed when the laser was slow Q-switched, a period of 8.5ns is measured, corresponding to a cavity length of 128cm. The actual optical cavity length is now 121cm (to account for the optical thickness of the etalon), so the effective intermode spacing has been reduced by 5.5%, in good agreement with the above calculation ($\alpha_n = 5.3\%$).

This is considered to be of minor importance in our telescopic resonator, but it should be taken into account when performing mode selectivity calculations, especially with short laser resonators incorporating high reflectivity etalons when the effect can be quite significant (for instance, example (i) above).

4.3.5 Cavity losses as a result of a tilted intracavity transmission etalon

When using a transmission etalon as a mode selector, it is necessary to adjust its angle so that lasing from its surfaces is suppressed. Multiple reflections within the etalon now walk off, and for a finite diameter laser beam this results in an angle-dependent power loss. Hercher (1969) quotes an approximate formula for single-pass power loss

$$\ell \simeq 4 R \frac{t}{D} \frac{\theta}{n} \qquad 4.75$$

where t is the thickness of the etalon, D is the diameter of the beam and θ is the angle of tilt from the beam direction. Experimental measurements of etalon transmission as a function of angle (Peterson and Yariv, 1966) indicate that for small angles of incidence the linear dependence of loss with angle in equation 4.75 is approximately obeyed, but with the numerical factor 4 replaced by 6, i.e.

$$\ell = 6 R \frac{t}{D} \frac{\theta}{n} \qquad 4.76$$

For the etalon used in our telescopic resonator, R = 0.72, t = 1cm, D ≃ 4mm, n = 1.45, equation 4.76 predicts a loss $\ell = 7.45\theta$. We have typically worked with θ up to 12mrad, which implies a maximum loss ℓ = 8.7% For a laser output of 80mJ, we would therefore expect to lose several milliJoules of useful energy as an off-axis beam. A strong reflected beam from the etalon was indeed observed, although no measurement has been made of the energy it contained. There was, however, sufficient energy to burn polaroid film and remove black anodising from aluminium, and from this we estimate that it contained ∿1-10mJ. Clearly this represents a significant loss, and suggests that a correctly designed resonant reflector output coupler, which is inherently free from walk-off loss, would be a better choice in this respect. At the end of this chapter we include some suggestions concerning the use of single-plate uncoated resonant reflectors for single-frequency laser operation.

4.4 Experimental

In sections 4.1 to 4.3 we have developed an analytical treatment of frequency-selection in pulsed lasers, and considered how practical limitations can degrade the expected performance. In this section we describe the experimental results obtained from an application of pre-lase triggered Q-switching to the telescopic resonator described in Chapter Three (for a brief introduction to slow Q-switching techniques, see section 4.1).

4.4.1 The resonator

The Q-switched telescopic resonator has already been shown in figure 3.8, and this same figure is repeated here, renumbered figure 4.15, for ease of reference. Frequency-selection was achieved by using an intracavity Fabry-Perot etalon, of thickness t = 1cm and power reflectivities (measured) R = 0.72. This was held in a temperature controlled oven, and mounted in the laser between the high reflectivity mirror and Pockels cell. The reasons for this choice of position for the etalon are the same as those for the Pockels cell, and are discussed in the cavity alignment procedure, section 3.3.2. As a result of absorption and walk-off losses in the etalon (see section 4.3.5, and also Peterson and Yariv, 1966), we found that to maintain an output energy of 80mJ an increase in pump energy from 42J to 51J was necessary when the etalon was inserted.

Drawing on the earlier sections of this chapter, we calculate the expected performance of the laser as follows. The ideal fractional mode selectivity per cavity round trip, ε_T, introduced by this etalon is 8.12×10^{-2}, where we have used data from table 4.1 (corrected for frequency pulling, as discussed in section 4.3.4), and equation 4.42(b). This gives the ratio of adjacent mode powers at the time switching occurs, $P_n(t_s)/P_m(t_s) = 1.9 \times 10^{16}$, which has been calculated using equation 4.35 with $R_{1n}/R_{1m} = 1.0812$ and $q_{eff} = 480$. Finally, from section 4.3.1, equation 4.56, one would expect ~75% of the laser shots to be 'single mode' (using the criterion that 'single mode' operation means that less than 1% amplitude modulation would be visible if the pulses were displayed using a fast detector and oscilloscope).

In order to obtain the maximum mode selectivity, we temperature-tuned the resonant reflector so that a reflectivity peak coincided with the gain maximum of the laser rod. This was arranged by analysing the spectrum of the pre-lase Q-switched laser output using a plane-parallel Fabry-Perot interferometer after first frequency doubling the radiation in type I phasematched KD*P. For this experiment the intracavity etalon was omitted, so the frequencies of the laser output were determined by the position of the resonant reflector peaks. The resulting linewidth, calculated from equation 4.25(a) with q = 480, $C_E = 1.15$ and $\Delta_E = 0.57\text{cm}^{-1}$, is 0.015cm^{-1}, corresponding to roughly 4 longitudinal modes. Before taking any results, the flashlamps were run for approximately one hour to allow the coolant, and hence the laser rod, to

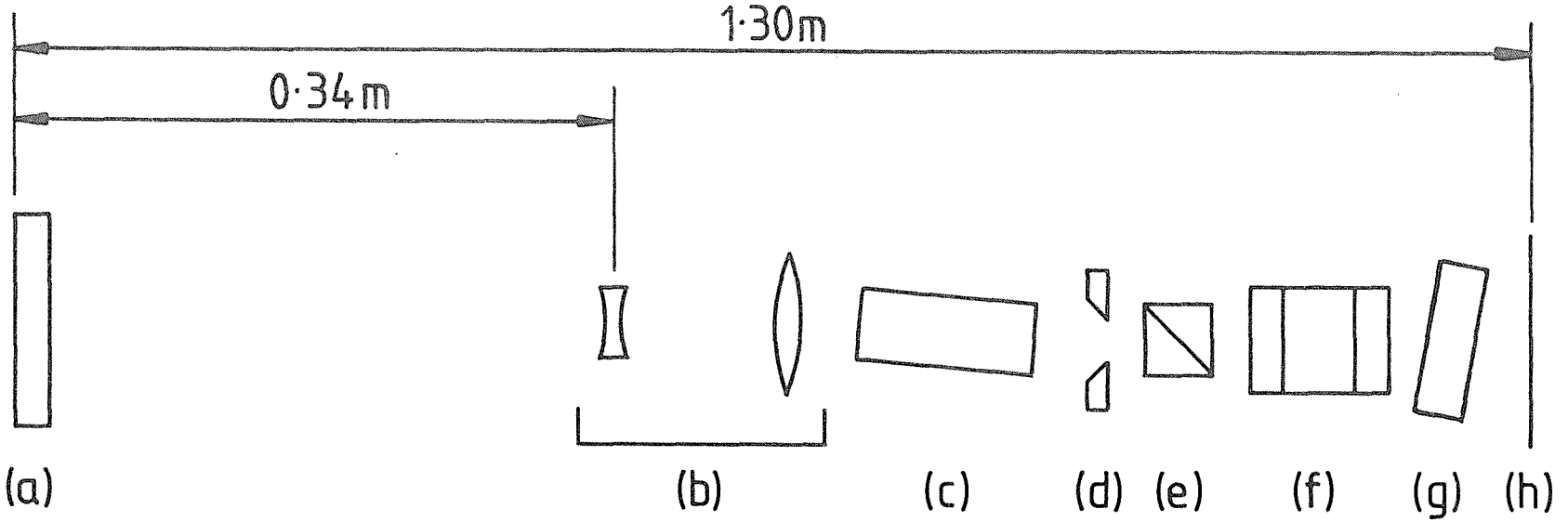

(a) Resonant reflector. 6mm thick.
(b) Telescope. Magnification=4
(c) Laser rod.
(d) Aperture. 6·25mm dia.
(e) Dielectric polariser.
(f) Pockels cell.
(g) Tilted etalon.
(h) Plane mirror. 93% reflectivity.

Figure 4.15: Pre-lase Q-switched telescopic resonator

reach a steady state. The resonant reflector was initially set to a temperature of 30°C, and was tuned in 1° increments up to 45°C. The output was analysed using an etalon characterised by $\Delta_E = 1.7cm^{-1}$, $F_E = 7$, arranged as shown in figure 4.16. The rings were observed at a distance of ∿1m from the etalon, and for most of the temperature range consisted of a single, sharp ring per free spectral range. However, when the resonant reflector temperature was set to 35 ± 0.5°C or 43 ± 0.5°C, a pattern of three rings per free spectral range was observed, the spacing between adjacent rings corresponding to the free spectral range of the resonant reflector. This indicates that for these temperatures, the resonant reflector peaks are symmetrically situated on either side of the gain maximum. The optimum temperatures for the resonant reflector were therefore ∿30°C and ∿39°C. For convenience, the temperature was set to the lower value of 30°C. It should be noted in passing that if the temperature of the coolant is changed, the temperature of the resonant reflector should also be reset. This is because the centre frequency of the fluorescence in Nd:YAG is temperature-dependent, changing by $-0.04cm^{-1}$ per degree centigrade (Kushida, 1969).

Alignment of the resonator is completed by ensuring that a transmission peak of the tilted etalon is centred on the gain maximum of the laser rod. We have found that this may be easily accomplished in the following way:

(a) Using an autocollimator, the etalon is aligned to make an angle of a few minutes of arc with the high reflectivity mirror. This is done to ensure that lasing cannot occur as a result of the reflection from the etalon. (Lasing occurs if the etalon is aligned to the resonant reflector to within ∿1 minute of arc.)

(b) The laser is now pumped, but with the Pockels cell supply set to the quarter-wave voltage, thereby suppressing laser action.

(c) The voltage is slowly reduced, until pre-lasing occurs (∿2.2 to 2.6kV for our laser), triggering the Q-switch via the detector and Marx Bank and producing Q-switched operation of the laser.

(d) A small increase is made to the voltage, with the effect of only just inhibiting lasing.

(e) The etalon is tilted. This moves a transmission peak towards the gain maximum, thus re-establishing Q-switched laser operation.

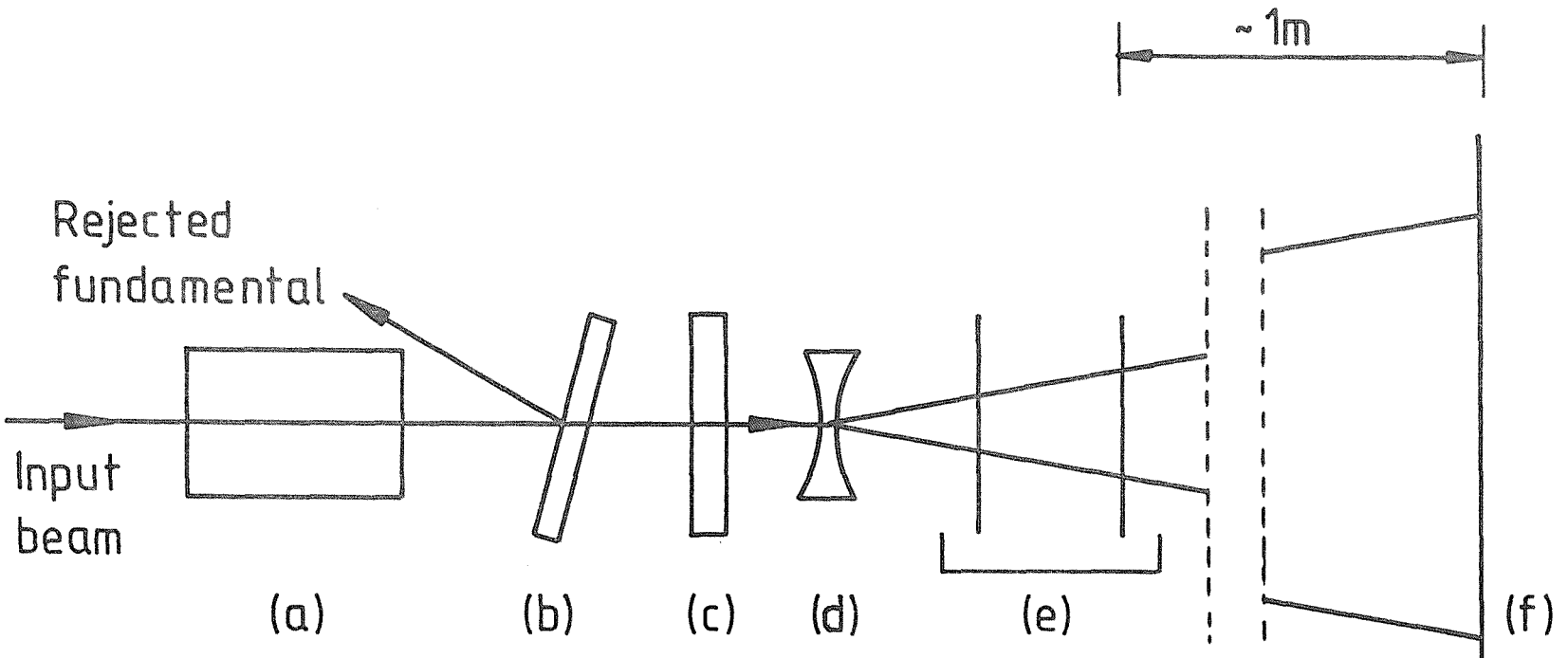

(a) Doubling crystal.

(b) Dichroic mirror. High reflectivity for 1·06μm, low reflectivity for 0·53μm

(c) KG3 filter.

(d) Lens. -5cm focal length

(e) Fabry - Perot interferometer.

(f) Screen.

Figure 4.16: The experimental arrangement used to set the resonant reflector temperature

By following steps (d) and (e) iteratively, the etalon transmission peak becomes progressively centred on the laser gain maximum, and also results in the Pockels cell voltage being set to its optimum value.

4.4.2 Evaluation of performance

The detection of a smooth pulse by a detection system of limited bandwidth may be the result of either single-frequency output, or the simultaneous oscillation of many randomly phased modes. In order to distinguish between these possibilities, the laser output was simultaneously monitored using:

(i) An ITT vacuum photodiode and Tektronix transient digitiser with a response time <1ns.

(ii) A defocussed confocal spherical Fabry-Perot interferometer (DFPS), characterised by $\Delta_E = 0.1cm^{-1}$, $F_E = 7$ for frequency doubled Nd:YAG radiation (Hercher, 1968; Bradley and Mitchell, 1968; Smith et al., 1972). The original specification of our instrument, as described by Smith et al., was $\Delta_E = 0.1cm^{-1}$, $F_E > 20$, and would therefore have had sufficient finesse to resolve two adjacent longitudinal modes of our laser. The degraded finesse, as deduced by measurement of the face reflectivity of the mirrors, is thought to be due to ageing of the soft dielectric coatings used. Single-mode operation of the laser has therefore been inferred by combining the interferometer and pulse waveform data.

Our typical experimental arrangement is illustrated in figure 4.17. The output from the laser was passed through a wedged beam splitter allowing a few percent of the beam energy to fall on the vacuum photodiode. The remainder of the beam was frequency doubled using type II phasematched KD*P, and the fundamental removed using the filters shown. The second harmonic was then passed through a beam-expanding telescope. The telescope lens spacing and telescope to DFPS spacing were adjusted to produce a collimated beam within the DFPS, where we have taken into account the fact that (as a result of their design) the DFPS mirror substrates have a focal length of 75cm. The fringe pattern of a DFPS is generated in the vicinity of the central plane of the instrument (Hercher, 1968), and this, in conjunction with the lenslike nature

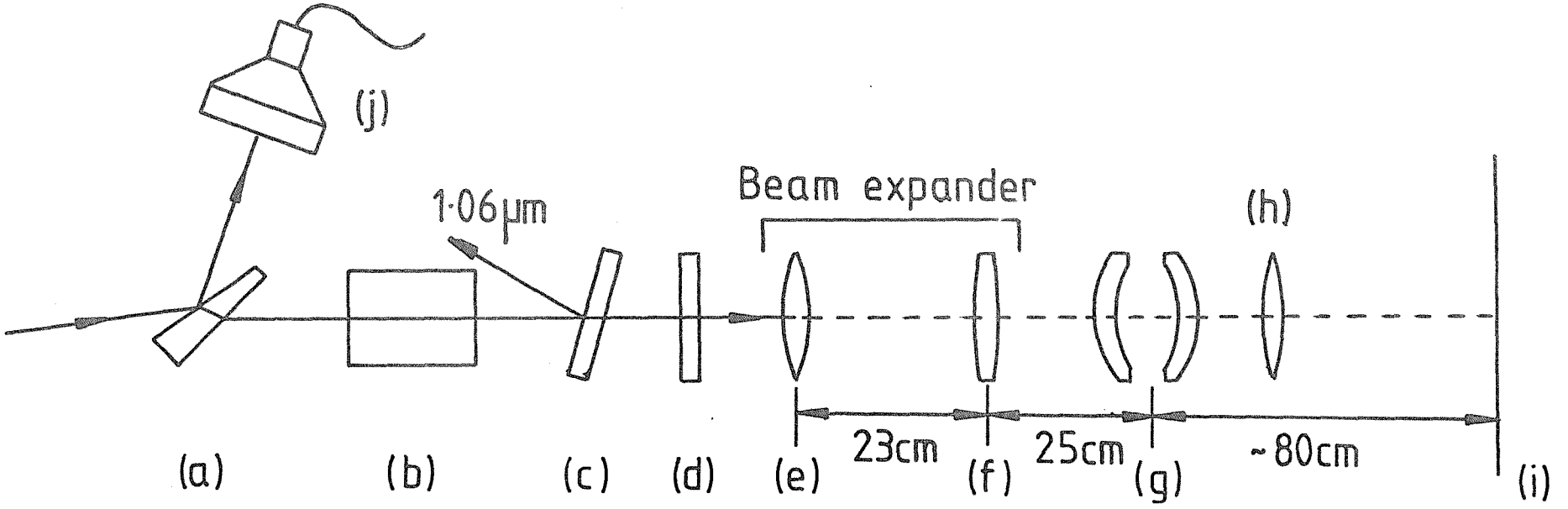

(a) Wedged beamsplitter.
(b) Frequency doubler.
(c) Dichroic mirror.
(d) KG3 filter.
(e) Lens. 5cm focal length.
(f) Lens. 30cm focal length.
(g) Fabry-Perot interferometer.
(h) Lens. 10cm focal length.
(i) Screen.
(j) Vacuum photodiode.

Figure 4.17: Experimental arrangement used for the evaluation of pre-lase Q-switched laser performance

of the mirror substrates, made it necessary to image the fringe pattern. This was achieved by using a lens, focal length 10cm, with an image to object distance of ∿80cm, arranged to give a magnification greater than unity. In the course of our experiments, however, it became clear that the pre-lase Q-switched linewidth was always less than the instrumental resolution of the interferometer ($0.014cm^{-1}$), and consequently we have had to rely on the additional observation of temporally smooth pulses as evidence of single longitudinal mode operation.

Initial tests performed on the laser gave disappointing (and misleading) results as a result of modulation of the pulse: a typical shot is illustrated in figure 4.18. The considerable depth of modulation was at first interpreted as being due to the presence of two modes in the laser output. However, whereas one might expect two oscillating modes of the laser to have random relative phase from shot-to-shot, resulting in the modulation of the pulse having random phase relative to the peak laser output, this was not observed experimentally: the modulation was fixed relative to the peak output. After some investigation we discovered that this effect resulted from a modulated cavity loss, caused by high frequency modulation of the Pockels cell voltage during and after switching. We significantly reduced the magnitude of this oscillation by incorporating a simple resistor-capacitor filter in the lead to the Pockels cell. This comprised a series resistance of 66Ω, and a high voltage disc ceramic capacitor of 300pF capacitance in parallel with the cell. This increased the fall time of the Pockels cell voltage from several nanoseconds to ∿80ns, but had no measurable effect on both fast and slow Q-switched laser output energy and pulse duration.

Typical performance as regards pulse smoothness is illustrated in figure 4.19, where we show ∿100 superimposed pulses recorded using a storage monitor in conjunction with the photodiode and transient digitiser. The laser was operating with an output energy of 80mJ at a repetition rate of 8Hz. The fixed pattern modulation of the pulses evident on the trace is due to a small amount of oscillation remaining on the Pockels cell voltage. By observing the behaviour of the output for periods of up to one hour, we found that single-frequency operation could be sustained for a maximum of 30 seconds (i.e. 240 shots), and this was followed by in general, a slightly shorter period during which

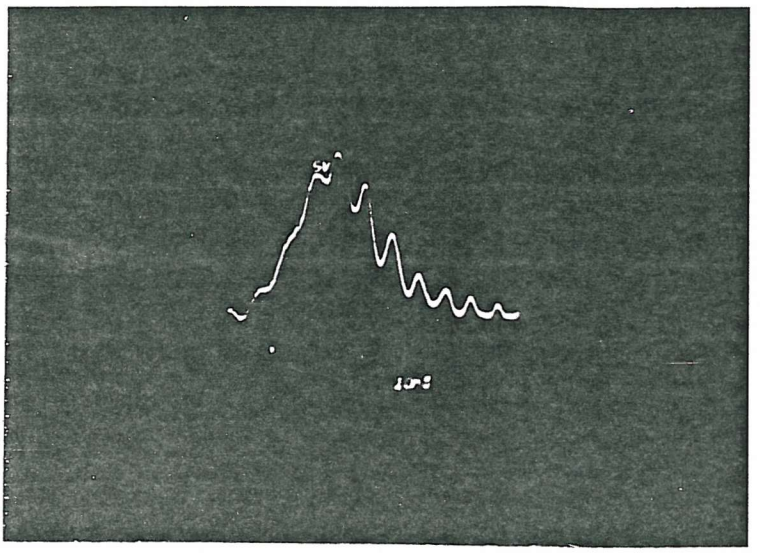

Figure 4.18: Temporal behaviour of the laser output in the presence of Pockels cell voltage modulation. 10ns per major horizontal division

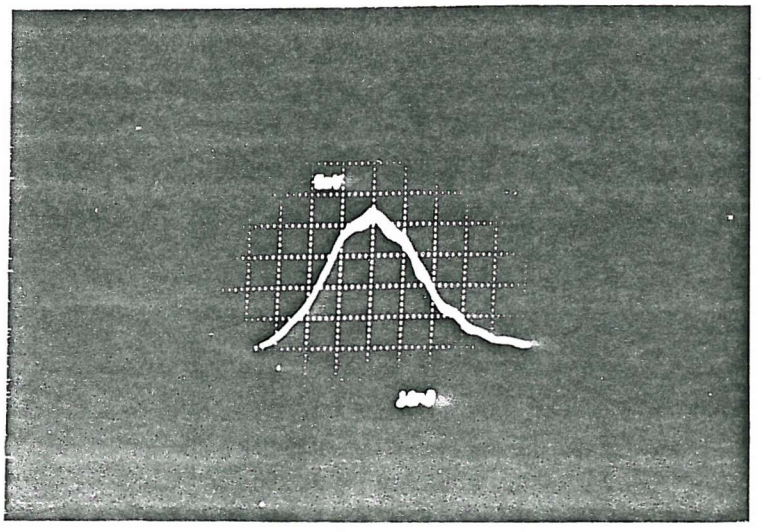

Figure 4.19: ∿100 superimposed, single-longitudinal mode pulses. 10ns per major horizontal division

the pulses showed deep modulation with a period equal to the cavity round trip time of 8.5ns. Based on these observations we estimate that approximately 60% of the laser pulses were single-mode, a figure which is in quite good agreement with the value of 75% calculated earlier. When mode beating was observed, indicating a drift in cavity mode frequencies, it was found that an angular adjustment to the etalon of ∿1mrad was sufficient to restore single-mode operation. An alternative, and more convenient method for ensuring coincidence of a cavity mode and etalon peak would be to use a wedged intracavity plate, mounted on a translation stage, to tune the optical cavity length. In this way, the etalon angle and temperature could be kept fixed, thereby ensuring coincidence of a transmission peak with the gain maximum of the laser and also keeping losses introduced by the etalon constant. Although this technique has not been tested as part of the work performed for this thesis, continuing work within the Laser Research Group has shown the practical advantages of this scheme (A.J. Berry, Private Communication).

A comparison of the transverse mode behaviour of the beam for the cases of fast and pre-lase Q-switching, both with and without the mode selecting etalon, revealed that there was no visible or measurable change in beam profile or divergence.

One troublesome aspect of the lasers' performance was the presence of a second, weaker pulse, which appeared 150-200ns after the main pulse and contains 21% of the total pulse energy. This behaviour, shown experimentally in figure 4.20, is due to a phenomenon known as spatial hole burning (Tang et al., 1963), and may be understood by considering the standing wave pattern set up in the laser rod when single-mode operation takes place. This causes a spatially periodic depletion of the inversion, leaving stored energy within the rod that can subsequently be extracted by a cavity mode of different frequency to the depleting mode. This problem is most severe if the rod is optically half-way between the mirrors, in which case it is the adjacent longitudinal mode which is best able to exploit the gain. With our experimental arrangement, and the physical limitations of the rail mounting system, the rod is ∿40cm from one mirror and ∿70cm from the other, suggesting that the second pulse may be at the adjacent mode frequency of the laser. Evidence for this was found by observing the behaviour of the second pulse over a period of some minutes. When the laser was producing a single-frequency first pulse, the peak of the second

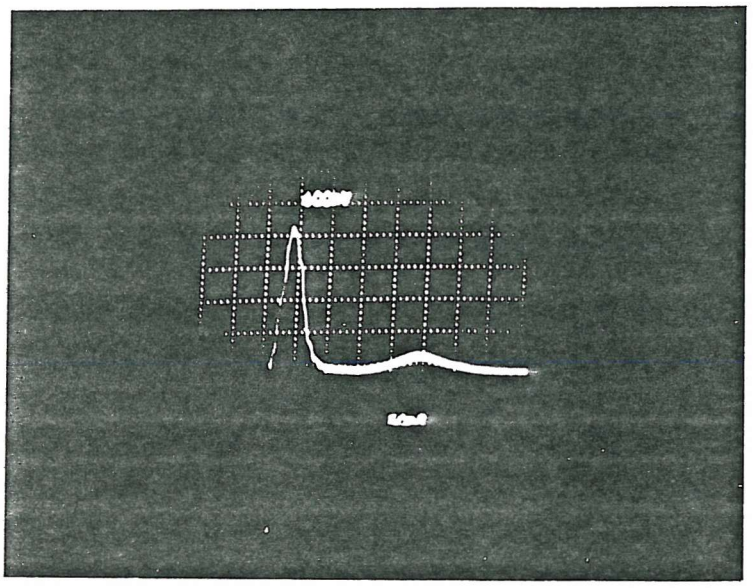

Figure 4.20: Temporal profile of an output pulse showing the presence of a secondary pulse caused by spatial hole burning. 50ns per major horizontal division

pulse occurred 150-200ns after the first. However, as the laser mode frequencies drifted relative to the etalon, the second pulse moved closer in time to the first, until the two pulses had some overlap, and the modulation that then resulted could be seen to have the cavity round trip frequency. Finally, the pulses merged completely, producing base line modulation of the composite pulse. In addition to this secondary pulse, there were also a few relaxation oscillation spikes, occuring about 500ns after the first, Q-switched pulse. The energy contained in these spikes is estimated to be about 13% of the total pulse energy. The spatial hole burning problem has been eliminated in c.w. Nd:YAG lasers by suppressing the standing wave behaviour in the laser rod, and two techniques exist which lend themselves to pulsed operation: (i) the use of a ring resonator (A.R. Clobes et al., 1972), (ii) forcing the laser to operate with circularly polarised light in the rod by placing a quarter-wave plate at each end of the rod (D.A. Draegert, 1972). However, in view of the extra complexity, expense and time that would have been involved in exploring these techniques, we have continued to operate the laser unchanged, accepting the presence of this second pulse, and taking account of the energy contained in it, and the relaxation oscillations, in subsequent experimental work.

4.5 Discussion and Recommendations for Further Work

In our study of pre-lase Q-switching we have found three main areas in which improvements could be made: (a) the fraction of shots which are single-mode, (b) pulse modulation caused by oscillation of the Pockels cell voltage, (c) spatial hole burning. We expand on these three points below.

(a) There are two aspects to the question of the fraction of single-mode shots of practical importance. Firstly, to enable the laser operator to quickly and easily correct for drift of cavity modes, one would like to ensure a slow, smooth variation with time of relative mode content. With the laser described in this thesis, single-mode operation was only observed for periods of less than 30 seconds, and this is thought to have been due to variations of the air temperature caused by nearby equipment cooling fans (see also section 4.3.2). Future work should therefore include the addition to the laser of a draught excluding or temperature-controlled box. Secondly, one should consider ways in which the fraction of single-frequency shots can be increased. In principle this may be achieved by increasing the selectivity of the mode-selecting etalon, reducing the cavity length, or

lengthening the pulse build-up time (see sections 4.2.4, 4.2.5 and 4.3.1). It is not obvious that increasing the face reflectivity and thickness of a tilted etalon necessarily results in greater mode selectivity, since walk-off as a result of the tilt leads to a degraded finesse, and also increased losses which decrease the output power of the laser. Furthermore, increasing the face reflectivity results in a greater susceptibility to damage. The second technique is not easily applicable to the telescopic resonator, since a reduction in cavity length must be accompanied by a reduction in output power to remain within the damage ratings of the laser components (see Chapter Two). The final technique, that of increasing the number of cavity round trips, could be usefully applied (Luther-Davies et al., 1979), provided the mechanical and thermal stability of the laser was sufficiently high (section 4.3.2).

Two methods of producing high mode selectivity, without the problems inherent in using a high finesse tilted intracavity etalon, must be mentioned, and provide a balance to the rather negative comments above. Firstly, one can use a multiple-plate resonant reflector (see, e.g. Watts, 1968). By exploiting multiple resonance effects, one can achieve a high degree of mode selectivity. At the same time, however, two problems exist with this device. (i) The design, construction and tuning of such a device is, in practice, difficult. (ii) As one increases the number of surfaces contributing to the resonances, so the peak reflectivity increases (see, e.g. Born and Wolf, 1975). For a two-plate reflector of plate index 1.5, one gets a peak reflectivity of 45%, as compared to a single-plate of reflectivity 15%. For the telescopic resonator this exposes damage sensitive components to a higher power level, which may be unacceptable. The second solution is to use a thick single-plate resonant reflector. From section 4.2.5, equation 4.41(b), one can see that by reducing Δ_E, so the mode selectivity increases. Calculation suggests that a thickness of about 10cm should be adequate for the telescopic resonator. However, because of the small value of Δ_E implied by this thickness, it is now possible for the laser to oscillate on several longitudinal modes separated by the free spectral range of the resonant reflector.† In practice, this problem can be cured by inserting a thin, uncoated, tilted etalon into the cavity, characterised by contrast and free spectral range C_E', Δ_E'. The ratio of mode powers at line centre and Δ_E away from

---

†This can be verified by rewriting equation 4.30 with Γ_{SQ} replaced by 2Δ and $\ell n2$ by ℓnx, where x is the ratio of mode powers at $^{SQ}\omega_0$ and $\omega_0 \pm \Delta$. For our typical values, using $q_{eff} = 480$ and $\Delta = \Delta_E$, one gets $x = 1.16$.

line centre can then be calculated using equations 4.43(b) and 4.42(b) with Δ_E, C_E and Δ replaced by Δ_E', C_E' and Δ_E.

(b) As we have shown, modulation of the Pockels cell voltage can have a severe effect on the temporal profile of the laser pulse. Although we have adopted a simple solution to this problem which in practice gives good results, a more acceptable long term solution would be a careful redesign of the Krytron switching circuitry responsible for removing the Pockels cell voltage. Alternatively, one might consider using a multiple transistor crowbar switch, which offers the advantages of clean, fast, jitter free switching (Luther-Davies et al., 1979, and Private Communication).

(c) Spatial hole burning is a problem common to all single-mode lasers, and, as mentioned in section 4.4.2, has two solutions which we were unable to pursue. An alternative is to move the laser rod closer to one end mirror with the result that only modes sufficiently removed from the main mode to be suppressed by the mode selecting etalon can exploit the remaining gain. This was tried in our laser by exchanging the positions of the Pockels cell, polariser, etalon and pump chamber (see figure 4.14). Unfortunately it proved to be impossible to suppress spurious lasing which occurred between the end mirror and Pockels cell, and the technique was consequently abandoned. Subsequent experiments, however, using a new laser head featuring a lower gain rod whose barrel had been 'profiled' to suppress superradiance, have been successful in the suppression of the secondary pulse by the above technique (A.J. Berry, Private Communication).

4.6 Conclusions

In this chapter we have investigated experimentally and theoretically the problems of controlling the linewidth of a Nd:YAG laser. In fact, the theoretical analysis is also applicable to other laser media, e.g. ruby. In particular the conditions required for single longitudinal mode operation of a Q-switched laser have been analysed. The influence of practical limitations, such as thermal and mechanical effects, has been considered, and their effect on the reliability of single-mode lasers quantified. Some mechanisms which are responsible for transient cavity length changes during the build-up of a selected single mode have been analysed, and numerical estimates have been made

concerning their magnitude in our experimental arrangements. With careful laser design, as regards mechanical stability and optical alignment, it is shown that these effects can be minimised to the extent that they may be safely ignored.

Experimental work has been performed on a pre-lase triggered telescopic resonator incorporating a tilted intracavity Fabry-Perot etalon to select a single longitudinal mode, and it has been shown that single-mode operation can be secured for about 60% of the laser shots. Typical operating conditions have been 8Hz repetition rate and 80mJ output energy. Pulse modulation as a result of oscillation of the Pockels cell voltage has been identified and minimised in a simple way, by incorporating an electrical filter in the high voltage lead to the cell.

The chapter has been concluded with some remarks concerning possible future development work on the resonator aimed towards improving the smoothness and repeatability of the laser pulses.

CHAPTER FIVE

APPLICATIONS USING THE OUTPUT FROM THE TELESCOPIC RESONATOR: FREQUENCY DOUBLING AND STIMULATED RAMAN SCATTERING

5.1 Introduction

In this chapter we describe two experiments in non-linear optics performed using the output from the telescopic resonator. First, in section 5.2 we discuss second harmonic generation. This was chosen since it is the simplest non-linear optics experiment, and offers the possibility of good agreement between detailed theory and experiment. Furthermore, it provided an opportunity to show the differences between using single and multi-longitudinal mode pump radiation. In section 5.3 we examine stimulated Raman scattering in Caesium vapour using the frequency doubled Nd:YAG radiation to pump the $6s_{1/2} - 5d_{5/2}$ Raman transition, thus generation Stokes radiation at 2.38μm. This work was performed because, as a result of other work in the laboratory, there was an interest in making a careful comparison of the calculated and measured values for Raman gain coefficient.

In both the frequency doubling and Raman scattering experiments we found good agreement between experimental observation and theoretical prediction.

5.2 Frequency Doubling

5.2.1 Large signal energy conversion efficiency for harmonic generation using a single-frequency pulsed laser

We begin by writing an expression for the fundamental field envelope within the non-linear crystal as a function of radial distance, r, from the beam axis and time, t, as

$$E_1(r,t) = E_{10} e^{-r^2/w_o^2} e^{-t^2/\tau^2} \qquad 5.1$$

where E_{10} is the peak E-field in the pulse, and we assume that the pulse is Gaussian in both the radial distance and in time, and also that diffraction of the beam may be neglected. Later in the analysis it will be found that considerable simplification can result from expressing the

electric fields in terms of a single variable. This may be achieved by writing $t' = w_o t/\tau$, and introducing a normalised variable, ρ, defined by

$$\rho = (r^2 + t'^2)^{\frac{1}{2}}/w_o$$

In this way, one can treat the variables x, y, t' in an analogeous way to the usual spatial coordinates, x, y, z, and exploit the 'spherical symmetry' by writing, instead of x, y, t', the corresponding spherical polar coordinates ρ, θ, ϕ. Equation 5.1, for example, may be rewritten

$$E_1(\rho) = E_{10}e^{-\rho^2} \qquad 5.2$$

The conversion of the fundamental field to the second harmonic may be exactly solved for infinite planewaves propagating in a lossless, infinite medium under the conditions of perfect phasematching (Armstrong et al., 1962; R.L. Byer; "Parametric oscillators and non-linear materials" in Harper and Wherrett, 1977). The solution may be written

$$E_2 = E_1 \tanh\left[\eta_s^{\frac{1}{2}}\right] \qquad 5.3(a)$$

where E_2 is the envelope of the second harmonic field. Alternatively, this can be rewritten in terms of a large signal, planewave, c.w. conversion efficiency

$$\eta_L^{(a)} \equiv \left|\frac{E_2}{E_1}\right|^2 = \tanh^2\left[\eta_s^{\frac{1}{2}}\right] \qquad 5.3(b)$$

where η_s is the small signal planewave conversion efficiency, defined in terms of material and laser parameters by

$$\eta_s = 2\left[\frac{2\pi}{\lambda}|d_{eff}|\ell\right]^2 \frac{I_{10}}{n^3 c \varepsilon_o} \qquad 5.4$$

In equation 5.4, λ and I_{10} are the wavelength and peak intensity of the

fundamental beam, ℓ is the length of the non-linear crystal, d_{eff} is the effective non-linear coefficient in units of mV^{-1}, and n is the refractive index. For the special case of a TEM_{00} pump beam of sufficiently large dimension for diffraction effects to be ignored, equation 5.3(a) can be applied point by point across the beam cross-section. Thus the second harmonic field, $E_2(e)$, is given by

$$E_2(\rho) = E_{10}e^{-\rho^2}\tanh\left[\eta_s^{\frac{1}{2}}\, e^{-\rho^2}\right] \qquad 5.5$$

The energy generated in the second harmonic pulse can be written in terms of the electric field as

$$\varepsilon_2 = \frac{\tau w_o^2}{2} nc\varepsilon_o \int_0^{2\pi}\int_0^{\pi}\int_0^{\infty} |E_2(\rho)|^2 \rho^2 \sin\theta \, d\rho \, d\theta \, d\phi \qquad 5.6$$

where we now exploit the spherical symmetry of the field. Substituting for $E_2(\rho)$ from equation 5.5 in equation 5.6, and performing the θ and ϕ integrations gives.

$$\varepsilon_2 = 4\pi\tau w_o^2 I_{10}\int_0^{\infty} \rho^2 e^{-2\rho^2}\tanh^2\left[\eta_s^{\frac{1}{2}} e^{-\rho^2}\right] d\rho \qquad 5.7$$

A similar treatment for the incident pump beam gives the fundamental pulse energy

$$\varepsilon_1 = \frac{1}{2}\sqrt{\frac{\pi}{2}}\,\pi\tau w_o^2 I_{10} \qquad 5.8$$

whence we find the pulsed, large signal energy conversion efficiency for a Gaussian fundamental beam

$$\eta_L^{(b)} \equiv \frac{\varepsilon_2}{\varepsilon_1} = 8\sqrt{\frac{2}{\pi}}\int_0^{\infty} \rho^2 e^{-2\rho^2}\tanh^2\left[\eta_s^{\frac{1}{2}} e^{-\rho^2}\right] d\rho \qquad 5.9$$

A similar analysis for a c.w. pump beam (White et al., 1970) yields a result similar to equation 5.9, viz.

$$\eta_L^{(c)} = 4\int_0^\infty \rho e^{-2\rho^2}\tanh^2\left[\eta_s^{\frac{1}{2}}e^{-\rho^2}\right]d\rho \qquad 5.10$$

in which the integral may be solved in closed form to yield

$$\eta_L^{(c)} = 1 - 2\eta_s^{-\frac{1}{2}}\tanh(\eta_s^{\frac{1}{2}}) + 2\eta_s^{-1}\ell n(\cosh(\eta_s^{\frac{1}{2}})) \qquad 5.11$$

Unfortunately, no closed solution has been found for the integral in equation 5.9, and consequently numerical integration has been used for its evaluation. However, small signal asymptotic solutions for all three cases can be easily written down, and are given by

$$\begin{aligned}
\eta_s^{(a)} &\simeq \eta_s && \text{(planewave, continuous)} \\
\eta_s^{(b)} &\simeq \eta_s/2\sqrt{2} && \text{(Gaussian, pulsed)} \\
\eta_s^{(c)} &\simeq \eta_s/2 && \text{(Gaussian, continuous)}
\end{aligned} \qquad \begin{matrix} 5.12 \\ (a,b,c) \end{matrix}$$

valid for $\eta_s << 1$. The conversion efficiencies defined by equations 5.3(b), 5.9 and 5.11 are plotted in figure 5.1 as a function of the small signal asymptotic conversion efficiency, defined for the three cases by equations 5.12.

The expected differences in conversion efficiency, which arise because η_s is defined in terms of the peak intensity of the beam, are largely removed from figure 5.1 by the renormalisations above (equations 5.12). We notice, however, that there still remains a difference between the three cases studied for large conversion efficiencies; a c.w. Gaussian beam has a lower conversion efficiency than c.w. planewaves, and a pulsed Gaussian beam has a lower efficiency still. Furthermore, in a realistic comparison of these three situations, one must also bear in mind that the peak intensity that can be experienced by the crystal is limited by the damage threshold, and so the differences in overall maximum energy conversion are greater than the curves in figure 5.1 show. Thus, for a pulsed Gaussian beam, the maximum conversion efficiency is in the range ∿40-60%, but for the same peak intensity, the c.w. planewave would give ∿80-95% conversion efficiency.†

---

†These results are based on published damage thresholds for KDP, KD*P and CD*A (Koechner, 1976), assuming a maximum crystal length, ℓ, equal to 4cm.

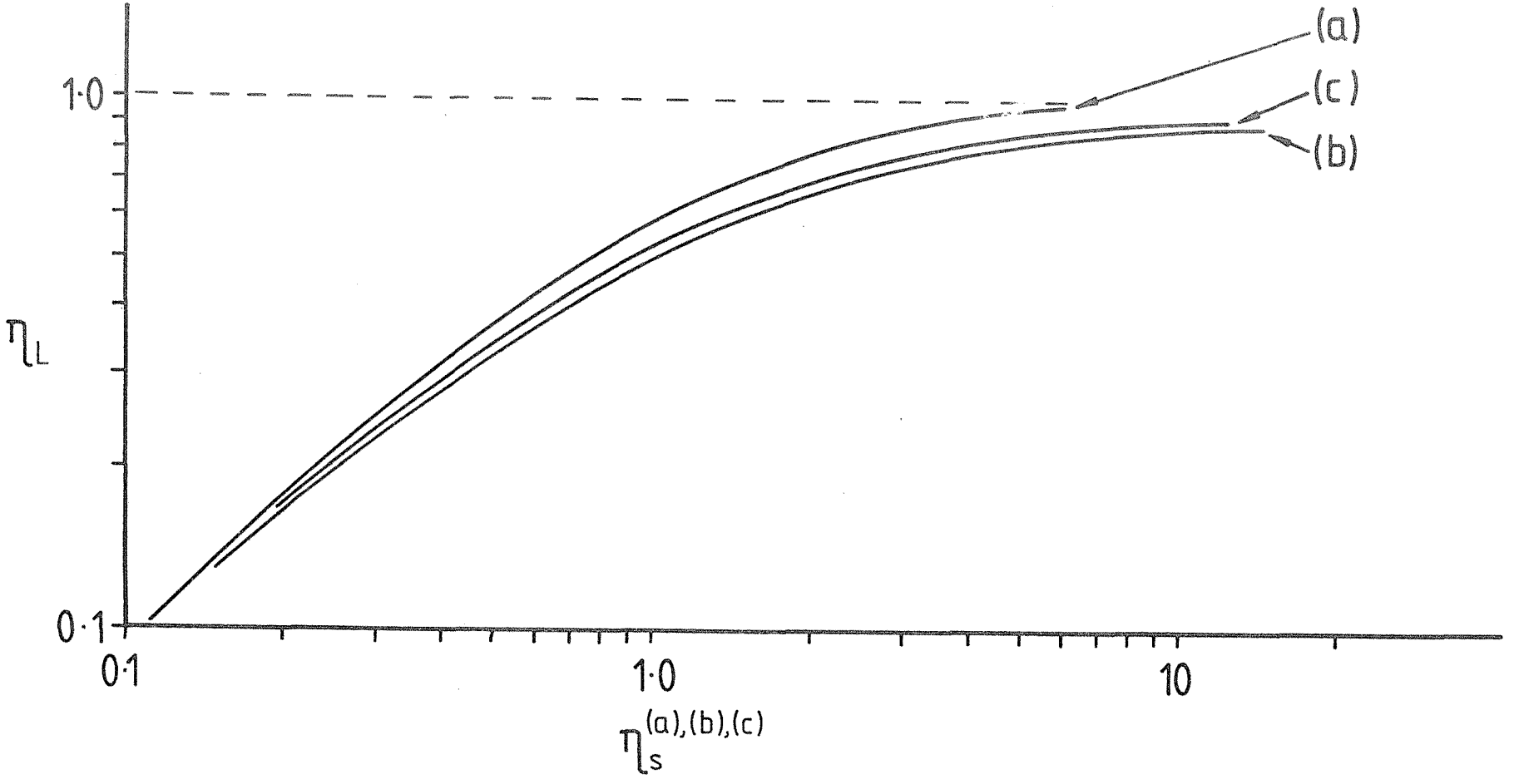

Figure 5.1: Large signal conversion efficiency, η_L, as a function of small signal asymptotic conversion efficiency, η_s. (a) Planewave pump, (b) Pulsed Gaussian pump, (c) c.w. Gaussian pump.

The experimentally determined parameters most often associated with a pulsed laser are the spot-size w, the pulse length (FWHM), $\tau_{1/2}$, and the energy, $\mathcal{E}$. It is easy to verify that the relationship between $\tau_{1/2}$ and τ is

$$\tau_{1/2} = (2\ell n2)^{\frac{1}{2}}\tau \qquad 5.13$$

and, in conjunction with equation 5.8 gives a useful equation relating the peak intensity to the measured parameters

$$I_{10} = 4\left[\frac{\ell n2}{\pi^3}\right]^{\frac{1}{2}} \frac{\mathcal{E}_1}{\tau_{1/2}w^2}$$

$$= 0.598 \frac{\mathcal{E}_1}{\tau_{1/2}w^2} \qquad 5.14(a)$$

It is also useful to note that a similar expression relates $\mathcal{E}_1$ and $\tau_{1/2}$ to the peak power in the pulse

$$P_{10} = 2\left[\frac{\ell n2}{\pi}\right]^{\frac{1}{2}} \frac{\mathcal{E}_1}{\tau_{1/2}}$$

$$= 0.939 \frac{\mathcal{E}_1}{\tau_{1/2}} \qquad 5.14(b)$$

As an example of the use of figure 5.1, consider a beam from a Nd:YAG laser which is characterised by w = 1mm, $\tau_{1/2}$ = 30ns, $\mathcal{E}_1$ = 100mJ, incident on a type II phasematched KD*P crystal of length ℓ = 2.5cm and refractive index n = 1.47 for which $|d_{eff}| = 4.98 \times 10^{-13} mV^{-1}$ (Koechner, 1976). From equation 5.14, one finds the peak beam intensity $I_{10} = 2.00 \times 10^{12} Wm^{-2}$ (within a factor of two of the damage threshold published by Koechner (1976)), and hence, using equations 5.4 and 5.12(b), $\eta_S^{(b)} = 0.903$. We therefore predict a conversion efficiency, using figure 5.1, of 47% (c.f. 85% using planewave theory, assuming a uniform beam intensity of I_{10}).

5.2.2 Experimental results

In this section we discuss the results obtained on frequency doubling of the output from the telescopic resonator. This work was performed at different times throughout the resonator experimental

programme, using various doubling crystals and input intensities, and with the resonator both fast and pre-lase Q-switched. Rather than giving a complete description of all the experimental arrangements used, we confine our discussion to general points concerning the experimental method, and summarise our results in table 5.2.

Three frequency doubling crystals were used in this work, type I phasematched KD*P, type II phasematched KD*P, and type I phasematched CD*A. The physical and optical characteristics of these crystals are listed in table 5.1, where we have drawn on data contained in Koechner (1976). The KD*P crystals were mounted in cells (and filled with an inert index matching fluid (FC104)) equipped with antireflection coated windows. These two crystals were cut for critical phasematching, and operation at room temperature. The CD*A, however, was cut for non-critical phasematching, and since this requires a crystal temperature in the range 90-100^{o}C, the doubler was mounted in a temperature-controlled oven.

Our typical experimental arrangement is illustrated in figure 5.2. The doubling crystals were mounted in an angular adjusting mount, and the doubled radiation reflected into a pyroelectric energy meter using a dichroic mirror having a reflectivity of 0.99 for 532nm radiation. Any remaining 1.06μm radiation was removed using a piece of KG3 glass which had a measured transmission of 77% for the green light. When doubling was performed using KD*P, a positive lens was placed between the laser and crystal to collimate the beam. This was necessary because the angular divergence of the laser output (0.86mrad) is comparable to the acceptance angle for efficient doubling in critically phasematched KD*P (0.67mrad for our crystal. See Koechner (1976).). Results were obtained by first measuring the energy of the 1.06μm beam using a cone calorimeter placed between the lens (if used) and the doubler. The doubled radiation was then measured, after optimisation of the crystal angle, on the pyroelectric energy meter. These two readings were then corrected to allow for the various filters, and also the Fresnel reflections at the entrance and exit faces of the cell. The results of these measurements are listed in table 5.2, along with theoretical prediction of the output energy and conversion efficiency. These calculations were performed in the following way:

(a) Slow Q-switching. When the laser is operated in this way, the output energy is divided in the ratio 0.66:0.21:0.13 between the primary

Table 5.1: Physical and optical characteristics of the doubling crystals

Crystal	Length ℓ (cm)	Ordinary refractive index @ 1.06μm n_o	Phasematching angle θ_m	$\lvert d_{eff} \rvert$ mV^{-1}
Type I KD*P	2.4	1.47	40.5^o	3.25×10^{-13}
Type II KD*P	2.4	1.47	40.5^o	4.94×10^{-13}
Type I CD*A	2.0	1.55	90.0^o	4.31×10^{-13}

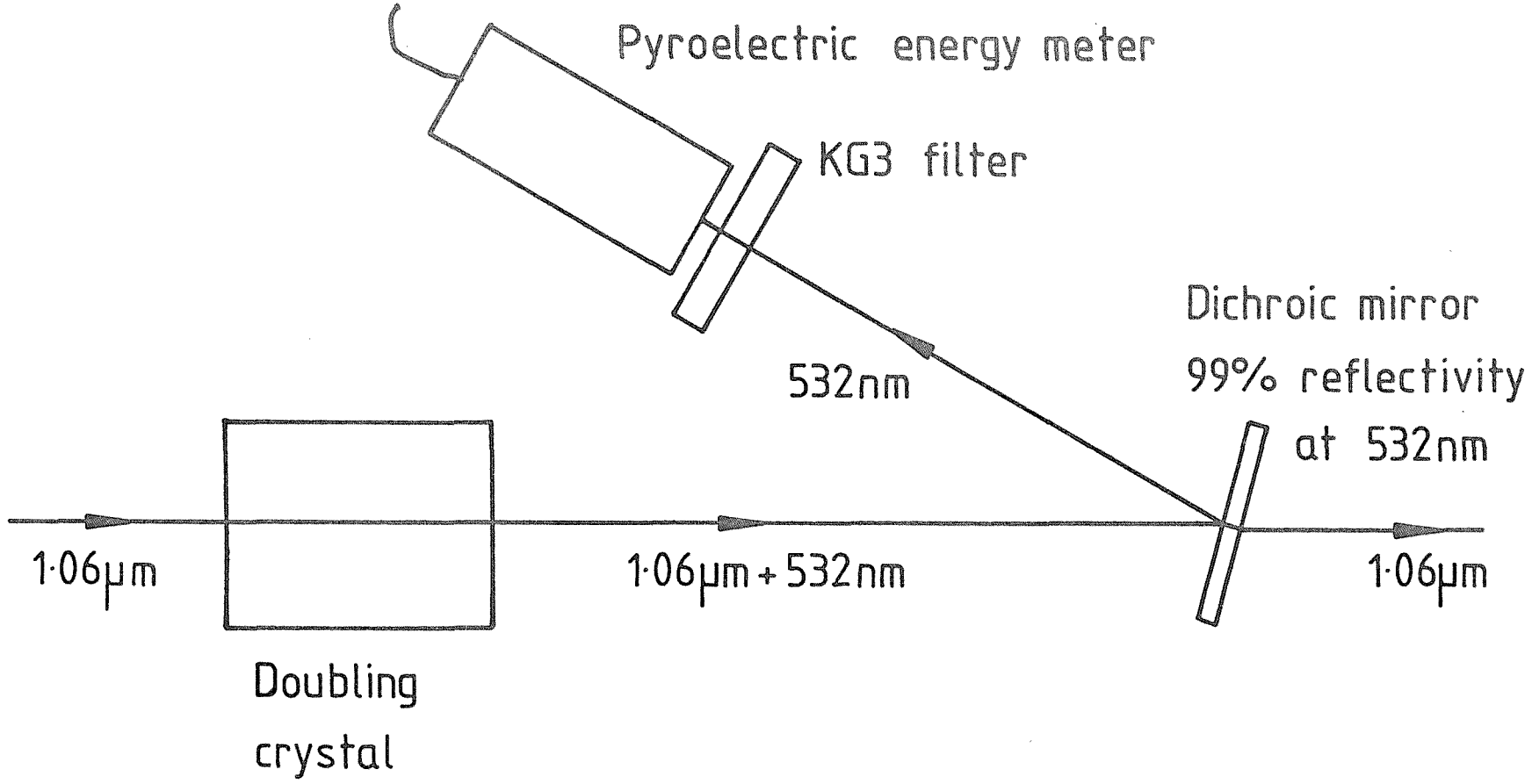

Figure 5.2: Experimental arrangement used to measure harmonic conversion efficiency

Table 5.2: Performance of frequency doubled telescopic resonator

Crystal	Q-switching technique	Input energy (mJ)	Input spot-size (mm)	Measured		Theoretical	
				Energy (mJ)	Efficiency	Energy (mJ)	Efficiency
KD*P Type I	SLOW	75.0	1.0	5.5	7.3%	8.0	10.7%
		45.4	1.9	2.8	6.2%	2.1	4.6%
	FAST	42.4	1.0	11.3	26.7%	5.7	13.4%
		75.0	1.0	16.7	22.3%	15.4	20.5%
KD*P Type II	SLOW	75.0	1.0	12.3	16.4%	14.9	19.9%
	FAST	75.0	1.0	24.9	33.2%	28.0	37.3%
CD*A Type I	SLOW	73.0	0.52	17.5	24.0%	20.2	27.7%
	FAST	83.0	0.52	43.1	51.9%	44.0	53.0%

pulse (length 30ns), secondary spatially hole-burnt pulse (length 75ns), and a later train of relaxation oscillation spikes (section 4.4.2). This final component of the laser output will give a negligible contribution to the total frequency doubled output energy, and is consequently neglected in the calculation. The theory of section 5.2.1 was applied separately to the primary and secondary pulses, and the contributions added together and listed in the table. We note the fact that the predicted output energy is 20-30% higher than the observed output for all three crystals. One possible reason why this should be so is that no account has been taken in our calculations of the absorption of the fundamental and second harmonic radiation by the crystal. The measured absorption of the type II KD*P doubler used in our experiments is 14% at 1.06μm and 4% at 532nm, and would thus account for much of the discrepancy.

(b) Fast Q-switching. When fast Q-switched the laser produces a single pulse 30ns long (for our operating conditions), with no evidence of relaxation oscillations. The predicted energy in the table has therefore been calculated (for reasons of comparison) by assuming that the pulse is single-frequency, and applying the theory in section 5.2.1. For conversion efficiencies $\lesssim$20%, the predicted energy is somewhat lower than was observed experimentally, whereas for higher conversions, the two values are comparable. This is because the theoretical treatment presented earlier applies to a single-mode pump field, which is not the case for our fast Q-switched laser. The effect of a multi-frequency pump laser on harmonic generation is to enhance the average second harmonic output. For low conversion efficiencies, one can show that the factor by which the second harmonic output is increased is $(2 - 1/n)$, where n randomly phased modes are present in the pump field (N. Bloembergen, in Fox, 1963; Zernike and Midwinter, 1973). For large conversion efficiencies, however, this factor approaches one (Hagen and Magnante, 1969).

An interesting consequence of the frequency doubling process is that, in the small signal region, the second harmonic pulse grows with a spot-size and pulse length foreshortened by a factor $1/\sqrt{2}$ as compared with the fundamental. This can be seen from equation 5.5, by writing $\tanh(\eta_s^{\frac{1}{2}} e^{-\rho^2}) \simeq \eta_s^{\frac{1}{2}} e^{-\rho^2}$. We illustrate this effect experimentally in figure 5.3, where we show the temporal behaviour of the fundamental and second harmonic pulses. For this measurement, the laser was pre-lase

(a)

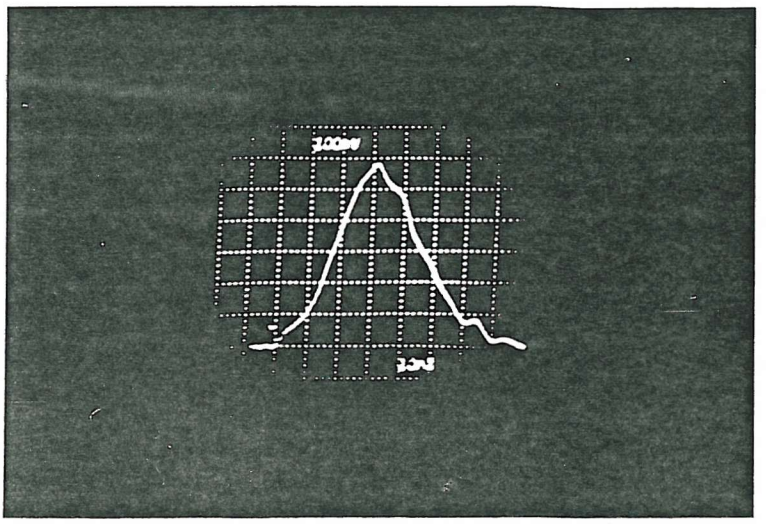

(b)

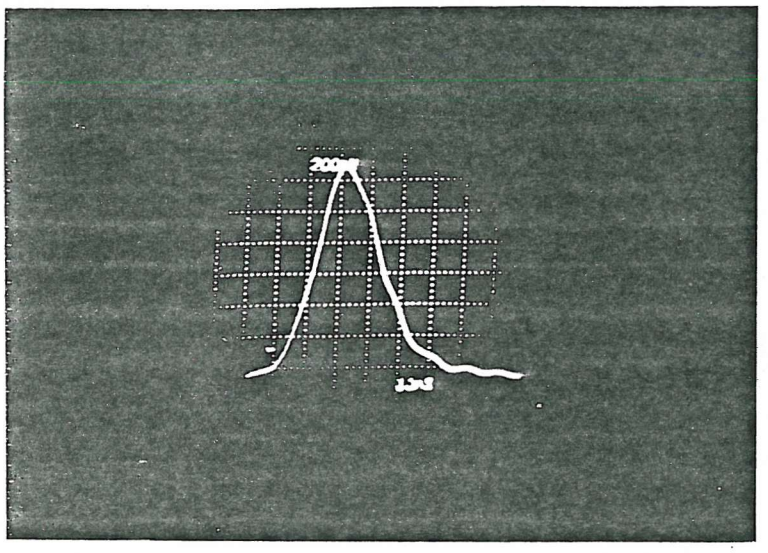

Figure 5.3: Temporal profile of the fundamental and second harmonic, for frequency doubling of a single-frequency Nd:YAG laser in type II phasematched KD*P
(a) Fundamental. Pulse length 29ns
(b) Second harmonic. Pulse length 21ns

Q-switched, and frequency doubled in type II phasematched KD*P. The ratio of pulse lengths, as measured from figure 5.2, is 21/29 = 0.72, and is in good agreement with the theoretical prediction of 0.71.

5.3 Stimulated Raman Scattering of Frequency Doubled Nd:YAG Radiation Via the $6s_{1/2} - 5d_{5/2}$ transition in Caesium Vapour

5.3.1 General

The Raman scattering process under study in this section is illustrated in figure 5.4. A pump wave $\lambda_P = 532nm$ is used to generate a frequency shifted Stokes wave of wavelength $\lambda_S = 2.38\mu m$. This transition was chosen for study since it is potentially of interest for tunable infra-red generation, but earlier work on this transition (Hodgson, 1979; Wyatt and Cotter, 1980) had indicated inconsistencies in the published threshold pump intensity. Clearly, a TEM_{00}, single-frequency pump would permit an ideal examination of this process. Consequently, we begin section 5.3 with some general comments concerning Raman scattering, and then obtain a theoretical prediction of Raman gain coefficient and threshold power. In section 5.3.4, experimental work is described which gives results in quite good agreement with the theoretical prediction.

A planewave analysis of the wave equations describing Raman scattering (see, e.g. Hanna et al., 1979) yields the well known result for the small signal growth of the Stokes wave intensity as a function of distance:

$$I_S(z) = I_{SO}\exp(g_R I_{PO} z) \qquad 5.15$$

In equation 5.15, I_{SO} and I_{PO} are the Stokes and pump intensities at the input face (Wm^{-2}) and g_R is the Raman gain coefficient (mW^{-1}), related to the Raman polarisability, α_R, by

$$g_R = \frac{\omega_S}{\epsilon_o^2 c^2 \hbar} \frac{N}{\Gamma} |\alpha_R|^2 \qquad 5.16$$

where ω_S is the Stokes frequency ($rad.s^{-1}$), N is the number density of atoms associated with the transition (m^{-3}), and Γ (angular frequency) is the Raman linewidth (full-width half-maximum). Implicit in our definition of α_R is an orientation average and sum over level degeneracies;

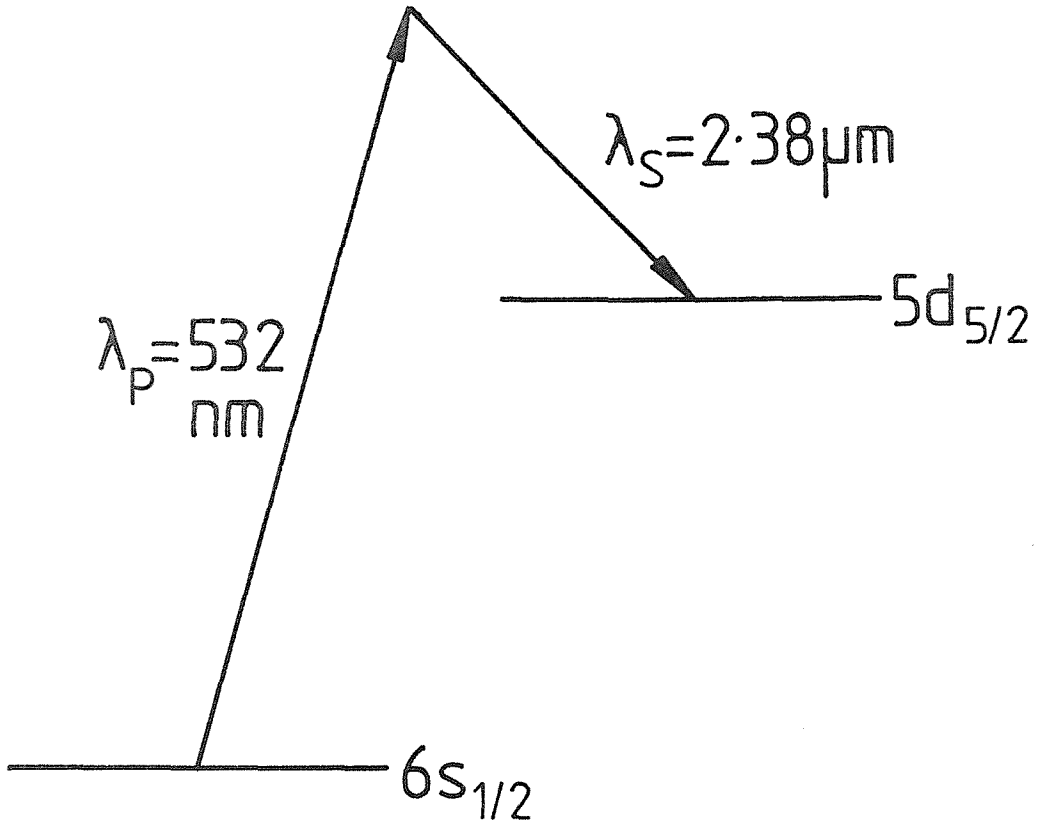

Figure 5.4: Raman scattering in Caesium

the numerical factors introduced by these considerations are discussed in some detail by Yuratich and Hanna (1976).

Note that, in equation 5.15, one requires some input noise intensity, I_{SO}, at the Stokes frequency. Although one could, in principle, inject radiation at the Stokes frequency, the approach most commonly adopted is to rely on the weak noise intensity at the Stokes frequency generated by spontaneous Raman scattering at the input end of the medium. As a result of the small signal behaviour predicted by equation 5.15, the generated Stokes intensity shows a very rapid dependence on pump intensity, and consequently one associates with the process a "threshold" pump intensity which is required to bring the Stokes wave to a detectable level. This choice of threshold is, of course, arbitrary, since it depends on the sensitivity of the detector. However, one can show that for most practical purposes, an adequate definition of threshold is

$$g_R(I_{PO}z)_{TH} \sim 30 \qquad 5.17$$

(see, for instance, the detailed discussion of this subject in Hanna et al., 1979).

In the derivation of equation 5.16, it is assumed that the linewidth of the pump laser is much less than the linewidth of the Raman transition, a requirement which may be loosely interpreted by saying that the non-linear medium response is able to follow the amplitude fluctuations of the pump wave envelope. For the opposite extreme, i.e. when the pump linewidth is much greater than the Raman linewidth, the medium response tends to follow the average pump intensity (Akhmanov et al., 1974). This has the result that equations 5.15 and 5.16 may still be used, but with I_{PO} replaced by $\bar{I}_{PO}$, the pump intensity averaged over the fluctuations. However, consider the case in which we fulfill the condition that the pump laser linewidth is much less than the Raman linewidth, but is not monochromatic. In this case, one can envisage the situation in which the pump has amplitude fluctuations which are perhaps too fast to be followed by the detection system, but which can be followed by the Raman medium. One normally deduces the Raman gain coefficient by using equation 5.17, and the measured threshold intensity. If, as discussed above, the detection system has a limited bandwidth, the observed intensity will not be the true intensity, and consequently

inaccuracies can occur in the value of g_R. We illustrate this point in the experimental section (5.3.4), where we measure the Raman gain coefficient for Caesium vapour (for which Γ is estimated to be $0.26cm^{-1}$) for $\lambda_p = 532nm$, for the two cases when the pump laser was (i) pre-lase Q-switched, (ii) fast Q-switched (when we estimate the linewidth of the frequency doubled radiation to be $\sim 0.1cm^{-1}$). A large difference in threshold energy was observed in these two cases.

5.3.2 Calculation of the gain coefficient, g_R

Drawing on results published in Yuratich and Hanna (1976), we write

$$|\alpha_R| = \frac{2}{\sqrt{75}} \frac{e^2}{\hbar} \left| \sum_i r_{fi}\, r_{ig} \left[\frac{1}{\Omega_{ig} - \omega_p} + \frac{1}{\Omega_{ig} + \omega_s} \right] \right| \qquad 5.18$$

where r_{fi}, r_{ig} are the radial matrix elements coupling the final Raman level ($5d_{5/2}$) and ground level ($6s_{1/2}$) to some intermediate level i; Ω_{ig} is the frequency (in angular units) of the intermediate state to ground state transitions, and, as a result of the selection rules associated with this process, the sum over intermediate states runs only over the $p_{3/2}$ states. The multiplying factor $2/\sqrt{75}$ applies where both pump and Stokes beams are linearly polarised in the same direction. Matrix elements for the alkali metals have been obtained by computer calculation by Eicher (1975), and tabulated in atomic units. It is useful, therefore, to cast equation 5.18 into a form which facilitates easy calculation,

$$|\alpha_R| = \frac{2}{\sqrt{75}} \frac{e^2 a_0^{\,2}}{200\pi c\hbar} \left| \sum r_{fi}\, r_{ig} \left[\frac{1}{\Omega_{ig} - \omega_p} + \frac{1}{\Omega_{ig} + \omega_s} \right] \right| \qquad 5.19$$

where r_{fi}, r_{ig} are now in atomic units, Ω_{ig}, ω_p, ω_s are in wave numbers, and a_0 is the Bohr radius, $5.29 \times 10^{-11}m$. In table 5.3 we list the values of r_{fi}, r_{ig} and Ω_{ig} relevant to the calculation. Using $\omega_p = 18797cm^{-1}$, $\omega_s = 4199.9cm^{-1}$ and equation 5.19 one calculates $|\alpha_R| = 2.39 \times 10^{-39} Cm^2V^{-1}$.

Calculation of the Raman gain coefficient can be performed once we have deduced a value for the ratio N/Γ relevant to our experimental arrangement. The two broadening mechanisms responsible for the linewidth of Caesium vapour in the temperature and pressure range of interest are

Table 5.3: Numerical data used in the calculation of Raman polarisability

Transition i-g	Ω_{ig} (cm^{-1})	r_{gi} (a.u.)	r_{if} (a.u.)
$6s_{1/2} - 6p_{3/2}$	11732.4	-5.68	5.69
$6s_{1/2} - 7p_{3/2}$	21946.7	-0.637	-1.27
$6s_{1/2} - 8p_{3/2}$	25791.8	-0.284	-0.354
$6s_{1/2} - 9p_{3/2}$	27682.0	-0.174	-0.179

Doppler broadening and pressure broadening. The well known formula for the Doppler broadened linewidth (see, e.g. Siegman, 1971) of a transition of frequency ω is

$$\Gamma_D = 2\omega \sqrt{2\ell n2 \frac{kT}{Mc^2}} \qquad 5.20$$

where M is the atomic mass. In our experimental arrangement, we have worked with T ≈ 1200K, and a vapour pressure of ∿20 torr. For T = 1200K, equation 5.20 predicts a linewidth (FWHM) of $3.14 \times 10^{-2}\text{cm}^{-1}$. Pressure broadening results in a linear dependence of linewidth on atomic number density, i.e. N/Γ_P = const. Measured values of N/Γ_P in the range $0.5\text{-}1 \times 10^{18}\text{cm}^{-2}$ have been published (Sayer et al., 1971; Wyatt and Cotter, 1980). In our calculations we will take the mean value of the quoted results, i.e. $N/\Gamma = 0.75 \times 10^{18}\text{cm}^{-2}$.

For our heatpipe oven, described later, we have an atomic number density of $2 \times 10^{17}\text{cm}^{-3}$, resulting in a pressure broadened linewidth of 0.27cm^{-1}. Strictly speaking, one should combine the pressure broadened and Doppler broadened contributions to give a Voigt profile. However, since we have $\Gamma_P >> \Gamma_D$, and also in view of the spread in values for N/Γ_P associated with pressure broadening, we will take the value for the Raman transition linewidth to be 0.27cm^{-1}. Furthermore, since the line broadening is dominated by pressure broadening, we can use $N/\Gamma = 0.75 \times 10^{18}\text{cm}^{-2}$ in equation 5.16. This yields a value for the Raman gain coefficient $g_R = 2.43 \times 10^{-11}\text{mW}^{-1}$.

5.3.3 Estimate of the pump power necessary to reach Raman threshold

A simple, order of magnitude estimate of the pump intensity required to reach Raman threshold can be made by using equation 5.17. For our experimental arrangement, the length of the Caesium vapour column is 1m, and so equation 5.17 gives $(I_{PO})_{TH} = 123\ \text{MWcm}^{-2}$. In practice, however, as in second harmonic generation, this planewave calculation is inadequate for accurate prediction, because of the Gaussian intensity profile of the beams. Also, the growth of the Stokes wave may be significantly influenced by diffraction, since the wavelength of the Stokes radiation is much longer than the pump wavelength. An analysis of this problem by Cotter et al. (1975) gives the following result for the threshold pump power

$$P_{pth} = \frac{1}{400\omega_s g_R}\left[1 + \left[1 + \frac{\omega_s}{\omega_p}\frac{\ell n\left[P_{sth}/P_{so}\right]}{\tan^{-1}(L/b_p)}\right]^{\frac{1}{2}}\right]^2 \qquad 5.21$$

where P_{sth}/P_{so} is the Stokes signal augmentation required to reach a detectable level, L is the length of the non-linear medium and b_p is the confocal parameter of the pump beam. ω_s and ω_p are in units of wavenumbers. In our experimental arrangement, confocal focussing was adopted, i.e. $L = b_p$, and we take as our threshold condition $\ell n\ P_{sth}/P_{so} = 30$. Inserting these values into equation 5.21 gives a predicted threshold pump power $P_{pth} = 409$kW.

5.3.4 Experimental

One of the problems associated with Raman scattering in Caesium vapour is the tendency for the atoms to form dimers, which cause absorption of the pump radiation (Lapp and Harris, 1966). Where a conventional heatpipe is used to contain the Caesium vapour, this can give rise to an increase in threshold (Wyatt and Cotter, 1980). However, Wyatt and Cotter discovered that the dimer density could be significantly reduced by superheating the portion of vapour through which the laser beam propagated, thereby thermally dissociating the dimers. Following this work, a "split-wick" heatpipe design (discussed in detail by Smith (1981)) has been adopted for the work discussed here, and is illustrated in figure 5.5. In this design, two short sections of stainless steel gauze at each end of the heated region of the pipe act as reservoirs for the liquid Caesium, and the section of pipe between the wicks, of length 1m, is heated to a temperature of $\sim 900^{\circ}C$ by direct resistive heating of the steel tubing. The buffer gas used to constrain the Caesium vapour to the heated region is argon. In practice it was found that argon can cause some reduction in the heatpipe transmission as a result of a fine mist of Caesium droplets at the buffer gas/Caesium interfaces. This is in agreement with observations made by Hodgson (1979), who avoided this problem by using helium as the buffer gas. However, our own experience with helium indicates that on cooling the pipe, the helium atoms become absorbed into the Caesium as it is allowed to cool at the end of the experiment. This then gives a misleading measure of the amount of helium in the pipe, and hence the partial pressure of Caesium vapour when reheated, possibly with more buffer gas added. This has led us to re-adopt argon as the buffer gas. When operated for the experiments performed for this thesis, the total pressure in the heatpipe

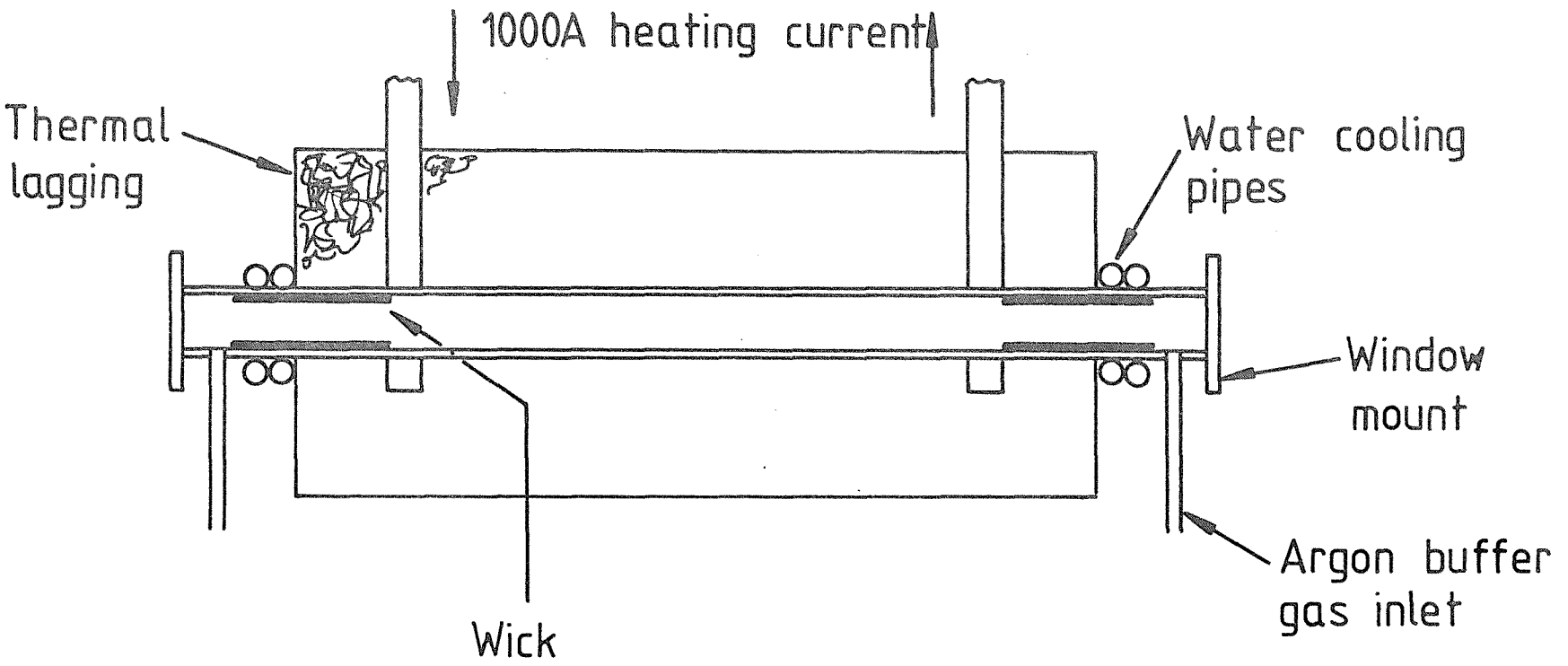

Figure 5.5: The split-wick heatpipe

was 25 torr, at an operating temperature of 940°C. Using the gas law, as applied to the superheated region of the pipe, these conditions indicate a Caesium atom number density of $2 \times 10^{17} cm^{-3}$.

The experimental arrangement used in our investigations is illustrated in figure 5.6, where we have, for clarity, omitted the various prisms used to steer the pump beam. The 1.06μm laser output was frequency doubled in either type I phasematched CD*A or type II phasematched KD*P, and focussed into the heatpipe using a 1m focal length lens. The focal length and position of the lens were chosen by calculation (Kogelnik and Li, 1966) to provide confocal focussing for the 1m long vapour column. Fine adjustments were made to the lens position to ensure that the beam focus was in the centre of the heatpipe. The fundamental radiation remaining after frequency doubling was removed using a dielectric mirror which rejected 99% of the fundamental while transmitting 95% of the second harmonic. After passing through the heatpipe, a diverging lens of focal length -5cm was used to spread the beam onto an RG715 filter, which absorbed the 532nm pump radiation while transmitting 85% at the Stokes wavelength. The radiation passed by this filter was then focussed, using a 10cm focal length lens, onto the entrance slit of a Hilger and Watts D330 grating monochromator. The output from the monochromator was detected using a Judson J12 room temperature Indium antimonide photodiode, used in the photoconductive mode, and loaded with a 50Ω termination. Alignment of the monochromator and detector was accomplished by operating the laser fixed-Q, removing the RG715 filter, and using the weak 532nm radiation to visually align the 10cm lens and monochromator. The detector was brought into alignment by adjusting its position to maximise the output signal. The Fresnel reflection from one face of the RG715 filter was allowed to fall onto a vacuum photodiode, after filtering the beam with a KG3 filter to remove any infra-red signal, to monitor the pump beam transmitted by the pipe. The input energy to the pipe was measured by using a pyroelectric energy meter just prior to the heatpipe, after first spreading the beam with a -5cm lens and blocking any remaining 1.06μm radiation using a KG3 filter. This measurement was then corrected for the measured transmission of KG3 at 532nm (0.77) and various Fresnel reflections to obtain the input energy to the pipe.

Typical results are illustrated in figure 5.7, where we show the pump input power, transmitted pump power and Stokes power for prelase Q-switched laser operation. These were obtained using the KD*P

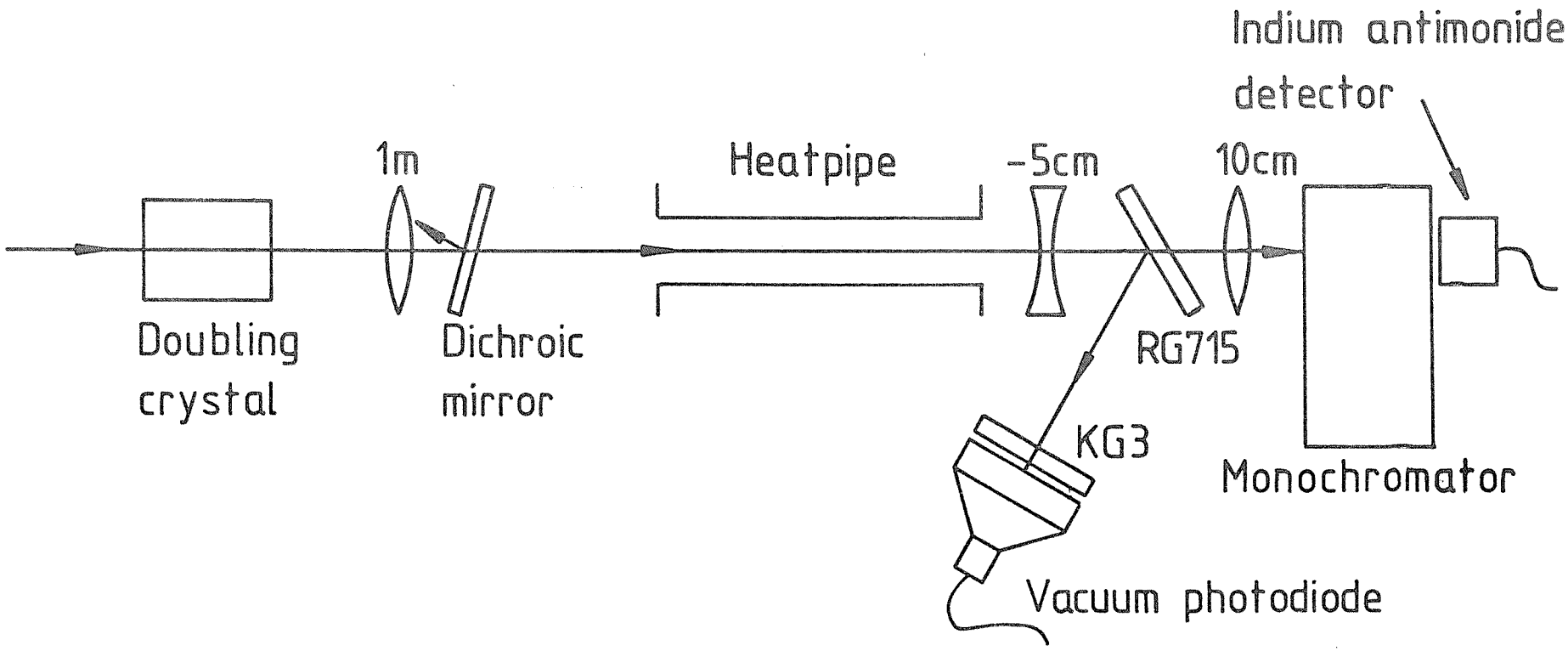

Figure 5.6: Raman scattering in Caesium vapour

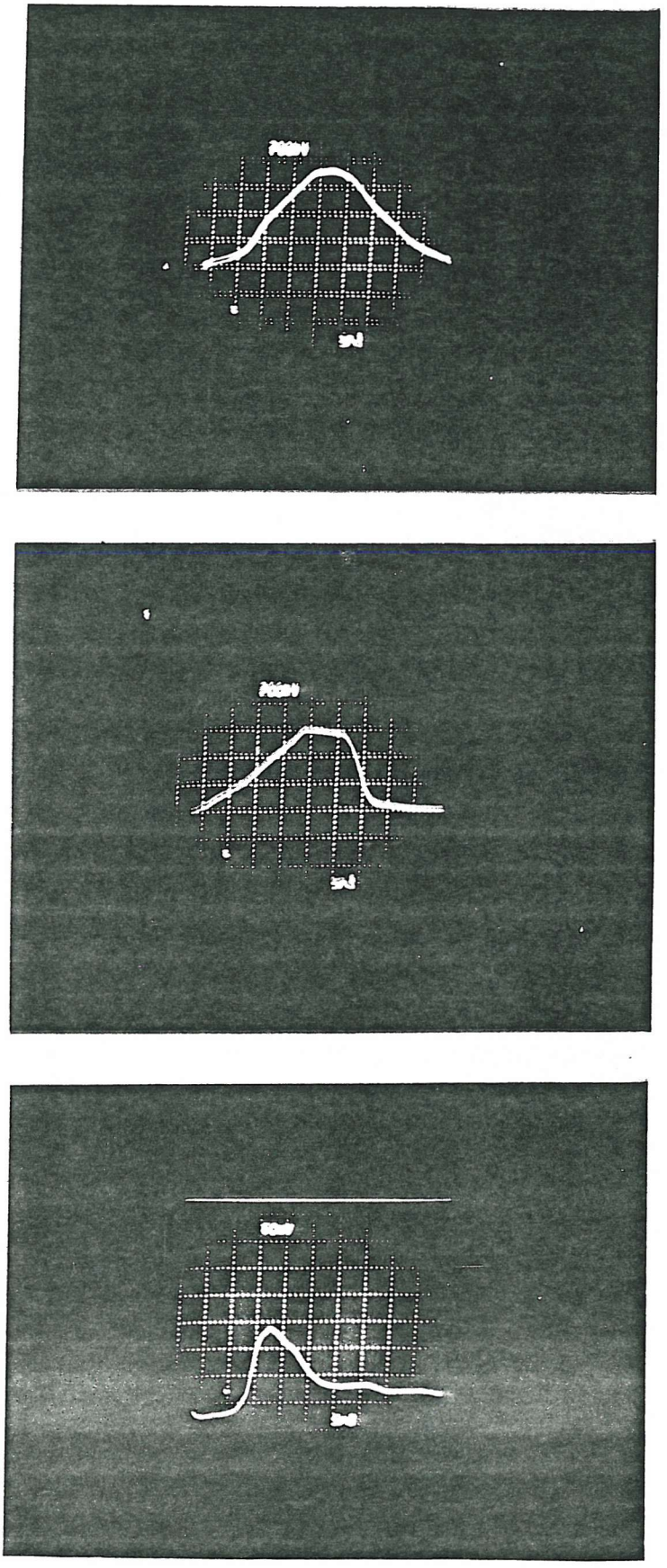

Figure 5.7: Raman scattering in Caesium vapour. Top trace: pump radiation. Middle trace: transmitted pump radiation. Bottom trace: Raman signal. 5ns per major horizontal division

doubling crystal, with 14mJ of 0.53μm input to the pipe. Threshold was determined with both the KD*P and CD*A crystals by adjusting the angle of the crystal to reduce the doubling efficiency. It was found that a 0.53μm pump level could be reached where no detectable Raman signal was present, but an estimated increase in pump energy of ∿0.5mJ was enough to restore a strong Raman output. The pump energy at which detectable Raman output ceased was measured to be 10.6mJ for both the KD*P doubler and also the CD*A doubler. With the full input of 14mJ to the pipe, the Raman signal showed a high degree of amplitude stability, and we illustrate this point in figure 5.8 where we show three random Raman pulses, taken at intervals of about ten seconds. When the laser was fast Q-switched, the threshold energy, measured in the same way as for pre-lase Q-switching, was found to be 8.3mJ, and is consistent with our earlier comments on the effect of pump linewidth on measured Raman threshold. The suggestion that the medium response is capable of following the peaks in the pump laser output is confirmed experimentally in figure 5.9, which is the Raman output signal obtained for a typical single fast Q-switched pump pulse. It can be seen that the Stokes pulse consists of four peaks, separated by half the pump laser cavity round trip time.

In order to compare our experimental measurements to the theoretical prediction of threshold pump power obtained in section 5.3.3 the transmission of the heatpipe was measured for unfocussed, 532nm wavelength, pre-lase Q-switched radiation with an energy of about 10mJ. This gave a heatpipe transmission of 56%. A check was made to ensure that no non-linear absorption processes were occurring by confirming that the pulse shape of the transmitted pulse was not distorted. Furthermore, it was found that the transmission of the heatpipe when focussed radiation was used (but Raman scattering was below threshold) was also 56%, indicating a constant absorption as a function of beam intensity for the experimental conditions used. We assume, for the purpose of calculation that this absorption is associated with the presence of dimers and scattering losses in the two short wick regions of the heatpipe. This means that only 75% of the input energy to the heatpipe is available for Raman scattering in the superheated portion of the pipe, and results in a threshold energy of 7.9mJ. From equation 5.14(b), with $\tau_{1/2}$ = 21ns, this gives a peak power of 350kW, and in view of the uncertainty involved in the parameter N/Γ, is in good agreement with the theoretical prediction of 409 kW.

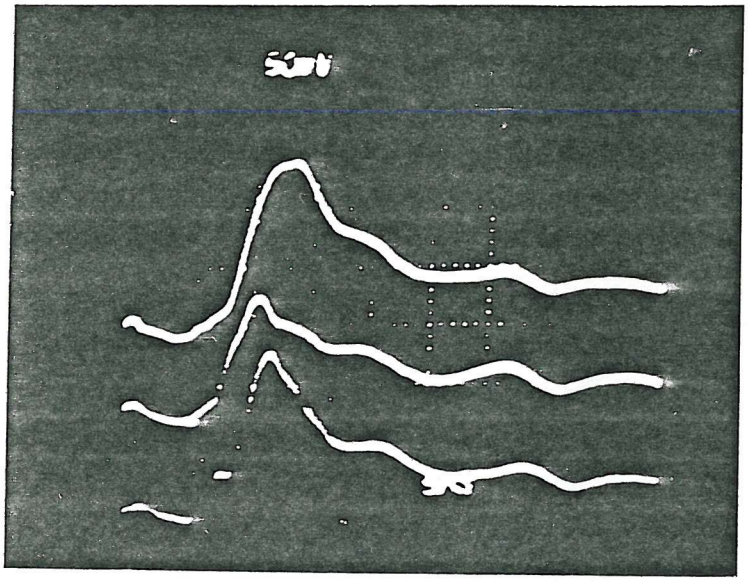

Figure 5.8: Three random Raman pulses. 5ns per major horizontal division

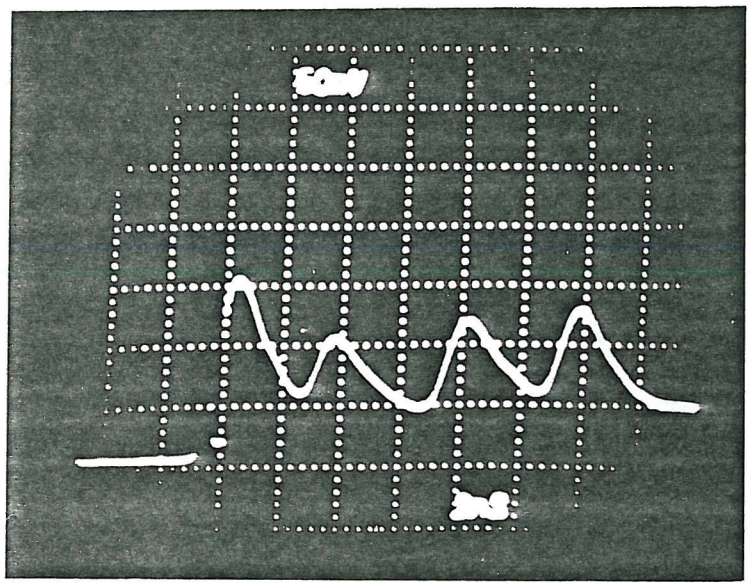

Figure 5.9: Typical Raman signal obtained when using a multi-longitudinal mode pump. 2ns per major horizontal division

5.4 Conclusion

In this chapter we have described the application of the telescopic resonator in two non-linear optical processes: frequency doubling and Raman scattering. For each of these experiments, the laser has been operated both single and multi-longitudinal mode. When operated single-longitudinal mode it has been shown that good agreement between detailed theoretical prediction and experiment is possible, thus indicating the usefulness of the single-mode laser as an analytical tool. When operated multi-longitudinal mode, however, we have shown that the higher peak intensity for a given pulse energy can lead to higher conversion efficiency (in the case of harmonic generation) and lower Raman threshold. Thus, the choice of single or multi-frequency laser operation depends on the priorities of the application.

CHAPTER SIX

CONCLUDING REMARKS

The analysis and experimental results presented in this thesis demonstrate the feasibility of telescopic resonators as a means of extracting high output power in a diffraction limited beam from a Nd:YAG laser. In addition to highly stable and repeatable performance both fixed-Q and fast Q-switched, we have shown that reliable single-longitudinal mode operation of the telescopic resonator can be obtained by using a single, tilted intracavity Fabry-Perot etalon. Furthermore, an analysis of frequency narrowing in pulsed lasers has led to simple compact formulae for the linewidth of a laser incorporating frequency selection, and also indicates the expected repeatability of single-mode operation.

In order to assess the usefulness of the laser, we have used it to measure the threshold power for Raman scattering in Caesium vapour of the Nd:YAG second harmonic. For both the harmonic generation and Raman scattering processes we found a good agreement between experimental observation and theoretical prediction, indicating the desirability in using a laser whose spatial and temporal profile can be analytically defined. In addition, we have shown that inaccuracies in the determination of Raman gain can result from the use of a multi-longitudinal mode pump laser.

In conclusion, it is hoped that the work presented in this thesis will give rise to further development work on the telescopic resonator with the aim of increasing the output energy and also improving the pulse repeatability when operated single-longitudinal mode.

APPENDIX 1: Calculation of diffraction loss for TEM_{00} and TEM_{10} modes

We consider a general resonator represented, as in figure A1.1(a), by two plane mirrors separated by a medium whose ray transfer matrix is $\begin{bmatrix} A & B \\ C & D \end{bmatrix}$ when traversed from left to right. Where an actual resonator mirror is curved, this is represented by a plane mirror and adjacent lens, and the lens is then included in the matrix $\begin{bmatrix} A & B \\ C & D \end{bmatrix}$. We assume the resonator contains an aperture diameter 2a, located at the surface of the right-hand mirror (figure A1.1(a)) and centred on the resonator axis. The round trip diffraction loss of this resonator is the same as the single-pass loss of the symmetric resonator in figure A1.1(b) in which the matrix $\begin{bmatrix} D & B \\ C & A \end{bmatrix}$ corresponds to the medium in figure A1.1(a) being traversed from right to left. Thus the overall matrix $\begin{bmatrix} A' & B' \\ C' & D' \end{bmatrix}$ of the symmetric resonator is

$$\begin{bmatrix} A' & B' \\ C' & D' \end{bmatrix} = \begin{bmatrix} A & B \\ C & D \end{bmatrix} \begin{bmatrix} D & B \\ C & A \end{bmatrix} = \begin{bmatrix} 2AD - 1 & 2AB \\ 2CD & 2AD - 1 \end{bmatrix}$$

where we have made use of the relation AD - BC = 1.

It can be shown (see e.g. Baues (1969)) that the diffraction loss of the above symmetric resonator is the same as that of an equivalent empty symmetric resonator having g parameter given by $g = A' = 2AD - 1$ and Fresnel number $N = a^2/\lambda B' = a^2/2\lambda AB$. From equation 2.16 we write $g = 2G_1G_2 - 1$ and since $G_1G_2 = \frac{1}{2}$ for a correctly adjusted dynamic stable resonator, it follows that the diffraction losses are the same as those of a symmetric resonator with g = 0, i.e. a confocal resonator. By substituting from equations 2.16 and 2.17(a) the expressions for A and B for a telescopic resonator, it is found that the Fresnel number N of this equivalent resonator is given by

$$N = \frac{a^2}{2\lambda M^2 L'(1 - L'/R_1)} \qquad \text{A1.1}$$

In the particular case where R_1 is plane this reduces to

$$N = \frac{a^2}{2\lambda M^2 L'} \qquad \text{A1.2}$$

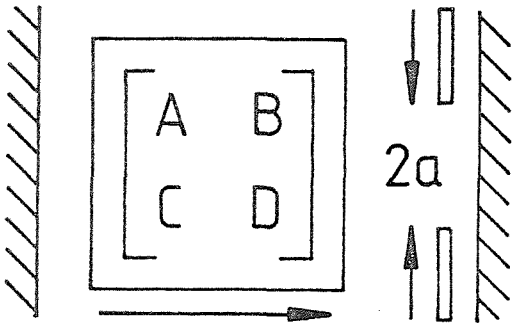

(a)

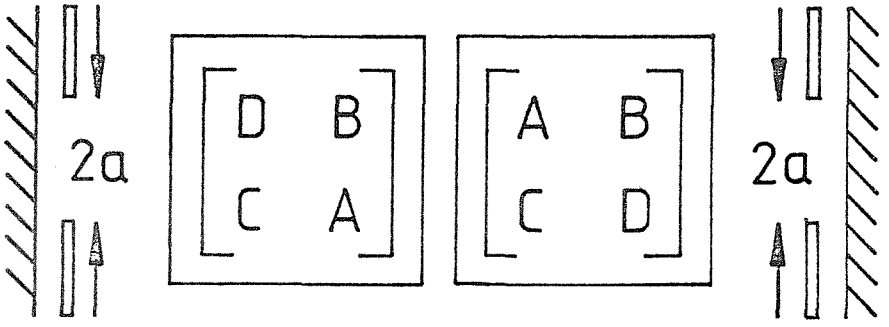

(b)

Figure A1.1: (a) Resonator with plane mirrors with an aperture of diameter 2a adjacent to the right-hand mirror, and separated by an optical medium whose ray transer matrix is $\begin{bmatrix} A & B \\ C & D \end{bmatrix}$ for propagation from left to right

(b) A round trip of the resonator in figure A1.1(a), starting from the aperture, and shown as an unfolded resonator

If the aperture in figure A1.1 had instead been located at the left-hand mirror, then a similar analysis shows that the round trip diffraction loss would be the same as that of an equivalent symmetric resonator whose Fresnel number is

$$N = \frac{a^2}{2\lambda BD} = \frac{a^2}{2\lambda L' \left(1 - \frac{M^2 L'}{R_2'}\right)} \qquad \text{A1.3}$$

Thus, as far as the mode-selectivity is concerned, it is immaterial whether the aperture is in the expanded or contracted beam, i.e. at the right-hand or left-hand mirror respectively, provided the aperture size is chosen to give the same value of N in either case.

APPENDIX 2: Calculation of the number of resonator round trips of growth experienced by laser radiation during Q-switching

Consider a laser into which radiation at a power P_{in} is injected at the time of Q-switching. Until saturation is reached, the power level in the resonator after q round trips, P(q), is given by

$$P(q) = P_{in}G^{q} \qquad \text{A2.1}$$

where G is the round trip loop gain of the resonator. This can be rearranged to give

$$q = \frac{\log(P(q)) - \log P_{in}}{\log G} \qquad \text{A2.2}$$

which can be used to find the number of round trips once P_{in}, P(q) and G are known. For the calculations in this thesis, we have taken the final laser power, P(q), to be equal to 1MW. Although equation A2.2 can be used to calculate the number of round trips when power is injected into the cavity (for instance, when the Q-switch is fully opened during pre-lase Q-switching), one often wishes to consider growth from noise. The noise power, P_0, at a frequency ν is related to the noise bandwidth $\delta\nu$ by

$$P_0 = h\nu\delta\nu \qquad \text{A2.3}$$

(see, e.g. Hanna et al., 1979). In our case, $\delta\nu$ is the bandwidth of final laser output. Thus for the case of fast Q-switching, when $\Gamma_{FQ} \simeq 0.3\text{cm}^{-1}$, we calculate $P_0 = 3.4 \times 10^{-9}$W, and therefore q = 30 for a typical loop gain G = 3. For the case of pre-lase Q-switching, where we assume that the output pulse is transform limited, the relevant bandwidth is $\delta\nu \simeq 0.44/\tau_{1/2}$ (Koechner, 1976), where $\tau_{1/2}$ is the FWHM pulse duration. Thus, for a 30ns pulse, $\delta\nu = 1.5 \times 10^{7}$Hz, and therefore $P_0 = 2.7 \times 10^{-12}$W.

APPENDIX 3: Determination of the optimum face reflectivities for a single-plate resonant reflector used as a mode selector

The power reflectivity for a single-plate resonant reflector whose thickness and refractive index are t and n, and whose faces have power reflectivities R_1, R_2, is given by (equation 4.37):

$$R = \frac{(\sqrt{R_1} - \sqrt{R_2})^2 + 4R\sin^2\delta/2}{(1 - R)^2 + 4R\sin^2\delta/2} \qquad \text{A3.1}$$

where $\delta/2 = 2\pi nt/\lambda$ and $R = \sqrt{R_1 R_2}$. Consider two adjacent laser modes, m and n, spaced by a frequency, Δ, and with mode n centred on a reflection maximum of the reflector. We require to find how the ratio R_n/R_m can be maximised by varying R_1 (or R_2).

For mode n, we have $\delta = 2p\pi$ (p is an integer), and so

$$R_n = \frac{(\sqrt{R_1} - \sqrt{R_2})^2}{(1 - R)^2} \qquad \text{A3.2}$$

For mode m, $\delta = 2p\pi \pm 2\pi\Delta/\Delta_E$, giving, after some manipulation

$$R_m \simeq \frac{(\sqrt{R_1} - \sqrt{R_2})^2}{(1 - R)^2} \cdot \left[1 - \left(2\pi \frac{\Delta}{\Delta_E}\right)^2 R\left\{\frac{1}{(\sqrt{R_1} + \sqrt{R_2})^2} - \frac{1}{(1 + R)^2}\right\}\right] \qquad \text{A3.3}$$

where we have used the approximation $2\pi\Delta/\Delta_E \ll 1$. Hence we find the ratio of reflectivities, r

$$r \equiv \frac{R_n}{R_m} = 1 - \left(\frac{2\pi\Delta}{\Delta_E}\right)^2 R\left\{\frac{1}{(\sqrt{R_1} + \sqrt{R_2})^2} - \frac{1}{(1 + R)^2}\right\} \qquad \text{A3.4}$$

For fixed $R = \sqrt{R_1 R_2}$, we look for the value of R_1 which maximises r. One can easily show

$$\frac{dr}{dR_1} = \left(2\pi \frac{\Delta}{\Delta_E}\right)^2 R \frac{1}{(\sqrt{R_1} + \sqrt{R_2})^3}\left[\frac{R}{R_1^{3/2}} - \frac{1}{R_1^{1/2}}\right] \qquad \text{A3.5}$$

thus giving $R_1 = R_2$ as the condition for maximum mode discrimination r.

APPENDIX 4: The relationship between the observed depth of modulation and ratio of mode powers for a laser operating on two longitudinal modes

Let the fields of the two modes, n and m, be

$$E_n = \hat{E}_n \cos(\omega_n t)$$
$$E_m = \hat{E}_m \cos(\omega_m t) \qquad \text{A4.1}$$

Suppose that these two modes are present simultaneously in the laser output, and that this output is detected by a square law detector. The output signal from the detector will be proportional to

$$(E_n + E_m)^2 = \hat{E}_n^2 \cos^2(\omega_n t) + \hat{E}_m^2 \cos^2(\omega_m t) + 2\hat{E}_n \hat{E}_m \cos(\omega_n t)\cos(\omega_m t) \qquad \text{A4.2}$$

Using the relationships

$$\cos^2(\omega_{n,m} t) = \tfrac{1}{2}\left[\cos(2\omega_{n,m} t) + 1\right]$$
$$\cos(\omega_n t)\cos(\omega_m t) = \tfrac{1}{2}\left[\cos(\omega_n + \omega_m)t + \cos(\omega_n - \omega_m)t\right] \qquad \text{A4.3}$$

and assuming that the detector averages over high frequency terms we arrive at a detector signal proportional to

$$\hat{E}_n \hat{E}_m \cos(\omega_n - \omega_m)t + \frac{\hat{E}_n^2}{2} + \frac{\hat{E}_m^2}{2} \qquad \text{A4.4}$$

Equation A4.4 describes a raised cosinusoidal signal of mean value $\hat{E}_n^2/2 + \hat{E}_m^2/2$ and peak-to-peak amplitude $2\hat{E}_n\hat{E}_m$.

Let

$$k = \frac{\text{peak-to-peak}}{\text{mean}} = \frac{4\hat{E}_n \hat{E}_m}{\hat{E}_n^2 + \hat{E}_m^2} \qquad \text{A4.5}$$

be a measure of the amount of mode beating. Solution of equation A4.5 for the ratio $(\hat{E}_n/\hat{E}_m)^2$, i.e. the ratio of the mode intensities, gives

$$\frac{I_n}{I_m} \equiv \left[\frac{\hat{E}_n}{\hat{E}_m}\right]^2 = \frac{8}{k^2}\left[1 + \left(1 - \frac{k^2}{4}\right)^{\frac{1}{2}}\right] - 1 \qquad \text{A4.6}$$

Typical values for k of experimental importance are $k << 1$, and equation A4.6 can be written in a more compact, approximate form:

$$\frac{I_n}{I_m} \simeq \frac{16}{k^2} \qquad \text{A4.7}$$

APPENDIX 5: Opt. Comm. 37 (5), 1981, 359-362

Large volume TEM_{oo} mode operation of Nd:YAG lasers

D.C. Hanna, C.G. Sawyers and M.A. Yuratich,

Department of Electronics,
University of Southampton,
Southampton SO9 5NH,
England.

Abstract

A stable resonator incorporating a suitably adjusted telescope allows operation of a NdYAG laser with a large volume TEM_{oo} mode. The resonator design allows excellent beam quality to be reliably maintained. TEM_{oo} energy in excess of 350mJ was obtained from a fixed Q laser. Q-switched energies have been kept at ∿100mJ to avoid damage but operation at ∿200mJ appears feasible.

There has been considerable recent work directed towards extracting as much energy as possible from a NdYAG laser in a 'diffraction-limited' or 'near-diffraction-limited' beam. A notable contribution was made by Herbst et al [1] who demonstrated the capability of an unstable resonator. However a disadvantage of the usual diffraction-coupled output from an unstable resonator is the hole in the near-field intensity distribution. This proves to be an inconvenient feature for a number of applications [2] and various other approaches have been tried in order to avoid this problem. One such approach, recently reported by Sarkies [3], involves a stable resonator containing a telescope. Small changes of telescope adjustment can affect the laser beam significantly (e.g. its divergence) and Sarkies adopted an adjustment which gave a good working compromise, i.e. a large output energy but with a divergence somewhat greater than diffraction-limited. These results stimulated our own investigations of the telescopic resonator, to see whether TEM_{oo} mode operation could be achieved with a large volume and with a degree of reliability which made it practicable. In the course of our investigations we became acquainted with the work of Steffen, Lortscher and Herziger [4,5] on what they refer to as 'dynamic stable resonators'. These publications appear not to have received wide recognition, but they contain the all-important recipe for reliable operation with a large volume TEM_{oo} mode, namely that the resonator must be designed so that the spot size in the laser rod is insensitive to fluctuations in the focal length of the pump-induced thermal lens.

Various resonator designs can achieve this insensitivity and the resonator incorporating a telescope is one†. We give here a simplified discussion of the resonator design, the detailed analytical treatment to be given in a further publication [6]. From our discussion it will be apparent that the correct choice of telescope adjustment is of crucial importance (but not critical to maintain once achieved) and failure to appreciate this fact has led to some disappointing earlier results with telescopic resonators (see e.g. [1]).

Resonator design

First we consider the resonator shown in Fig. 1a, with a plane mirror at one end and a spherical mirror, of curvature f_m, at the other end, this being represented by a lens of focal length f_m adjacent to a plane mirror. The laser rod, represented by the (thermally induced) lens of focal length f_R is also assumed for simplicity to be adjacent to the curved mirror, and the lens combination has a focal length f. The beam spot size w_1 at the laser rod is given by [7],

$$w_1^2 = (\lambda f/\pi).\sqrt{L/(f-L)} \qquad (1)$$

Thus an arbitrarily large spot size can be obtained by making f large, i.e. by arranging that $f_m \simeq -f_R$. However it can also be shown that the fractional change of spot size, $\frac{\delta w}{w}$, produced by a fractional change, $\delta f_R/f_R$, of the rod focal length is given by

$$\frac{\delta w}{w} = \frac{1}{4}\left(\frac{f-2L}{f-L}\right).(1+f_R/f_m)^{-1}\ \frac{\delta f_R}{f_R} \qquad (2)$$

Thus a large spot, which requires $(1+f_R/f_m) \ll 1$, would generally imply large fluctuations $\frac{\delta w}{w}$, as a result of shot-to-shot variations of pump energy and hence of f_R. This would tend to make the laser

† Steffen et al [4] briefly mention this possibility but give no indication of having used such an arrangement.

performance unreliable. However equation (2) shows that the spot size is insensitive to fluctuations of f_R if the cavity length L is chosen to satisfy the condition f=2L, thus giving a spot size $w_1 = \sqrt{\lambda f/\pi} = \sqrt{2L\lambda/\pi}$. Steffen et al [4] confirmed experimentally that this condition did indeed permit reliable operation with a large mode volume although the disadvantage of this design was the inconvenient resonator length implied by the large value of f. One way to get around this inconvenience is to use a short radius convex mirror, the approach taken by Steffen et al [4,5]. Alternatively one can use a telescope arrangement as shown in fig. 1b, with the advantage over the convex mirror resonator of not producing such a small spot on the mirror [6]. One can best understand the role of the telescope by considering, for simplicity, a short telescope of magnification M (where $f_2=-Mf_1$, see fig. 1b) located close to the laser rod. Thus the lens focal lengths are taken to be short compared to the resonator length. It can be shown that for small defocussing δ of the telescope i.e. where the lens spacing is $f_1+f_2+\delta$ and $|\delta/f_1| \ll 1$, the telescope has two main effects: it changes the beam spot size by a factor $\sim M$ and it changes the wavefront curvature as though it consisted of a single lens of focal length $f_T = -f_1 f_2 M/\delta = f_2^2/\delta$. Thus the telescope can be adjusted to achieve compensation of the thermal lens f_R by making $f_T \simeq -f'$ where f' now refers to the focal length resulting from the combination of f_R and f_m, i.e. $1/f' = 1/f_R + 1/f_m$. The effect of the magnification M is to modify the condition for insensitivity of spot size to variations of f_R. This becomes $f/M^2=2L$ where f is the focal length resulting from the combination of f_T, f_R and f_m i.e. $1/f = 1/f_T + 1/f'$. The spot size in the laser rod is again given by $w_1=\sqrt{\lambda f/\pi}$, which can also be written as $w_1=M\sqrt{2L\lambda/\pi}$. Thus introducing the correctly adjusted telescope allows the same large mode volume in the laser rod to be maintained but with a reduction of cavity length by M^2. The main limitation of this

approach is that it exposes components in the reduced beam to higher intensity and thus greater damage risk.

So far our discussion has assumed a simplified resonator with the lenses close to one mirror, whereas in a practical resonator the optical components have a finite size and are therefore located some distance from the mirror. A more realistic treatment is then needed for accurate results and we have made exact calculations using a computer to carry out ray transfer matrix operations. In addition we have developed an approximate analysis [6] leading to simple analytical expressions for spot-size which agree very closely with these exact calculations. Fig. 2 shows the results of exact calculations of spot-size versus telescope defocussing with parameters corresponding to a particular resonator that we have tested experimentally. The main feature to notice is the broad flat minimum for spot-size in the laser rod (upper curve), implying insensitivity of spot-size to δ. Note that a change of δ with f_R fixed is equivalent to a change of f_R (due to changed pump conditions) with δ fixed, since both correspond to a change of combined focal length f. Thus fig. 2 also represents a plot of spot size versus f_R. The minimum of the upper curve therefore implies insensitivity to fluctuations in f_R. The desired operating point is at the bottom of this minimum and the telescope must therefore be defocussed by the correct amount to ensure this. Incorrect telescope adjustment could lead to operation on the steep sides of the minimum and unreliable performance would result. Our procedure for checking the correctness of the telescope adjustment is described in the experimental section.

Experimental

In arriving at a resonator design the main parameters to be chosen are spot-size w_1 in the laser rod, resonator length L and magnification M. In fact these are related and the relationship for the simplified resonator of Fig. 1b has already been given, viz. $w_1=M\sqrt{2L\lambda/\pi} = \sqrt{\lambda f/\pi}$. Our approach has been to first choose a value of w_1 which makes good use of the available volume of laser medium. In practice the maximum value of w_1 may be limited by optical quality of the medium, the uniformity of pumping and the presence of thermally induced birefringence [8]. The laser used in our experiments was a NdYAG laser, with a rod of 75mm length and 9mm diameter pumped by twin close-coupled flashlamps [J.K. Lasers]. We have found it easy to operate with w_1=2.5mm and it is likely that even larger spot-size would be feasible. With w_1 chosen, the choice of values for L and M is made to give an acceptable compromise between a small M and hence an inconveniently large L or small L and hence large M which may then lead to excessive intensity in the contracted beam. When L (and hence M) have been chosen the value of f is fixed ($f=2M^2L$ for the simplified resonator) and this in turn fixes δ through the relations $1/f=1/f_T+1/f_R+1/f_m$ and $f_T=f_2^2/\delta$ .This assumes f_R to be known — we have measured f_R for various lamp powers P and found that the relation $f_R(m)= 2.7/P(kW)$ is obeyed [see 8]. With the design value of δ fixed, the telescope is first adjusted to be exactly collimated (using an autocollimator), then a calculated correction is made for dispersion so that it is collimated for 1.06μm, and finally the design value of δ is introduced. With the telescope so adjusted further adjustments are made to the lasers as follows. (i) The mirror alignment

is adjusted for maximum output energy. (ii) A circular aperture to select the TEM_{oo} mode is inserted and centred. In practice we have found that the aperture diameter should be ~1.5 times the calculated spot diameter at the point of insertion to ensure suppression of the TEM_{01} mode. For convenience the aperture is used in the expanded beam. (iii) Fine adjustment of δ is made until the beam circularity and uniformity, as seen from burn patterns on photographic paper have been optimised.

Measurements of beam intensity profile and beam divergence have then been made using a Si photodiode array. Observations have been made for a number of resonator mirror combinations, at various pump levels, both on the expanded and contracted beams and for fixed-Q and Q-switched operation. It has been found under these various conditions that by adopting the alignment procedure outlined above an excellent beam quality can be achieved and reliably maintained, with the measured profile and divergence agreeing to within experimental accuracy with values calculated from the design equations. A typical resonator design that we have used is specified by the parameters given in fig. 2. With this resonator and with fixed-Q operation, a TEM_{oo} output energy of 350mJ has been obtained for a flashlamp input energy of 55J. When Q-switched we have operated at lower energy to avoid damage to the small lens of the telescope and to the reflector for the contracted beam. A resonant reflector (spectrosil B) and uncoated lens (BK7) have been used, taking the contracted beam as output. At first, using a lens whose surface finish was suspect, it was found that damage to the lens was sustained at 150mJ output whereas the resonant reflector was unscathed.

With a replacement lens (also BK7), the output has been deliberately restricted to ∿100mJ and no sign of damage found after more than 10^5 shots. As a test of the laser's reliability we have run it at the ∿100mJ level continuously for one hour at 8 Hz without any adjustment. No special efforts were made to stabilise the laser mechanically or thermally. During this time the burn patterns at a distance of several metres from the output mirror were examined periodically. The burn patterns remained visually identical, with perfect circularity and complete freedom from any structure, diffraction rings, etc. We have found that TEM_{01} mode operation can be induced by small displacements of the aperture off-axis (the two lobes then have quite different intensities); even a small admixture of TEM_{01} mode is then visually detectable in the burn patterns. No sign of TEM_{01} operation was found during the one hour trial.

In conclusion we have obtained reliable operation of a NdYAG laser with a large volume TEM_{00} mode of excellent purity. A design procedure for achieving this by using a telescopic resonator has been outlined. A change of pumping conditions, e.g. repetition rate or input energy, only requires a (readily calculable) adjustment of telescope spacing. Q-switched output energies have been limited to 100mJ in our experiments but no attempt has been made to optimise the design as far as damage threshold is concerned. With optimisation and by paying attention to the choice and protection of the vulnerable components (e.g. by eliminating dust) it is believed that Q-switched TEM_{oo} outputs at ∿200mJ would be a practical possibility.

This work has been supported by a grant from the Science Research Council and one of us (C.G.S.) wishes to acknowledge support from the S.R.C. and UKAEA (Culham Laboratory) in the form of a Case Studentship. We also wish to acknowledge helpful discussions with Dr. P.H. Sarkies and assistance in the latter phase of the work from Mr. A.J. Berry.

References

1. R.L. Herbst, H. Komine and R.L. Byer, Opt. Commun. 21, (1977), 5.

2. D.C. Hanna and L.C. Laycock, Opt. Quant. Elect. 11, (1979), 153.

3. P.H. Sarkies, Opt. Commun. 31, (1979), 189.

4. J. Steffen, J.P. Lörtscher and G. Herziger, IEEE J. Quant. Elec. QE-8, (1972), 239.

5. J.P. Lörtscher, J. Steffen and G. Herziger, Opt. Quant. Elect. 7, (1975), 505.

6. D.C. Hanna, C.G. Sawyers and M.A. Yuratich (in preparation).

7. H. Kogelnik and T. Li, Applied Optics, 5, (1966),1550.

8. W. Koechner, Solid State Laser Engineering, Vol. 1, Springer Series in Optical Sciences, Springer-Verlag 1976.

Figure Captions

Fig. 1a Resonator with laser rod (focal length f_R) close to mirror of curvature f_m. The focal length, f, of the lens combination is given by $1/f = 1/f_R + 1/f_m$.

Fig. 1b Resonator with laser rod (focal length f_R) close to a plane mirror and incorporating a short telescope of magnification M ($f_2 = -Mf_1$) close to the laser rod.

Fig. 2 Spot sizes w_1 (in laser rod) and w_2 (on left hand mirror) versus telescope defocussing δ, with f_R fixed (5 m), or equivalently versus f_R with δ fixed at -6.2 mm. The laser parameters are as follows:- A=0.55m, B=0.37m, C=0.16m

$f_1 = -0.05$m, $f_2 = 0.20$ m, M= 4

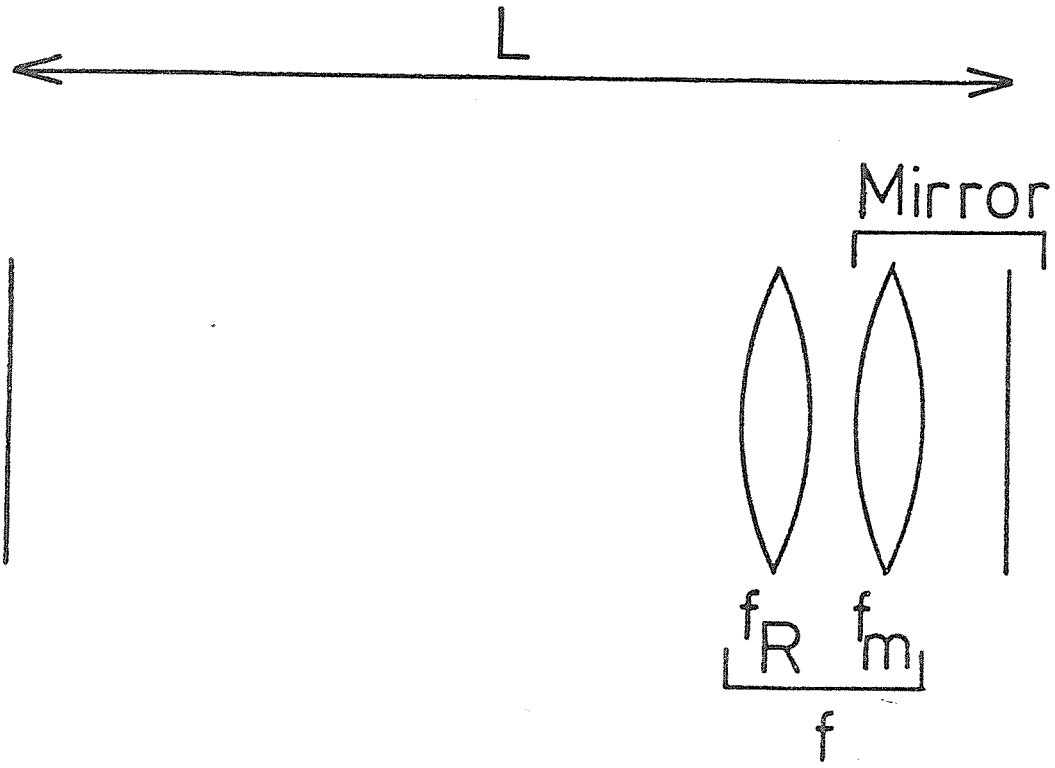
L
Mirror
f_R
f_m
f

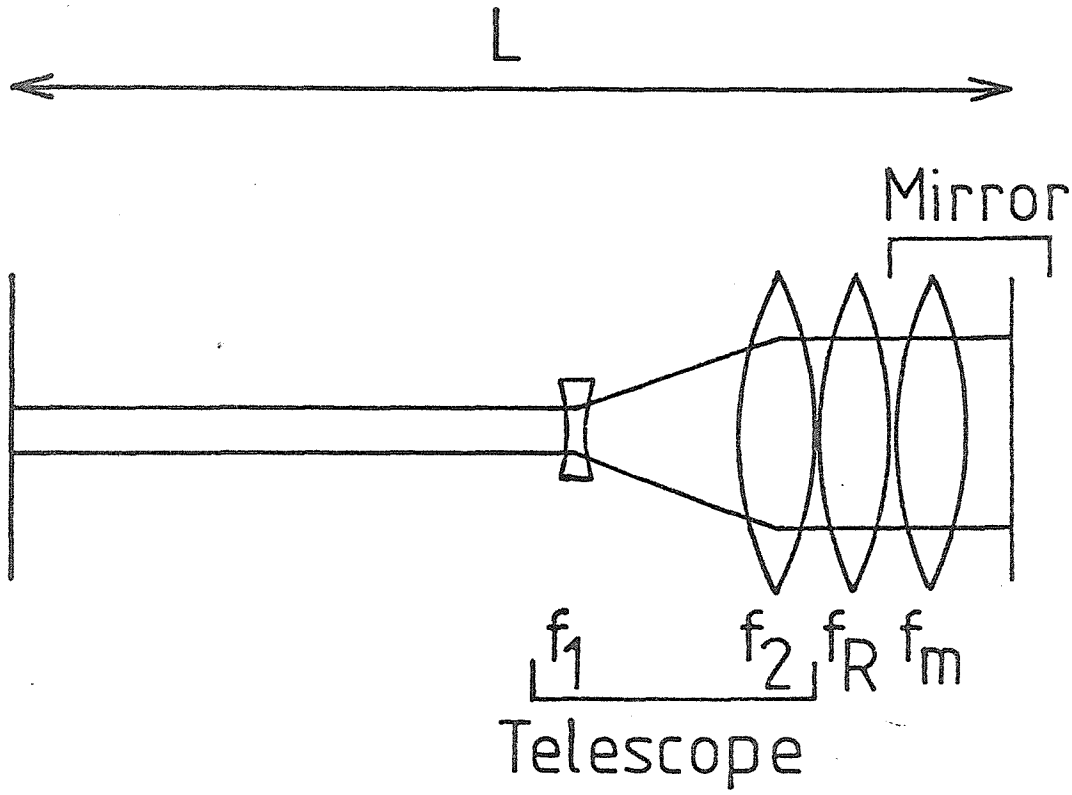
L
Mirror
f1
f2
fR
fm
Telescope

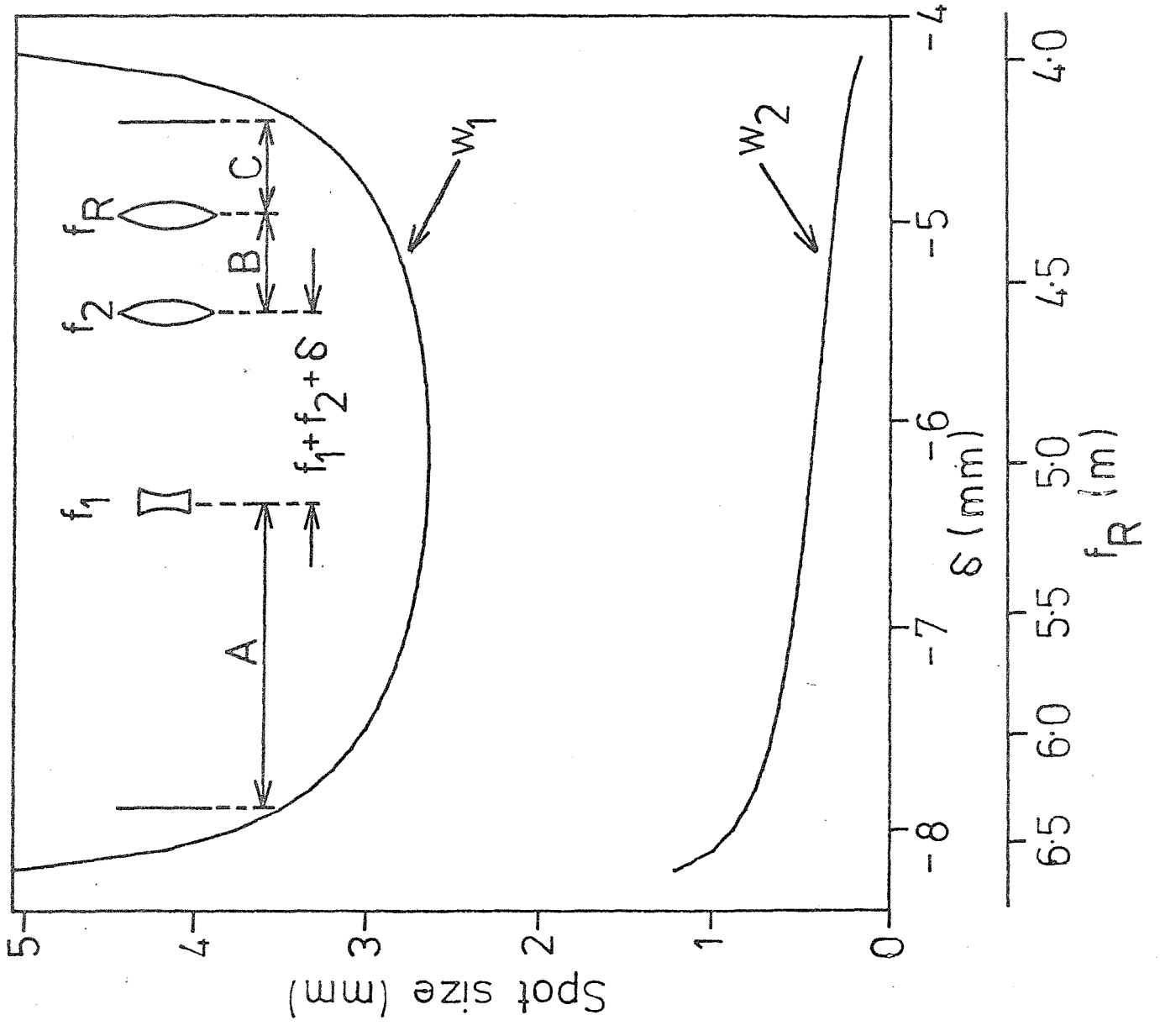
Spot size (mm)
0
1
2
3
4
5
w_1
w_2
f_1
f_2
f_R
A
B
C
$f_1+f_2+\delta$
-4
-5
-6
-7
-8
δ (mm)
4·0
4·5
5·0
5·5
6·0
6·5
f_R (m)

REFERENCES

S.A. AKHMANOV, Yu. E. D'YAKOV, L.I. PAVLOV:
"Statistical phenomena in Raman scattering stimulated by a broad-band pump",
Sov. Phys. JETP, 39 (3), (1974), 249-256.

J.A. ARMSTRONG, N. BLOEMBERGEN, J. DUCUING, P.S. PERSHAN:
"Interactions between light waves in a non-linear dielectric",
Phys. Rev. 127 (6), (1962), 1918-1939.

M.I. BAKLUSHINA:
"Evolution of the changes induced in the refractive properties of a gas by stimulated Raman scattering",
Sov. Phys. JETP, 46 (3), (1977), 436-442.

G.D. BALDWIN, E.P. REIDEL:
"Measurements of dynamic optical distortion in Nd-doped glass laser rods",
Jnl. App. Phys. 38 (7), (1967), 2726-2738.

P. BAUES:
"Huygens' principle in inhomogeneous, isotropic media and a general integral equation applicable to optical resonators",
Opto-Electron. 1, (1969), 37-44.

D.D. BHAWALKAR, L.G. NAIR, S.C. MEHENDALE:
"Effect of an internal Fabry-Perot etalon on the modes of a resonator",
Opt. Commun. 23 (3), (1977), 427-429.

G.C. BJORKLUND:
"Effects of focussing on third-order non-linear processes in isotropic media",
IEEE Jnl. Quant. Electron. QE-11 (6), (1975), 287-296.

M. BORN, E. WOLF:
"Principles of optics",
Pergamon Press, 1975.

D.J. BRADLEY, C.J. MITCHELL:
"Characteristics of the defocussed spherical Fabry-Perot interferometer as a quasi-linear dispersion instrument for high resolution spectroscopy of pulsed laser sources",
Phil. Trans. Roy. Soc. A 263, (1968), 209-223.

G. BRASSART, G. BRET, J.M. MARTEAU:
"Laser declenche a haut rendement",
Opt. Commun. 23 (3), (1977), 327-329.

D. BUA, D. FRADIN, M. BASS:
"A simple technique for longitudinal mode selection",
IEEE Jnl. Quant. Electron. QE-8 (12), (1972), 916-917.

L.W. CASPERSON, S.D. LUNNAM:
"Gaussian modes in high loss resonators",
App. Opt. 14 (5), (1975), 1193-1199.

R.B. CHESLER, D. MAYDAN:
"Convex-concave resonators for TEM_{00} operation of solid-state ion lasers",
Jnl. App. Phys. 43 (5), (1972), 2254-2257.

P.E.L. CLARKE:
"OPTIC: A program for Gaussian beam propagation in optical systems",
A report submitted for B.Sc. Electronics, University of Southampton, June 1980.

A.R. CLOBES, M.J. BRIENZA:
"Single-frequency travelling-wave Nd:YAG laser",
App. Phys. Letts. 21, (1972), 265-267.

D. COTTER, D.C. HANNA, R. WYATT:
"Infra-red stimulated Raman generation: effects of gain focussing on threshold and tuning behaviour",
App. Phys. 8, (1975), 333-340.

D.A. DRAEGERT:
"Efficient single-longitudinal-mode Nd:YAG laser",
IEEE Jnl. Quant. Electron. QE-8 (2), (1972), 235-239.

S.V. EFIMOVSKIĬ, I.G. ZUBAREV, A.V. KOTOV:
"Tunable Raman laser based on the third Stokes component of liquid nitrogen",
Sov. Jnl. Quant. Electron. 7 (9), (1978), 1155-1156.

H. EICHER:
"Third-order susceptibility of alkali metal vapours",
IEEE Jnl. Quant. Electron. QE-11 (4), (1975), 121-130.

J. FOX (Editor):
"Proceedings of the symposium on optical masers",
Polytechnic press of the Polytechnic Institute of Brooklyn, 1963.
(Distributed by Interscience.)

J.P. GORDON, R.C.C LEITE, R.S. MOORE, S.P.S. PORTO, J.R. WHINNERY:
"Long-transient effects in lasers with inserted liquid samples",
Jnl. App. Phys. 36 (1), (1965), 3-8.

A.Z. GRASIUK:
"High-power tunable IR Raman and optically pumped molecular lasers for spectroscopy",
App. Phys. 21, (1980), 173-180.

A.Z. GRASIUK, I.G. ZUBAREV:
"High-power tunable IR Raman lasers",
App. Phys. 17, (1978), 211-232.

A.Z. GRASYUK, V.F. EFIMKOV, I.G. ZUBAREV, A.V. KOTOV, V.G. SMIRNOV:
"Active media, designs and plans for powerful Raman lasers",
in "Lasers and their application to physicsl experiments".
Scientific reports of P.N. Lebedev Physical Institute, USSR Academy of Sciences, Vol. 91, (1977), 116-146.
English translation: pp115-147.

J.B. GRUN, A.K. McQUILLAN, B.P. STOICHEFF:
"Intensity and gain measurements on the stimulated Raman emission in liquid O_2 and N_2",
Phys. Rev. 180 (1), (1969), 61-68.

W.E. HAGEN, P.C. MAGNANTE:
"Efficient second-harmonic generation with diffraction-limited and high-spectral radiance Nd:glass lasers",
Jnl. App. Phys. 40 (1), (1969), 219-224.

D.C. HANNA, L.C. LAYCOCK:
"An unstable resonator Nd:YAG laser",
Opt. Quant. Electron. 11, (1979), 153-160.

D.C. HANNA, B. LUTHER-DAVIES, H.N. RUTT, R.C. SMITH:
"A two-step Q-switching technique for producing high power in a single longitudinal mode",
Opto-Electronics 3, (1971), 163-169.

D.C. HANNA, B. LUTHER-DAVIES, R.C. SMITH:
"Active Q-switching technique for producing high laser power in a single longitudinal mode",
Electron. Letts. 8 (15), (1972), 369-370.

D.C. HANNA, B. LUTHER-DAVIES, R.C. SMITH:
"Single longitudinal mode selection of high power actively Q-switched lasers",
Opto-Electronics 4, (1972), 249-256.

D.C. HANNA, C.G. SAWYERS, M.A. YURATICH:
"Large volume TEM_{00} mode operation of Nd:YAG lasers",
Opt. Commun. 37 (5), (1981), 359-362.

D.C. HANNA, M.A. YURATICH, D. COTTER:
"Non-linear optics in free atoms and molecules",
Springer series on Optical Sciences, Vol. 17.
Springer-Verlag, 1979.

P.G. HARPER, B.S. WHERRETT (Editors):
"Non-linear optics",
Academic Press, 1977.

R.L. HERBST, H. KOMINE, R.L. BYER:
"A 200mJ unstable resonator Nd:YAG oscillator",
Opt. Commun. 21 (1), (1977), 5-7.

M. HERCHER:
"Single-mode operation of a Q-switched ruby laser",
App. Phys. Letts. 7 (2), (1965), 39-41.

M. HERCHER:
"The spherical mirror Fabry-Perot interferometer",
App. Opt. 7 (5), (1968), 951-966.

M. HERCHER:
"Tunable single mode operation of gas lasers using intracavity tilted etalons",
App. Opt. 8 (6), (1969), 1103-1106.

R.T. HODGSON:
"Stimulated electronic Raman scattering from the $6s^2S_{1/2}$ to the $5d^2D_{5/2}$ state of Caesium",
App. Phys. Letts. 34 (1), (1979), 58-60.

W. KOECHNER:
"Solic-state laser engineering",
Springer series in Optical Sciences, Vol. 1.
Springer-Verlag, 1976.

H. KOGELNIK:
"Imaging of optical modes - resonators with internal lenses",
Bell Sys. Tech. Jnl., March (1965), 455-495.

H. KOGELNIK, T. LI:
"Laser beams and resonators",
App. Opt. 5 (10), (1966), 1550-1567.

S.B. KORMER, V.D. NIKOLAEV, V.D. URLIN:
"Divergence of the radiation from a Raman laser with a slowly relaxing active medium",
Sov. Jnl. Quant. Electron. 9 (2), (1979), 220-222.

T. KUSHIDA:
"Linewidths and thermal shifts of spectral lines in Neodymium-doped Yttrium Aluminium Garnet and Calcium Fluorophosphate",
Phys. Rev. 185, (1969), 500-508.

M. LAPP, L.P. HARRIS:
"Absorption cross sections of alkali-vapour molecules: I. Cs_2 in the visible. II. K_2 in the red",
Jnl. Quant. Spectros. Radiat. Trans. 6, (1966), 169-179.

L.C. LAYCOCK:
"Development of lasers for coherent anti-Stokes Raman spectroscopy",
Ph.D. Thesis, University of Southampton, 1978.

T. LI:
"Diffraction loss and selection of modes in maser resonators with circular mirrors",
Bell Sys. Tech. Jnl. 44, (1965), 917-932.

J.P. LÖRTSCHER, J. STEFFEN, G. HERTZIGER:
"Dynamic stable resonators: a design procedure",
Opt. Quant. Electron. 7, (1975), 505-514.

B. LUTHER-DAVIES, V. DEL PIZZO:
"A simple pulse tailoring/synchronisation system for laser plasma interaction experiments",
Opt. Commun. 30 (3), (1979), 403-408.

A. OWYOUNG, E.D. JONES:
"Control of temporal and spectral jitter in single mode pulsed Nd:YAG oscillators",
Rev. Sci. Inst. 49 (2), (1978), 266-267.

D.G. PETERSON, A. YARIV:
"Interferometry and laser control with solid Fabry-Perot etalons",
App. Opt. 5 (6), (1966), 985-991.

P.H. SARKIES:
"A stable YAG resonator yielding a beam of very low divergence and high output energy",
Opt. Commun. 31 (2), (1979), 189-191.

C.G. SAWYERS:
"High power tunable infra-red generation by four wave mixing in cryogenic liquids",
Mini-Thesis, University of Southampton, 1979.

B. SAYER, R. WANG, J.C. JEANNET, M. SASSI:
"Absorption measurements of quadrupole transition probabilities 6S - nD in Caesium vapour",
Jnl. Phys. B 4 (4), (1971), L20-L23.

A.E. SIEGMAN:
"An introduction to lasers and masers",
McGraw-Hill, 1971.

T. SINNOTT, J. MEYER, H. MENNICKE:
"Investigation of tunable stimulated Raman scattering by light mixing in liquid N_2",
Jnl. App. Phys. 48 (11), (1977), 4480-4483.

D.C. SMITH:
"High power laser propagation: thermal blooming",
Proc. IEEE 65 (12), (1977), 1679-1714.

G.C. SMITH:
Mini-Thesis, in preparation.

R.C. SMITH, Y.A. ABDUL-RAHMAN, G.W. BEESLEY, F.T. BELL, P.E. ONGLEY:
"A prototype de-focussed confocal Fabry-Perot spherical interferometer (DFPS)",
Opt. Laser Tech., February (1972), 13-18.

W.R. SOOY:
"The natural selection of modes in a passive Q-switched laser",
App. Phys. Letts. 7 (2), (1965), 36-37.

J. STEFFEN, J.P. LÖRTSCHER, G. HERTZIGER:
"Fundamental mode radiation with solid-state lasers",
IEEE Jnl. Quant. Electron. QE-8 (2), (1972), 239-245.

C.M. STICKLEY:
"7B2 - Laser brightness gain and mode control by compensation for thermal distortion",
IEEE Jnl. Quant. Electron. QE-2 (9), (1966), 511-518.

C.L. TANG, H. SATZ, G. DE MARS:
"Spectral output and spiking behaviour of solid-state lasers",
Jnl. App. Phys. 34, (1963), 2289-2295.

Y.S. TOULOUKIAN, R.W. POWELL, C.Y. HO, P.G. KLEMENS:
"Thermophysical properties of matter" Volume 2,
IFI/Plenum, 1970.

W.G. WAGNER, B.A. LENGYEL:
"Evolution of the giant pulse in a laser",
Jnl. App. Phys. 34 (7), (1963), 2040-2046.

J.F. WARD, G.H.C. NEW:
"Optical third harmonic generation in gases by a focussed laser beam",
Phys. Rev. 185 (1), (1969), 57-72.

J.K. WATTS:
"Theory of multiplate resonant reflectors",
App. Opt. 7 (8), (1968), 1621-1623.

C.J. WEST, C. HULL:
"International critical tables of numerical data, physics, chemistry and technology",
McGraw-Hill, 1933.

D.R. WHITE, E.L. DAWES, J.H MARBURGER:
"Theory of second-harmonic generation with high-conversion efficiency",
IEEE Jnl. Quant. Electron. QE-6 (12), (1970), 793-796.

E. WILD, M. MAIER:
"Thermal blooming in liquid N_2 during high repetition rate stimulated Raman scattering",
Jnl. App. Phys. 51 (6), (1980), 3078-3080.

R. WYATT, D. COTTER:
"Tunable infra-red generation using the 6s - 5d Raman transition in Caesium vapour",
App. Phys. 21, (1980), 199-204.

M. YAMAZAKI, T. OGAWA:
"Temperature dependences of the refractive indices of $NH_4H_2PO_4$, KH_2PO_4, and partially deuterated KH_2PO_4",
Jnl. Opt. Soc. Am. 56 (10), (1966), 1407-1408.

M.A. YURATICH, D.C. HANNA:
"Non-linear atomic susceptibilities",
Jnl. Phys. B 9 (5), (1976), 729-749.

F. ZERNIKE, J.E. MIDWINTER:
"Applied non-linear optics",
Wiley Interscience, 1973.

ACKNOWLEDGEMENTS

I wish, in particular, to thank Dr. D.C. Hanna and Dr. M.A. Yuratich, whose advice, guidance and encouragement in the course of this work have been invaluable. Also, I would like to acknowledge the financial support of the S.E.R.C. and U.K.A.E.A. (Culham Laboratories) during the first three years of my studentship. I also wish to thank the many members of the Laser Research Group for innumerable discussions and ideas, and in particular, Dave Hearn whose fertile mind and nimble wit have produced relevant ideas and served, at times, to maintain a degree of sanity. My thanks also go to Dr. J.K. Wright and Dr. P.H. Sarkies of J.K. Lasers Ltd. for fruitful discussions and the loan of countless items of equipment crucial to this work.

Thanks also, to Sue Frier, for her patient deciphering of my handwriting in typing this thesis.

Lastly, my thanks to my wife Carole, for her encouragement and support over the past four years, and persuading me on occasions that things could only get better!